Studies of Endohedral Metallofullerenes, Metal Carbides and Fullerene Derivatives by Fourier Transform Ion Cyclotron Resonance Mass Spectrometry

by

Rui Zhang

This thesis is submitted in the fulfillment of the requirement for the degree of Doctor of Philosophy

School of Chemistry

University of New South Wales

October 2001

This thesis is dedicated to

Shouxun Zhang

Declaration

I hereby declare that this thesis is my own work and that, to the best of my knowledge and belief, it contains no material previously published or written by another nor material which to substantial extent has been accepted for an award of any other degree or diploma of a university or other institute of higher learning except where due acknowledgement is made in the text of this thesis.

Rui Zhang

Abstract

Laser ablation Fourier transform ion cyclotron resonance mass spectrometry was used in the study of endohedral metallofullerenes, metal carbide clusters and selected fullerene derivatives.

Laser ablation Fourier transform ion cyclotron resonance mass spectrometry was employed to study the carbon precursor effect in the formation of endohedral metallofullerene ions. Carbon thermal black and pyrolysed Koppers coal-tar (KCT) pitch were investigated primarily by mixing compounds containing selected metals from group IIA (Ca and Ba), IIIB (Y and La) and lanthanide (Ce, Pr, Nd and Sm) in the periodic table. Endohedral metallofullerene cations $M@C_{2n}^+$ (n is observed equal or greater than 22) were detected by Laser ablation Fourier transform ion cyclotron resonance mass spectrometry from all these metals. A preliminary investigation of macroscopic production of endohedral metallofullerenes using pyrolysed KCT-pitch as the carbon precursor showed that the energy used in such production was about three orders of magnitude lower than that required for graphite.

Laser ablation Fourier transform ion cyclotron resonance mass spectrometry studies also show a correlation between endohedral metallofullerenes $M@C_{2n}$ and their corresponding metal carbide clusters MC_n ($n < 10$). These two types of clusters are formed from the same target but by different laser pulse widths and laser energies. For metals that are not observed to form endohedral metallofullerenes, such as Nb and Ta, only metal carbide cluster cations are detected in the form of $M_xC_y^+$ ($x = 1 - 13$; $y = 0 - 14$) with the M_4 series were observed as the most abundant species.

Gas-phase ion-molecule reactions between yttrium-/lanthanum-carbide cluster cations (MC_2^+, MC_4^+ and MC_6^+) and methanol, hydrogen sulfide, benzene, benzenethiol and cyclohexane were investigated. These cluster ions were capable of dehydrogenating the reagent molecules to form covalently bonded structures in the initial stage. Clustering processes were observed in the reactions with benzene and cyclohexane that yield condensation products formed by weak covalent interactions. Gas-phase studies of these metal carbide cluster ions also show that the increasing number of carbon atoms in these clusters effectively reduces their reactivity towards reagent molecules.

Quantum chemical calculations using density functional theory reveal that the ground state geometry for LaC_2^+, LaC_4^+ and LaC_6^+ is a fan shaped structure, with LaC_6^+ being non-planar. The calculation results for gas-phase reaction products of LaC_n^+ (n = 2 and 4) with benzene reveal lanthanum forms two La-C covalent bonds with the reactant molecule in the initial stage, which might have the carbon ligands involved. Further reaction products formed structures mostly by weak covalent interactions between lanthanum and carbon *Pi* bond.

Several amino acid types of fullerene derivatives together with cyano-fullerenes and fluorinated fullerenes were investigated by ESI-FTICR mass spectrometry. The cationic molecular species are mostly formed by protonation or alkali-metal ion addition. Deprotonation, chemical reduction and cyano-addition are responsible for the observation of anionic species.

Acknowledgements

It would have been impossible to complete this project and thesis work without the encouragement and help from many people including friends and family members.

First of all, I sincerely thank my principle supervisor Associate Prof. Gary Willett and co-supervisor Dr. Keith Fisher. The guidance and advice that I have received from them have enlightened me in many aspects in my research. Both of them have become known to me long before the beginning of this thesis work, and I was always impressed by their down-to-earth personality and earnest attitude towards scientific research. I feel very grateful to have known them and I believe what I have learnt from them will greatly benefit my future career.

I would also like to thank Dr. Derek Smith for his inspiring advice. I am especially impressed by his clear analysis of many problems that we have encountered. His thoughtful suggestions have helped me with the research in this thesis.

Special thanks are paid to Dr. Bill Burch from Tetley Medical for his trust in providing me the support for this project. Without his scientific and financial assistance, I would not have been able to undertake the work in this thesis. For this I am extremely grateful.

Special thanks are also paid to several group members including Ms. Femia Hopwood, Dr. Paul Greenwood, Dr. John El-Nakat, Dr. Harry Rose, Dr. Phillip Jackson, Dr. Sejin Jeong, Ms. Adriana Dinca and Dr. Mansoor Ahmad.

I would also like to thank Mr. Paul Khallahan from the mechanical workshop at UNSW and to Mr. John Morgan from electronic shop at UNSW for their assistance in

making and repairing equipments. Special thanks are paid to Mr. Hongsit Chan for his support in solving many computer problems that I have encountered.

I would like to thank Prof. Yohji Achiba and Dr. Shinzo Suzuki from Tokyo Metropolitan University in Japan for their kindness in helping me to carry out endohedral metallofullerene studies using their fullerene generator and time-of-flight mass spectrometer.

I also appreciate the suggestions and advice from Professor Zhen Gao from the State Key Laboratory of Molecular Reaction Dynamics, Institute of Chemistry, The Academy of Science, P. R. China. I would like to acknowledge Prof. Liangbing Gan from Chemistry Department, Peking University, P. R. China, Dr Gerry Gadd from Australian Nuclear Science and Technology Organization, Dr Paul Keller from Wollongong University, Dr Barrie Peel and Dr George Khairallah from La Trobe University for supplying a variety of the fullerene derivative samples. I am also grateful to Dr Barrie Peel for his assistance with the molecular orbital calculations.

Several friends have provided strong support during this study. Among them, I would like to thank Miss Ceri Addis from Bristol, UK. It was her financial assistance made it possible for me to come to Australia in 1989. Ceri has also been my spiritual support over the years. Her cheerful personality and encouraging words have pulled me through many difficult times.

Mr. Reg Wilson and Mrs. Kathleen Wilson from Sydney have been my long-time Australian friends. I have always regarded them as my Australian family. Both of them have devoted a large amount of time and energy to make me feel being part of their family. I must say it was through them that I learned about Australia. I have become

very fond of this land and its people so much so that I became determined to be one of them. I am extremely grateful to both them.

Finally, I would like to thank my parents and my younger sister Yue for their love and support. They are caring people who have always encouraged me to move forward. I believe that I am a lucky person to have such nice family, and I know I will always love them deeply wherever I travel to.

List of Abbreviations

AO	*Atomic Orbital*
APCI	*Atmospheric Pressure Chemical Ionization*
B3	*Hybrid 3-Parameter (Density Functional Method)*
BIRD	*Blackbody Irradiation Dissociation*
CASSCF	*Complete Active Space Self Consistent Field*
CI	*Chemical Ionization or Configuration Interaction*
CID	*Collision Induced Dissociation*
CPU	*Central Processing Unit*
CTB	*Carbon Thermal Black*
DFT	*Density Functional Theory*
DLV	*Direct Laser Vaporization*
EA	*Electron Affinity*
ECD	*Electron Capture Dissociation*
ECP	*Effective Core Potential*
EI	*Electron Ionization*
EIS	*External Ion Source*
ESI	*Electrospray Ionization*
ESR/EPR	*Electron Spin Resonance/Electron Paramagnetic Resonance*
FAB	*Fast Atom Bombardment*
FD	*Field Desorption*
FTICR-MS	*Fourier Transform Ion Cyclotron Resonance Mass Spectrometry*
FWHM	*Full Width at Half Maximum*
GC	*Gas Chromatography*

GSALDI	*Graphite Surface-Assisted Laser Desorption Ionization*
GTO	*Gaussian-Type Orbital*
HF	*Hartree-Fock*
HG	*Harmonic Generator*
HOMO	*Highest Occupied Molecular Orbital*
HPLC	*High Performance Liquid Chromatography*
IE	*Ionization Energy*
IR	*Infrared*
IRMPD	*Infrared Multiphoton Dissociation*
IUPAC	*International Union of Pure and Applied Chemistry*
KCT-pitch	*Koppers Coal-Tar pitch*
KE	*Kinetic Energy*
LA	*Laser Ablation*
LD	*Laser Desorption*
LCAO	*Linear Combination of Atomic Orbital*
LDA	*Local Density Approximation*
LUMO	*Lowest Unoccupied Molecular Orbital*
LYP	*Lee-Yang-Parr*
MALDI	*Matrix Assisted Laser Desorption Ionization*
MetCar	*Metallocarbohedrene*
MO	*Molecular Orbital*
MS^n	*Tandem Mass Spectrometry*
Nd-YAG	*Neodymium(+3) -Yttrium Aluminum Garnet*
NMR	*Nuclear Magnetic Resonance*
ORI	*On-Resonance Irradiation*

PA	*Proton Affinity*
PAHs	*Polycyclic Aromatic Hydrocarbons*
PC	*Personal Computer*
PES	*Photoelectron Spectroscopy*
QEA	*Quadrupolar Excitation Axialization*
REMPI	*Resonance Enhanced Multiphoton Ionization*
rf	*radio-frequency*
RHF	*Restricted Hartree-Fock*
SCF	*Self Consistent Field*
SIMS	*Secondary Ion Mass Spectrometry*
SORI	*Sustained Off-resonance Irradiation*
STM	*Scan Tunneling Microscopy*
STO	*Slater-Type Orbital*
SWIFT	*Stored Waveform Inverse Fourier Transformation*
SWNT	*Single Wall Nanotube*
TEM	*Transmission Electron Microscopy*
TMP	*Turbo-Molecular Pump*
TOF-MS	*Time-Of-Flight Mass Spectrometry*
UHF	*Unrestricted Hartree-Fock*
UHV	*Ultrahigh Vacuum*
UV-vis	*Ultraviolet-visible*
XPS	*X-ray Photoelectron Spectroscopy*
ZEKE	*Zero Electron Kinetic Energy*

Table of Contents

Chapter One

General Introduction

1.1 Aim and Outline of this Research Project

The primary goal of the research in this thesis is to apply Fourier transform ion cyclotron resonance (FTICR) mass spectrometry to investigate fullerenes, endohedral metallofullerenes and its related precursors and derivatives.

The laser ablation ionization method is used to study the formation of fullerenes and endohedral metallofullerenes from various carbonaceous materials. Small metal-carbide clusters that are related to endohedral metallofullerenes are investigated by means of gas-phase ion-molecule reactions and quantum chemical (DFT) calculations. Various fullerene derivatives are studied by the electrospray ionization method in order to reveal their gas-phase ion chemistry.

1.2 A Brief History of Fourier Transform Ion Cyclotron Resonance Mass Spectrometry

Fourier transform ion cyclotron resonance mass spectrometry, being a versatile and informative modern analytical technique, has found broad applications in natural science. Over the past three decades, both its theoretical fundamentals as well as its applications have undergone an explosive development.

The methodology which FTICR mass spectrometry adopted can be traced back to as early as 1949 when a group of physicists, Sommer, Thomas and Hipple introduced the 'Omegatron' to measure the cyclotron frequencies of ions constrained in a magnetic field.[1-3] The core of this omegatron consisted of flat metal plates or electrodes to which radio frequency and direct current (DC) voltages were applied. The ion motion in this instrument was constrained to circular orbits perpendicular to the magnetic field and no

constraint by the magnetic field along the parallel. Ions were stopped escaping axially by applying a DC electric field onto the electrode plates that were set perpendicular to the magnetic field. Although this device exhibited relatively low mass resolution by today's standards, these scientists had predicted that the mass resolving power of the ion cyclotron resonance technique is the same as the frequency resolving power. They pointed out that one of the most important applications of ICR spectroscopy would be in precise mass measurement and they demonstrated that isobars H^+ and D^+ could be readily separated.[4]

During the 1960's, prototypes of ion cyclotron resonance mass spectrometers were introduced and developed by Wobschall at Cornell,[5,6] Llewellyn at Varian[7] and Baldeschwieler's group at Standford.[8,9] These instruments had an improved mass range and resolution compared to the omegatron and used a marginal oscillator ion detector. Ions were generated by electron ionization and drifted through the ICR cell on the order of milliseconds. They demonstrated that by scanning the magnetic field, ions of various masses could be brought into resonance in sequence. But because ions quickly drifting out of the ICR cell, the possible detection time and the mass resolution for the observed ions were limited.

A breakthrough of ICR mass spectrometry came in 1970 when McIver[10] demonstrated that ions could be formed, trapped and detected in a single ICR cell. Ions were no longer allowed to drift through the cell but permitted to remain in an enclosed ion trajectory in the ICR cell on the order of many seconds. Ions of various masses were excited sequentially using a swept-frequency pulse and detected by a capacitance bridge.[11]

In 1974, Comisarow and Marshall[12-14] introduced the Fourier transform data reduction method to the ICR mass spectrometry. This innovative combination

revolutionized the ICR mass spectrometry. Since then, a new name, Fourier transform ion cyclotron resonance mass spectrometry has been given to this powerful analytic technique, and an enormous number of studies have been carried out on both instrumental development and its chemical applications. Up till the end of year 2000, there are some four thousand publications have been listed by the database Scifinder® that are closely related to the FTICR mass spectrometry studies.

During the 1980's, several new features were added to the FTICR mass spectrometry and they have made significant improvement in many aspects of this new technique. The utilization of ultrahigh-vacuum and strong-field superconducting magnets,[15] as predicted by theoretical studies,[16,17] have significantly improved ion trapping efficiency, and ions can be trapped in the ICR cell on the order of many hours. These developments have also enhanced the mass resolution, especially for high-mass ions. The applications of a frequency scan instead of a magnetic field scan,[18,19] made it possible for fast signal acquisition over a wide mass range.

Meanwhile, various new ICR cell designs have been investigated in order to improve the ICR cell performance. A cylindrical ICR cell was used to avoid side-band effect that was observed in McIver's cubic cell.[20,21] To reduce the space-charge effect and to eliminate harmonic peaks, an elongated ICR cell was investigated.[22] In order to improve the electromagnetic field homogeneity, some modification were made to the cylindrical cell, a rf-shimmed ICR cell with hemispherical end caps was used.[23-24] For the same reason, an 'infinity' cell was designed by Caravatti,[25,26] and an open geometry ICR cell was introduced by Wang and Marshall.[27] Note that some of the concepts presented here will be explained in the later discussion.

Another important development of FTICR mass spectrometry at this time was the coupling of various external ionization methods.[28] Along with the FTICR mass

spectrometry development, ionization methods have undergone many changes in order to meet analytical chemistry demands. Many new ionization methods such as fast atom bombardment (FAB),[29] matrix-assisted laser desorption ionization (MALDI)[30] and electrospray ionization (ESI)[31] were developed to facilitate the study of different types of samples, either in the form of gas, liquid or solid. Unlike the electron ionization (EI) method, which was used internally by FTICR mass spectrometry at the beginning, most of the new ionization methods have been applied externally to a FTICR mass spectrometer. This new design has made FTICR mass spectrometry a very versatile technique and capable of analyzing a broad range of samples. Detailed description of these ionization methods will be present in later sections of this chapter where ion generation method is the focus of the discussion.

Over the years, many researchers, besides those mentioned above, have made significant contributions to the FTICR mass spectrometry development. Their contributions have broadened and deepened the fields that FTICR mass spectrometry involved. Among them, Kofel, McMahon and coworkers developed high-pressure FTICR mass spectrometry, which enabled the use of external ionization sources.[28,32,33] Brauman and coworkers developed an infrared laser photophysics method for the study of gas-phase ions.[34,35] Other researchers like Eyler, Dunbar, Freiser and Cooks have or had been the major developers of the gas-phase ion chemistry. Readers are directed to comprehensive reviews for detailed description of their research works.[36-39]

1.3 The Fundamentals of FTICR Mass Spectrometry

The fundamental principle of FTICR mass spectrometry is represented by a simple relationship between the ion cyclotron frequency and it's mass.[39] As shown in Equation 1-01, in a uniform magnetic field B, which is well defined, the ion cyclotron frequency

ω is proportional to the magnetic field strength B and inversely proportional to the mass-to-charge ratio (m/q or m/z).

$$\omega = \frac{qB}{m} \qquad (1\text{-}01)$$

Where q is the electric charge carried by the ion.

Many important features of FTICR mass spectrometry including the mass range, mass resolution and mass accuracy can be derived from this basic principle. In practice, these features are not only confined by theoretical barriers, but also limited by instrumental conditions. Equation 1-01 also indicates that FTICR mass analysis is an ion energy free technique. This eliminates the need for ion energy focusing which is the fundamental concern for some other mass spectrometry techniques such as time-of-flight mass spectrometry.

1.3.1 Mass Range

According to the Equation 1-01, the mass range measured by FTICR mass spectrometry reflects the range of frequency measurement. In theory, as the detected ion mass becomes smaller, the corresponding frequency increases significantly. This effect often sets a low m/z end limit for signal digitization. On the other hand, the ion cyclotron frequency at high mass range (m/z >5,000) is of such small value that the electronic noise can interfere with ion detection. Also, as the mass of ions becomes larger, the so-called 'magnetron motion'[40-42] can become very severe, and it can significantly affect the mass resolution. These problems can be overcome to some extend by using improved electronics[43] as well as higher strength of magnetic field. [44]

1.3.2 Mass Resolution

The unique ultrahigh mass resolution of FTICR mass spectrometry was first noted by Comisarow and Marshall,[12,45] As illustrated in Equation 1-02,[37] the mass resolution

(R) is directly proportional to the observation time (transient) and to the magnetic field strength, but inversely proportional to the mass-to-charge ratio m/z.

$$R = \frac{m}{\Delta m} = \frac{\omega}{\Delta \omega} \ (\Delta\omega : FWHH) \leq 1.7 \times 10^{7} \frac{zBt}{m} \qquad (1\text{-}02)$$

where m is the mass of the analyte molecule, ω is the ICR frequency of the corresponding ion, $FWHH$ is the full width at half height of a peak, z is the electronic charge carried by the ion, B is the magnetic field strength and t is the observation time.

In the ICR cell, the ion cyclotron frequency is measured by the image current induced by the ion cyclotron motion. This image current can be affected by many factors and the most significant one is the so-called collision damping effect. That is an ion in the ion packet moving coherently in the cyclotron motion can break out from the packet through collisions, and high pressures in the ICR cell therefore result in rapid signal decay producing a low-resolution spectrum. On the other hand, at ultrahigh vacuum, the transient can last for tens of seconds producing an ultrahigh-resolution spectrum. The pressure effect on the mass resolution is shown in equation 1-03.[37]

$$R = \frac{m}{\Delta m} = \frac{\omega}{\Delta \omega} \leq 8.65 \times 10^{-10} \frac{zB}{mp}\left(\frac{\xi}{n}\right) \qquad (1\text{-}03)$$

Where ξ/n is the collisional damping frequency.

Under normal laboratory conditions, the mass resolution is also limited by the instrumentation, especially the computer memory size. As the analog-to-digital conversion (ADC) needs to be twice the size of the highest frequency of the corresponding mass to be measured, the computer memory must be capable of collecting enough long transients to achieve desired mass resolution. Freiser had shown that for a mass spectrum which was applied with an rf chirp from 0 - 2 MHz (at 3 T), which corresponds to the mass range of 23 - ∞ (m/z), the ADC rate is required to be 4

MHz, and for computer memory capacity of 256 K, data could only be collected for 64 ms, despite the fact that the transient may have barely begun to decay at that point.[37]

An alternative way to achieve higher mass resolution is to perform so-called 'heterodyne' or 'narrow band' experiment for which a narrow frequency range is covered around a chosen reference frequency. The higher the resolution desired, the narrower the mass range observed, but such an experiment diminishes the multi-channel advantage of FTICR mass spectrometry for mass measurement.

Today, the ever-increasing computer memory size and computing speed has gradually eliminated some of the instrumental limitation for high-resolution mass measurement. The latest computer workstations that are installed for FTICR mass spectrometers are often capable of acquiring over 1 MB size broad band mass spectrum that possess enough data points at high m/z to obtain mass resolution that was only achievable by the narrow band experiment five years ago. Meanwhile, application of a higher strength superconducting magnet (up to 25 T)[46] also significantly enhances the mass resolution.

1.3.3 Mass Accuracy

The precision of ion cyclotron frequency measurements, in some cases, can be as high as one part in 10^9, but such precision does not directly translate into mass accuracy. While routine mass analysis fits in well with the basic equation 1-01 at unit mass, a number of instrumental and experimental limitations including space-charge effects, inhomogeneity in the magnetic field and a non-uniform static electric field can cause disturbances in the ion motion and consequently affects the mass accuracy.

Several mass calibration procedures[47-49] have been proposed and one of the procedures that is commonly used is based on Equation 1-04.[50]

$$m = \frac{\gamma}{f_{obs}} + \frac{\beta}{f_{obs}^2} \qquad (1\text{-}04)$$

Where $\gamma = qB / 2\pi$, $\beta = -2qG_TV_{eff} / 4\pi^2$ and f_{obs} is the observed ion cyclotron frequency. G_T is the geometry factor for the trapping field and V_{eff} is the effective cell trapping potential.

This method was derived taking into account the space-charge effects and assumes that the ion space-charge potential is time invariant and quadratic. Ledford et al. had shown that using such method, ions formed by EI from 1,1,1,2-tetrachloroethane over a m/z range 117 to 135 had an average error of 0.4 ppm for 15,000 ions in the cell. As the number of ions increased to 120,000, the mass accuracy was decreased and the range of residual errors increased from 11 to 36 ppm.[50] It is clear that this method did not take full account of space-charge effect. It was shown by this method, however, the space-charge effect could be reduced dramatically by applying a higher strength magnetic field, and a 36 ppm error on the 1.2 T would be reduced to 1 ppm at 7.2 T.

Another important consideration in obtaining high mass accuracy is the digital resolution. The same number of data points acquired for the transient is used in plotting the frequency or mass spectrum. In a wide-band experiment covering a full mass range, this may mean that a peak in the spectrum is defined by only a few points, and it is quite possible that there is no point exactly at the true peak maximum. This problem will be solved through the improvement of computer digital precision.

The current level of mass accuracy for FTICR mass spectrometry is in the sub-ppm range and improves with the application of higher magnetic field and better digital resolution. The investigation into the fine details of the space-charge effect and nonideal electric fields is expected to provide better methods for the mass calibration, and subsequently improves the mass accuracy.[51]

1.4 Ion Formation and Ion Analysis in FTICR mass spectrometry

Like all other mass spectrometry techniques, the simple truth is, FTICR mass spectrometry is based on the study of ionic species in the gas-phase. Sample atoms or molecules have to be ionized prior to mass analysis in the FTICR mass spectrometer. Various ionization methods have been developed to facilitate the study of different forms of samples. Once ions are generated, they can be mass detected or manipulated in the ICR cell. The basic events in each FTICR mass spectrometry experiment include ion generation, ion excitation and ion detection.

1.4.1 Ion Generation

The principle of the ionization process is to remove electron(s) from neutrals to form positively charged ions (cations), or to attach electron(s) to neutrals to form negatively charged ions (anions). Over the last half century, a number of ionization techniques have been developed and they have been coupled with FTICR mass spectrometer to study samples range from small gaseous organic molecules[51] to large biochemical polymers.[53,54]

1.4.1.1 Electron Ionization and Chemical Ionization

The first ionization method which was used in the FTICR mass spectrometer was electron ionization,[12] for which gas-phase sample atoms/molecules were ionized by a beam of electrons emitted from a filament in the EI source. The electron energy is typically around 70 eV. The energetic electron ejects another electron out of a neutral molecule to form a positively charged radical cation $M^{\bullet+}$ (M is a closed-shell species).

$$M + e \longrightarrow M^{\bullet+} + 2e \qquad (1\text{-}05)$$

In many cases, this ionization process can be very destructive, and the sample molecule dissociates to produce fragment ions. In order to produce high abundance of molecular ion by EI, low ionization energies between 10 - 20 eV are often used.[55-57]

For the negative-ion, a sample molecule attaches with an electron to form a molecular radical anion $M^{\bullet -}$ (M is a closed-shell species).

$$M + e \longrightarrow M^{\bullet -} \qquad (1\text{-}06)$$

In order to analyze chemically labile molecules, an EI derived ionization method – chemical ionization (CI)[58-62] was introduced. Later, another ionization method called field ionization (FI)[63,64] was also developed. These ionization methods are generally less destructive and molecular species are likely to be formed.

In the chemical ionization process, a mixture of volatile sample vapor and excessive amount of CI reagent gas such as methane are present in the EI ion source. An electron beam with electron energy of 50-500 eV is produced by the EI source and bombards the reagent gas. The CI reagent gas is ionized, and then undergoes a series of chemical reactions with the sample molecules to produce protonated species $[M+H]^+$, where M is the analyte molecule.

1.4.1.2 Field Ionization and Field Desorption Ionization

The field ionization source consists of an anode or emitter, which may be a thin wire, a sharp edge or blade, or a sharp tip; and a cathode, which is a fine slit or hole according to the shape of the emitter. High voltage (kV) is applied to the emitter to provide a field between the two electrodes on the order of 2 V $Å^{-1}$.[64] In such a field the potential wall of the analyte molecule is distorted such that an electron can 'tunnel' from the molecule into a vacant Fermi level of the emitter metal. The ion so produced is immediately accelerated by the field through the slit into the mass analyzer. The residence time that ions spend in the ionization source is very short and there is little energy transferred to sample molecules during the ionization process. These factors give a high probability of producing a molecular ion. Based on the principle of field ionization, field desorption ionization (FDI) method was developed for the study of

thermally labile, polar and non-volatile compounds. Ions are generated by ion-molecule reaction type processes leading to $[M+H]^+$ or $[M+alkali]^+$ in contrast with field ionization, where $M^{\cdot+}$ are form. The coupling of FDI and FTICR mass spectrometry was experimented by Wanczek and co-workers using a high precision multi-purpose solid sample probe.[65]

The ionization methods described so far (excluding FID) mostly require the vaporization of a sample into the gas-phase prior to the ionization and they are generally not feasible for the analysis of nonvolatile and thermally labile compounds.

1.4.1.3 Fast Atom Bombardment

In the early 1980's, a new ionization method was introduced by Devienne and coworkers called fast atom bombardment.[29] While studying the sputtering of metals by a molecular beam they discovered that the bombardment of a solid target with high energetic neutral particles produced ion signals. This effect was extensively studied in the following years by the same group of researchers using various neutral molecular beams and a range of target materials by means of mass spectrometry detection. It should be noted that Barber and co-workers have done most of the developmental work for organic analysis using FAB technique.[66] It was shown by many studies that organic, inorganic materials, biological samples could be easily ionized and yielded strong ion signals with this FAB technique.[67-70]

1.4.1.4 Secondary Ion Mass Spectrometry

Secondary ion mass spectrometry (SIMS) was developed at same time as the FAB method was introduced. It employed an ion beam to sputter a solid surface and yielded secondary ions for mass spectrometric detection. In SIMS experiments, an energetic (0.1 keV ion^{-1}) ion (such as Cs^+) beam impinges upon a solid sample, so that particles including ions and neutrals are ejected out of the surface. As the liberated species stem

from very shallow depth (< 1 nm), these species carry information about the composition of the target surface. By continuing bombardment with the primary ion beam, the depth profile of the surface composition can be established. It is for this reason that SIMS has been mainly used for surface science studies.[71-73] The latest commercial FTICR mass spectrometers such as the Bruker BioAPEX series have the capability to adapt a SIMS ionization source.

1.4.1.5 Laser Desorption and Laser Ablation Ionization

Another important step in the development of ionization methods was the application of pulsed lasers. The fundamental process of laser ionization involves single photon or multi-photon absorption by the sample molecules. The term laser desorption is generally referred to as the method of producing molecular species,[74] while laser ablation is referred to as the photodecomposition of the sample material.[75-77] Both terms are vaguely defined, and no clear line can be drawn in between the two processes. It has been shown that in the laser desorption process, however, the ion energy profile fits in a pseudo-Maxwellian distribution with average ion energy of a few eV;[78] while in the laser ablation process, ion energy distribution appears to be a more random pattern with an average ion energy often greater than 100 eV.[79]

In laser ablation experiments, a high-energy laser is often used. Ions, neutrals and electrons are simultaneously produced in a broad range of kinetic energies. The ion-to-neutral ratio in the laser plume is often less then 10^{-4}.[80] The exact mechanism associated with the laser ablation process is not fully understood even though a considerable number of studies have been carried out under different experimental conditions.[81] The general conclusion, however, is that the laser ablation ionization process can have several alternatives and competing pathways involving photodecomposition and ion-molecule reactions. These different pathways are shown

under the change of laser wavelength from ultraviolet to visible and infrared with wide power range applied (20 – 10^{12} Wcm^{-2}).[82] On the other hand, laser desorption requires low laser power that desorbs predominantly neutral molecules to form ions with relatively small amount of excess energy. Laser desorption offers a mean of generating high-mass ions with minimum of fragmentation, which is advantageous for the study of thermally labile compounds and large biopolymers such as peptides and proteins. Another important ion formation mechanism in the laser desorption process is the formation of adduct ions including the attachment of electrons.

1.4.1.6 Matrix-Assisted Laser Desorption Ionization

An alternative laser desorption method that has been widely used is called matrix assisted laser desorption ionization or MALDI.[83-85] In a MALDI experiment, the sample material is mixed with excess amount of matrix material. The chosen matrix often absorbs the laser irradiation with higher efficiency then the analyte, and thus the sample molecules mostly remain intact during the MALDI process. Upon the laser irradiation, the matrix molecules are preferentially ionized and through the ion-molecule reactions, an ionic species such as a proton is transferred from the matrix ion to the sample molecule to form $[M+H]^+$ (in positive-ion mode) where M is the neutral sample molecule. Like laser desorption or laser ablation experiments, MALDI involves very complicated processes with many different pathways for ion formation. Several mechanisms have been proposed including multi-photon ionization, energy pooling and excited state proton transfer.[86-91] These mechanisms have important bearings in defining the optimized experimental conditions in terms of the state of the sample and desorption laser energies. The term 'sweet-spot' is often used to describe the sample conditions that consistently produce abundant signals in the MALDI experiment.

On the other hand, the selection of a matrix can be critical for successful ion detection in a MALDI experiment. The selection of a matrix for a particular type of compound can be unique. There is no general guideline for matrix selection, however, a wide range of matrices have been investigated and most of them have been used for the study of biopolymer compounds.[87,92-101]

1.4.1.7 Electrospray Ionization

Another important ionization method that has been developed parallel to MALDI is electrospray ionization. ESI has substantially changed the practice of mass spectrometry because of its applicability to the analysis of large bio-molecular species. It is a technique of high sensitivity, broad utility and facility to interface with many separation techniques, such as liquid chromatography (LC) and capillary electrophoresis (CE).

The concept of electrospray ionization was introduced by Malcolm Dole in the 1960's,[102,103] and it was introduced to mass spectrometry by Fenn and coworkers in the early 1980's.[31] The ESI ion source, in principle, can be considered as an electrochemical cell. Ionic species in the spray solution undergo charge separation under the influence of a strong electrical field. Depending on the polarity of the electrical field applied, the spray droplets contain excessive amount of either positive or negative charges. The solvent in the droplet quickly evaporates as the droplet move through the hot drying gas (typically N_2). This desolvation process increases the repulsion between the charges on the droplet's surface and causes coulomb explosion of the droplet. Smaller droplets produced by the coulomb explosion are further desolvated and produce even smaller droplets. This shrinking-and-exploding process goes on repeatedly till the gas-phase ions are formed.

For many covalent molecules, ion formation in ESI is achieved by either a direct redox process or an ion-addition mechanism. Ions that are often added to neutral molecules during the ESI process include the proton, alkali metal ions and NH_4^+ for positive ions; OH^-, halogen anions and basic group ions for negative ions.

Multiply charged ions are often observed in ESI for compounds with molecular weight greater than ~1,000 Da.[104] Since the observed mass in FTICR mass spectrometry is shown as the mass-to-charge ratio (m/z), this multiple charging effect fractionates the molecular mass for macromolecules including polymers and biological compounds that brings them into the m/z range of high mass resolution.

1.4.1.8 Other Ionization Methods

Over the years, many other ionization methods have also been developed for specific mass spectrometry tasks. These include 252-Cf plasma desorption,[105-107] supersonic expansion cluster ion source,[106,107] glow-discharge ionization,[110-114] atmospheric pressure chemical ionization (APCI),[115,116] microspray,[117] nanospray[118] and capillary electrophoresis ionization.[119,120]

As mentioned earlier, in the original design of an FTICR mass spectrometry ion source the EI source was fitted inside the ICR cell and it limited the use of other alternative ionization methods. The latest FTICR mass spectrometers, however, are often equipped with a range of external ionization sources including those mentioned above. In an external ionization source, ions are generated in the high-pressure region and transferred into the ultrahigh vacuum ICR cell by ion guide components.[121-126]

1.4.2 Ion Excitation

Once ions are present in the ICR cell, they are trapped along the magnetic field lines by the electric potentials applied on the end plates of the cell, while the magnetic field constrains the ions to move in circular orbits perpendicular to the magnetic field

lines referred as an ion cyclotron motion.[127] As indicated by Equation 1-01, ion cyclotron frequency is independent of the ion energy. In other words, ions of same m/z can have the same ion cyclotron frequency but different translational energies (velocities). It is also possible that these ions are located in the different regions in the cell. Such incoherent motion cannot produce an image current on the receiver plates of an ICR cell. To solve this problem, a frequency-swept rf pulse is applied to the two excitation-plates of the ICR cell. The irradiation effectively excites ions into larger cyclotron orbits and ions of same m/z value are brought into phase to form an ion packet. This has raised a question, however, about the coulomb repulsion between the ions in the packet. It has been observed that as the number of ions (same m/z value) increases, its corresponding mass spectrometric signal has become broadened. This is the so-called 'space-charge effect'.[50,128-131] For ultrahigh resolution mass measurement, the mass shift caused by the space-charge effect can be significant. It is therefore important to keep the ion population small in the ICR cell since the space-charge effect increases with higher ion population in the cell.

During the excitation, the radius of ion cyclotron orbits can be calculated by Equation 1-07.[130-132]

$$r = \frac{V_{pp} t}{2Bd} \qquad (1\text{-}07)$$

Where V_{pp} is the peak-to-peak rf voltage (applied to the pair of excitation plates) amplitude, t is the duration of the rf excitation pulse, B is the magnetic field strength and d is the diameter of the ICR cell (cylindrical).

An important feature of Equation 1-07 is that the ion cyclotron radius is independent of the ICR frequency and this means for ions of a certain m/z, the excitation only becomes effective when the applied swept rf frequency comes into

resonance with the ion cyclotron frequency. This is the key feature of ICR technique. The frequency-sweep ion-excitation method 'chirp' adopted by FTICR mass spectrometry is based on such a principle.[133,135,136]

1.4.3 Ion Detection

The detection of ions starts at the end of ion excitation. The coherent ICR motion of ion packets induces an image current in the receiver plates of the ICR cell. This image current is also referred to as a transient, a time domain signal or a free ion decay signal. For each ion ensemble at a particular m/z, the corresponding image current is represented by a single frequency sine wave. As in most of FTICR mass spectrometry experiments, ions of many different m/z values are presented in the ICR cell simultaneously, their ICR frequency sine waves are superimposed and presented as a complex transient signal. This transient is then converted into a voltage signal, which is amplified, digitized and recorded by the computer.[132] The Fourier transform algorithm effectively extracts each individual sine wave and translates it into the corresponding ICR frequency. Based on the Equation 1-01, the frequency domain spectrum can be readily transformed into its corresponding mass spectrum.

1.4.4 Tandem Mass Spectrometry

One of the outstanding features of FTICR mass spectrometry is its unique ion trapping capability, which enables multi-stage ion manipulations. This is called tandem mass spectrometry, which is described as MS^n. Tandem mass spectrometry is extremely useful for the ion structure elucidation and gas-phase ion-molecule reaction studies. Over the years, FTICR technique has adapted many new designs that have facilitated MS^n experiments. The use of the pulsed molecular valve has assisted ion cooling in the ICR cell.[137] Ion ejection techniques such as stored waveform inverse Fourier transform (SWIFT),[138-142] introduced by Marshall and co-workers, have improved the

precision of ion selection and resulted in clean ion isolation. Ion fragmentation methods such as on-resonance irradiation collision-induced dissociation (ORI-CID), sustained off-resonance irradiation collision-induced dissociation (SORI-CID),[143-146] blackbody irradiation dissociation (BIRD),[147,148] infrared multiphoton dissociation (IRMPD)[149-151] and electron capture dissociation (ECD)[151-162] have become standard techniques for ion structure studies.

FTICR mass spectrometry experiments are carried out as events of a series of pulses termed as a 'pulse sequence'. The mass spectrometric events occur as the result of executing the pulse steps in the sequence, which sends commands to the FTICR mass spectrometer. Tandem mass spectrometry experiments are accomplished by executing additional steps of pulses in the FTICR pulse sequence. For each stage of MS experiments, the basic pulse sequence includes ion selection/isolation; ion excitation (optional); time delay for reaction or CID. Ion-molecule reactions and ion-dissociation processes are often combined in the gas-phase studies in order to reveal the structure or the reactivity of both parent ions and the daughter ions. As it will be shown in the later chapters, both ORI-CID and SORI-CID are applied to this current study.

1.4.4.1 On-Resonance Irradiation Collision-Induced Dissociation

The ORI-CID experiment is carried out by translationally exciting the selected ion continuously for periods of up to hundreds of microseconds after which the ions can undergo collisions with the collision gas atoms or molecules to fragment. The applied excitation frequency precisely matches the cyclotron frequency of the selected ions. The selected ions constantly acquire energy during the ion-excitation and ions follow an outward spiral trajectory.[163]

The center-of-mass translational kinetic energy (in eV) of an activated ion, E_k^{com} is given by following equation:[161]

$$E_k^{com} = \frac{m_t}{m_t + m_p} \times \frac{S_e^2 V_{pp}^2}{d^2} \times \frac{t_{rf}^2 q}{8m_p} \quad (1\text{-}08)$$

Where m_t is the target atom or molecular mass; m_p is the parent ion mass; S_e is the geometry factor of the ICR cell; V_{pp} is the peak-to-peak voltage of the rf pulse; d is the diameter of the ICR cell; t_{rf} is the length of the rf excitation pulse and q is the electronic charge.

The ion collision frequency during the ion activation N_c can be calculated by following equation: [164]

$$N_c = \frac{\pi q(\gamma_t + \gamma_p)^2 C_n V_{pp} t_{rf} S_e}{2m_p d} \quad (1\text{-}09)$$

Where γ_t is the average radius of the target atom or molecule; γ_p is the average collision radius of the parent ion; C_n is the number density of the target gas atoms or molecules.

Based on equation 1-08 and equation 1-09, the ORI excitation can effectively increase the transitional energy of the selected ion in a relative short period of time, but the collision frequency can be low in this process. For an ion at m/z 200 Da, with collision gas pressure of $1x10^{-9}$ mbar of argon in the cell (7 T), the number of collisions during a 50 μs of excitation (*Vpp* = 100 V) is in the single collision regime. This result implies that the ORI-CID technique is more efficient for low-mass ions as the center-of-mass translational energy acquired by the selected-ion is more significant in a single collision. It also implicates that the limited number of collisions during the ORI excitation may not be able to provide sufficient energy for large mass ions to fragment.

1.4.4.2 Sustained Off-Resonance Irradiation Collision-Induced Dissociation

In order to improve the CID efficiency for large mass ions, an alternative excitation method sustained off-resonance irradiation collision-induced dissociation or SORI-

CID[143,144,147,165] has been developed to provide the mass-selected ion with sufficient translational energy to dissociate. This method applies an excitation rf frequency offset to the ion cyclotron frequency of the mass selected ion. The excitation effectively accelerates-decelerates the chosen ion and the change of the excitation energy follows a sine wave function. The alternating cycles are sustained for the whole excitation period up to many seconds.

During the SORI process, the average kinetic energy E_{av}^{K} of the ions over long periods and in the absence of collisions is described by the following equation: [165-167]

$$E_{av}^{K} = \frac{qE_0^2}{8\pi q} \times \frac{\nu_c}{(\nu_c - \nu)^2} \qquad (1\text{-}10)$$

In which E_o is the excitation field amplitude corrected for the cylindrical cell, B is the magnetic field strength and q is the electronic charge. The variables, ν_c and ν are the natural ion cyclotron frequency and off-resonance frequency respectively.

The SORI-CID is a low energy process and the average energy that ions acquired in each collision is less then 10 eV. However, as the selected-ion undergoes enormous number of collisions during SORI-CID experiment, energy is constantly dumped to the selected-ion via collisions and it is therefore more advantageous for the large mass ions to fragment as they can accumulate the energy more efficiently than smaller ions.

1.5 Chemical Applications of FTICR Mass Spectrometry

Over the last thirty years, the fields that FTICR mass spectrometry have been applied covering nearly very area of natural science including almost all the branches of chemistry. FTICR mass spectrometry is not only a unique tool for chemical analysis, but also a unique environment for the study of chemistry fundamentals. Several disciplines have been formed during the advancing years of FTICR mass spectrometry. These include gas-phase ion chemistry, cluster chemistry, biological applications and

many other chemistry or physics related studies. It is beyond the scope of this thesis work to present a comprehensive review of these studies, brief descriptions are given below on the development of the major fields that have involved FTICR mass spectrometry.

1.5.1 Gas-Phase Ion Chemistry

The FTICR mass spectrometry has enabled studies of gas-phase chemical reactions under defined chemical and physical conditions that are impossible to achieve in the condensed phase. The effect of solvent, ligands and counter ions can be mostly eliminated in the gas-phase studies and the intrinsic properties of the investigated ions, such as the ionization energy (IE), electron affinity (EA), proton affinity (PA) and rate constant for many reactions can be determined in a direct manner.

Several features have made FTICR mass spectrometry superior to many other mass spectrometric methods in the study of gas-phase ion chemistry. Firstly, the ICR cell combines the reaction chamber and ion detector, which eliminates the need of additional mass analyzer for the ion detection. The application of the so-called double resonance technique permits unambiguous determination of reactant and product ion relationships.[8,168] Ion activation by rf excitation can be used to overcome the energy barrier that in some instances can facilitate endothermic reactions. The wide range of external ion sources that are commonly coupled to FTICR instruments allows the study of unusual gas-phase species that may not be observed in the condensed phase. For example, the study of ion-molecule reactions between laser generated 'bare' transition metal ions and hydrocarbon molecules have revealed the catalytic properties of transition metals at the molecular level.[169-174]

Gas-phase ion chemistry can be generally divided into two categories, gas-phase organic ion chemistry and gas-phase organometallic ion chemistry. The gas-phase

organic ion chemistry involves nucleophilic anions, electrophilic cations and some unusual ionic species such as distonic radical ions and fullerene ions. The nucleophilic anion reactions can occur as substitution, elimination, addition/elimination and reduction reactions. The organometallic reactions on the other hand often involve gas-phase 'bare' metal ions or ligated metal ions in the reaction with di- or tri-atomic molecules including larger alkanes, unsaturated hydrocarbons and many other small organic molecules. Comprehensive reviews are available for extensive discussions of these studies.[175,176]

It is also possible to carry out kinetic studies by FTICR mass spectrometry experiments. A so-called 'kinetic method' has been established by Cooks and co-workers to determine important chemical properties such as proton affinity, gas-phase basicity and thermodynamic constants for gas-phase ionic species.[177-180] Although the kinetic method was first established with sector instruments, FTICR mass spectrometry has also played important role in the later studies.

1.5.2 Cluster Chemistry

Another important field that FTICR mass spectrometry has been heavily applied to is gas-phase cluster chemistry. For many years, atomic and molecular clusters have been a main focus of research both in physics and chemistry. The unique chemical and physical properties possessed by cluster species have made an important attribution to the new field in material science termed as 'nanotechnology', for which cluster materials at nanometer scale plays a central role.[181]

The concept of a 'cluster' covers a wide range of atomic and molecular species and it is difficult to give a clear definition. It is generally referred to as the aggregation of atoms or molecules either with strong covalent interaction or weak interaction by nucleophilic or electrophilic attractions.

The early study of gas-phase clusters was promoted by the demand of understanding many physical processes such as the condensation and forces that control the crystal growth of semiconductors. The study of vapor components in the equilibrium with molten metals yielded the earliest reports of gas-phase inorganic clusters.[182-184]

A large amount of early cluster work was carried out using the Kundsen or effusion cell technique, which applied resistive-heating to generate gas-phase clusters including alloys,[185-188] metal carbides[189-197] and mixtures. The invention of supersonic expansion cluster source has enabled studies of weakly-bound rare gas clusters[198-201] and alkali metal clusters[202,203] that require low internal energy for stabilization. The application of pulsed laser in either direct laser ablation mode or combined with supersonic expansion source has remarkably broadened the field of cluster chemistry.[204] Gas-phase bare metal clusters, metal oxide clusters and metal sulfide clusters are readily produced by these methods. The most impressive cluster study, however, has been the discovery of caged carbon clusters named *fullerenes*, which resulted in the award of the Nobel Prize to its three major discoverers, Kroto, Smalley and Curl.[205]

The composition of clusters can be either homogeneous such as in fullerenes or heterogeneous as in metal-oxide clusters or metal sulfide clusters, and the size of clusters is in the range that bridges between atomic/molecular species and bulk materials. Clusters are therefore referred to as 'the fifth state of matter'.[206]

Combined with various ion-dissociation techniques such as collision-induced-dissociation and photodissociation, FTICR mass spectrometry can provid crucial information on cluster bonding energies, ionization potential and electron/proton affinities.[207]

The development of new ionization methods such as ESI in recent years has enabled the study of gas-phase cluster ions formed from closed-shell precursors. The formation of this type of cluster ions results from the nucleophilic or electrophilic attraction between a central ion and neutral molecules, generally, there is no electron exchange energy involved. For example, electrospray of an alkali halide salt solution such as NaI/MeOH generates weakly bound cluster ions $(NaI)_nNa^+$ and $(NaI)_nI^-$ (n= 1 - ~30, the number n varies with the ESI condition).

1.5.3 Biological Macromolecules

In recent years, ionization techniques such as ESI and MALDI have made a strong impact on biological science. Combined with separation techniques such as gas-phase chromatography and high performance liquid chromatography, mass spectrometry has become the 'real-time' analysis method for research in biological and microbiological science.[208]

One crucial step in this development has been the application of electrospray ionization method to mass spectrometry because it enables sample molecules to be introduced into mass spectrometer via the solution phase. The ability to form multiply charged ions by ESI process has been, in many cases, an advantage for mass spectrometry, especially for FTICR mass spectrometry studies. It allows high molecular weight species to be observed in the low m/z region (< ~1,000 Da) with high-mass resolution. In such a low m/z region, FTICR mass spectrometer has sufficient resolving power to provide isotopic information for multiply charged ions. By accurate mass measurement, sometimes the elemental composition of certain ions can be correctly assigned. To date, a single biological molecule (DNA) with molecular masses up to a hundred mega-Dalton has been detected by ESI-FTICR mass spectrometry which carries ~ 30,000 charges.[209]

The strong demand for structure elucidation of large biomolecules has promoted the development of various ion-dissociation techniques and new computer software for mass spectrometry. Ion-dissociation techniques such as SORI-CID, BIRD, IRMPD and ECD have become the essential tool in peptide sequencing and protein structure mapping. The latest computer software designed for mass spectrometry often contain databases or have interfaced with on-line databases to provide information on peptides and proteins.[210] Also, the hydrogen-deuterium (H/D) exchange method has provided a convenient way to probe the protein-folding process.[211-215]

1.6 Fullerene Chemistry

1.6.1 The Discovery of Fullerenes

Fullerenes are a family of cage-like pure carbon molecules that consist of twelve pentagon rings and different number of hexagon rings. They are the third form of carbon allotropes beside diamond and graphite.[216-220] The fullerene C_{60}, being the first molecule in the series that has all its pentagons completely separated by the hexagons, forms a truncated icosoahedral structure. C_{60} was first named buckminsterfullerene for its resemblance to the architectural structure - geodesic dome, which was designed by American architect and constructor, Buckminster Fuller.[218]

The discovery of fullerenes is a result of gas-phase study of carbon clusters, which has its roots in the astrophysics relating to interstellar absorption bands.[221-223] In 1984, a group of scientists from *Exxon Research* studied the abundance of carbon clusters generated by laser vaporization of graphite resulting in the surprising observation that only even-numbered clusters were presented in the C_{40} - C_{200} ion mass range.[224] Later, Smalley, Kroto et al. explained the abundance of these even-numbered carbon clusters was the result of formation of cage-like molecules containing a central cavity and they named these molecules *fullerenes*.[218] The photodissociation experiments performed by

the Smalley group on a FTICR mass spectrometer, using a selected range of fullerene ions, showed that these fullerene ions fragmented by emitting C_2 units under the irradiation of XeCl excimer laser.[225] Based on the experimental observation, the same research group developed a mechanism called the 'Pentagon Rule' to explain the stability of the fullerene carbon clusters.[226,227] It states that the energetically most favored form of any open graphite sheet is one, which is:

(a) made up solely of pentagons and hexagons

(b) and has as many pentagons as possible

(c) while avoiding adjacent pentagons.

They pointed out that C_{60} is the first pentagon rule structure that can close. Many theoretical studies have been carried out to confirm the fullerene cage structures and to probe their chemical properties.[228-241] Interestingly, the earliest chemical calculations had predicted the cage structure of fullerene C_{60} long before the experimental evidence was obtained.[242]

1.6.2 Fullerene Generation and Characterization

If fullerenes had not been made in bulk quantities, they would probably have remained only of the interest to a handful of spectroscopists, especially mass spectrometrists. In 1990, Kratschmer and co-workers developed a method, which allowed fullerenes to be generated in gram quantities, and they obtained the crystal structures of pure C_{60} by X-ray diffraction of a microcrystalline powder of C_{60}.[243,244] The method involved evaporation of graphite by resistive heating. Graphite rods were used as electrodes in the atmosphere of ~100 Torr helium. The resulting black soot was collected from the evaporation chamber and dispersed in benzene. It produced a wine-red solution. The dissolved material was analyzed by laser desorption mass spectrometry and it showed predominately C_{60} with less than 10% of C_{70}. This method

was later modified by using direct current discharge between the two graphite electrodes and it is the method now used commerically.[227]

The characterization of fullerenes has been carried out by many analytical methods including various mass spectrometry techniques,[245-247] NMR,[248-251] FTIR,[252,253] UV-vis[254-256] and X-ray diffraction.[242,257,258]

It has been confirmed by these analytical methods that there are two types of bonding presented in the fullerene C_{60}, the so-called 6-6 (1.38Å) and 6-5 (1.45Å) carbon-carbon bonds (see the insert). In contrast, C_{70} consists of eight types of C-C bonds.

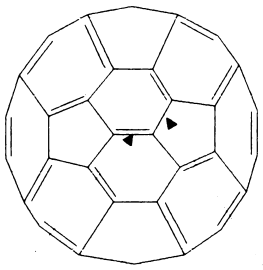

6-6 C-C bond 6-5 C-C bond

Fullerene C_{60}

1.6.3 Fullerene Derivatization

Since macroscopic amounts of fullerenes have become commercially available, a broad range of fullerene-chemistry studies has been carried out and the majority of these studies are aimed at adding functional groups to the fullerene frame.

Fullerenes are unique molecules in terms of their structures that extend in three dimensions in space, and their chemical reactivity is thus determined by such a spatial structure. The stability of C_{60} is based on being the smallest caged molecule in which all the 12 pentagons are isolated from each other by hexagons. A hexagon containing three π–bonds and fused to two pentagons can be represented in the three possible ways, each existing as a resonating pair. Of six possible structures, in one structure there is no double bond at the 5-6 ring junctions. A double bond in a five-member ring increases strain and therefore decreases stability. For fullerenes to be structurally stable, all the double bonds should be placed in such a manner that there would be no

double bonds at the 5-6 ring junctions. Theoretical calculations show that 12,500 resonant structures are possible for C_{60}.[259]

The C=C bonds of C_{60} react like those of very electron-deficient arenes or alkenes, therefore C_{60} as whole behaves as an electron-deficient 'superalkene' rather than as a 'superaromatic' molecule. Based on such chemical character, the modification of fullerenes has been attempted mainly by adding functional group(s) on to the exterior carbon frame of fullerenes. The exohedral addition reactions can occur through cycloaddition, radical and nucleophilic addition, hydrogenation, oxidation, halogenation reactions and complex formation with transition metals. The conjugated π–system in C_{60} is not completely delocalized and the electrophilic double bonds [6-6] on C_{60} can readily add nucleophiles and radicals. Mass spectrometry studies have shown that C_{60} can add up to 34 methyl radicals and it is therefore referred to as a 'radical sponge'.[260]

Cycloaddition to fullerenes gives mainly monoaddition products, commonly, 1,2-addition to a 6-6 bond, which is energetically more favorable than addition to a 6-5 bond.[261] The reaction products are often used as the initial compound for further functionalization.

Nucleophilic addition to C_{60} gives, as a rule, monoadducts. Functional groups such as amino acid molecules, CN[262] and vinyl ethers group can add to the C_{60} fullerene and some of these reaction products are promising monomers for cationic polymerization.[263]

All the attempts to prepare completely hydrogenated fullerene $C_{60}H_{60}$ have been unsuccessful. This compound appears to be highly unstable due to the enormous strain, which arises upon the formation of twenty planar cyclohexane rings and numerous H-H interactions.[261] So far, fullerene hydrides with the compositions $C_{60}H_x$ (x = 2, 4, 18, 32, 36-50, 42-44) and $C_{70}H_x$ (x = 2, 4, 8, 10, 34-44) have been reported.[264]

The electronegative fullerene molecules can be easily reduced but are difficult to oxidize. The reaction of fullerene with oxygen, however, on exposure to UV light (in hexane) or heating (in the presence of oxygen) results in vigorous oxidation accompanied by fragmentation - the rupture of the C=C bonds in the fullerene cage. Upon irradiation, C_{60} initially passes into the triplet state, the transfer of energy from this species affords singlet oxygen, which oxidizes the fullerene.

The halogenation of fullerenes was achieved by reacting C_{60} with gaseous chlorine, fluorine and liquid bromine giving complex mixture of addition products. It has been considered that iodine does not react with fullerenes, but recently, a charge transfer complex involving iodine and C_{60} was reported.[265] Among the halogenated fullerene derivatives, fluorinated fullerenes have been mostly studied due to the interest of material science. Fluorofullerenes containing up to 60 fluorine atoms per molecule, including $C_{60}F_{48}$ can be prepared by fluorination with fluorine gas, while hyperfluorofullerenes $C_{60}F_{76}$ can be synthesized on treatment with fluorine with exposure to UV radiation.[266,267]

Polymerization of fullerenes has also been attempted by many researchers. Macromolecular fullerene derivatives facilitate the combination of unusual properties of fullerenes with the specific properties of many polymers. Thus macromolecular modification of fullerenes can provide and tailor polymeric materials with interesting properties, e.g. electronic, magnetic, mechanical, catalytic and optical properties. The synthesis of polymers containing fullerenes has been carried out following two main schemes, either the 'main-chain' or the 'side-chain' polymers.[268] These polymeric derivatives can be termed as polyfullerenes, indicating the covalent binding to a polymer and high molecular mass. Polymers containing fullerene molecules often show unusual properties that possess potential in material science. For example, the telechelic

polymer that bridges two fullerene molecules exhibits unusual photophysical and redox properties.[269] These polymers have been the focus of many studies of energy- and electron-transfer process. Mono- and ditelechelic polymers provide exotic molecules in which the fullerene core can be tethered to different chromophores. For example, monotelechelic, covalently linked, multi-chromophoric molecules, in which the bridge is a poly(norbornane-bicyclo[2,2,0]-hexane-hybrid oligomer, have been synthesized.[270]

1.6.4 Metallofullerenes

Shortly after the discovery of fullerenes, Heath et al. reported that lanthanum atom(s) could be encapsulated in the fullerene cages.[271] The name *endohedral metallofullerene* written as $A_m@C_{2n}$ (m = 1-3, n = 30-70) has been assigned to this new family of fullerenes where the symbol @ denotes that the metal atom (A) is located inside fullerene cage.[272,273]

As an example, Smalley and co-workers have shown in their pulsed-molecular-valve mass spectrometry (PMV-MS) experiment that a range of lanthanofullerene ions could be generated by laser ablation of a La_2O_3 doped graphite target. Endohedral metallofullerenes are very unusual molecules with regard to their structures. The carbon cage prevents the metal reacting with other chemicals and so the metal is 'inert'. Verification of this lack of reactivity was obtained with a cluster beam/ FTICR mass spectrometer by non-reactions with O_2, NO and NH_3.[274] Other evidence of metal encapsulation was shown by laser irradiation of $La@C_{60}^+$, which produces C_2 loss from the carbon cage until $La@C_{44}^+$, the predicted size of a carbon cage that is able to contain a lanthanum ion.

Endohedral metallofullerenes are predicted to have many potential applications in areas such as nonlinear optical devices and catalysts,[275] superconductors,[276] lasers and ferroelectric materials.[276,277] To date, the macroscopic production[278,279] and spectro-

scopic characterization[246,251,280-284] of endohedral metallofullerenes are still under investigation.

Laboratory scale chemical studies on endohedral metallofullerenes are difficult because these species can only be produced with very low yields and so there is a demand for other methods of production or the discovery of new precursors. So far, most of preparations have used graphite/metal or metal oxide mixtures as precursors with different vaporization sources.[285,286] Studies at the University of New South Wales, on the other hand have focused on the search for new carbon precursors for fullerene and metallofullerene.[287-299]

The use of metal doped graphite rods with the electric arc vaporization method[243] and the laser ablation-furnace method[300,301] represent the two important methods for metallofullerene production. Of these two methods, the electric arc technique is preferred for macroscopic production but this method has yields of less than 0.1% even for the most abundant metallofullerenes (for example, La@C_{82})[302] that can be isolated.

Purification of the metallofullerenes is time consuming and requires preparative scale HPLC to produce only milligram quantities of the metallofullerenes.[303-306] Although yields of fullerenes, such as C_{60}, from graphite are as high as 10% in arc experiments[307-309] and 40% in laser furnace experiments,[228] there has been no significant improvement in the low yields of endohedral metallofullerenes. Möschel et al. have reported a new method for metallofullerene synthesis that involved the evaporation of the carbon and barium metal in different regions of a radio frequency (rf) furnace.[310] They reported that this technique can enhance the formation of endohedral barium fullerenes.

1.7 Metallocarbohedrenes

Another important class of metal-carbon clusters discovered in recent years is called metallocarbohedrenes or metcars. Metcars are binary metal-carbon clusters in the form of M_xC_y (x= 1 - ~15; y= 0 - ~20). Multi-caged structures are proposed for clusters such as $M_8C_{12}^+$. As reported by Castleman et al., early transition metals such as Ti, Zr, Hf, V and Nb are capable of forming multi-metal/carbon binary clusters by ion-molecule reactions in a pulsed gas expansion laser ablation cluster source.[311-321] The experiments were performed using laser generated metal cluster ions to dehydrogenate gaseous alkanes that were seeded in the expansion gas.[312] $M_8C_{12}^+$ has been observed in predominant abundance among the metal carbide cluster ions and it is believed that the 'superabundance' of this species is related to its thermodynamic stability. Although the structures and heats of formation for most of the M_xC_y ions are still unknown, both theoretical and a range of experimental techniques have been employed to elucidate the structure of Ti_8C_{12}.[323-325] Unlike fullerenes or endohedral metallofullerenes, metcars are very reactive. The metal atoms in its structure are exposed and can easily react with other reagent molecules. Metcars therefore have not been made in bulk material and its research has been carried out mainly in the gas-phase and by theoretical studies.

An interesting phenomenon has been observed by comparing the formation of metallofullerenes and metcars. That is formation of these two types of clusters has shown to be metal selective. The metallofullerene related metals are mainly the group IIA and IIIB elements in the periodic table including lanthanides, and the metcar related metals are in the group IVB and VB. This metal selectivity reflects the intrinsic difference among the metallic elements with regard to the interaction with carbon.[326]

1.8 Carbon Nanotubes

The fullerene production method introduced by Krätschmer and Huffman,[243] which uses a high-current electric discharge to vaporize carbon electrodes in a helium buffer gas has been commonly used to produce large quantity of fullerenes. It was noticed by Ijima in 1992 that during such an electrical discharge, the graphite rod used as the cathode grows in its length as the result of the deposition of a new form of carbon material. He examined the carbon deposit collected on the cathode by transmission electron microscopy (TEM).[327,328] The TEM image revealed some tube-like cylindrical carbon material in the carbon deposit, and these carbon tubes comprised of hexagonal graphene sheets with a typical size of few nanometers in diameter. Later these carbon tubes were referred to as carbon nanotubes.[329]

Carbon nanotubes can be divided into two categories according to the number of carbon layers they contain. The first type is the single-wall nanotube (SWNT) which is close to an ideal fullerene fiber and its diameter is close to fullerenes and has single layer cylinder extending from end to end on the order of nanometers to milimeters.[330,331] The second type is multiwalled nanotubes (MWNT). They comprise concentric cylinders placed around a common central hollow, with spacing between the layers close to that of the interlayer distance in graphite of 0.34 nm. Closed-end carbon nanotubes are also observed in the initial discovery by Ijima, and similar to fullerenes, the capping curvature is caused by a number of five-member rings.

The time scale for the carbon nanotube formation is extremely short, a 5 nm diameter MWNT of 1 mm length grows in 10^{-4} s.[332] The arc discharge method produces stiff, near-perfect and whiskerlike MWNT, but the yield is limited and the material formed in the deposit contains substantial amounts of nanoparticles that have polyhedral shapes. Several other methods including catalytic growth[333] and catalyzed laser

ablation[334] have been developed to produce better defined larger scale carbon nanotubes. The catalytic growth method used a graphite rod with a hole in the center, which was packed with mixture of graphite powder and low percentage of transition metals such as Fe, Co and Ni.[335]

It is believed that carbon nanotubes will play an important role in nanotechnology – a fast developing field in material science. Some preliminary investigation has shown that carbon nanotubes can be used as molecular wires that permit a single electron to transmit through the tube.[336] They are also good media for absorbing hydrogen, which has the potential in the design of new generation of hydrogen batteries.[337]

1.9 The Methodology of Theoretical Studies - Quantum Chemical Calculations

Quantum chemical calculations have become very useful methods for investigating novel molecules and ions in recent years. Improved computer algorithms, faster computer processors, more efficient disk storage and overall improvements in software have enabled high quality results to be generated for a large range of molecular/ionic species. For this reason, some of the metal-carbon species and their derivatives that were observed in this project were investigated by quantum chemical calculations.

Quantum chemical calculations are concerned with predicting the properties of atomic or molecular system. They are based upon the fundamental laws of quantum mechanics and use a variety of mathematical transformation and approximation techniques to solve the fundamental equations.

Quantum mechanics states that the energy and other related properties of an atom or a molecule might be obtained by solving the Schrödinger equation:

$$\hat{H}\Psi = E\Psi \qquad (1\text{-}11)$$

Where the cap denotes an operator. Except for the smallest systems such as hydrogen-like species, the exact solutions to the Schrödinger equation are not

computationally practical. Electronic structure methods are therefore characterized by their various mathematical approximations to its solution. Three major classes of electronic structure methods have been developed including *semi-empirical* methods, *ab initio* methods and *density functional* methods. Although it is still under debate whether *density functional* methods are also *ab initio* methods, the main concern of this current study is not to address this question but to use these methods to investigate the species that are observed in the FTICR mass spectrometry experiments.

1.9.1 Hartree-Fock Theory

1.9.1.1 Born-Oppenheimer Approximation

As the exact solution to the Schrödinger equation is not possible for any but the most trivial molecular systems, a number of simplifying assumptions have been used to yield approximate solutions for a large range of molecules. The Born-Oppenheimer approximation is the first of several approximations used to simplify the solution of the Schrödinger equation. It simplifies general molecular problem by separating nuclear and electronic motions. This approximation is based on the fact that the mass of a typical nucleus is thousands of times greater than that of an electron. Nuclei move very slowly with respect to the electrons, and electrons react essentially instantaneously to changes in the nuclear position. The electron distribution within a molecular system depends on the positions of the nuclei, and not on their velocities. In other words, the electronic motion can be described as occurring in a field of fixed nuclei.

For molecular systems, the full Hamiltonian can be expressed as:

$$\hat{H} = \hat{T}^{e} + \hat{T}^{N} + \hat{V}^{e-N} + \hat{V}^{e-e} + \hat{V}^{N-N} \qquad (1\text{-}12)$$

The first two terms on the right hand side of the equation are the kinetic energy operators. The other three terms describe the potential energies in the system. '$\hat{V}^{e-N}$'

is the electron-nuclei attraction potential, '$\hat{V}^{e-e}$' and '$\hat{V}^{N-N}$' are the electron-electron and nuclei-nuclei Coulomb repulsion potentials respectively.

The Born-Oppenheimer approximation allows two parts of the problem to be solved independently. It is therefore possible to construct an electronic Hamiltonian, which neglect the kinetic energy term for the nuclei.

$$\mathrm{H}^{e} = -\frac{1}{2}\sum_{i}^{e}\nabla_{i}^{2} - \sum_{i}^{e-N}\sum_{I}\left(\frac{Z_I}{\left|\vec{R}_I - \vec{r}_i\right|}\right) + \sum_{i}^{e-e}\sum_{j<i}\left(\frac{1}{\left|\vec{r}_i - \vec{r}_j\right|}\right) + \sum_{I}^{N-N}\sum_{J<I}\left(\frac{Z_I Z_J}{\left|\vec{R}_I - \vec{R}_J\right|}\right) \tag{1-13}$$

Note that this equation is expressed in atomic units ($a_0 = h^2/4\pi^2 m_e e^2$).

This Hamiltonian is then used in the Schrödinger equation describing the motion of electrons in the field of fixed nuclei.

$$\mathrm{H}^{e}\Psi^{e}\left(\vec{r},\vec{R}\right) = \mathrm{E}^{eff}\left(\vec{R}\right)\Psi^{e}\left(\vec{r},\vec{R}\right) \tag{1-14}$$

The solution to this equation for the electronic wavefunction is the effective nuclear potential function E^{eff}, which depends on the nuclear coordinates and describes the potential energy surface for the system. Accordingly, E^{eff} is also used as the effective potential for the nuclear Hamiltonian.

$$\mathrm{H}^{N} = T^{N}\left(\vec{R}\right) + \mathrm{E}^{eff}\left(\vec{R}\right) \tag{1-15}$$

This Hamiltonian is used in the Schrödinger equation for nuclear motion, describing the vibrational, rotational and translational states of the nuclei. Solving the nuclear Schrödinger equation is necessary for predicting the vibrational spectra on all operators and functions.

1.9.1.2 Self-Consistent Field and Hartree-Fock Theory

For the various approximation methods that have been used, they are faced with a basic question as how to find a one-electron Hamiltonian $\hat{H}_i$ and to use a one-electron

Schrödinger equation to obtain the one-electron wavefunction φ_i and its orbital energy E_i, ultimately to establish the full wavefunction and to resolve the total energy of the system.

The first method that provided solution to this problem was introduced by Hartree in 1928, and it is now known as the method of *self-consistent fields* (SCF). This technique was later modified by Fock and Slater to include the effect of electron exchange, and commonly referred to as the Hartree-Fock (HF) method or Hartree-Fock theory.

The assumption behind this technique is that any one electron moves in a potential, which is a spherical average of the potential due to all the other electrons. Then the Schrödinger equation is integrated numerically for that electron and that average potential. This supposes that a wavefunction for all the other electrons are already known so that their average potential can be evaluated. This is in general not the case, and so the calculation is started by guessing the form of their wavefunctions. The Schrödinger equation for the electron of interest is then solved, and the wavefunction so found is used in the calculation of the potential experienced by one of the other electrons. The latter's Schrödinger equation is then solved, and in turn is used to refine the average potential experienced by another electron. This is repeated for all the electrons in the system, and the potential experienced by the first electron can be recalculated. Usually this refined potential differs from the original guess, and so the whole cycle is repeated until the solutions for all the electrons are unchanged in a cycle of calculation – then the orbitals are *self-consistent*.

1.9.1.3 Linear Combination of Molecular Orbitals

In order to describe molecular structures, the concept of *molecular orbitals* (MO) was developed that supposes the individual electrons of a molecule can each be thought

of as occupying an orbital that spreads throughout the nuclear framework. The procedure to construct molecular orbitals is called *the linear combination of atomic orbitals* (LCAO) method, which models the molecular orbitals by expressing them as linear combinations of the atomic orbitals of the parent atoms.

An individual molecular orbital is defined as:

$$\phi_i = \sum_{\mu=1}^{N} c_{\mu i} \chi_\mu \qquad (1\text{-}16)$$

where the coefficients $c_{\mu i}$ are known as the molecular expansion coefficients. ϕ_i and χ_μ represent an arbitrary molecular orbital and its basis function respectively. The basis functions $\chi_1 \ldots \chi_N$ are also chosen to be normalized.

For LCAO to be accomplished, the set of molecular expansion coefficients $c_{\mu i}$ in equation 1-16 has to be obtained. Hartree-Fock theory takes advantage of the variational principle, which states that for the ground-state of any antisymmetric normalized function of the electronic coordinates, which denoted as Ξ, the expectation value for the energy corresponding to Ξ will always be greater than the energy for the exact wavefunction:

$$E(\Xi) > E(\Psi); \quad \Xi \neq \Psi \qquad (1\text{-}17)$$

In other words, the energy of the exact wavefunction serves as a lower boundary to the energies calculated by any other normalized antisymmetric function. Thus, the problem becomes to find the set of coefficients that minimize the energy of the resultant function.

The variation principle leads to the following equation describing the molecular orbital expansion coefficients, $c_{\mu i}$, derived by Roothaan and Hall:

$$\sum_{\nu=1}^{N} (F_{\mu\nu} - \varepsilon_i S_{\mu\nu}) C_{\mu i} = 0 \qquad \mu = 1, \ 2, \ \ldots, \ N \qquad (1\text{-}18)$$

This equation can be presented in matrix form:

$$FC = SC\varepsilon \tag{1-19}$$

Where each element is a matrix and ε is a diagonal matrix of orbital energies, each of its elements ε_i is the one-electron orbital energy of molecular orbital χ_i. F is called the Fock matrix, and it represents the average effects of the field of all the electrons on each orbital. For a closed shell system, its elements are:

$$F_{\mu\nu} = H_{\mu\nu}^{core} + \sum_{\lambda=1}^{N}\sum_{\sigma=1}^{N} P_{\lambda\sigma}\left[\langle\mu\nu|\lambda\sigma\rangle - \frac{1}{2}\langle\mu\lambda|\nu\sigma\rangle\right] \tag{1-20}$$

where $H_{\mu\nu}^{core}$ is another matrix representing the energy of a single electron in the field of the bare nuclei, and P is the density matrix, defined as:

$$P_{\lambda\sigma} = 2\sum_{i=1}^{occupied} c_{\lambda i}^{*} c_{\sigma i} \tag{1-21}$$

The coefficients are summed over the occupied orbitals only, and the factor of two comes from the fact that each orbital holds two electrons.

Finally, the matrix S from Equation 1-19 is the overlap matrix, indicating the overlap between orbitals. Both Fock matrix (through the density matrix) and the orbitals depend on the molecular orbital expansion coefficient. Thus, Equation 1-19 is not linear and must be solved iteratively. At convergence, the energy is at a minimum, and the orbitals generate a field, which produces the same orbitals, accounting for the method's name *self-consistent field.* The solution produces a set of orbitals, both occupied ($\phi_{i,j,\ldots}$) and virtual (unoccupied, conventionally denoted $\phi_{a,b,\ldots}$). The total number of orbitals is equal to the number of the basis function used.

The term $\langle\mu\nu|\lambda\sigma\rangle$ in Equation 1-20 signifies the *two-electron repulsion integrals.* Under the Hartree-Fock treatment, each electron sees other electrons as an average distribution; there is no instantaneous electron-electron interaction included. Higher-

level methods attempt to remedy this neglect of electron correlation in various ways that will be discussed later.

1.9.1.4 Correlation of Electron Spins with Molecular Orbitals

The wavefunctions Ψ that describe the electronic structures of the system must satisfy some basic criteria. First, Ψ must be *normalized* in order to give meaningful answers to the electron distribution probability. The normalization condition is expressed as:

$$\int \Psi^* \Psi d\tau = 1 \qquad (1\text{-}22)$$

The integration being over all the space. Ψ and its first derivative should also be continuous in order to define a second order derivative for frequency calculations.

Another major criteria is that Ψ must be *antisymmetric*, meaning that it must change sign when two identical particles are interchanged. For a simple function, antisymmetry means that the following relation holds:

$$f(i,j) = -f(j,i) \qquad (1\text{-}23)$$

For an electronic wavefunction, antisymmetry is a physical requirement following from the fact that electrons are Fermions, (Fermions are particles possessing the properties of antisymmetry and a half-integral spin quantum numbers). It is essentially a requirement that Ψ agree with the results of experimental physics. More specifically, this requirement means that the following relation holds:

$$\Psi\left(\vec{r}_1,\ldots,\vec{r}_i,\ldots,\vec{r}_j,\ldots,\vec{r}_n\right) = -\Psi\left(\vec{r}_1,\ldots,\vec{r}_j,\ldots,\vec{r}_i,\ldots,\vec{r}_n\right) \qquad (1\text{-}24)$$

Fock and Slater realized that the Hartree method did not treat electron spin explicitly, and that wavefunctions for electrons should be antisymmetric. Electrons can have spin up (+1/2) or down (-1/2). The electron spin functions are defined as α and β for which:

$$\alpha(\uparrow)=1 \quad \alpha(\downarrow)=0$$
$$\beta(\uparrow)=0 \quad \beta(\downarrow)=1 \tag{1-25}$$

The α function is 1 for a spin up electron and the β function is 1 when the electron is spin down. The notation $\alpha(i)$ and $\beta(i)$ will designate the values of α and β for electron *i*; thus $\alpha(1)$ is the value of α for electron 1.

Multiplying a molecular orbital functions by α and β will include electron spin as part of the overall electronic wavefunction Ψ. The product of the molecular orbital and a spin function is defined as a *spin orbital*, a function of both the electron's location and its spin.

Note that in equation 1-26, when the molecular orbital components are orthonormal, so are the spin orbitals. Each row of this determinant is formed by representing all possible assignments of electron *i* to all orbital-spin combinations. Swapping two electrons corresponds to interchanging two rows of the determinant, which will result in changing its sign. This determinant mixes all of the possible orbitals of all the electrons in the molecular system to form the wavefunction.

$$\Psi(\vec{r}) = \frac{1}{\sqrt{n!}} \begin{vmatrix} \phi_1(\vec{r_1})\alpha(1) & \phi_1(\vec{r_1})\beta(1) & \phi_2(\vec{r_1})\alpha(1) & \phi_2(\vec{r_1})\beta(1) & \cdots & \phi_{\frac{n}{2}}(\vec{r_1})\alpha(1) & \phi_{\frac{n}{2}}(\vec{r_1})\beta(1) \\ \phi_1(\vec{r_2})\alpha(2) & \phi_1(\vec{r_2})\beta(2) & \phi_2(\vec{r_2})\alpha(2) & \phi_2(\vec{r_2})\beta(2) & \cdots & \phi_{\frac{n}{2}}(\vec{r_2})\alpha(2) & \phi_{\frac{n}{2}}(\vec{r_2})\beta(2) \\ \vdots & \vdots & \vdots & \vdots & & \vdots & \vdots \\ \phi_1(\vec{r_i})\alpha(i) & \phi_1(\vec{r_i})\beta(i) & \phi_2(\vec{r_i})\alpha(i) & \phi_2(\vec{r_i})\beta(i) & \cdots & \phi_{\frac{n}{2}}(\vec{r_i})\alpha(i) & \phi_{\frac{n}{2}}(\vec{r_i})\beta(i) \\ \phi_1(\vec{r_j})\alpha(j) & \phi_1(\vec{r_j})\beta(j) & \phi_2(\vec{r_j})\alpha(j) & \phi_2(\vec{r_j})\beta(j) & \cdots & \phi_{\frac{n}{2}}(\vec{r_j})\alpha(j) & \phi_{\frac{n}{2}}(\vec{r_j})\beta(j) \\ \vdots & \vdots & \vdots & \vdots & & \vdots & \vdots \\ \phi_1(\vec{r_n})\alpha(n) & \phi_1(\vec{r_n})\beta(n) & \phi_2(\vec{r_n})\alpha(n) & \phi_2(\vec{r_n})\beta(n) & \cdots & \phi_{\frac{n}{2}}(\vec{r_n})\alpha(n) & \phi_{\frac{n}{2}}(\vec{r_n})\beta(n) \end{vmatrix} \tag{1-26}$$

1.9.1.5 Methods for Open-Shell Systems

The discussions above have only considered the restricted Hartree-Fock (RHF) method, which applies to the closed-shell systems. For open-shell systems, an

unrestricted Hartree-Fock (UHF) method, capable of treating unpaired electrons, is needed. In this case, the alpha and beta electrons are in different orbitals, resulting in two sets of molecular orbital expansion coefficients:

$$\phi_i^{\alpha} = \sum_{\mu} c_{\mu i}^{\alpha} \chi_{\mu}$$
$$\phi_i^{\beta} = \sum_{\mu} c_{\mu i}^{\beta} \chi_{\mu} \qquad (1\text{-}27)$$

The two sets of coefficients result in two sets of Fock matrices (and their associated density matrices), and ultimately to a solution producing two sets of orbitals. These separate orbitals produce proper dissociation to separate atoms, correct delocalized orbitals for resonant systems, and other attributes characteristic of open shell systems. However, eigenfunctions are not pure spin states, but contain some amount of spin contamination from higher states (for example, doublets are contaminated to some degree by functions corresponding to quartets and higher states).

1.9.2 Electron Correlation Methods

As explained above, the Hartree-Fock method provides an inadequate treatment of the correlation between the motions of electrons within a molecular system, especially that arising between electrons of opposite spin.

When Hartree-Fock theory fulfills the requirement that $|\Psi^2|$ be invariant with respect to the exchange of any two electrons by antisymmtrizing the wavefunction, it automatically includes the major correlation effects arising from pairs of electrons with the same spin. This correlation is termed *exchange correlation.* However, the motion of electrons of opposite spin remains uncorrelated under Hartree-Fock theory.

Any method which goes beyond SCF in attempting to treat this phenomenon properly is known as an *electron correlation* method (despite to the fact that HF method

does include some correlation effects) or a *post-SCF* method. Two different approaches will be discussed briefly below.

1.9.2.1 Configuration Interaction

The configuration interaction method begins by noting that exact wavefunction Ψ cannot be expressed as a single determinant, as HF theory assumes. CI proceeds by constructing other determinants that replace one or more occupied orbitals within the Hartree-Fock determinant with a virtual orbital.

In a *single substitution*, a virtual orbital, such as ϕ_a, replaces an occupied orbital ϕ_i within the determinant. This is equivalent to exciting an electron to a higher energy orbital. Similarly, in a *double substitution*, two occupied orbitals are replaced by virtual orbitals:

$$\phi_\alpha \leftarrow \phi_i ; \phi_\beta \leftarrow \phi_j$$

$$\Psi_{i\alpha} = |\phi_1, \ \ldots \ \phi_i, \ \phi_{\alpha+1}, \ \ldots \ \phi_{i-1}, \ \phi_\alpha \ \ldots \ \phi_n| \qquad (1\text{-}28)$$

Triple substitutions would exchange three orbitals, and so on.

If the wavefunction Ψ is formed as a linear combination of the Hartree-Fock determinants and all possible substituted determinants, then the method is called full configuration interaction or full CI. The wavefunction Ψ can be expressed as:

$$\Psi = b_0\Psi_0 + \sum_{s>0} b_s\Psi_s \qquad (1\text{-}29)$$

Where the 0-indexed term is the Hartree-Fock level, and s runs over all possible substitutions. The b's are the set of coefficients to be solved for, again by minimizing the energy of the resultant wavefunction.

Equation 1-29 represents a mixing of all of the possible electronic states of the molecule, all of which have some probability of being attained according to the laws of quantum mechanics. Full CI is the most complete non-relativistic treatment of the

molecular system possible, within the limitations imposed by the modeling the electron density in accordance with the definition (and constraints) of the basis set in use.

The full CI method has many of the desirable features of a theoretical model. It is well-defined, size-consistent, and variational. However, it is also very cost-expensive and impractical for all but the smallest systems.

1.9.2.2 Møller-Plesset Perturbation Theory

Another approach to electron correlation is Møller-Plesset (MP) perturbation theory. Qualitatively, Møller-Plesset perturbation theory adds higher excitation to Hartree-Fock theory as a non-iterative correction, drawing upon techniques from the area of mathematical physics known as many-body perturbation theory.

Perturbation theory is based upon dividing the Hamiltonian into two parts:

$$H = H_0 + \lambda V \tag{1-30}$$

$\mathbf{H}_0$ is soluble exactly, and λV is a *perturbation* applied to $\mathbf{H}_0$. λV is a correction, which is assumed to be small in comparison to $\mathbf{H}_0$. (Note that the perturbation operator V is not related to the potential energy.) The assumption that V is a small perturbation to H_0 suggests that the perturbed wavefunction and energy can be expressed as a power series in V.

$$\begin{aligned} \Psi &= \Psi^{(0)} + \lambda\Psi^{(1)} + \lambda^2\Psi^{(2)} + \lambda^3\Psi^{(3)} + \cdots \\ \mathrm{E} &= \mathrm{E}^{(0)} + \lambda\mathrm{E}^{(1)} + \lambda^2\mathrm{E}^{(2)} + \lambda^3\mathrm{E}^{(3)} + \cdots \end{aligned} \tag{1-31}$$

The perturbed wavefunction and energy are substituted back into the Schrödinger equation. After expanding the products, and by equating the coefficients on each side of the equation for each power of λ, a series of relations representing successively higher orders of perturbation can be formed.

The n^{th} order (MPn) corrected wavefunction may be used to calculate the $(2n+1)^{th}$ order energy correction. At MP_2 level, the energy correction will always have negative

value, which means lowering the energy. However, MP perturbation theory is capable of overcorrecting the energy by higher order corrections, which indicated by the energy corrections sometimes being positive.

1.9.3 Basis Sets

Classic Hartree-Fock and post-Hartree-Fock methods use Gaussian-type orbitals (GTO's) or Slater-type orbitals (STO's) to represent the atomic orbitals in the linear combination of atomic orbital (LCAO) method. The quality and accuracy of the calculation results are very sensitive to the number of basis functions or the basis set that is used in the calculation. In practice, however, the increasing number of basis functions imposes a significant computational strain and limits the size of the system that can be studied.

1.9.4 Effective Core Potentials and Relativistic Effects

For systems containing heavy atoms such as the third-row transition metals, the relativistic contraction of core orbitals results in a significant alteration of calculated ground-state geometry. Neglect of the relativistic effects results in over estimation of bond distances involving heavy atoms by up to as much as 20%. On the other hand, if the core electrons of larger atoms can be treated as non-interacting potentials which is analogous to the use of effective core potentials (ECPs),[338-342] the number of the basis functions that are needed for the calculation can be reduced without significant loss of accuracy.

1.9.5 Density Functional Theory

Density functional theory-based methods ultimately derive from quantum mechanics research from the 1920's, especially the Thomas-Fermi-Dirac model and as well from Slater's fundamental work in quantum chemistry in the 1950's.[343-345] The DFT approach is based upon a strategy of modeling electron correlation via a general

functional of the electron density (a functional is a function whose definition is itself a function, in other words, a function of a function).

DFT methods owe their modern origins to the Hohenberg-Kohn theorem, published in 1964,[346] which demonstrated the existence of a unique functional which determines the ground-state energy and density exactly. The theorem, however, does not provide the form of this functional.

Following on the work of Kohn and Sham, the approximate functionals employed by current DFT methods partition the electronic energy into several terms:

$$E = E^{T} + E^{V} + E^{J} + E^{XC} \qquad (1\text{-}32)$$

where E^T is the kinetic energy term (arising from the motion of the electrons), E^V includes terms describing the potential energy of the nuclear-electron attraction and of the repulsion between pairs of nuclei, E^J is the electron-electron repulsion term (it is also described as the Coulomb self-interaction of the electron density), and E^{XC} is the exchange-correlation term and includes the remaining part of the electron-electron interaction. All terms except the nuclear-nuclear repulsion are functions of the electron density ρ.

$E^{T} + E^{V} + E^{J}$ corresponds to the classical energy of the charge distribution ρ. The E^{XC} term in Equation 1-32 accounts for the remaining terms in the energy including the exchange energy arising from the antisymmetry of the quantum mechanic wavefunction and the dynamic correlation in the motions of the individual electrons.

Hohernberg and Kohn demonstrated that E^{XC} is determined entirely by the electron density (or is a functional of the electron density). In practice, E^{XC} is usually approximated as an integral involving only the spin densities and possibly their gradients:

$$E^{XC}(\rho) = \int f\left(\rho_\alpha(\vec{r}), \rho_\beta(\vec{r}), \nabla\rho_\alpha(\vec{r}), \nabla\rho_\beta(\vec{r})\right) d^3\vec{r} \quad (1\text{-}33)$$

Here ρ_α and ρ_β are referred to the α and β spin density respectively, and ρ is referred to the total electron density $(\rho_\alpha + \rho_\beta)$.

E^{XC} is usually divided into separate parts, referred to as the exchange and correlation energy and actually correspond to same-spin and mixed spin interactions, respectively:

$$E^{XC}(\rho) = E^X(\rho) + E^C(\rho) \quad (1\text{-}34)$$

All three terms are again functionals of the electron density, and functionals define the two components on the right side of Equation 1-34 are termed exchange functionals and correlation functionals respectively. Both components can be of two distinct types: local functionals depend on only the electron density ρ, while gradient-corrected functionals depend on both ρ and its gradient, $\nabla\rho$. Note that this use of the term 'local' does not coincide with the use of a similarly named term in mathematics; both local and gradient-corrected functionals are local in the mathematical sense.

The local exchange functional is virtually always defined as follows:

$$E^X_{LDA} = -\frac{3}{2}\left(\frac{3}{4\pi}\right)^{1/3} \int \rho^{4/3} d^3\vec{r} \quad (1\text{-}35)$$

Where ρ is a function of $\vec{r}$. This form was developed to reproduce the exchange energy of a uniform electron cloud. By itself, however, it has a weakness in describing molecular systems.

Becke formulated the following gradient-corrected exchange functional based on the local density approximation exchange functional in 1988:[347]

$$E^X_{B88} = E^X_{LDA} - \gamma \int \frac{\rho^{4/3} x^2}{\left(1 + 6\gamma \sinh^{-1} x\right)} d^3\vec{r} \quad (1\text{-}36)$$

Where $x = \rho^{-4/3}\left|\nabla_\rho\right|$ and γ is a parameter chosen to fit the known exchange energies of the inert gas atoms. Becke defines its value as 0.0042 Hartrees (1 Hartree $= 4\pi^2 m_e e^4 / h^2$ = 27.2 eV). As Equation 1-36 makes clear, Becke's functional is defined as a correction to the local LDA exchange functional, and it succeeds in remedying many of the LDA functional's deficiencies.

Similarly, there are local and gradient-corrected correlation functionals. For example, The following is Perdew and Wang's formulation of the local part of their 1991 correlation functional:[348]

$$E^C = \int \rho \varepsilon_C\left(r_s\left(\rho(\vec{r})\right), \zeta\right) d^3\vec{r}$$

$$r_s = \left[\frac{3}{4\pi\rho}\right]^{1/3}$$

$$\zeta = \frac{\rho_\alpha - \rho_\beta}{\rho_\alpha + \rho_\beta}$$

$$\varepsilon_C(r_s,\zeta) = \varepsilon_C(\rho,0) + a_C(r_s)\frac{f(\zeta)}{f''(0)}\left(1-\zeta^4\right) + \left[\varepsilon_C(\rho,1) - \varepsilon_C(\rho,0)\right] f(\zeta)\zeta^4$$

$$f(\zeta) = \frac{\left[(1+\zeta)^{4/3} + (1-\zeta)^{4/3} - 2\right]}{\left(2^{4/3} - 2\right)} \qquad (1\text{-}37)$$

r_s is termed the density parameter and ζ is the relative spin polarization, ζ = 0 corresponds to equal α and β densities, ζ = 1 corresponds to all α density, and ζ = -1 corresponds to all β density. Note that f (0) = 0 and f ($\pm$ 1) = 1.

The general expression for ε_C involves both r_s and ζ. Its final term performs an interpolation for mixed spin cases. The following function G is used to compute the values of $\varepsilon_C(r_s,0)$, $\varepsilon_C(r_s,1)$ and -$a_C(r_s)$:

$$G(r_s, A, \alpha_1, \beta_1, \beta_2, \beta_3, \beta_4, P) = -2A(1+\alpha_1 r_s)\ln\left(1+\frac{1}{2A(\beta_1 r_s^{1/2}+\beta_2 r_s+\beta_3 r_3^{3/2}+\beta_4 r_s^{P+1})}\right)$$

(1-38)

In this equation, all the arguments to G except r_s are parameters chosen by Perdew and Wang to reproduce accurate calculations on uniform electron clouds. The parameter sets differ for G when it is used to evaluate each of $\varepsilon_C(r_s,0)$, $\varepsilon_C(r_s,1)$ and $-a_C(r_s)$. In an analogous way to the exchange functional we examined earlier, a local correlation functional may also be improved by adding a gradient correction.

Pure DFT methods are defined by pairing an exchange functional with a correlation functional. For example, the well-known BLYP functional pairs Becke's gradient-corrected exchange functional with the gradient-corrected correlation functional of Lee, Yang and Parr.[349]

In actual practice, self-consistent Kohn-Sham DFT calculations are performed in an iterative manner that is analogous to an SCF computation. This similarity to the methodology of Hartree-Fock theory was pointed out by Kohn and Sham.[350]

Hartree-Fock theory also includes an exchange term as part of its formulation. Recently, Becke has formulated functionals that include a mixture of Hartree-Fock and DFT exchange along with DFT correlation, conceptually defining E^{XC} as:

$$E_{hybrid}^{XC} = c_{HF}E_{HF}^{X} + c_{DFT}E_{DFT}^{XC} \qquad (1\text{-}38)$$

Where the c's are constants. For example, a Becke-style three-parameter functional may be defined via the following expression:

$$E_{B3LYP}^{XC} = E_{LDA}^{X} + c_0\left(E_{HF}^{X} - E_{LDA}^{X}\right) + c_X\Delta E_{B88}^{X} + E_{VWN3}^{C} + c_C\left(E_{LYP}^{C} - E_{VWN3}^{C}\right) \qquad (1\text{-}40)$$

Here, the parameter c_0 allows any admixture of Hartree-Fock and local density approximation (LDA) local exchange to be used. In addition, Becke's gradient correction to LDA exchange is also included, scaled by the parameter c_x. Similarly, the

Vosko-Wilk-Nusair 3 correlation functional (VWN3) local correlation functional is used, and it may be optionally corrected by the Lee-Yang-Parr (LYP) correlation correction via the parameter c_C. In the Becke-style 3-parameter density (B3LYP) functional (using the Lee-Yang-Parr correlation functional), the parameters values are those specified by Becke, which he determined by fitting to the atomization energies, ionization potentials, proton affinities and first-row atomic energies in the G1 molecule set: $c_0 = 0.20$, $c_x = 0.72$ and $c_C = 0.81$. Note that Becke used the Perdew-Wang 1991 correlation functional[351] in his original work rather than VWN3[352] and LYP. The fact that the same coefficients work well with different functionals reflects the underlying physical justification for using such a mixture of Hartree-Fock and DFT exchange first pointed out by Becke.[353]

1.10 References

(1) Sommer, H.; Thomas, H. A.; Hipple, J. A. *Phys. Rev.* **1949**, *76*, 1877.

(2) Sommer, H.; Thomas, H. A. *Phys. Rev.* **1950**, *78*, 806.

(3) Sommer, H.; Thomas, H. A.; Hipple, J. A. *Phys. Rev.* **1951**, *82*, 697.

(4) Nachtrieb, R.; LaBombard, B.; Thomas, Jr. E. *Rev. Sci. Instru.* **2000**, *71*, 4107.

(5) Wobschall, D.; Graham, J. R., Jr.; Malone, D. P. *Phys. Rev.* **1963**, *131*, 1565.

(6) Wobschall, D. *Rev. Sci. Instrum.* **1965**, *36*, 466.

(7) Llewellyn, P. M. *"Ion Cyclotron Resonance Mass Spectrometer Having Means for Detecting the Energy Absorbed by Resonant Ions",* U.S.A. Patent No. 3,390,265, Issued 09 June, **1968**.

(8) Anders, L. R.; Beauchamp, J. L.; Dunbar, R. C.; Baldeschwieler, J. D. *J. Chem. Phys.* **1966**, *45*, 1062.

(9) Baldeschwieler, J. D. *Science* **1968**, *159*, 263.

(10) McIver, R. T., Jr. *Rev. Sci. Instrum.* **1970**, *41*, 555.

(11) McIver, R. T., Jr.; Hunter, R. L.; Ledford, E. B., Jr.; Locke, M. J.; Francl, T. J. *Int. J. Mass Spectrom. Ion Phys.* **1981**, *39*, 65.

(12) Comisarow, M. B.; Marshall, A. G. *Chem. Phys. Lett.* **1974**, *25*, 282.

(13) Comisarow, M. B.; Marshall, A. G. *Chem. Phys. Lett.* **1974**, *26*, 489.

(14) Comisarow, M. B.; Marshall, A. G. *Can. J. Chem.* **1974**, *52*, 1997.

(15) Allemann, M.; Kellerhals, H.; Wanczek, K. P. *Chem. Phys. Lett.* **1980**, *75*, 328.

(16) Laukien, F. *Proc. 35th Am. Soc. Mass Spectrom. Conf. on Mass Spectrom. & Allied Topies*, (American Society for Mass Spectrometry) **1987**, *Denver*, 112.

(17) Allemann, M.; Kellerhals, H.; Wanczek, K. P. *Int. J. Mass Spectrom. Ion Proc.* **1983**, *46*, 139.

(18) Hunter, R. L.; McIver, R. T., Jr. *Am. Lab.* **1977**, *9*, 13.

(19) McIver, R. T., Jr.; Ledford, E. B., Jr.; Hunter, R. L. *J. Chem. Phys.* **1980**, *72*, 2535.

(20) Lee, S.-H.; Wanczek, K.-P.; Hartmann, H. *Adv. Mass Spectrom.* **1980**, *8B*, 1645.

(21) Allemann, M.; Kellerhals, H. P.; Wanczek, K. P. *Chem. Phys. Lett.* **1981**, *84*, 547.

(22) Hunter, R. L.; Sherman, M. G.; McIver, R. T., Jr. *Int. J. Mass Spectrom. Ion Phys.* **1983**, *50*, 259.

(23) Hanson, C. D.; Castro, M. E.; Kerley, E. L.; Russell, D. H. *Anal. Chem.* **1990**, *62*, 520.

(24) Wang, M.; Marshall, A. G. *Anal. Chem.* **1989**, *61*, 1288.

(25) Sievers, H. L.; Gruetzmacher, H.-F.; Caravatti, P. *Int. J. Mass Spectrom. Ion Proc.* **1996**, *157*, 233.

(26) Caravatti, P.; Allemann, M. *Org. Mass Spectrom.* **1991**, *26*, 514.

(27) Wang, M.; Marshall, A. G. *Anal. Chem.* **1990**, *62*, 515.

(28) Kofel, P.; Allemann, M.; Kellerhals, H.; Wanczek, K. P. *Int. J. Mass Spectrom. Ion Proc.* **1985**, *65*, 97.

(29) Devienne, F. M.; Roustan, J.-C. *"The Encyclopedia of Mass Spectrometry: Ionization Methods"* Eds., Gross, M. L.; Caprioli, R. (Pergamon Press) **2001,** 153.

(30) Hillenkamp, F.; Karas, M.; Holtkamp, D.; Klusener, P. *Int. J. Mass Spectrom. Ion Proc.* **1986**, *69*, 265.

(31) Yamashita, M.; Fenn, J. B. *J. Phys. Chem.* **1984**, *88*, 4671.

(32) Kofel, P.; Allemann, M.; Kellerhals, H.; Wanczek, K. P. *Int. J. Mass Spectrom. Ion Proc.* **1989**, *87*, 237.

(33) Kofel, P.; McMahon, T. B. *Int. J. Mass Spectrom. Ion Proc.* **1990**, *98*, 1.

(34) Rosenfeld, R. N.; Jasinski, J. M.; Meyer, F. K.; Brauman, J. I. *J. Am. Chem. Soc.* **1982**, *104*, 658.

(35) Meyer, F. K.; Jasinski, J. M.; Rosenfeld, R. N.; Brauman, J. I. *J. Am. Chem. Soc.* **1982**, *104*, 663.

(36) Freiser, B. S. "*Organometallic Ion Chemistry" (Understanding Chemical Reactivity, Vol. 15) Ed.* Freiser, B. S. (Kluwer Academic) **1996**, 1.

(37) Freiser, B. S. *"Techniques for the Study of Ion Molecule Reactions*", Eds. Farrar, J. M.; Saunders, W. H., Jr. (John Wiley & Sons: New York) **1988**, 61.

(38) Shirts, R. B. *"Gaseous Ion Chemistry*" Ed. Futrell, J. H. (John Wiley & Sons: New York) **1986**, 100.

(39) Weller, R. R.; McMahon, T. J.; Freiser, B. S. *"Lasers and Mass Spectrometry*" Eds. Lubman, D. M.; Stark, H. (Oxford University Press: New York) **1989**, 249.

(40) Francl, T. J.; Fukuda, E. K.; McIver, R. T., Jr. *Int. J. Mass Spectrom. Ion Proc.* **1983**, *50*, 151.

(41) Dunbar, R. C.; Chen, J. H.; Hays, J. D. *Int. J. Mass Spectrom. Ion Phys.* **1984**, *57*, 39.

(42) Dunbar, R. C. *Int. J. Mass Spectrom. Ion Proc.* **1984**, *56*, 1.

(43) Amster, J. I.; McLafferty, F. W.; Castro, M. E.; Russell, R. B.; Cody, J. R. B.; Ghaderi, S. *Anal. Chem.* **1986**, *58*, 458.

(44) Marshall, A. G.; Guan, S. H.; Eyler, J. R. *Rapid Comm. Mass Spectrom.* **1996**, *10*, 1814.

(45) Comisarow, M. B.; Marshall, A. G. *J. Chem. Phys.* **1976**, *64*, 110.

(46) Shi, S. D. H.; Drader, J. J.; Hendrickson, C. L.; Marshall, A. G. *J. Am. Soc. Mass Spectrom.* **1999**, *10*, 265.

(47) Comisarow, M. B. *Adv. Mass Spectrom.* **1980**, *8*, 1698.

(48) Ledford, E. B.; Ghaderi, S.; White, R. L.; Spencer, R. B.; Kulkarni, P. S.; Wilkins, C. L.; Gross, M. L. *Anal. Chem.* **1980**, *52*, 463.

(49) Francl, T. J.; Sherman, M. G.; Hunter, R. L.; Locke, M. J.; Bowers, W. D.; McIver, R. T., Jr. *Int. J. Mass Spectrom. Ion Proc.* **1983**, *54*, 189.

(50) Ledford, J. E. B.; Rempel, D. L.; Gross, M. L. *Anal. Chem.* **1984**, *56*, 2744.

(51) Marshall, A. G. *Int. J. Mass Spectrom.* **2000**, *200*, 331.

(52) Johlman, C. L.; White, R. L.; Wilkins, C. L. *Mass Spectrom. Rev.* **1983**, *2*, 389.

(53) Lorenz, S. A.; Maziarz, E. P.; Wood, T. D. *App. Spectros.* **1999**, *53*, 18A.

(54) McLafferty, F. W.; Senko, M. W.; Little, D. P.; Wood, T. D.; O'Connor, P. B.; Speir, J. P.; Chorush, R. A.; Kelleher, N. L. *Adv. Mass Spectrom.* **1995**, *13*, 115.

(55) Hickham, W. M.; Berg, D. "*Advance in Mass Spectrometry*" (Pergamon Press: New York) **1959**, 10.

(56) Foti, S.; Montando, G. *"The Encyclopedia of Mass Spectrometry: Ionization Methods"* Eds., Gross, M. L.; Caprioli, R. (Pergamon Press: New York) **2001,** 22.

(57) Boerboom, A. J. H. *"The Encyclopedia of Mass Spectrometry: Ionization Methods"* Eds., Gross, M. L.; Caprioli, R. (Pergamon Press: New York) **2001,** 41.

(58) Ghaderi, S.; Kulkarni, P. S.; Ledford, E. B.; Wilkins, C. L.; Gross, M. L. *Anal. Chem.* **1981**, *53*, 428.

(59) Hunter, R. L.; McIver, R. T., Jr. *Anal. Chem.* **1979**, *51*, 699.

(60) Munson, M. S. B.; Field, F. H. *J. Am. Chem. Soc.* **1966**, *88*, 2621.

(61) Munson, B. *Anal. Chem.* **1971**, *43, 22.*

(62) Munson, B. *Anal. Chem.* **1977**, *49*, 772.

(63) Beckey, H. D. "*Field Ionization Mass Spectroscopy*" (Pergamon Press: Oxford) **1977,** 25.

(64) Beckey, H. D.; Hoffmann, G.; Maurer, K. H.; Winkler, H. U. *Anal. Chem.* **1970,** 42, 626.

(65) Ipezsa, I.; Knoll, H.; Wanczek, K.-P.; Linden, H. B. *Proc. 36th Am. Soc. Mass Spectrom. Conf. on Mass Spectrom. & Allied Topics (American Society for Mass Spectrometry),* **1988**, *San Francisco*, 590.

(66) Williams, D. H.; Bradley, C.; Bojesen, G.; Santikarn, S.; Taylor, L. C. E. *J. Am. Chem. Soc.* **1981**, *103*, 5700.

(67) Barber, M.; Bordoli, R. S.; Elliott, G. J.; Sedgwick, R. D.; Tyler, A. N. *Anal. Chem.* **1982**, *54*, 645.

(68) Doerr, M.; Luderwald, I.; Schulten, H.-R. *Fresenius Z Anal. Chem.* **1984**, *318*, 339.

(69) Baldwin, M. A.; Proctor, C. J.; Amster, I. J.; McLafferty, F. W. *Int. J. Mass Spectrom. Ion Proc.* **1983**, *54*, 97.

(70) Dell, A. *Adv. Carbohydr. Chem. Biochem.* **1987**, *45*, 19.

(71) Vickerman, J. C. "*ToF-SIMS: Surface Analysis by Mass Spectrometry*" Eds. Brown, A.; Reed, N. M. (Oxford University Press: New York) **1989,** 15.

(72) Pauw, D. E. *Mass Spectrom. Rev.* **1986**, *5*, 191.

(73) Winograd, N.; Garrison, B. J. "*Methods of Surface Characterisation*" Eds. Czanderna, A. W.; Hurcules, D. M. (Oxford University Press: New York) **1991**, 45.

(74) Zakett, D.; Schoen, A. E.; Cooks, R. G.; Hemberger, P. H. *J. Am. Chem. Soc.* **1981**, *103*, 1295.

(75) Dunbar, R. C.; Hutchinson, B. B. *J. Am. Chem. Soc.* **1974**, *96*, 3816.

(76) Garrison, B. J.; Srinivasan, R. *Appl. Phys. Lett.* **1984**, *44*, 849.

(77) Srinivasan, R.; Leigh, W. J. *J. Am. Chem. Soc.* **1982**, *104*, 6784.

(78) Van der Peyl, G. L.; Van der Zande, W. J.; Kistermaker, P. G. *Int. J. Mass Spectrom. Ion Proc.* **1984**, *62*, 51.

(79) Brown, R. S.; Weil, D. A.; Wilkins, C. L. *Macromolec.* **1986**, *19*, 1255.

(80) Mowry, C. D.; Johnston, M. V. *J. Phys. Chem.*, **1994**, *98*, 1904.

(81) Stöckle, R.; Setz, P.; Deckert, V.; Lippert, T.; Wokaun, A.; Zenobi, R. *Anal. Chem.* **2001**, *73*, 1399.

(82) Lindner, B.; Seydel, U. *Anal. Chem.* **1985**, *57*, 895.

(83) Karas, M.; Bahr, U.; Hillenkamp, F. *Int. J. Mass Spectrom. Ion Proc.* **1989**, *92*, 231.

(84) Karas, M.; Bahr, U.; Giessman, U. *Mass Spectrom. Rev.* **1991**, *10*, 335.

(85) Beavis, R. C. *Org. Mass Spectrom.* **1992**, *27*, 653-659.

(86) Staneke, P. O.; Nibbering, N. M. M. *Spectroscopy* **1997**, *13*, 145.

(87) Zenobi, R.; Knochenmuss, R. *Mass Spectrom. Rev.* **1999**, *17*, 337.

(88) Cramer, R.; R. F. Haglund, J.; Hillenkamp, *Proc. 45th Am. Soc. Mass Spectrom. Conf. on Mass Spectrom. & Allied Topics (American Society for Mass Spectrometry),* **1997**, *Palm Springs*, 123.

(89) Bencsura, A.; Sadeghi, M.; Vertes, A. *Proc. 44th Am. Soc. Mass Spectrom. Conf. on Mass Spectrom. & Allied Topics (American Society for Mass Spectrometry),* **1996**, *Portland*, 566.

(90) Knochenmuss, R.; Dubois, F.; Dale, M. J.; Zenoba, R. *Rapid Commun. Mass Spectrom.* **1996**, *10,* 67.

(91) Scrivener, E.; Fong, K.; Lloyd, P. M.; Malroney, D. R.; Haddleton, D. M.; Eason, M.; Derrick, P. J. *Proc. 44th Am. Soc. Mass Spectrom. Conf. on Mass*

Spectrom. & Allied Topics (American Society for Mass Spectrometry), **1996**, *Portland*, 746.

(92) van Baar, B. L. M. *FEMS Microbiol. Rev.* **2000**, *24*, 193.

(93) Roepstorff, P. *"Proteomics in Functional Genomics"*, Eds. Jollès, P.; Jörnvall, H. (Basel: Birhäuser Verlag) **2000**, 81.

(94) Wunschel, D. S.; Muddiman, D. C.; Smith, R. D. *Adv. Mass Spectrom.* **1998**, *14*, 377.

(95) Krause, J. L.; Schlunegger, U. P. *Proc. 45th Am. Soc. Mass Spectrom. Conf. on Mass Spectrom. & Allied Topics (American Society for Mass Spectrometry),* **1997**, *Palm Springs*, 732.

(96) Hettich, R. L.; Stemmler, E. A. *Rapid Commun. Mass Spectrom.* **1996**, *10*, 321.

(97) Zaluzec, E. J.; Gage, D. A.; Watson, J. T. *Protein Expression Purif.* **1995**, *6*, 109.

(98) Solouki, R.; Gillig, K. J.; Russell, D. H. *Anal. Chem.* **1994**, *66*, 1583.

(99) Solouki, T.; Russell, D. H. *Appl. Spectrosc.* **1993**, *47*, 211.

(100) Beavis, R. C.; Chait, B. R.; Creel, H. S.; Fournier, M. J.; Mason, T. L.; Tirrell, D. A. *J. Am. Chem,. Soc.* **1992**, *114*, 7584.

(101) Hillenkamp, F.; Karas, M.; Beavis, R. C.; Chait, B. T. *Anal. Chem.* **1991**, *63*, 1193A.

(102) Dole, M.; Mack, L. L.; Hines, R. L.; Mobley, R. C.; Ferguson, L. D.; Alice, M. B. *J. Chem. Phys.* **1968**, *49*, 2240.

(103) Dole, M.; Hines, R. L. *Macromol.* **1968**, *1*, 96.

(104) McEwen, C. N.; Larsen, B. S. *"Electrospray Ionization Mass Spectrometry "* Ed. Cole, R. B. (John Wiley & Sons: New York), **1997**, 177.

(105) Viswanadham, S. K.; Hercules, D. M.; Weller, R. R.; Giam, C. S. *Biomedical and Environ. Mass Spectrom.* **1987**, *14*, 43.

(106) Loo, J. A.; Williams, E. R.; Amster, I. J.; Furlong, J. J. P.; Wang, B. H.; McLafferty, F. W.; Chait, B. J.; Field, F. H. *Anal. Chem.* **1987**, *59*, 1880.

(107) Williams, E. R.; McLafferty, F. W. *J. Am. Soc. Mass Spectrom.* **1990**, *1*, 427.

(108) Alford, J. M.; Williams, P. E.; Trevor, D. J.; Smalley, R. E. *Int. J. Mass Spectrom. Ion Proc.* **1986**, *72*, 33.

(109) Smalley, R. E. *Anal. Instru.* **1988**, *17*, 1.

(110) Barshick, C. M.; Eyler, J. R. *J. Am. Soc. Mass Spectrom.* **1992**, *3*, 122.

(111) Limbach, P. A.; Marshall, A. G.; Duckworth, D. C.; Buchanan, M. V. *Proc. 41th Am. Soc. Mass Spectrom. Conf. on Mass Spectrom. & Allied Topics (American Society for Mass Spectrometry),* **1993**, *San Francisco*, 112.

(1120) Watson, C. H.; Wronka, J.; Laukien, F. H.; Barshick, C. M.; Eyler, J. R. *Anal. Chem.* **1993**, *65*, 2801.

(113) Watson, C. H.; Wronka, J.; Laukien, F. H.; Barshick, C. M.; Eyler, J. R. *Spectrochim. Acta, Part B* **1993**, *48B*, 1445.

(114) Goodner, K. L.; Milgram, K. E.; Watson, C. H.; Eyler, J. R.; Dejsupa, C.; Barshick, C. M. *J. Am. Soc. Mass Spectrom.* **1996**, *7*, 923.

(115) Macha, S. F.; McCarley, T. D.; Limbach, P. A.; Green, J. G.; Savickas, P. *Proc. 46th Am. Soc. Mass Spectrom. Conf. on Mass Spectrom. & Allied Topics (American Society for Mass Spectrometry),* **1998**, *Orlando*, 345.

(116) Takada, Y.; Sakairi, M.; Koizumi, H. *Anal. Chem.* **1995**, *34*, 1474.

(117) Liu, C.; Muddiman, D. C.; Tang, K.; Smith, R. D. *J. Mass Spectrom.* **1997**, *32*, 425.

(118) Karas, M.; Bahr, U.; Dulcks, T. *Anal. Chem.* **2000**, *366*, 669.

(119) Smith, R. D.; Wahl, J. H.; Goodlett, D. R.; Hofstadler, S. A. *Anal. Chem.* **1993**, *65*, 574A.

(120) Valaskovic, G. A.; Kelleher, N. L.; McLafferty, F. W. *Science* **1996**, *273*, 1199-1202.

(121) McIver, R. T., Jr. *"Electronic Microcopier Apparatus"* U.S.A. Patent No. 4,523,235, Issued 13 August, **1985**.

(122) Meek, J. T.; Stockton, G. W. *"Fourier Transform Ion Cyclothon Resonance Mass Spectrometer with Spatially Separated Sources and Detector"* U.S.A. Patent No. 4,686,365, Issued 11 August, **1987**.

(123) Ghaderi, S.; Vosburger, O.; Littlejohn, D.; Shohet, J. L. *"Mass Spectrometer with Remote Ion Source"*, U.S.A. Patent No. 4,739,165, Issued 19 April, **1988**.

(124) Tang, L.; Hettich, R. L.; Hurst, G. B.; Buchanan, M. V. *Rapid Commun. Mass Spectrom.* **1995**, *9*, 731.

(125) Mordehai, A.; S. E. Buttrill, J. *Proc. 44th Am. Soc. Mass Spectrom. Conf. on Mass Spectrom. & Allied Topics (American Society for Mass Spectrometry),* **1996**, *Portland*, 771.

(126) Guan, S.; Marshall, A. G. *J. Am. Soc. Mass Spectrom.* **1995**, *7*, 101.

(127) McIver, R. T., Jr.; Dunbar, R. C. *Int. J. Mass Spectrom. Ion Phys.* **1971**, *7*, 471.

(128) Uechi, G. T.; Dunbar, R. C. *J. Am. Soc. Mass Spectrom* **1992**, *3*, 734.

(129) Jeffries, J. B.; Barlow, S. E.; Dunn, G. H. *Int. J. Mass Spectrom. Ion Proc.* **1983**, *54*, 169.

(130) Ledford, E. B., Jr.; Rempel, D. L.; Gross, M. L. *Int. J. Mass Spectrom. Ion Proc.* **1983**, *55*, 143.

(131) Meek, J. T.; Millen, W. G.; Francl, T. J.; Stockton, G. W.; Thomson, M. L.; Wayne, R. S.; *Proc. 35th Am. Soc. Mass Spectrom. Conf. on Mass Spectrom. & Allied Topics (American Society for Mass Spectrometry),* **1987**, *Denver*, 411.

(132) Comisarow, M. B. *J. Chem. Phys.* **1978**, *69*, 4097.

(133) Marshall, A. G.; Roe, D. C. *J. Chem. Phys.* **1980**, *73*, 1581.

(134) McIver, J., R. *Am. Lab.*, **1980**, 12, 1830.

(135) Hearn, B. A.; Watson, C. H.; Baykut, G.; Eyler, J. R. *Int. J. Mass Spectrom. Ion Proc.* **1990**, *95*, 299.

(136) Noest, A. J.; Kort, C. W. F. *Compu. Chem.* **1982**, *7*, 81.

(137) Smalley, R. E.; Levy, D. H.; Wharton, L. *J. Chem. Phys.* **1976**, *64*, 3266.

(138) Hsu, A. T.; Hunter, W. W., Jr.; Schmalbrock, P.; Marshall, A. G. *J. Magn. Reson.* **1987**, *72*, 75.

(139) Guan, S. *J. Chem. Phys.* **1989**, *91*, 775.

(140) Guan, S.; McIver, R. T., Jr. *J. Chem. Phys.* **1990**, *92*, 5841.

(141) Guan, S. *J. Chem. Phys.* **1990**, *93*, 8442.

(142) Guan, S.; Marshall, A. G. *Anal. Chem.* **1993**, *65*, 1288.

(143) Heck, A. J. R.; De Koning, L. J.; Pinkse, F. A.; Nibbering, N. M. M. *Rapid Commun. Mass Spectrom.* **1991**, *5*, 406.

(144) Fujiwara, M.; Naito, Y. *Rapid Commun. Mass Spectrom.* **1999**, *13*, 1633.

(145) Naito, Y. *J. Mass Spectrom. Soc. Jpn.* **1999**, *47*, 297.

(146) Zhong, W.; Shukla, A. K.; Futrell, J. H.; Ridge, D. P.; Wysocki, V. H.; *Proc. 45th Am. Soc. Mass Spectrom. Conf. on Mass Spectrom. & Allied Topics (American Society for Mass Spectrometry),* **1997**, *Palm Springs*, 305.

(147) Dunbar, R. C.; McMahon, T. B. *Science* **1998**, *279*, 194.

(148) Nichols, L. S.; Sena, M.; Richardson, D.; Eyler, J. *Proc. 218th ACS National Meeting* (American Chemical Society), **1999**, *New Orleans*, 1105.

(149) Surya, P.I.; Roth, L.M.; Ranatunga, D.R.A.; Freiser, B.S. *J. Am. Chem. Soc.*, **1996**, *118*, 1118.

(150) Peiris, D. M.; Riveros, J. M.; Eyler, J. R. *Int. J. Mass Spectrom. Ion Proc.* **1996**, *159*, 169.

(151) Peiris, D. M.; Yang, Y.; Ramanathan, R.; Williams, K. R.; Watson, C. H.; Eyler, J. R. *Int. J. Mass Spectrom. Ion Proc.* **1996**, *157*, 365.

(152) Zubarev, R. A.; Kelleher, N. L.; McLafferty, F. W. *J. Am. Chem. Soc.* **1998**, *120*, 3265.

(153) Cerda, B. A.; Horn, D. M.; Breuker, K.; Carpenter, B. K.; McLafferty, F. W. *Eur. Mass Spectrom.* **1999**, *5*, 335.

(154) Kruger, N. A.; Zubarev, R. A.; Horn, D. M.; McLafferty, F. W. *Int. J. Mass Spectrom.* **1999**, *185*, 787.

(155) Kruger, N. A.; Zubarev, R. A.; Carpenter, B. K.; Kelleher, N. L.; Horn, D. M.; McLafferty, F. W. *Int. J. Mass Spectrom.* **1999**, *182*, 1.

(156) Zubarev, R. A.; Kruger, N. A.; Fridriksson, E. K.; Lewis, M. A.; Horn, D. M.; Carpenter, B. K.; McLafferty, F. W. *J. Am. Chem. Soc.* **1999**, *121*, 2857.

(157) Mirgorodskaya, E.; Roepstorff, P.; Zubarev, R. A. *Anal. Chem.* **1999**, *71*, 4431.

(158) Zubarev, R. A.; Horn, D. M.; Fridriksson, E. K.; Kelleher, N. L.; Kruger, N. A.; Lewis, M. A.; Carpenter, B. K.; McLafferty, F. W. *Anal. Chem.* **2000**, *72*, 563.

(159) Zubarev, R. A.; Fridriksson, E. K.; Horn, D. M.; Kelleher, N. L.; Kruger, N. A.; Lewis, M. A.; Carpenter, B. K.; McLafferty, F. W. *Mass Spectrom. Biol. Med.* **2000**, *22*,111.

(160) Horn, D. M.; Ge, Y.; McLafferty, F. W. *Anal. Chem.* **2000**, *72*, 4778.

(161) McLafferty, F. W.; Horn, D. M.; Breuker, K.; Ge, Y.; Lewis, M. A.; Cerda, B.; Zubarev, R. A.; Carpenter, B. K. *J. Am. Soc. Mass Spectrom.* **2001**, *12*, 245.

(162) Shi, S. D. H.; Hemling, M. E.; Carr, S. A.; Horn, D. M.; Lindh, I.; McLafferty, F. W. *Anal. Chem.* **2001**, *73*, 19.

(163) Marshall, A.G.; Wang, T.-C.L.; Ricca, T.L. *J. Am. Chem. Soc.*, **1985**, *107*, 7893.

(164) Hop, C. E. C. A.; McMahon, T. B.; Willett, G. D. *Int. J. Mass Spectrom. Ion Proc.* **1990**, *101*, 191.

(165) Gauthier, J. W.; Trautman, T. R.; Jacobson, D. B. *Anal. Chim. Acta* **1991**, *246*, 211.

(166) Huang, Y. L.; Pasa-Tolic, L.; Guan , S. H.; Marshall, A. G. *Anal. Chem.* **1994**, *66*, 4385.

(167) Senko, M. W.; Speir, J. P.; McLafferty, F. W. *Anal. Chem.* **1994**, *66*, 2801.

(168) Beauchamp, J. L.; Armstrong, J. T. *Rev. Sci. Instrum.* **1969**, *40*, 123.

(169) Huang, Y.; Hill, Y. D.; Sodupe, M.; Bauschlicher, C. W.; Freiser, B. S. *Inorg. Chem.* **1991**, *30*, 3822.

(170) Xiang, X.; Tollens, F. R.; Marshall, A. G. *Organometallics* **1995**, *14*, 542.

(171) Carroll, J. J.; Haug, K. L.; Weisshaar, J. C.; Blomberg, M. R. A.; Siegbahn, P. E. M.; Svensson, M. *J. Phys. Chem.* **1995**, *99*, 13955.

(172) Schroeder, D.; Schwarz, H. *Angew. Chem., Int. Ed. Engl.* **1995**, *34*, 1973.

(173) Berg, C.; Schindler, T.; Niedner-Schatteburg, G.; Bondybey, V. E. *J. Chem. Phys.* **1995**, *102*, 4870.

(174) Berg, C.; Beyer, M.; Schindler, T.; Niedner-Schatteburg, G.; Bondybey, V. E. *J. Chem. Phys.* **1996**, *104*, 7940.

(175) Eller, K.; Schwarz, H. *Chem. Rev.* **1991**, *91*, 1121.

(176) Gronert, S. *Chem. Rev.* **2001**, *101*, 329.

(177) Yang, S. S.; Chen, G.; Ma, S.; Cooks, R. G.; Gozzo, F.; Eberlin, M. N. *J. Mass Spectrom.* **1995**, *30*, 807.

(178) Patrick, J. S.; Yang, S. S.; Cooks, R. G. *J. Am. Chem. Soc.* **1996**, *118*, 231.

(179) Nourse, B. D.; Cooks, R. G. *Int. J. Mass Spectrom. Ion Proc.* **1991**, *106*, 249.

(180) Cooks, R. G.; Patrick, J. S.; Kotiaho, T.; McLuckey, S. A. *Mass Spectrom. Rev.* **1994**, *13*, 287.

(181) Grobert, N.; Hare, J. P.; Hsu, W. K.; Kroto, H. W.; Pidduck, A. J.; Reeves, C. L.; Terrones, H.; Terrones, M.; Trasobares, S.; Vizard, C.; Wallis, D. J.; Walton, D. R. M.; Wright, P. J.; Zhu, Y. Q. *AIP Conf. Proc.* (American Institute of Physics) **1998**, *442*, 29.

(182) Honing, R. E. *J. Chem. Phys.* **1953**, *21*, 573.

(183) Honing, R. E. *J. Chem. Phys.* **1954**, *22*, 126.

(184) Honing, R. E. *J. Chem. Phys.* **1954**, *22*, 1610.

(185) Gingerich, K. A.; Kingcade, J. E., Jr.; Stickney, M. J.; Chandrasekharaiah, M. S. *J. Less-Common Met.* **1988**, *143*, 373.

(186) Hartmann, A.; Weil, K. G. *High Temp. Sci.* **1990**, *27*, 31.

(187) Gingerich, K. A.; Blue, G. D. *J. Chem. Phys.* **1973**, *59*, 185.

(188) Choudary, U. V.; Gingerich, K. A.; Cornwell, L. R. *Metall. Trans., A* **1977**, *8A*, 1487.

(189) Pelino, M.; Haque, R.; Bencivenni, L.; Gingerich, K. A. *J. Chem. Phys.* **1988**, *88*, 6534.

(190) Pelino, M.; Gingerich, K. A.; Haque, R.; Kingcade, J. E. *J. Phys. Chem.* **1985**, *89*, 4257.

(191) Kingcade, J. E., Jr.; Cocke, D. L.; Gingerich, K. A. *High Temp. Sci.* **1983**, *16*, 89.

(192) Haque, R.; Gingerich, K. A. *J. Chem. Phys.* **1981**, *74*, 6407.

(193) Gingerich, K. A.; Pelino, M.; Haque, R. *High Temp. Sci.* **1981**, *14*, 137.

(194) Gingerich, K. A.; Choudary, U. V.; Krishnan, K.; Hilpert, K. *J. Chem. Phys.* **1985**, *83*, 1237.

(195) Gingerich, K. A.; Pupp, C.; Campbell, B. E. *High Temp. Sci.* **1972**, *4*, 236.

(196) Pelino, M.; Gingerich, K. A. *J. Phys. Chem.* **1989**, *93*, 1581.

(197) Cocke, D. L.; Gingerich, K. A. *J. Chem. Phys.* **1972**, *57*, 3654.

(198) Echt, O.; Sattler, K.; Recknagel, E. *Phys. Rev. Lett.* **1981**, *47*, 1121.

(199) Harris, I. A.; Kidwell, R. S.; Northby, J. A. *Phys. Rev. Lett.* **1984**, *53*, 2390.

(200) Kreisle, D.; Echt, O.; Knapp, M.; Recknagel, E. *Phys. Rev. A: Gen. Phys.* **1986**, *33*, 768.

(201) Harris, I. A.; Norman, K. A.; Mulkern, R. V.; Northby, J. A. *Chem. Phys. Lett.* **1986**, *130*, 316.

(202) Kappes, M. M.; Radi, P.; Schaer, M.; Yeretzian, C.; Schumacher, E. *Z. Phys. D: At., Mol. Clusters* **1986**, *3*, 115.

(203) Knight, W. D.; De Heer, W. A.; Clemenger, K.; Saunders, W. A. *Solid State Commun.* **1985**, *53*, 445.

(204) Kappes, M. M. "*Laser ablation: Principles and Applications*" Ed. Miller, J. C. (Springer-Verlag: New York) **1994**,185.

(205) Levinovitz, A. W.; Ringertz, N. *"The Nobel Prize: The First 100 Years",* (Imperial College Press and World Scientific Publishing Co. Pte. Ltd.) **2001**, 120.

(206) Knight, A. E. W. *Chem. Aust.* **1991**, 11, 328.

(207) Jellinek, J.; Krissinel, E. B. "*Theory of Atomic and Molecular Clusters with a Glimpse at Experiments*" Ed. Jellinek, J. (Springer-Verlag, Heidelberg) **1999**, 277.

(208) Noble, C. A.; Prather, K. A. *Mass Spec. Rev.* **2000** *19*, 248.

(209) Chen, R.; Cheng, X.; Mitchell, D. W.; Hofstadler, S. A.; Wu, Q.; Rockwood, A. L.; Sherman, M. G.; Smith, R. D. *Anal. Chem.* **1995**, *67*, 1159.

(210) Berman, H. M.; Westbrook, J.; Feng, Z.; Gilliland, G.; Bhat, T. N.; Weissig, H.; Shindyalov, I. N.; Bourne, P. E. *Nucleic Acids Res.* **2000**, *28*, 235.

(211) Miranker, A.; Robinson, C. V.; Radford, S. E.; Aplin, R. T.; Dobson, C. M. *Science* **1993**, *262*, 896.

(212) Farmer, T. B.; Caprioli, R. M. *NATO ASI Ser., Ser. C* **1996**, *475*, 61.

(213) Akashi, S.; Naito, Y.; Takio, K. *Anal. Chem.* **1999**, *71*, 4974.

(214) Akashi, S.; Naito, Y.; Takio, K. *Anal. Chem.* **2000**, *72*, 259.

(215) Katta, V.; Chait, B. T. *Rapid Commun. Mass Spectrom.* **1991**, *5*, 214.

(216) Cox, D. M.; Reichman, K. C.; Kaldor, A. *J. Chem. Phys.* **1988**, *88*, 1588.

(217) Kroto, H. W. *Nature* **1987**, *329*, 529.

(218) Kroto, H. W.; Heath, J. R.; O'Brien, S. C.; Curl, R. F.; Smalley, R. E. *Nature* **1985**, *318*, 162.

(219) Klein, D. J.; Schmalz, T. G.; Hite, G. E.; Seitz, W. A. *J. Am. Chem. Soc.* **1986**, *108*, 1301.

(220) Curl, R. F.; Smalley, R. E. *Science* **1988**, *242*, 1017.

(221) Hare, J. P.; Kroto, H. W. *Symp. Int. Astron. Union* **1992**, *150*, 47.

(222) Kroto, H. *Science* **1988**, *242*, 1139.

(223) Kroto, H. W.; Prassides, K.; Endo, M.; Jura, M. "*Fullerenes: Status and Perspectives*", Eds. Taliani, C.; Ruani, G.; Zamboni, R. (World Scientific) **1992,** 12.

(224) Rohlfing, E. A.; Cox, D. M.; Kaldor, A. *J. Chem. Phys.* **1984**, *81*, 3322.

(225) Maruyama, S.; Lee, M. Y.; Haufler, R. E.; Chai, Y.; Smalley, R. E. *Z. Phys. D: At., Mol. Clusters* **1991**, *19*, 409.

(226) Curl, R. F.; Smalley, R. E. *Sci. Amer.* **1991**, *1*, 32.

(227) Haufler, R. E.; Chai, Y.; Chibante, L. P. F.; Conceico, J.; Jin, C.; Wang, L. S.; Maruyama, S.; Smalley, R. E. *Mater. Chem. Res. Soc. Proc.*, **1991,** *3*, 70.

(228) Stanton, R. E. *J. Phys. Chem.* **1992**, *96*, 111.

(229) Negri, F.; Orlandi, G.; Zerbetto, F. *Chem. Phys. Lett.* **1992**, *190*, 174.

(230) Matsuzawa, N.; Dixon, D. A. *J. Phys. chem.* **1992**, *96*, 6872.

(231) Yoshida, M.; Osawa, E. *Fuller. Sci. Tech.* **1993**, *1*, 55.

(232) Hrusak, J.; Schwarz, H. *Chem. Phys. Lett.* **1993**, *205*, 187.

(233) Ciufolini, M. A. *"Buckminster Fullerenes"*, Eds. Ciufolini, M. A.; Billups, W. E. (John Wiley & Sons: New York), **1993**, 1.

(234) Gotschy, B.; Klos, H.; Schütz, W.; Denninger, G.; Hirsch, A. ; Winter, H. *"Electronic Properties of Fullerenes"*, Springer Series in Solid State Science **1993,** *117,* 363.

(235) Bakowies, D.; Walter, T. *J. Am. Chem. Soc.* **1991**, *113*, 3704.

(236) Bakowies, D.; Thiel, W. *Chem. Phys. Lett.* **1992**, *192*, 236.

(237) Bakowies, D.; Buhl, M.; Thiel, W. *Chem. Phys. Letters* **1995**, *247*, 491.

(238) Scuseria, G. E. *Chem. Phys. Lett.* **1991**, *176*, 423.

(239) Scuseria, G. E.; Murray, R. L. *Science* **1994**, *263*, 791.

(240) Scuseria, G. E. *Science* **1996**, *271*, 942.

(241) Shvartsburg, A. A.; Hudgins, R. R.; Dugourd, P.; Jarrold, M. F. *J. Phys. Chem. A* **1997**, *101*, 1684.

(242) Yoshida, Z.; Osawa, E. *Aromaticity Kagakudojin* **1971**, 3, 174.

(243) Krätschmer, W.; Lamb, L. D.; Fostiropoulos, K.; Huffman, D. R. *Nature* **1990**, *347*, 354.

(244) Ajie, H.; Alvarez, M. M.; Anz, S. J.; Beck, R. D.; Diederich, F.; Fostiropoulos, K.; Huffman, D. R.; Kraetschmer, W.; Rubin, Y.; et al. *J. Phys. Chem.* **1990**, *94*, 8630.

(245) Shinohara, H.; Sato, H.; Saito, Y.; Izuoka, A.; Sugawara, T.; Ito, H.; Sakurai, T.; Matsuo, T. *Rapid Commun. Mass Spectrom.* **1992**, *6*, 413.

(246) Wurz, P.; Lykke, K. R.; Pellin, M. J.; Gruen, D. M.; Parker, D. H. *Vacuum* **1992**, *43*, 381.

(247) Parker, D. H.; Wurz, P.; Chatterjee, K.; Lykke, K. R.; Hunt, J. E.; Pellin, M. J.; Hemminger, J. C.; Gruen, D. M.; Stock, L. M. *J. Am. Chem. Soc.* **1991**, *113*, 7499.

(248) Meijer, G.; Bethune, D.S. *J. Chem. Phys.* **1990**, *93*, 7800.

(249) Johnson, R. D.; Yannoni, C. S.; Salem, J.; Meijer, G.; Bethune, D. S. *Phys.* **1991**, *41*, 20.

(250) Johnson, R. D.; Meijer, G.; Salem, J. R.; Bethune, D. S. *J. Am. Chem. Soc.*, **1992**, *114*, 3320.

(251) Kikuchi, K.; Nakahara, N.; Wakabayashi, T.; Suzuki, S.; Shiromaru, H.; Miyake, Y.; Saito, K.; Ikemoto, I.; Kainosho, M.; Achiba, Y. *Nature* **1992**, *357*, 142.

(252) Katayama, N.; Miyatake, Y.; Ozaki, Y.; Kikuchi, K.; Achiba, Y.; Ikemoto, I.; Iriyama, K. *Fullerene Sci. Technol.* **1993**, *1*, 329.

(253) Harada, Y.; Ohyama, T.; Otsuka, E.; Tashiro, K.; Kobayashi, M.; Ito, H.; Matsuo, T.; Saito, Y.; Shinohara, H. *J. Phys. Soc. Jpn.* **1993**, *62*, 1427.

(254) Heath, J. R.; Curl, R. F.; Smalley, R. E. *J. Chem. Phys.* **1987**, *87*, 4236.

(255) Hare, J. P.; Kroto, H. W.; Taylor, R. *Chem. Phys. Lett.* **1991**, *177*, 394.

(256) Achiba, Y.; Nakagawa, T.; Matsui, Y.; Suzuki, S.; Shiromaru, H.; Yamauchi, K.; Nishiyama, K.; Kainosho, M.; Hoshi, H. *Chem. Lett.* **1991**, 23, 1233.

(257) Liu, S.; Lu, Y.; Kappes, M. M.; Ibers, J. A. *Science* **1991**, *254*, 408.

(258) Kawada, H.; Fujii, Y.; Nakao, H.; Murakami, Y.; Watanuki, T.; Suematsu, H.; Kikuchi, K.; Achiba, Y.; Ikemoto, I. *Phys. Rev. B* **1995**, *31*, 8723.

(259) Geckeler, K. E.; Samal, S. *Polym. Int.* **1999**, *48*, 743.

(260) Diederich, F.; Gomez-Lopez, M. *Chem. Soc. Rev.* **1999**, *28*, 263.

(261) Hirsch, A. *Synthesis* **1995**, 895.

(262) Khairallah, G.; Peel, J. B. *Chem. Phys. Lett.* **1997**, *268*, 218.

(263) Okamura, H.; Murata, Y.; Mineda, M.; Komatsu, K.; Miyamoto, T.; Wan, T. S. *J. Org. Chem.* **1996**, *61*, 8500.

(264) Bergosh, R. G.; Meier, M. S.; Cooke, J. A. L.; Spielmann, H. P.; Weedon, B. R. *J. Org. Chem.* **1997**, *62*, 7667.

(265) Nakashima, S.; Norimoto, M.; Harima, H.; Hamanaka, Y.; Grigoryan, L.S. Tokumoto, M. *Chem. Phys. Lett.* **1997**, *268*, 359

(266) Touhara, H.; Okino, F. *Adv. Inorg. Fluorides* **2000**, 555.

(267) Boltalina, O. V. *J. Fluorine Chem.* **2000**, *101*, 273.

(268) Amato, I. *Science* **1991**, *254*, 30.

(269) Geckeler, K.E. "*Telechelic Polymers: Synthesis and Applications*", Ed. Goethals, E. (CRC Press, Boca Raton) **1989**, 229.

(270) Khan, S. I.; Oliver, A. M.; Paddon-Row, M. N.; Rubin, Y. *J. Am. Chem. Soc.* **1993**, *115*, 4919.

(271) Heath, J. R.; O'Brien, S. C.; Zhang, Q.; Liu, Y.; Curl, R. F.; Tittel, F. K.; Smalley, R. E. *J. Am. Chem. Soc.* **1985**, *107*, 7779.

(272) Chai, Y.; Guo, T.; Jin, C.; Haufler, R. E.; Chibante, L. P. F.; Fure, J.; Wang, L.; Alford, J. M.; Smalley, R. E. *J. Phys. Chem.* **1991**, *95*, 7564.

(273) Stevenson, S.; Burbank, P.; Harich, K.; Sun, Z.; Dorn, H. C.; van Loosdrecht, P. H. M.; deVries, M. S.; Salem, J. R.; Kiang, C.-H.; Johnson, R. D.; Bethune, D. S. *J. Phys. Chem. A* **1998**, *102*, 2833.

(274) Weiss, F. D.; Elkind, J. L.; O'Brien, S. C.; Curl, R. F.; Smalley, R. E. *J. Am. Chem. Soc.* **1988**, *110*, 4464.

(275) Beyers, R.; Kiang, C.-H.; Johnson, R. D.; Salem, J. R.; Vries, M. S. d.; Yannoni, C. S.; Bethune, D. S.; Dorn, H. C.; Burbank, P.; Harich, K.; Stevenson, S. *Nature* **1994**, *370*, 196.

(276) Hebard, A. F.; Rosseinsky, M. J.; Haddon, R. C.; Murphy, D. W.; Glarum, S. H.; Palstra, T. T. M.; Ramirez, A. P.; Kortan, A. R. *Nature* **1991**, *350*, 600.

(277) Bethune, D. S.; Johnson, R. D.; Salem, J. R.; Vries, M. S. d.; Yannoni, C. S. *Nature* **1993**, *366*, 123.

(278) Moro, L.; Ruoff, R. S.; Becker, C. H.; Lorents, D. C.; Malhotra, R. *J. Phys. Chem.* **1993**, *97*, 6801.

(279) Gillan, E. G.; Yeretzian, C.; Min, K. S.; Alvarez, M. M.; Whetton, R. L.; Kaner, R. B. *J. Phys. Chem.* **1992**, *96*, 6869.

(280) Weaver, J. H.; Chai, Y.; Kroll, G. H.; Jin, C.; Ohno, T. R.; Haufler, R. E.; Guo, T.; Alford, J. M.; Conceicao, J.; Chibante, L. P. F.; Jain, A.; Palmer, G.; Smalley, R. E. *Chem. Phys. Lett.* **1992**, *190*, 460.

(281) Ding, J.; Yang, S. *Angew. Chem. Int. Ed. Engl.* **1996**, *35*, 2234.

(282) Luberek, J.; Wendin, G. *Chem Phys Lett.* **1996**, *248*, 147.

(283) Rubsam, M.; Pluschau, M.; Schweitzer, P.; Dinse, K. P.; Fuchs, D.; Rietschel, H.; Michel, R. H.; Benz, M.; Kappes, M. M. *Chem. Phys. Lett.* **1995**, *240*, 615.

(284) Ding, J.; Lin, N.; Weng, L.; Cue, N.; Yang, S. *Chem. Phys. Lett.* **1996**, *261*, 92.

(285) McElvany, S. W. *J. Phys. Chem.* **1992**, *96*, 4935.

(286) O'Keefe, A. O.; Ross, M. M.; Baronavski, A. P. *Chem. Phys. Lett.* **1986**, *130*, 17.

(287) Rose, H. R.; Smith, D. R.; Vassallo, A. M. *Energy Fuels* **1993**, *7*, 319.

(288) Rose, H. R.; Dance, I. G.; Fisher, K. J.; Smith, D. R.; Willett, G. D.; Wilson, M. A. *Org. Mass Spectrom.* **1994**, *29*, 470.

(289) Rose, H. R.; Dance, I. G.; Fisher, K. J.; Smith, D. R.; Willett, G. D.; Wilson, M. A. *J. Chem. Soc., Chem. Commun.* **1993**, 941.

(290) Rose, H. R.; Smith, D. R.; Fisher, K. J.; Dance, I. G.; Willett, G. D.; Wilson, M. A. *Org. Mass Spectrom.* **1993**, *28*, 825.

(291) Greenwood, P. F.; Strachan, M. G.; El-Nakat, H. J.; Willett, G. D.; Wilson, M. A.; Attalla, M. I. *Fuel* **1990**, *69*, 257.

(292) Greenwood, P. F.; Strachan, M. G.; Willett, G. D.; Wilson, M. A. *Org. Mass Spectrom.* **1990**, *25*, 353.

(293) Greenwood, P. F.; Dance, I. G.; Fisher, K. J.; Willett, G. D.; Pang, L. S. K.; Wilson, M. A. *Org. Mass Spectrom.* **1991**, *26*, 920.

(294) Dance, I. G.; Fisher, K. J.; Willett, G. D.; Wilson, M. A. *J. Phys. Chem.* **1991**, *95*, 8425.

(295) Wilson, M. A.; Pang, L. S. K.; Quezada, R. A.; Fisher, K. J.; Dance, I. G.; Willett, G. D. *Carbon* **1993**, *31*, 393.

(296) Mackey, D. W. J.; Burch, W. M.; Dance, I. G.; Fisher, K. J.; Willett, G. D. *Nucl. Med. Commun.* **1994**, *15*, 430.

(297) Pang, L. S. K.; Prochazka, L.; Quezada, R.; Wilson, M. A.; Pallasser, R.; Fisher, K. J.; FitzGerald, J. D.; Taylor, G. H.; Willett, G. D.; Dance, I. G. *Energy and Fuels* **1995**, *9*, 38.

(298) Hopwood, F. G.; Fisher, K. J.; Greenhill, P.; Willett, G. D.; Zhang, R. *J. Phys. Chem. B* **1997**, *101*, 10704.

(299) Hopwood, F. G.; Dance, I. G.; Fisher, K. J.; Willet, G. D.; Wilson, M. A.; Pang, L. S. K.; Hanna, J. V. *Org. Mass Spectrom.* **1992**, *27*, 1006.

(300) Guo, T.; Nikolaev, P.; Thess, A.; Colbert, D. T.; Smalley, R. E. *Chem. Phys. Lett.* **1995**, 240, 49.

(301) Iijima, S.; Wakabayashi, T.; Achiba, Y. *J. Phys. Chem.* **1996**, *100*, 5839.

(302) Kikuchi, K.; Suzuki, S.; Nakao, Y.; Nakahara, N.; Wakabayashi, T.; Shiromaru, H.; Saito, K.; Ikemoto, I.; Achiba, Y. *Chem. Phys. Lett.* **1993**, *216*, 67.

(303) Kikuchi, K.; Nakao, Y.; Achiba, Y.; Nomura, M. "*Fullerenes - Recent Advances in the Chemistry and Physics of Fullerenes and Related Materials*", Ed. Ruoff, R. S. (Electrochemical Society) **1994**, *1*,1300.

(304) Kikuchi, K.; Nakao, Y.; Suzuki, S.; Achiba, Y.; Suzuki, T.; Maruyama, Y. *J. Am. Chem. Soc.* **1994**, *116*, 9367.

(305) Michel, R. H.; Fuchs, D.; Beck, R. D.; Kappes, M. M. *Proc. 38th Robert A. Welch Found. Conf. Chem. Res.* **1995,** 38.

(306) Sun, D.; Liu, Z.; Guo, X.; Xu, W.; Liu, S. *J. Phys. Chem.* **1997**, *101*, 3927-3930.

(307) Anderson, P. E.; Anderson, T. T.; Dyer, P. L.; Dykes, J. W.; Irons, S. H.; Smith, C. A.; Kylin, R. D.; Klavins, P.; Liu, J. Z.; Shelton, R. N. "*Fullerenes - Recent*

Advances in the Chemistry and Physics of Fullerenes and Related Materials", Ed. Ruoff, R. S. (Electrochemical Society) **1994**, *1*,180.

(308) Ross, M. M.; Nelson, H. H.; Callahan, J. H.; McElvany, S. W. *J. Phys. Chem.* **1992**, *96*, 5231.

(309) Mittelbach, A.; Honle, W.; Schnering, H. G. v.; Carlsen, J.; Janiak, R.; Quast, H. *Angew. Chem. Int. Ed. Engl.* **1992**, *31*, 1640.

(310) Moschel, C.; Jansen, M. *Chem. Ber./Recueil* **1997**, *130*, 1761.

(311) Wei, S.; Guo, B. C.; Purnell, J.; Buzza, S.; Castleman, A. W., Jr. *Science* **1992**, *256*, 818.

(312) Wei, S.; Guo, B. C.; Purnell, J.; Buzza, S.; Castleman, A. W., Jr. *J. Phys. Chem.* **1992**, *96*, 4166.

(313) Wei, S.; Guo, B. C.; Deng, H. T.; Kerns, K.; Purnell, J.; Buzza, S. A.; Castleman, A. W., Jr. *J. Am. Chem. Soc.* **1994**, *116*, 4475.

(314) Cartier, S. F.; May, B. D.; Toleno, B. J.; Purnell, J.; Wei, S.; Castleman, A. W., Jr. *Chem. Phys. Lett.* **1994**, *220*, 23.

(315) Cartier, S. F.; Chen, Z. Y.; Walder, G. J.; Sleppy, C. R.; Castleman, A. W., Jr. *Science* **1993**, *260*, 195.

(316) Cartier, S. F.; May, B. D.; Castleman, A. W., Jr. *J. Am. Chem. Soc.* **1994**, *116*, 5295.

(317) Cartier, S. F.; May, B. D.; Castleman, A. W., Jr. *J. Phys. Chem.* **1996**, *100*, 8175.

(318) Castleman, A. W., Jr.; Guo, B.; Wei, S. *Int. J. Mod. Phys. B* **1992**, *6*, 3587.

(319) Castleman, A. W., Jr.; Guo, B. C.; Wei, S.; Chen, Z. Y. *Plasma Phys. Controlled Fusion* **1992**, *34*, 2047.

(320) Guo, B. C.; Kerns, K. P.; Castleman, A. W., Jr. *Science* **1992**, *255*, 1411.

(321) Guo, B. C.; Wei, S.; Purnell, J.; Buzza, S.; Castleman, A. W., Jr. *Science* **1992**, *256*, 515.

(322) Guo, B. C.; Castleman, A. W., Jr. *Adv. Met. Semicond. Clusters* **1994**, *2*, 137.

(323) Rohmer, M.-M.; Benard, M.; Poblet, J.-M. *Chem. Rev.* **2000**, *100*, 495.

(324) Wei, S.; Guo, B. C.; Purnell, J.; Buzza, S.; Castleman, Jr., A. W. *J. Phys. Chem.* **1993**, *93*, 9559.

(325) Rohmer, M.-M.; Benard, M.; Poblet, J.-M. *Met. Clusters Chem.* **1999**, *3*, 1664.

(326) Zhang, R.; Fisher, K. J.; Smith, D. R.; Willett, G. D., *Proc. 49th Am. Soc. Mass Spectrom. Conf. on Mass Spectrom. & Allied Topics (American Society for Mass Spectrometry),* **2001**, *Chicago*, 432.

(327) Iijima, S. *Nature* **1991**, *354*, 56.

(328) Iijima, S.; Ajayan, P. M.; Ichihashi, T. *Phys. Rev. Lett.* **1992**, *69*, 3100.

(329) Tanaka, K. "*The Science and Technology of Carbon Nanotubes*" Eds., Yamabe, T.; Fukui, K. (Elsevier: New York) **2002,** 2.

(330) Iijima, S.; Ichihashi, T. *Nature* **1993**, *363*, 603.

(331) Iijima, S. *Mater. Sci. Eng., B* **1993**, *B19*, 172.

(332) Gamaly, E. G.; Ebbesen, T. W. *Phys. Rev. B: Condens. Matter* **1995**, *52*, 2083.

(333) Birkett, P. R.; Cheetham, A. J.; Eggen, B. R.; Hare, J. P.; Kroto, H. W.; Walton, D. R. M. *Chem. Phys. Lett.* **1997**, *281*, 111.

(334) Thess, A.; Lee, R.; Nikolaev, P.; Dai, H. J.; Petit, P.; Robert, J.; Xu, C. H.; Lee, Y. H.; Kim, S. G.; Rinzler, A. G.; Colbert, D. T.; Scuseria, G. E.; Tomanak, D.; Fischer, J. E.; Smalley, R. E. *Science* **1996**, *273*, 483.

(335) Seraphin, S.; Zhou, D. *J. Electrochem. Soc.* **1995**, *142*, 290.

(336) Kazaoui, S.; Minami, N.; Matsuda, N.; Kataura, H.; Achiba, Y. *Appl. Phys. Lett.* **2001**, *78*, 3433.

(337) Fujiwara, A.; Ishii, K.; Suematsu, H.; Kataura, H.; Maniwa, Y.; Suzuki, S.; Achiba, Y. *Chem. Phys. Lett.* **2001**, *336*, 205.

(338) Brooks, M. S. S.; Johansson, B.; Eriksson, O.; Skriver, H. L. *Physica B+C* **1986**, *144*, 1.

(339) Christiansen, P. A.; Ermler, W. C.; Pitzer, K. S. *Annu. Rev. Phys. Chem.* **1985**, *36*, 407.

(340) Delgado-Barrio, G.; Fernandez-Rico, J.; Varade, A. *Theor. Chem.* **1988**, *43*, 159.

(341) Kahn, L. R.; Hay, P. J.; Cowan, R. D. *J. Chem. Phys.* **1978**, *68*, 2386.

(342) Basch, H.; Topiol, S. *J. Chem. Phys.* **1979**, *71*, 802.

(343) Slater, J. C. *Phys. Rev.* **1953**, *91*, 528.

(344) Slater, J. C.; Koster, G. F. *Phys. Rev.* **1954**, *94*, 1498.

(345) Slater, J. C. *Phys. Rev.* **1955**, *98*, 1039.

(346) Hohenberg, P. C.; Kohn, W. *Phys. Rev. B* **1964**, *136*, 864.

(347) Becke, A. D. *Phys. Rev. A*, **1988**, *38*, 3098.

(348) Perdew, J. P.; Chevary, J. A.; Vosko, S. H.; Jackson, K. A.; Pederson, M. R.; Singh, D. J.; Fiolhais, C. *Phys. Rev. B: Condens. Matter* **1992**, *46*, 6671.

(349) Lee, C.; Yang, W.; Parr, R. G. *Phys. Rev. B: Condens. Matter* **1988**, *37*, 785.

(350) Kohn, W.; Sham, L. J. *Phys. Rev.* **1965**, *140*, A1133.

(351) Perdew, J. P.; Yang, W. *Phys. Rev. B* **1991**, *45*, 13244.

(352) Vosko, S. H.; Wilk, L.; Nusair, M. *Can. J. Phys.* **1980**, *58*, 1200.

(353) Becke, A. D. *J. Chem. Phys.* **1993**, *98*, 5648.

Chapter Two

Experimental and Instrumentation

2.1 Introduction

Several instruments including two different models of Fourier transform ion cyclotron resonance mass spectrometers (Bruker CMS-47X and BioAPEX II) have been used in this study. Both FTICR mass spectrometers were used with various ionization methods in order to produce gas-phase ionic species from different form of samples. For instance, the direct laser ablation ionization method was used to generate gas-phase metallofullerene ions from carbonaceous materials containing metal compounds. The electrospray ionization method was chosen to produce charged species from solutions containing fullerene derivatives. The characterization of KCT-pitch residues was carried out by the graphite surface-assisted laser desorption ionization (GSALDI) method. In this chapter, the discussion is focused on the main features of the two FTICR mass spectrometers.

Other instruments including a laser furnace fullerene/metallofullerene generator were constructed for a metallofullerene production experiment, and an apparatus was built for the pyrolysis of KCT-pitch, the material that was used as the carbon precursor for metallofullerenes. The characterization of KCT-pitch pyrolysis residues and the metallofullerenes soot were carried out on a home-built reflectron TOF mass spectrometer. Details of these instruments will be given in the later chapters wherever they become relevant.

The quantum chemical calculations using density functional theory have been employed for the study of small metal-carbon clusters and their gas-phase ion-molecule

reaction products. The method used for the calculations will be described in Chapter Four.

2.2 The Bruker CMS-47X Fourier Transform ICR Mass Spectrometer

The laser ablation experiments described in this thesis were first performed on a Bruker CMS-47X FTICR mass spectrometer coupled with a Spectra-Physics DCR 11 Nd-YAG laser. This FTICR mass spectrometer consists of several components including an unshielded 4.7 T superconducting magnet, a vacuum system which incorporates an ICR cell, and an Aspect 3000 Computer. Figure 2-01 is a schematic diagram of this instrument. Figure 2-02 shows the actual setup of the instrument in the laboratory.

2.2.1 The 4.7 T Superconducting Magnet

The superconducting magnet is an essential component of the FTICR mass spectrometer and the uniform magnetic field combined with a static electric field confines the ion cyclotron motion in ICR cell. Theoretical studies have shown that the mass resolution, signal to noise ratio and the collision frequency between ions and neutral species are proportional to the magnetic field strength.[1] It is therefore advantageous for FTICR mass spectrometer to operate at the highest possible magnetic field strength. To date, high strength superconducting magnets up to 11.5 T have become commercially available for FTICR mass spectrometers.

Detailed descriptions and the operational principles for superconducting magnet can be found elsewhere.[2] In particular, the superconducting magnet in the CMS-47X FTICR mass spectrometer consists of a coil, which is wound from NbTi superconducting wire with a single filament and/or multi filaments in a protective matrix of copper. The superconducting magnet is operated at a constant temperature of 4.2 K, maintained by immersing the magnet in a cryostat of liquid helium.

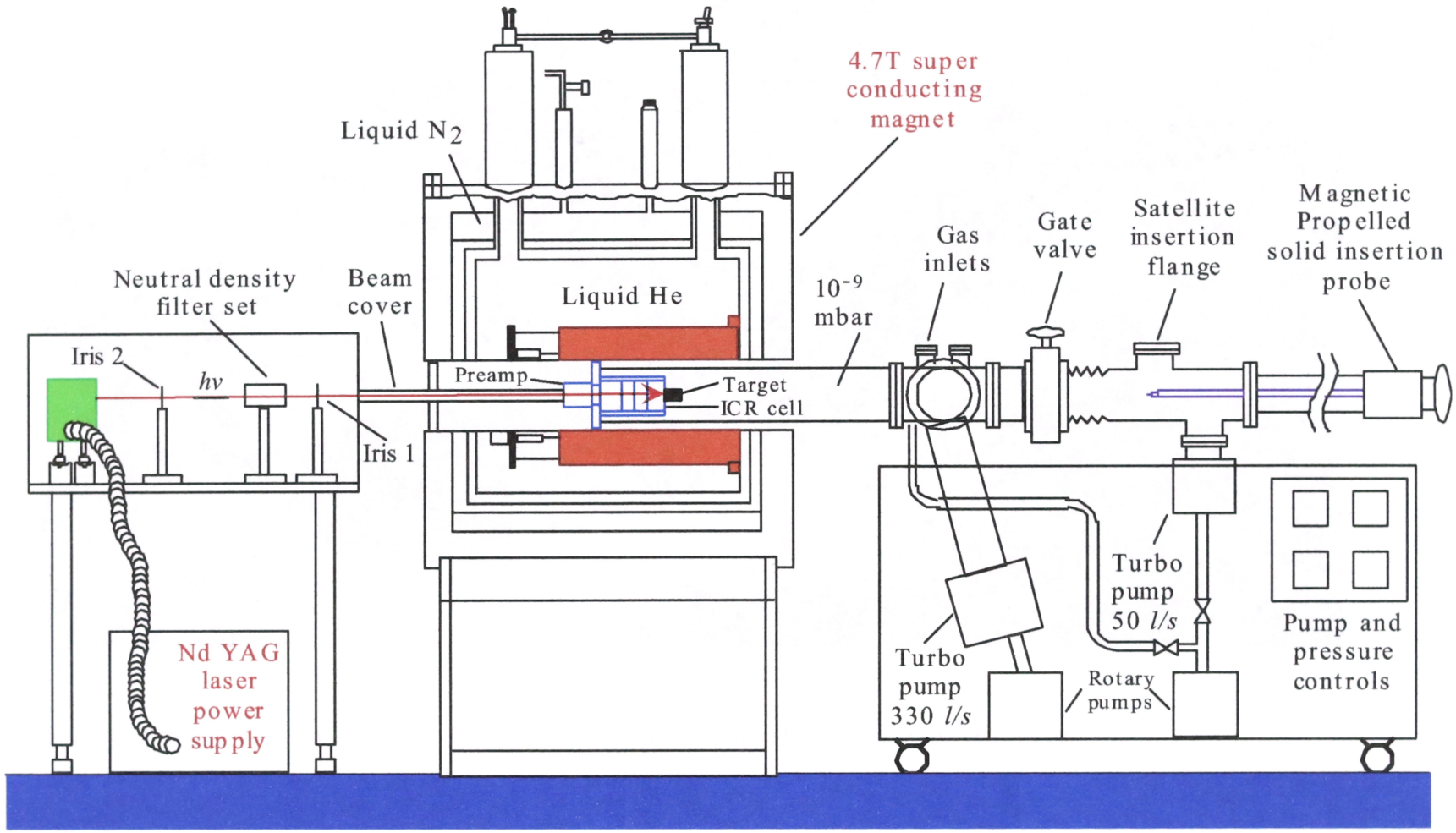

Figure 2-01 *Schematic of Bruker CMS-47 FTICR Mass Spectrometer with Spectra-Physics DCR-11 Nd-YAG laser*

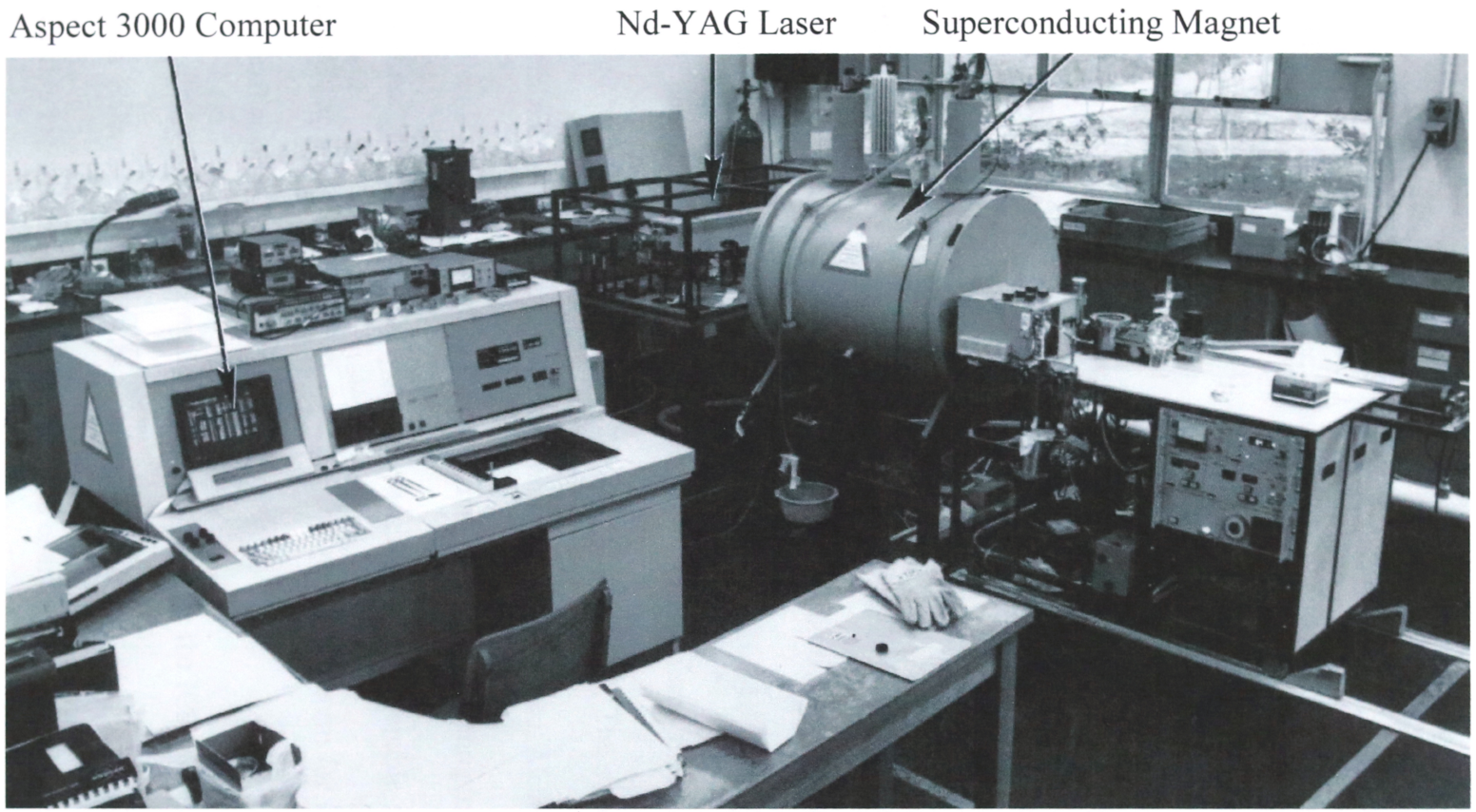

Figure 2-02 Laboratory setup of the Bruker CMS-47X laser ablation FTICR mass spectrometer.

The vessel containing liquid helium is surrounded by a liquid nitrogen cryostat and shield. Both the helium and nitrogen vessels are enclosed and insulated by separate vacuum cases.

The superconducting magnet has a 150 mm bore. During the operation of the FTICR mass spectrometer, the UHV chamber sits inside the bore of the superconducting magnet with the ICR cell located at the center of the magnet.

2.2.2 The Vacuum System

The operation of CMS-47X FTICR mass spectrometer requires high vacuum for ion detection. The ion trapping efficiency and mass resolution are functions of the pressure in the ICR cell.[3] As samples are normally loaded into the ICR cell from a region at atmospheric pressure, differential pumping is necessary for the system to operate. Figure 2-03 is a schematic of the vacuum system in the CMS-47X FTICR mass spectrometer. The high vacuum (typically 10^{-9}-10^{-7} mbar) in the stainless steel UHV chamber is maintained by a Balzer 330 Ls^{-1} turbo molecular pump (TPU-330) backed by a three-phase Alcatel (2012A) rotary pump. The solid insertion probe inlet system and/or gas inlet system are pumped by a second Alcatel rotary pump and a smaller Balzers turbo molecular pump (TPU-50) at pumping speed of 50 Ls^{-1}. Modification has been made on this vacuum system to enable the use of small turbo molecular pump (TPU-50) to evacuate the gas inlet system for lower pressure than its original design.

The pressure in the vacuum chamber housing the ICR cell is monitored constantly by a Balzers UHV ionization gauge (IMG 070). For some CID and ion-molecule reaction experiments, the pressure in this chamber is also monitored by a Varian UHV multi-gauge (Cat No. 971-5007) for automated pressure readings, which is controlled by a software program.

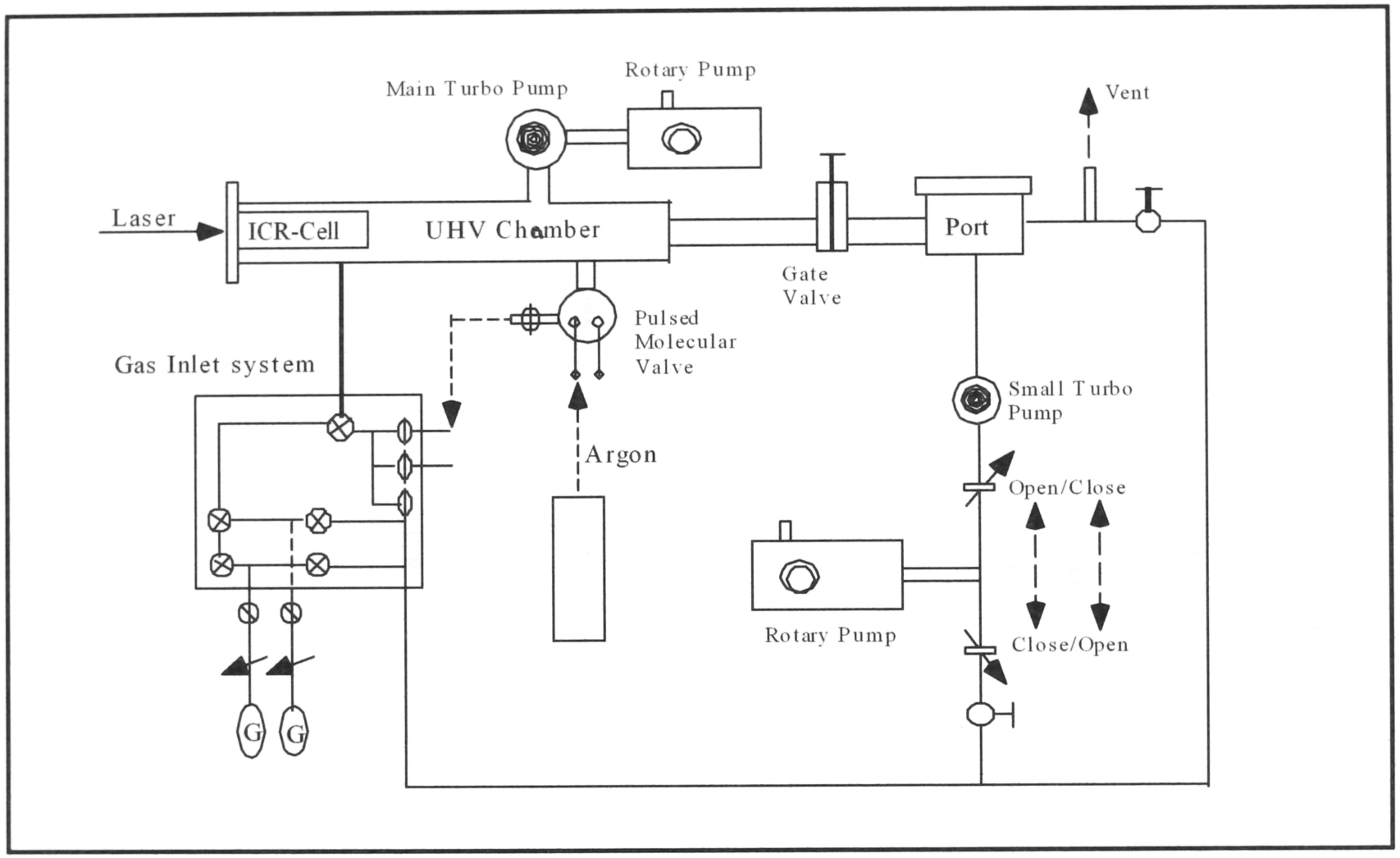

Figure 2-03 A schematic of the vacuum system of Bruker CMS-47X FT/ICR mass spectrometer.

2.2.3 The Ion Cyclotron Resonance Cell

The heart of the FTICR mass spectrometer is the ion cyclotron resonance cell. Various geometric shapes of the ICR cells have been used during the development of the FTICR mass spectrometry. The early stage of the theoretical studies about ion motion in the ICR cell including ion trajectories, excitation and the derivation of ion motion equations were accomplished in the cubic cell.[4-7] The results have been modified to adapt to other shapes of the ICR cells including the elongated rectangular cell,[8,9] cylindrical cell[10] or Penning trap.[10,11] The experimental results in terms of mass resolution and mass accuracy have shown little difference among the various shapes of ICR cells and this has also been confirmed by theoretically studies.[12] The choice of the geometry of the ICR cell is therefore mainly based on its compatibility with the superconducting magnet and design of the UHV chamber. Currently, the two major FTICR mass spectrometer suppliers, Bruker Daltonics and IonSpec, have both adopted the cylindrical cell design for their FTICR instruments.

2.2.3.1 The Modification of Spectrospin ICR Cell for the Laser Ablation Experiments

The cylindrical ICR cell in the CMS-47X FTICR mass spectrometer was originally designed only for electron ionization experiments. In order to carry out laser ablation experiments, it was necessary to modify the ICR cell to allow the focussed laser beam to be directed onto the sample target in the cell. This modification was made by former members of this research group at the UNSW and the new ICR cell was constructed at the school of chemistry workshop. Figure 2-04 shows the modified cylindrical ICR cell used in this study. The x-y-z axial coordinates allow spatial definition within the cell. The ICR cell consists of three pairs of electrically isolated titanium cell plates: the round trapping plates (d = 60mm) sits perpendicular to the z-axial, the cylindrical excitation and ion signal receiver plates (r =30 mm; l = 60 mm) are arranged parallel and surround

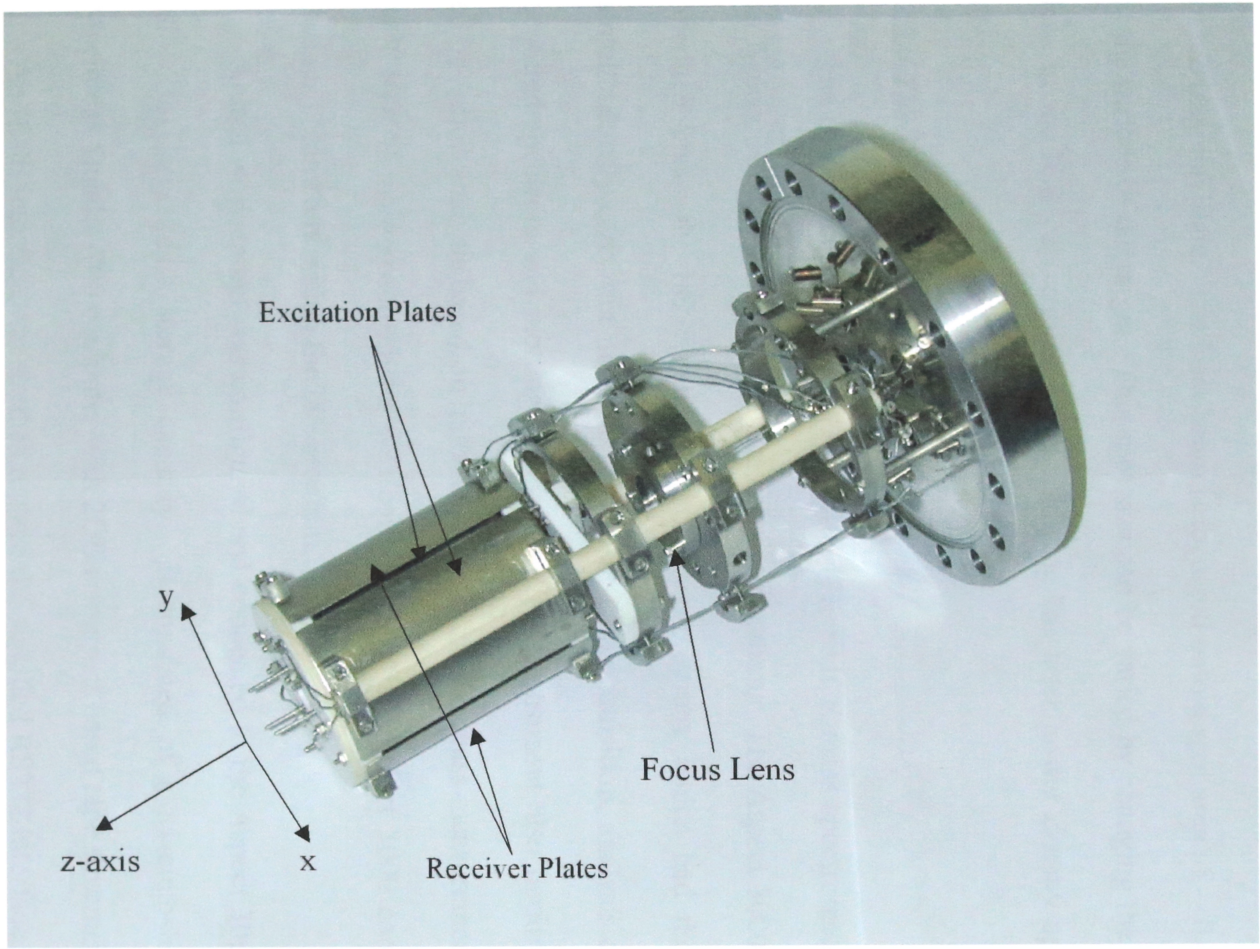

Figure 2-04 Standard ICR cell in CMS-47X FTICR mass spectrometer (modified for the internal laser ablation experiments).

the z-axial. The respective plate pairs are each opposite and form an enclosed cylindrical cell.

In order to use high laser energy for the laser ablation experiment, the laser beam is focussed by a UV grade quartz lens (CVI; f = 101.6 mm; d = 25 mm; AR/AR coated for 1064 nm) in the ICR cell. The quartz lens is placed perpendicular to the z-axial in front of the trapping plate. The laser beam is focussed onto a spot area of ~ 0.4 mm diameter at the surface of the target. This spot size can be varied by changing the position of the lens in the ICR cell, consequently changing the laser power density applied onto the target.

2.2.4 The Data Processing Unit

The data processing unit on the CMS-47X FTICR mass spectrometer consisted of an Aspect 3000 minicomputer and a data workstation. The Aspect 3000 minicomputer operated under the I89 commercial software program, which had the capability to simultaneously carry out multi-tasks such as data acquisition, analysis of a previously acquired spectrum and plotting or printing. The instrument also performed elemental composition analysis based on high-resolution accurate mass measurement. The CMS-47X FTICR mass spectrometer was controlled by the Aspect 3000 computer through various parameters within the I89 program.

A data workstation was configured and connected to the Aspect 3000 computer to allow for larger data storage capacity. It consisted of a Macintosh SI and /or a Macintosh Quadra-700 computer with 2GB retrospect based tape streamer.

An IEEE interface was used to replace the supplied RS232 interface in between the Aspect and the Macintosh system, which allowed the data to be transferred in parallel rather than in series. A software program 'ICR plotter', written by Mr. John Morgan from the electronic workshop at School of Chemistry, was used on the Macintosh

computer to allow FTICR mass spectra to be displayed and saved as either ASCII or Igor binary files. The commercial graphics package Igor® (WaveMetrics Inc.) was used to plot and modify these mass spectra so they can be incorporated with other software programs such as Microsoft Word.

2.2.5 The Nd-YAG Laser and Optics

The Nd-YAG laser used in the laser ablation experiment produces a coherent, monochromatic, high intensity light beam, which is made up of photons of identical phase, direction and amplitude. The generation of a laser light requires four basic elements: an active medium, an excitation mechanism, a feedback mechanism and an output coupler. The theoretical discussion and laser applications can be found in detail elsewhere.[13-16]

2.2.5.1 The Nd-YAG Medium and the Optical Resonator

Among all the solid-state laser media, the neodymium-doped yttrium aluminum garnet (Nd-YAG) has been well studied and best understood in terms of its spectroscopic properties. The generation of Nd-YAG laser beam involves four stages of transition as shown in the Figure 2-05. The active media is the triple-charged neodymium ion Nd^{3+}, which is excited optically by a flash lamp and emits photons that match the principle absorption bands in the red and near infrared region. The excitation for Nd^{3+} takes about 200 μs. Excited electrons then drop to the $^4F_{3/2}$ energy level, which is metastable with respect to the other excited states. Electrons occupying the $^4F_{3/2}$ state have a relatively long lifetime of about 230 μs. The electron population at $^4F_{3/2}$ state rapidly increases as the excited state electrons continue to flow down from above. The $^4I_{11/2}$ energy level, on the other hand is a less populated state. Electrons in $^4I_{11/2}$ state are quickly relaxed to the ground state and result in the population inversion between the

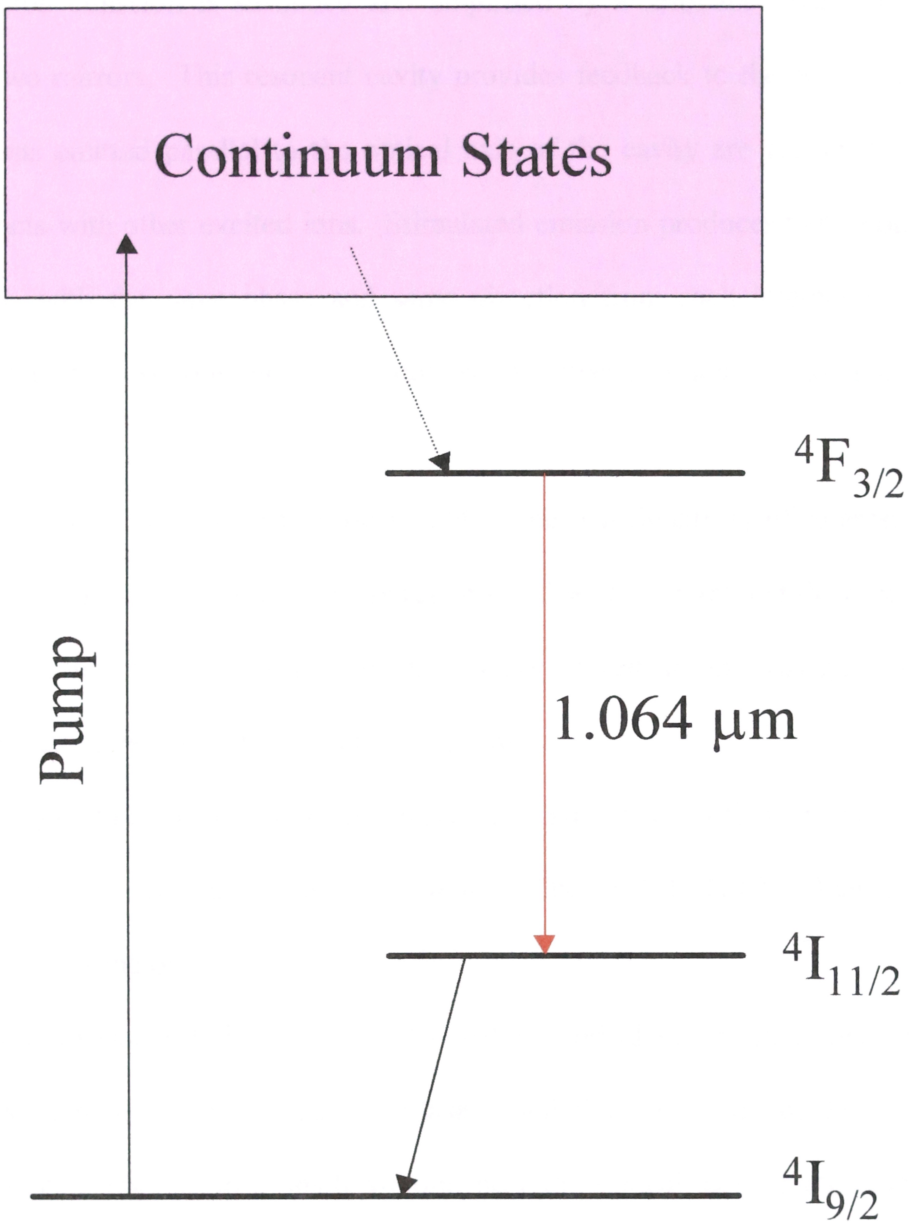

Figure 2-05 Photon Emission Scheme for the Nd-YAG Laser

$^4F_{3/2}$ state and $^4I_{11/2}$ state. The photon emitted through this transition process has wavelength of 1064 nm.

The photon emission is sustained and amplified by a resonant cavity, which is defined by two mirrors. This resonant cavity provides feedback to the active medium Nd^{3+}. Photons emitted parallel to the optical axis of the cavity are reflected, and in return, interacts with other excited ions. Stimulated emission produces two photons of equal energy, with the same phase and same direction from each interaction. This photon doubling process continues until equilibrium between excitation and emission is reached.

The two mirrors are coated to reflect light at the wavelength(s) of interest while transmitting all others. One of the mirrors reflects 100% of the light and the other – the output coupler transmits a fraction of the energy stored in the cavity, and this transmitted radiation becomes the output laser beam.

The configuration of the optical resonators can be classified in two major categories: *stable resonator* and *unstable resonator*. The DCR-11 Nd-YAG laser has an unstable type of resonator.

In a *stable resonator*, light is reflected toward the optical axis by its cavity mirrors, and contained along the primary axis of the laser irradiation. This type of the resonator can only extract energy from a small volume near the optical axis of the resonator, which limits the energy of the output. By contrast, the *unstable resonator* reflects the light away from the axis and produces a large diameter laser beam. In the unstable resonator, the energy extraction from the active media is through a larger cross-section and therefore becomes more efficient. Figure 2-06 illustrates the two types of resonators.

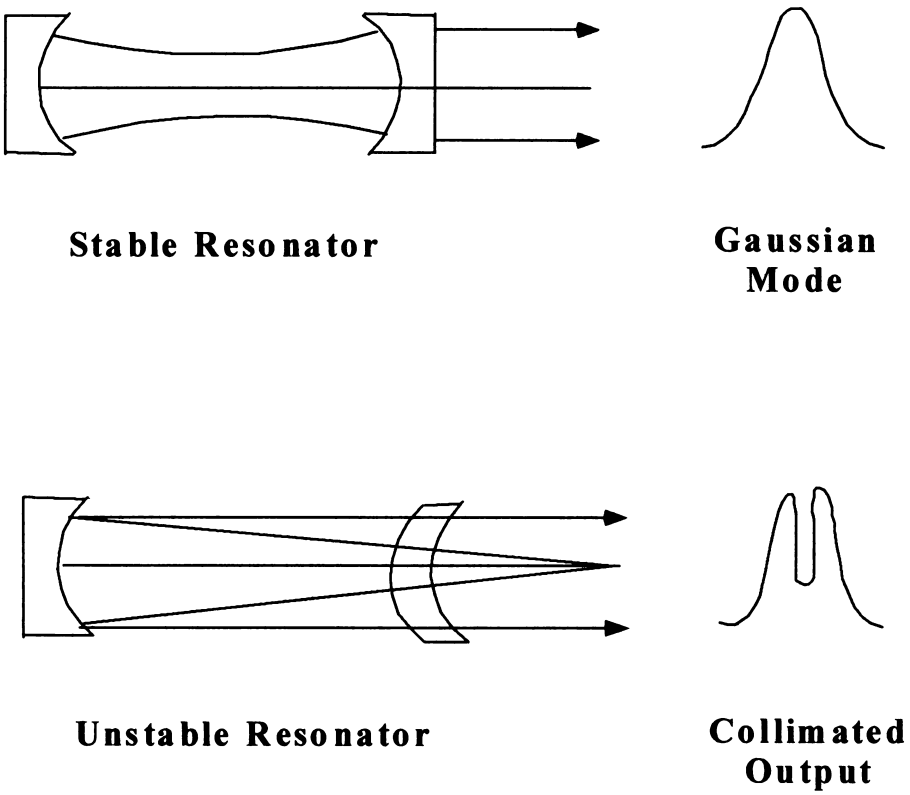

Figure 2-06 Stable and unstable resonator configurations

The output coupler in the DCR-11 laser has a small high reflector mounted on a clear substrate. This reflector lies on the optical axis of the resonator. Energy escapes the resonator by diffracting around this 'dot' reflector, which gives the 'diffraction coupled resonator' (DCR) its name.

2.2.5.2 Q-switch and Long Pulse

During the population inversion, if oscillation can be prevented and energy can be quickly released, the laser will emit a short pulse of high intensity light. This can be achieved by applying an electro-optic Q-switch, which introduces high cavity loss to prevent oscillation. As illustrated in the Figure 2-07, the Q-switch comprises a polarizer, a quarter-wave plate and Pockels cell. Applying high voltage to the crystal in the Pockels cell changes its polarization retardation characteristics, which determines whether the Q-switch is open (low loss) or closed (high loss).

If no voltage is applied (Q-switch closed), the Pockels cell does not affect the polarization of light passing through it. When light enters the polarizer it becomes vertically polarized. The quarter-wave plate then converts the light to circular polarization. As the circular polarized light returns from the high reflector, the quarter-wave plate converts it to horizontal polarization. Because the polarizer only transmits vertically polarized light, it reflects the light out of the resonator, so the cavity loss is high. With voltage applied (Q-switch open), the Pockels cell cancels the polarization retardation of the quarter-wave plate, so the light remains vertically polarized and transmitted with minimal loss. The resultant pulse of Q-switch is < 25 ns, and the peak optical power can be as high as tens of megawatts.

An alternative 'long pulse' mode of operation is built in to the DCR-11. Voltage is applied to the Pockels cell as soon as the flash lamp fires, and the Q-switch is held open for the entire lamp firing. The result is a train of pulses about 230 μs long, with a

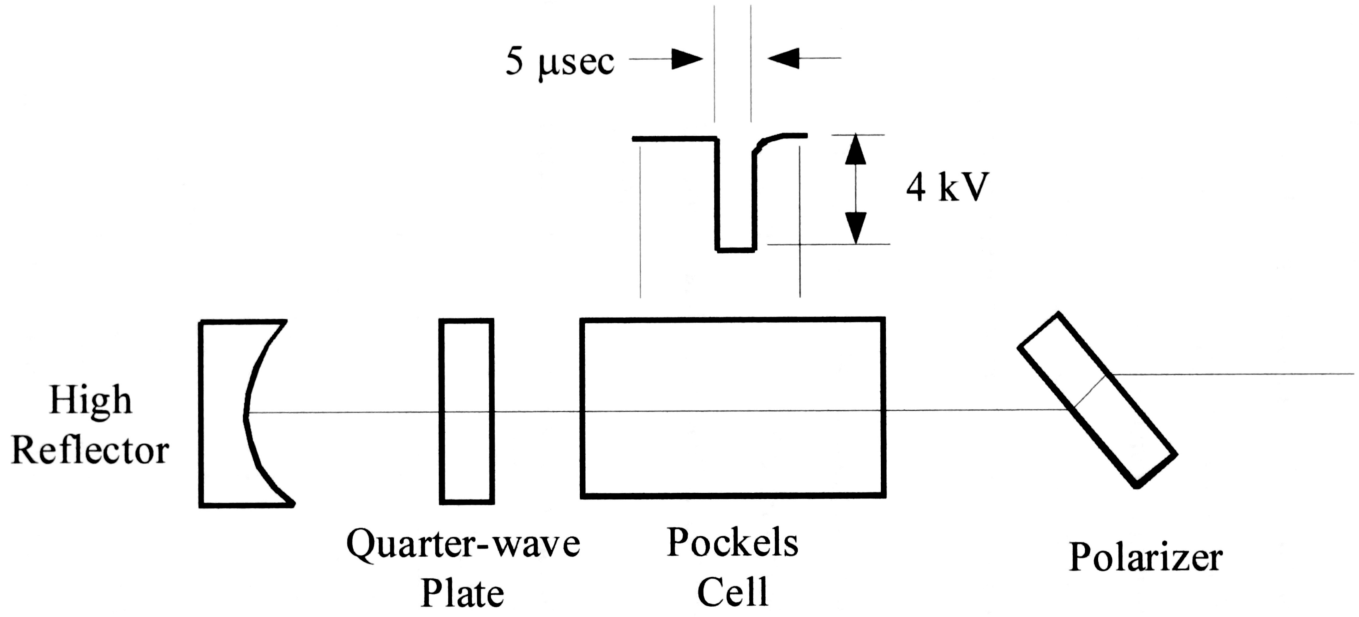

Figure 2-07 The Q-switch comprises a polarizer, a quarter-wave polarization rotator, and a Pockels Cell.

separation between individual pulses of 2 - 4 μs. The total energy of the pulse train is similar to that of a single Q-switch pulse. This long pulse mode allows safer alignment and setup, and is useful in experiments where total pulse energy, rather than its distribution in time, is of the main interest.

2.2.5.3 The Harmonic Generator

The short pulse of high peak power of the Q-switch laser pulse permits wavelength conversion through several nonlinear processes, such as frequency doubling, frequency mixing, dye laser pumping or Raman frequency conversion. The interaction between the fundamental (1064 nm) laser beam and the crystal produces a secondary beam with half of the fundamental wavelength which is frequency doubled. Such device is called harmonic generator.

Using the harmonic generator, the fundamental wavelength infrared irradiation (1064 nm) can be converted into its second (532 nm), third (355 nm) or fourth (266 nm) harmonics. The pulse energy and pulse widths of these harmonic wavelengths are illustrated in the Table 2-01.

Table 2-01. Specifications of the frequency harmonics of DCR-11 Nd-YAG laser.

	Harmonic		
	2	3	4
Wavelength (nm)	532	355	266
Q-switch Pulse Width (ns)	6-7	5-6	4-5
Pulse Energy (mJ)	135	60	30

The converted harmonic irradiation still contains a residue of the fundamental irradiation. The monochromatic harmonic laser beam is produced by passing the emerging beam through a Pellin Broca prism, (1" Fused Silica-type PLBC-10UV)

which refracts different wavelength of laser beams at different angles. (Figure 2-08) By rotating the Pellin Broca rotary support, desired wavelength of laser beam can be directed to the sample target.

The third and fourth harmonics cannot be simultaneously generated. The third harmonic is formed by the summation of the fundamental and the second harmonic. The fourth harmonic is generated by frequency doubling of the second harmonic of which itself is obtained by frequency doubling of the fundamental irradiation.

2.3 The BioAPEX II 70e Fourier Transform ICR Mass Spectrometer

The second FTICR mass spectrometer used in this thesis work was a Bruker BioAPEX II 70e FTICR mass spectrometer. This new generation of FTICR mass spectrometer incorporates many new outcomes of the latest theoretical and experimental studies of FTICR mass spectrometry. Although the fundamental principles are the same for both BioAPEX II 70e and CMS-47X FTICR mass spectrometers, there is a major difference between the two instruments. The CMS-47X FTICR mass spectrometer was designed mainly for the internal (in the ICR cell) ion generation, while the BioAPEX II 70e is designed primarily for the use of external ionization sources. Ionization methods such as ESI, APCI and MALDI can be easily incorporated with BioAPEX II 70e FTICR mass spectrometer, with about 20 minutes changeover time for the different ion sources.

The BioAPEX II 70e FTICR mass spectrometer consists of several components including a 7 T passive shielded superconducting magnet, the vacuum system, the ion optics voltage supply, the external ion sources, the SGI data processing computer and the Unix O_2 workstation. A brief discussion will be presented here regarding the new features of this FTICR instruments. A schematic of this BioAPEX II 70e FTICR mass spectrometer is shown in Figure 2-09.

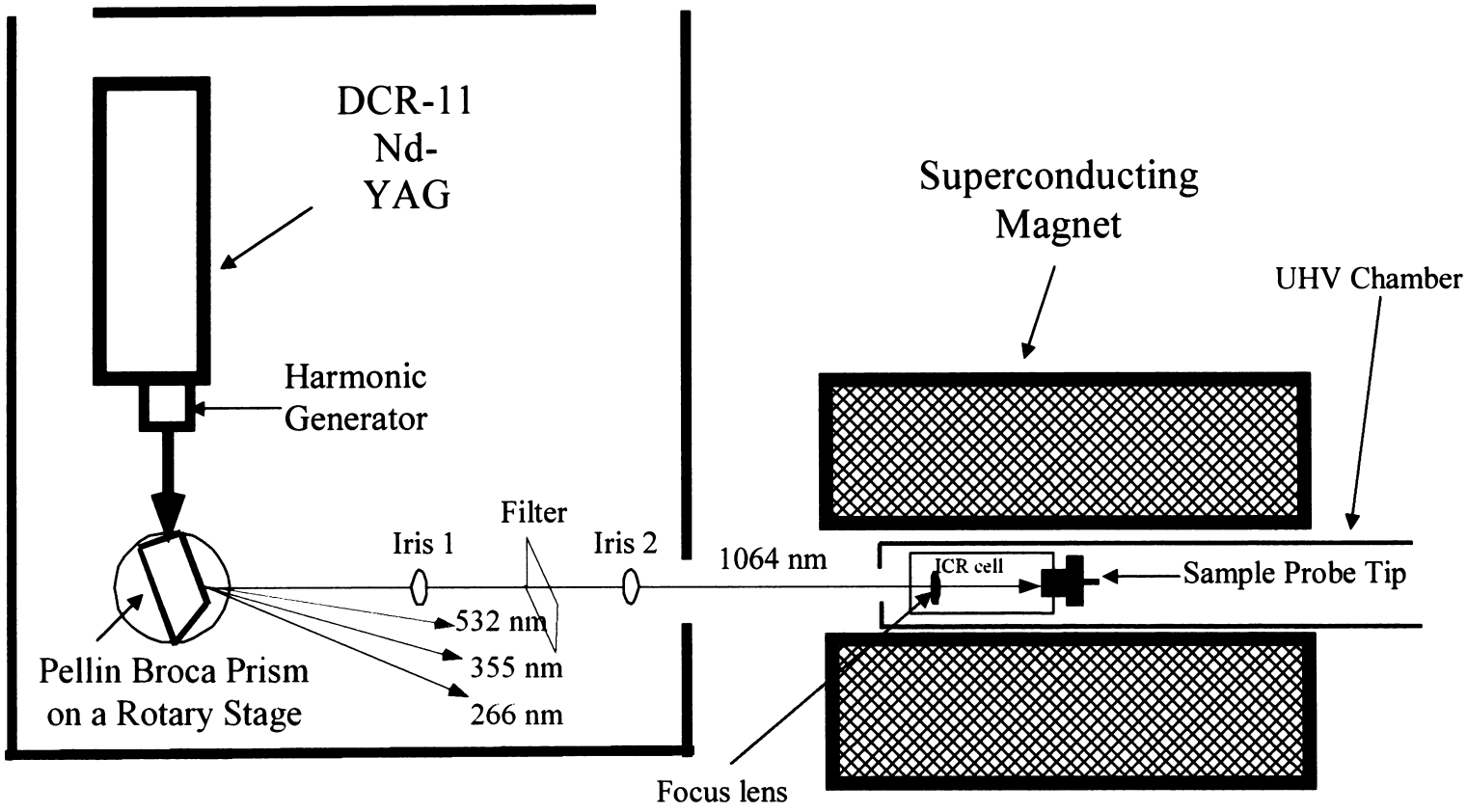

Figure 2-08 A schematic of Pellin Broca prism and the separation of frequency harmonic laser beams.

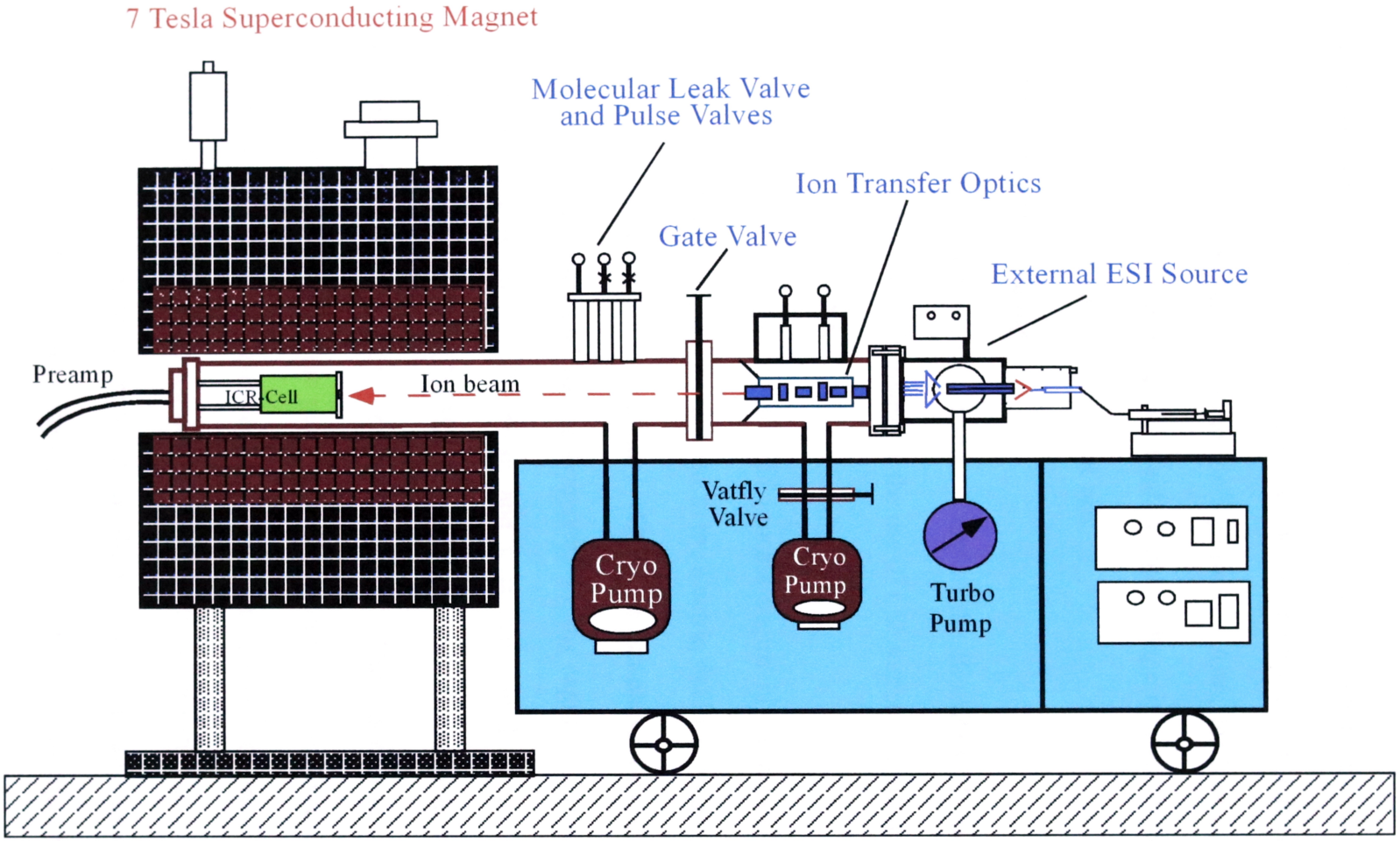

Figure 2-09 A schematic of Bruker BioAPEX II 70 e FTICR mass spectrometer equipped with an electrospray ionization source.

2.3.1 The Vacuum System and Ion Optics

As BioAPEX II FTICR mass spectrometer is designed to operate with various external ion sources; ions that are generated in the ion source have to be transferred from a high-pressure atmospheric region to the ultrahigh vacuum ICR cell, differential pumping has to be established in the ion's pathway. Also, for ions to overcome the repulsion from the fringing magnetic field, a high-voltage is used for the ion transfer optics in order to inject ions in to the ICR cell.

2.3.1.1 Differential Pumping

Figure 2-10 illustrates the vacuum system on the BioAPEX II 70e FTICR mass spectrometer. The example is given for the use of ESI source and differential pumping is indicated in this schematic.

Gas-phase ion formation in the ESI process begins in the atmospheric pressure region where charged droplets are formed in the electric field between the spray needle tip and the entrance-end of the capillary. Once the gas-phase ions are formed, they travel through a capillary and then a skimmer. In this capillary-skimmer region, the pressure is typically 10^{-2} ~ 10^{-4} mbar, and it is maintained by an Edwards turbo molecular pump (Model: EXT250H). After the skimmer, a hexapole ion trap and an extraction plate are located in the ion source chamber. This chamber is evacuated by an Edwards CoolStar 800 cryogenic pump and the pressure is maintained in the range of 10^{-5} ~ 10^{-7} mbar. Ions are extracted by the extraction plates on the ESI source and transferred into the ultrahigh vacuum (UHV) chamber by a series of ion steering and focusing lenses. The major components of the ion optics are also located in the ion source chamber. In the ion focussing region, the pressure is maintained by an Edwards CoolStar 400 cryogenic pump and the pressure is in the range of 10^{-7} ~ 10^{-9} mbar. Finally, ions enter the UHV chamber where the ICR cell is located and the pressure in

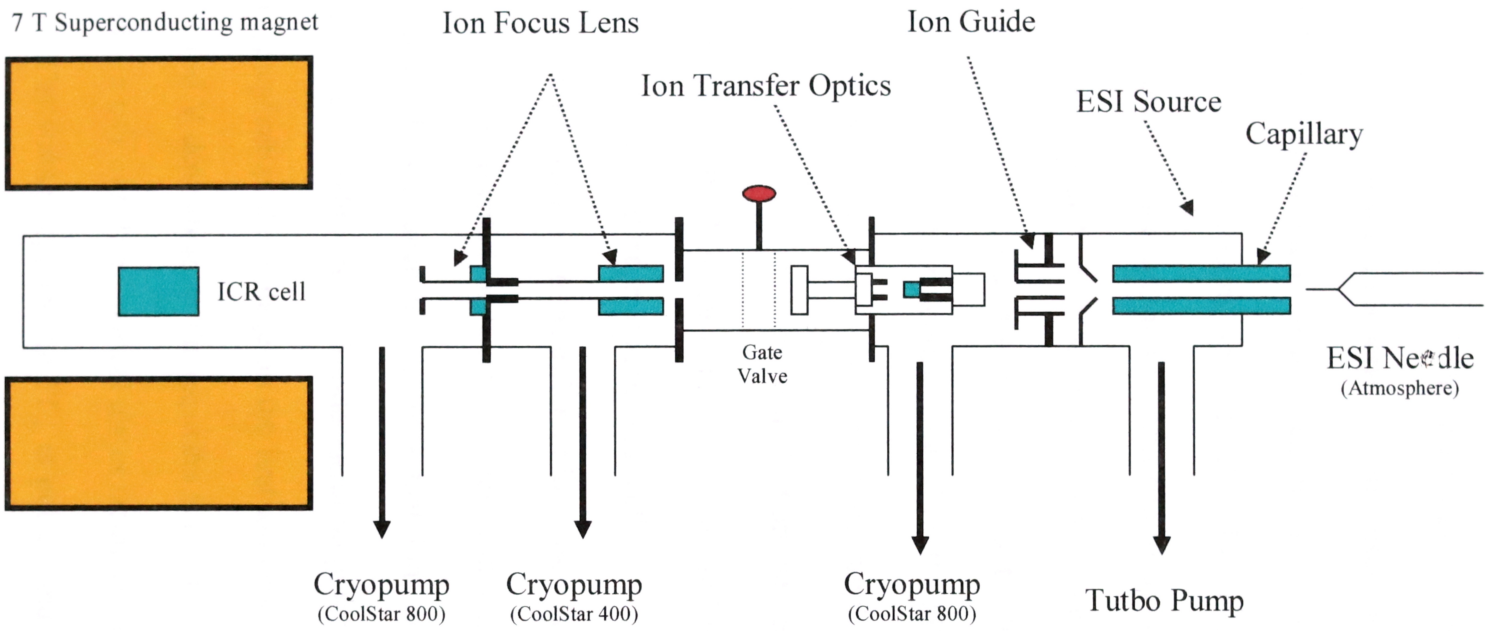

Figure 2-10 A schematic of differential pumping system on the Bruker BioAPEX II 70e FTICR mass spectrometer.

this region is typically 10^{-9} ~ 10^{-11} mbar which is maintained by another Edwards CoolStar 800 cryogenic pump.

2.3.1.2 The Ion Transfer Optics and Potential Gradient

As illustrated in Figure 2-11, the ion transfer optics on BioAPEX II 70e FTICR mass spectrometer consists of a series of ion lenses including ion steering optics PL1, PL2/DPL2, PL4/DPL4, high voltage element HVO (~ 2.5 kV), ion deflection optics XDFL and YDFL, ion focusing optics FOCL1, PL9 and FOCL2. The last parts of the ion transfer optics are located on the front-end of the ICR cell, EV1 and EV2/DEV2. The high voltage applied on some of these lenses was used for ions to overcome the magnetic fringing field during their transmission to the ICR cell.

Figure 2-12 shows the potentials applied on the different ion lenses under normal experimental conditions. Some of the lenses are supplied with pulsed voltages that are arranged in sequence with the rf pulse applied on the ESI hexapole ion trap or the pulse extraction plates on the MALDI ion source. This pulsing function enables a packet of ions to be dispatched and trapped in the ICR cell.

The potential gradient on the different ion lenses is arranged in a way that ions are generated in a low potential ion source (~ a few volts) and trapped at similar potential in the ICR cell. This arrangement ensures that ions are not acquiring excess energy through the electric field acceleration-deceleration process.

In a typical setup, the voltage on the first ion lens PL_1 can be adjusted in the range on 0 ~ +/-180 V depending on the experimental conditions and ion detection polarity. Next to PL_1, a pair of half-cylindrical plates facing each other horizontally form the ion lens PL_2. The voltage applied on PL_2 is pulsed and a potential difference DPL_2 is applied on the two half plates. In a similar fashion, a pair of half-cylindrical plates (PL_4) is placed vertically behind the PL_2 plates, and a voltage difference DPL_4 is

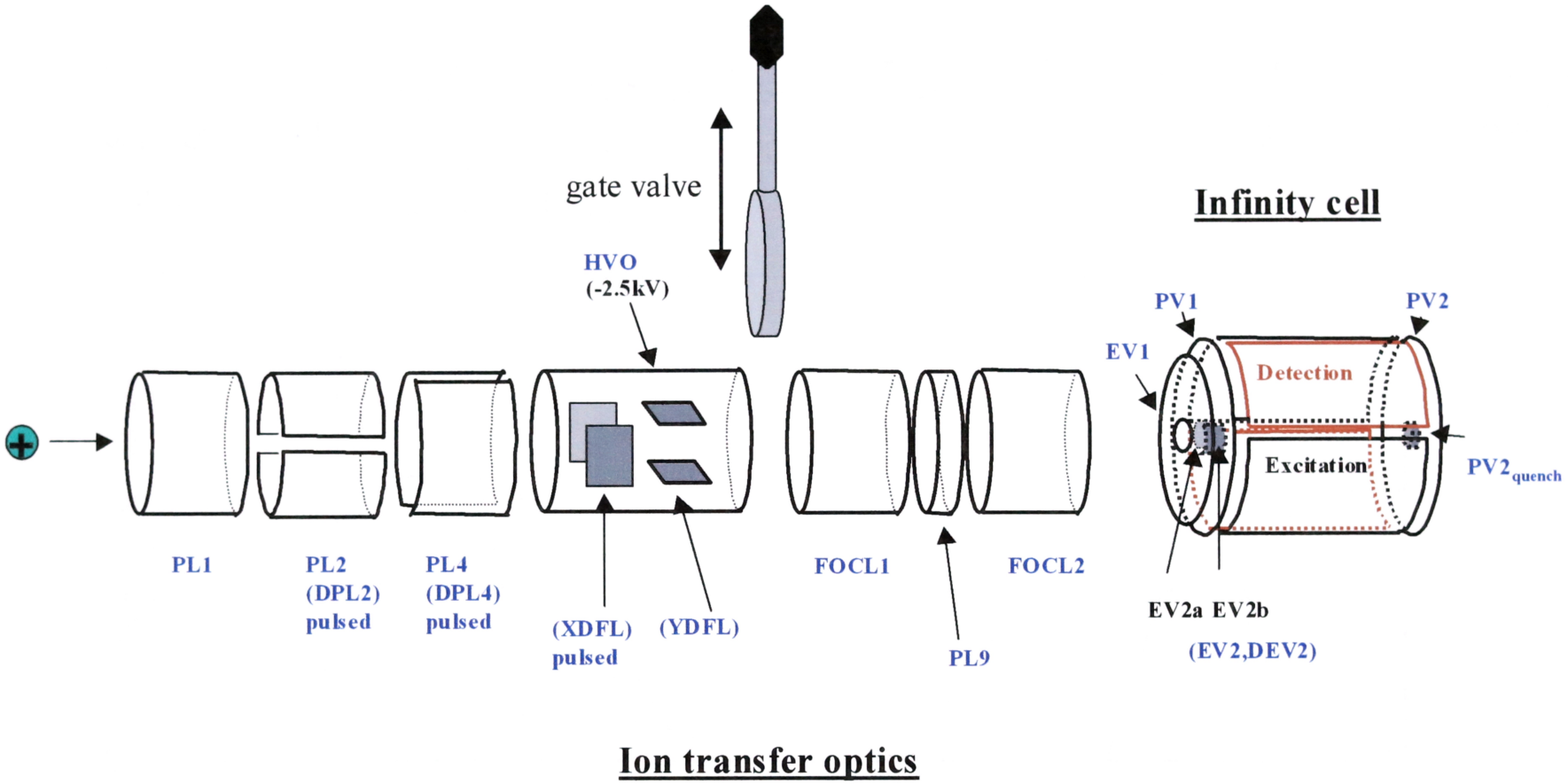

Figure 2-11 Schematic of the ion transfer optics and the infinity cell of Bruker BioAPEX II 70e FT/ICR Mass Spectrometer.

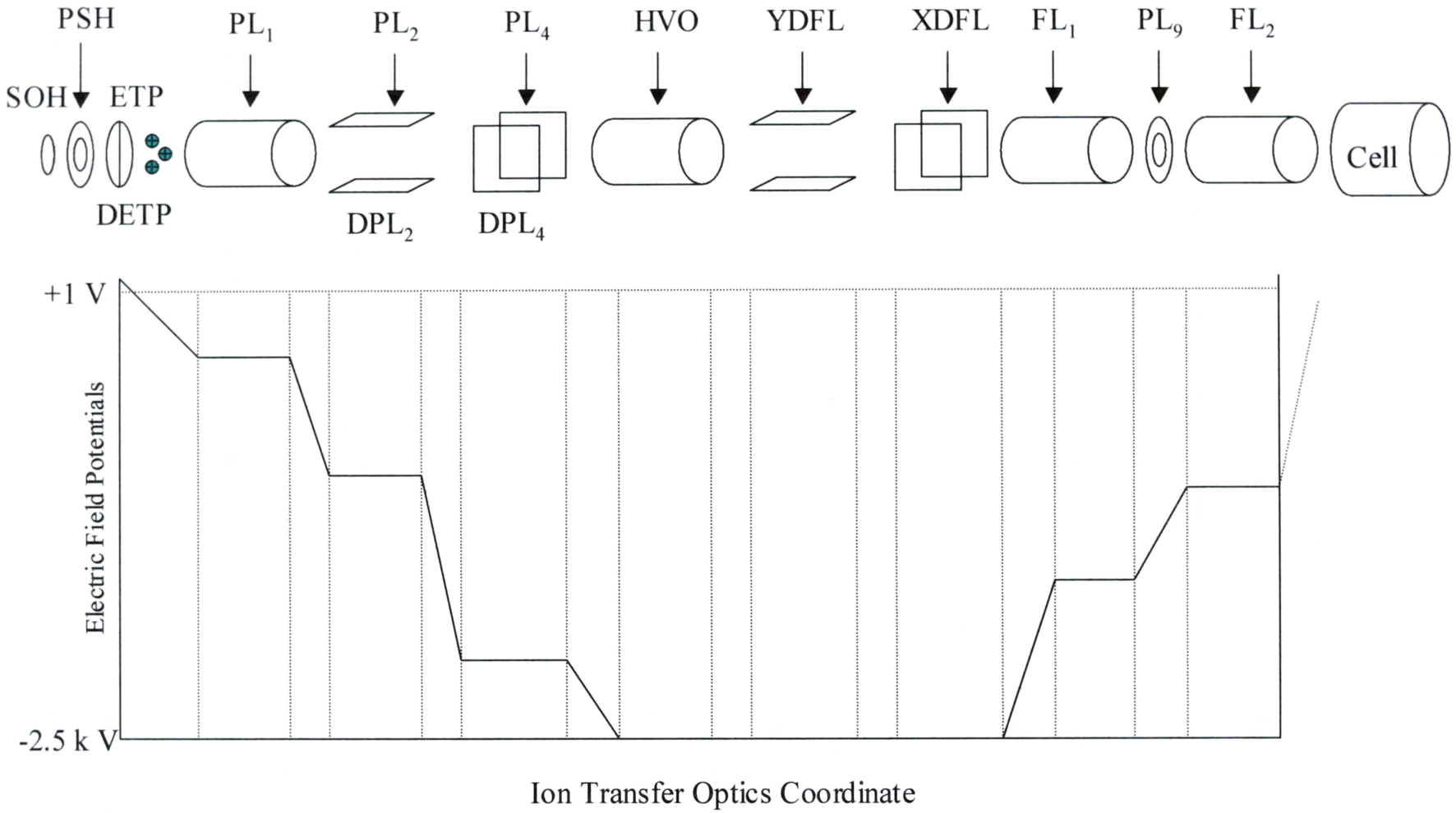

Figure 2-12 electric potential diagram for the ion transfer optics of Bruker BioAPEX II 70e FT/ICR mass spectrometer.

applied to these two plates. The voltage applied to PL_4 is also pulsed. The PL_1, PL_2/DPL_2 and PL_4/DPL_4 form the 'ion beam steering' lenses to give ions a guided acceleration. The high voltage of +/-2.5 kV is applied on a cylindrical ion lens behind PL_4, which incorporates with two pairs of flat deflection plates XDFL and YDFL. These two sets of deflection plates are arranged in horizontal and vertical positions respectively. The potential on the XDFL and YDFL can be adjusted between 0 ~ +/-180 V, which steers the ion packet and injects it into the UHV chamber. The einzel lens $FOCL_1$, PL_9 and $FOCL_2$ arranged downstream in the the line focuses the ion beam into the ICR cell. The potentials applied on these three lenses also form a part of the potential gradient, which decelerate ions before they enter the cell.

The final stages of the potential gradient are the voltages set on the ICR cell trapping plates. The cell parameters EV_1, EV_2/DEV_2, PV_1 and PV_2 can be tuned collectively to control ion accumulation and ion trapping. The element EV_1 acts as a fine adjustment to the ion's energy before entering the cell. EV_2 and DEV_2 together control the Sidekick™ (detailed in later section) mechanism for ion accumulation. EV_2 defines the center potential at the cell entrance while DEV_2 controls the voltage gradient across the cell entrance.

2.3.2 The 'Infinity' ICR Cell

The Bruker BioAPEX II 70e FTICR mass spectrometer is equipped with a special ICR cell called the 'infinity' cell. The standard ICR cell has uniformed potential applied on the two trapping plates at each end of the cell. A major drawback of this configuration is that during the ion excitation, some non-linear effects, such as the coupling of axial and radial motions can cause undesired ion ejection along the z-axis of the ICR cell. This is so-called 'z-ejection'.[5,17,18] It has been shown that excitation of the axial motion is especially effective for frequencies equal to $2\omega_t$ and $\omega_c+2\omega_t$ where ω_c is

the cyclotron frequency and ω_t is the trapping frequency. To eliminate such unwanted ion ejection, Caravatti and Allemann designed a pair of eleven-segment trapping plates with different potentials applied on each segment to match the potential gradient of the rf excitation field.[19] Such ICR cell then behaves, with respect to the electric rf excitation field, like an infinitely long cell. Viewed from inside the cell, the two trapping plates act as rf mirrors and give the ions the 'illusion' of an infinitely long rf field. Caravatti and Allemann showed the infinity cell effectively eliminates the excitation-ejection at frequency of $\omega_c+2\omega_t$ and produces signal to noise ratios that are greatly improved.

In the Bruker infinity cell, all electroplates are made of titanium and gold-plated. The eleven-segment trapping plate PV_1 and PV_2 are designed and arranged in the way that was described in the Allemann's report.[19] The additional plates outside the PV_1 are the EV_1 and two EV_2 half-plates.

2.3.3 Ion Trapping

The ion trapping by BioAPEX II 70e FTICR mass spectrometer can be performed in several ways. These include the Sidekick™ ion trapping, gated ion trapping (either static or dynamic) and collision gas-assisted dynamic ion trapping.

2.3.3.1 Sidekick™ Ion Trapping

The Sidekick™ ion trapping method is used mainly for fast routine mass analysis. Following the ion injection event, a potential difference DEV_2 is applied on the two EV_2 half-plates that are mounted outside the first trapping plate PV_1 (see Figure 2-11). This potential difference exerts a force upon ions entering the cell, which is perpendicular to the z-axis of the cell so it pushes ions into ion cyclotron orbits. The advantage of Sidekick™ ion trapping method is that a wide mass range of ions can be trapped in the cell and it is easy to operate. As most of the ions are pushed off from the centerline of

the cell, this method is not feasible for the electron-capture dissociation (ECD) or infrared multiphoton dissociation (IRMPD) experiments, which requires ions to be presented close to the z-axis of the cell.

2.3.3.2 Gated Ion Trapping

Another ion trapping method is based on the time-of-flight of ions and gating the ICR cell at a proper time. This ion trapping method can be performed in either static or dynamic ways. The static ion trapping is to set the trapping potential at a constant value and whether ions can be detected relies critically on the flight times of the ions. On the other hand, the dynamic ion trapping is to have the trapping potential pulsed on the trapping plates and the length of the pulse can be manually tuned to enhance the signal intensity. The gated trapping can keep the ions on axis therefore convenient for the ECD and IRMPD experiment. The disadvantage of this method is that narrow mass range of ions can be trapped and the trapping efficiency is relatively low.

2.3.3.3 Collision Gas assisted Dynamic Ion Trapping

The third ion trapping method is collision gas assisted dynamic ion trapping which introduces collision gas (pulsed) into the ICR cell to quench ions, and applies a pulsed potential on the trapping plate to trap the ions. This ion trapping method can efficiently reduce the ion energy spread, which is reflected by the flight time of the ions. A wide mass range of ions can be trapped by this method. As the pulsed gas has to be pumped away before the detection, this ion trapping method is a slow process, and the mass range is still limited by the time-of-flight effect.

The effect of collision gas-assisted dynamic ion trapping has been experimented in this current study. The cooling process is most effective for high m/z ions (> ~1,000 Da). For example, the laser desorption experiment of fullerene soot using Nd-YAG laser (1064 nm) shows that only a small number of fullerene ions including mainly C_{60}^+

and C_{70}^+ are detected (Figure 2-13a). Very few high fullerene ions are presented in this mass spectrum. However, by pulsing methanol into the ICR cell, not only C_{60}^+ and C_{70}^+ signals enhanced, but also many larger fullerene ions are detected (Figure 2-13b). The two experiments are performed under the same laser energy at the same target spot, so the observation of larger fullerene ions clearly demonstrated the effect of collision gas in helping to cool and trap ions.

2.3.4 External Ionization Sources

The Bruker BioAPEX II 70e FTICR mass spectrometer is equipped with a range of ionization sources including EI/CI, ESI, nanospray, APCI, MALDI and a supersonic expansion cluster ion source. In this thesis work, the ESI and MALDI ion sources were mostly used, and a brief introduction will be given here for the two types of ion sources.

2.3.4.1 The External Electrospray Ionization Source

For routine ESI experiments, the experimental setup and operation is as following: A Cole-Parmer (Vernon Hills, Illinois) syringe pump is used to produce a sample flow at 60 μl/h by pressing a syringe (250 μl) that contains the sample solution at a concentration of 100 μg/l. The syringe needle is connected to the spray needle via Teflon tubing, and the spray needle is 0.1 mm in diameter. This spray needle is positioned at about 1 cm from the end of a quartz-capillary, which is coated with a thin nickel film at both ends. For the negative-ion detection, approximately + 4 kV is applied to the entrance-end of the capillary facing the spray. This high voltage creates a strong electric field between the capillary and the spray needle to initiate the ion formation from the spray. The end plate and the mesh cylinder surrounded the spray needle are held at ~ + 2.5 kV. Heated drying gas (N_2, 300 °C) is directed towards the spray from the gap between the end plate and the capillary. Voltages ranging from – 400 V to 400 V are applied to the exit-end of the capillary. A skimmer is located after

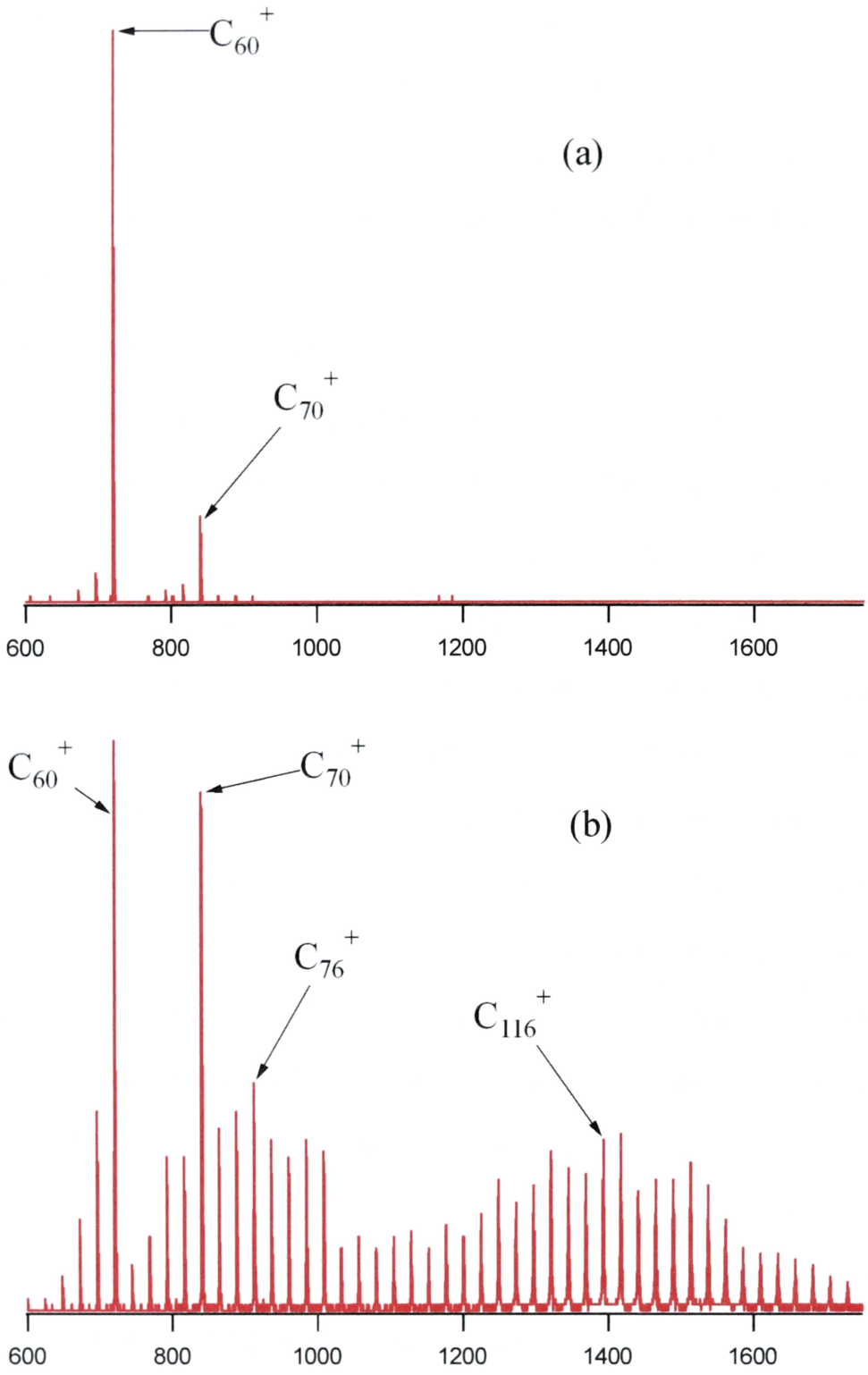

Figure 2-13 Collision gas assisted ion trapping demonstrated by laser desorption of fullerene soot. (a) No collision gas in the ICR cell, (b) methanol pulsed into the ICR cell.

the exit end of the capillary and it is held at a low voltage (0 V to –20 V). Next, an rf/dc hexapole ion trap is used to accumulate ions prior to ejecting them to the ICR cell. A delay d_1 which ranges from 0.1 to several seconds is used for the ion accumulation. An ion packet is pulsed out from the hexapole ion trap and directed into the ICR cell by the ion transfer optics.

2.3.4.2 The External MALDI Source

The MALDI ion source as supplied has a 3 μW N_2 laser (UV) incorporated in the vacuum cart for the ionization. The UV laser beam is reflected and diverted onto the target by a pair of mirrors and focussed by an optical lens. A sample insertion probe is used to load samples from atmosphere pressure region into the high-vacuum ion-source. (Figure 2-14a). The sample holder can accommodate as many as 11 different samples (Figure 2-14b) at a time and they can be positioned into the focused laser beam in sequence by winding the insertion probe inward. The MALDI source consists of three electro-elements, the source housing (SOH), the pusher (PSH) and the extraction plate (ETP/DETP) as shown in Figure 2-15. Note that the extraction plates are taken away for the laser ablation experiment. Ions produced by the laser are confined by the electric field that is created by the combination of SOH and PSH potentials. The extraction plates are applied with a pulsed rf potential to extract ions out of the MALDI ion source. This potential is offset by the DETP parameter in the XMASS program. A coated filter, which is installed in the N_2 laser's pathway, varies the laser energy, and a CCD camera is mounted inside the MALDI source to view the sample.

2.3.4.3 The Modification of the MALDI Source for the Laser Ablation Experiments

In order to carry out laser ablation experiments on the BioAPEX II instrument, the external MALDI ion source was modified by the author to allow the use of a DCR-11 Nd-YAG laser for the ion generation.

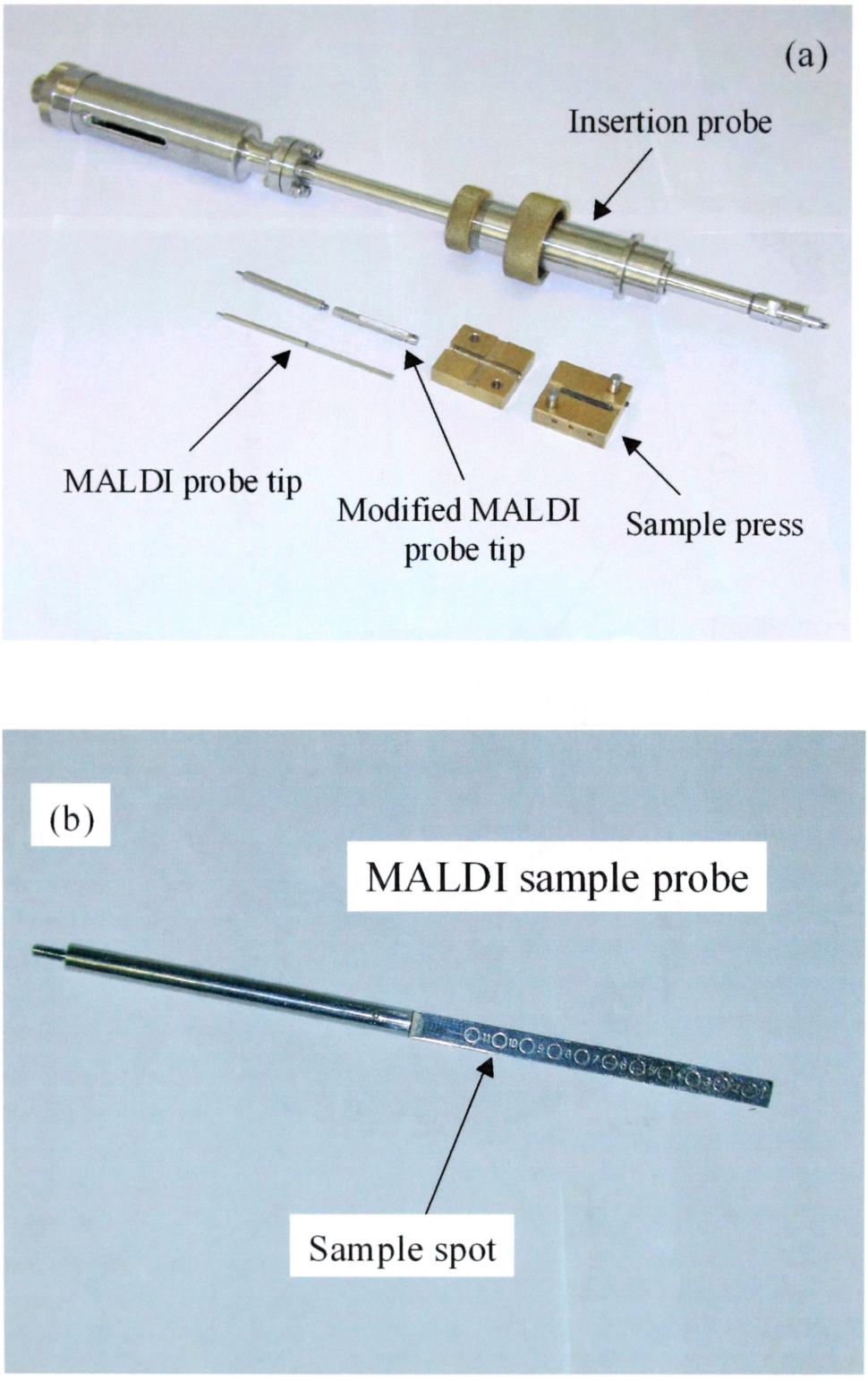

Figure 2-14 MALDI probe of BioAPEX II FT/ICR mass spectrometer (a) insertion probe and sample press. (b) MALDI sample probe.

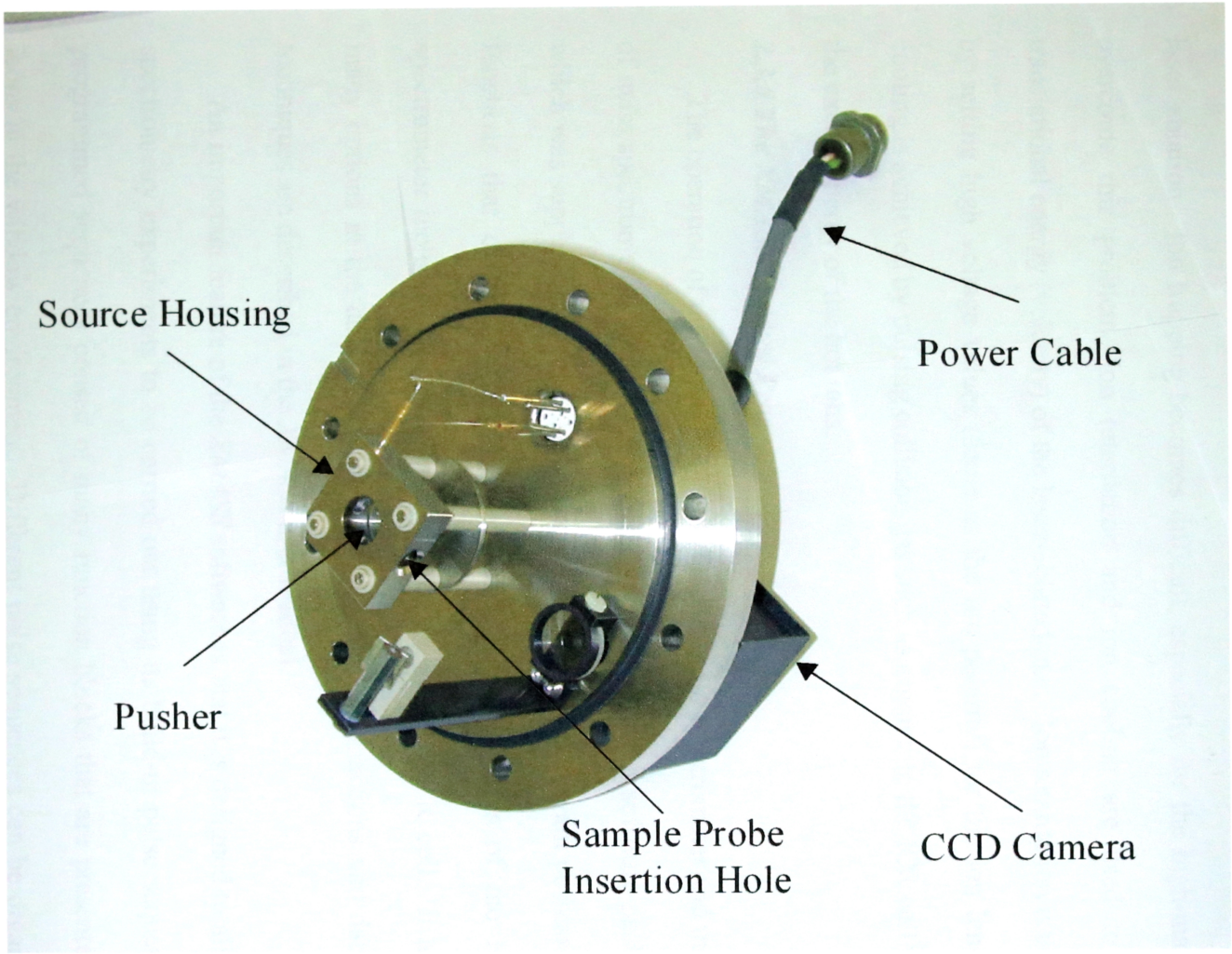

Figure 2-15 MALDI ion source of Bruker BioAPEX II 70e FT/ICR mass spectrometer.

Figure 2-16 is a schematic which shows the Nd-YAG laser beam pathways in the experiment. The laser beam is reflected by an UV grade quartz Pellin Broca prism and three right-angle prisms. The laser energy is varied by neutral density filters set in the laser's pathway. Ions produced by this method can have much higher translational energy than the ions produced in the MALDI experiments as the result of high energy laser ablation. Ion trapping becomes difficult, especially for the high-mass ions. To overcome this problem, ion retardation and ion cooling are used to reduce the translational energy (velocity) of the laser-ablated ions. Ion retardation is accomplished by setting high voltage values (same as the ion polarity) for the ion lens PL_1. Ion cooling is achieved by pulsing collision gas such as argon into the ICR cell to take away the excess energy of the hot ions.

2.3.5 The XMASS Control Program

The operation of the BioAPEX II 70e FTICR mass spectrometer and the acquisition of mass spectrometry data are accomplished by the computer software package *XMASS* which was supplied by Bruker Daltonics Company. This program possesses numerous functions that control the voltages on different components of the FTICR mass spectrometer including the ion source, ion optics and the ICR cell. It also provides many options in the data processing. Details of these functions and data processing techniques are described in the *XMASS* user manual.

An important feature of the *XMASS* software is that it is designed to allow the mass spectrometry experiments to be carried out using its build-in pulse sequences. These programmed sequences consist of many function blocks that are presented as bitmap icons in the window environment. Different pulse sequences can be organized simply by activating the required bitmap icons. These pulse sequences are also user-accessible and can be easily modified by editing relevant function blocks in the program.

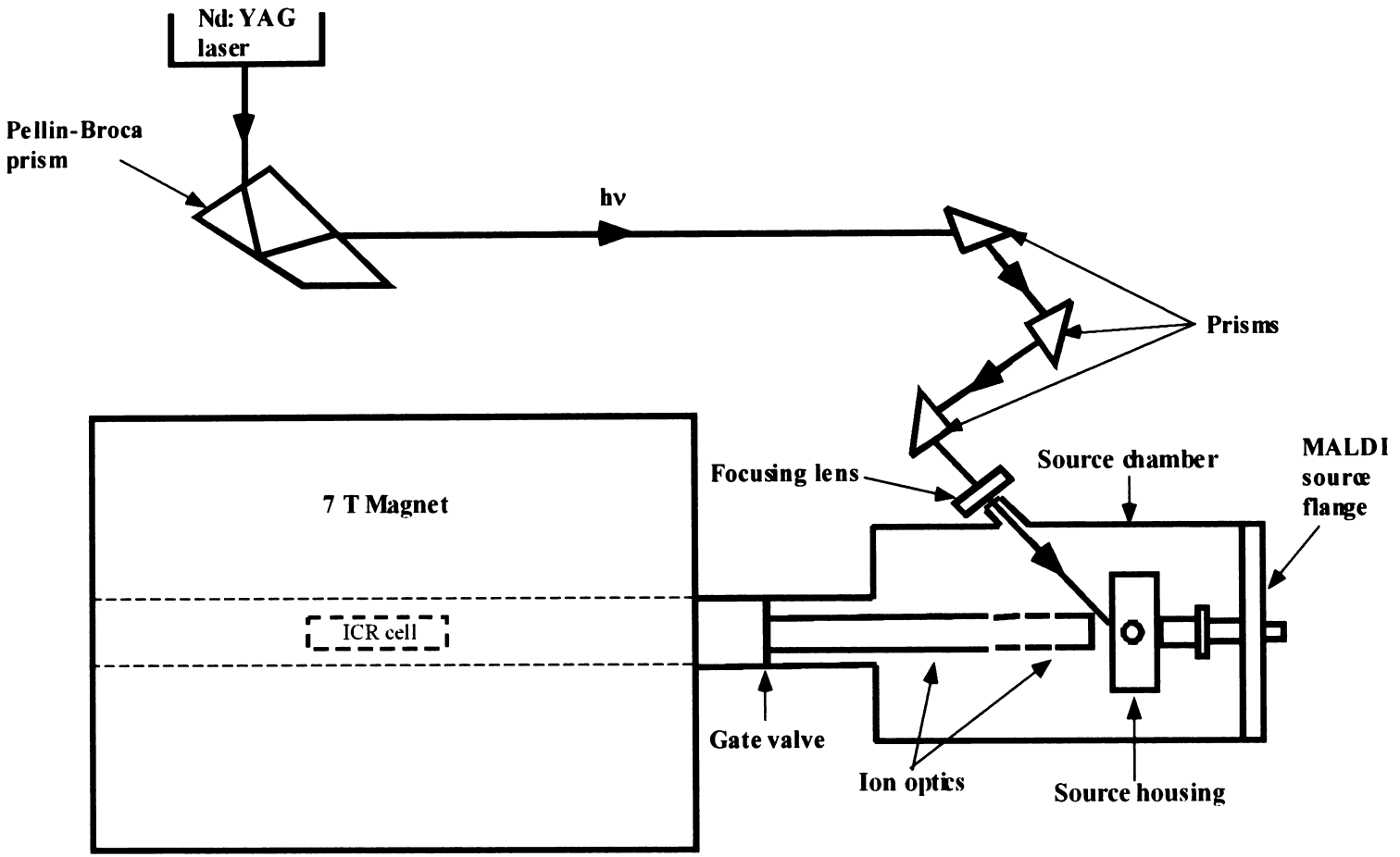

Figure 2-16 Schematic of the modified MALDI source for Bruker BioAPEX II FT/ICR mass spectrometer..

The mass spectrometry data obtained by the *XMASS* program can be saved as *ASCII* file (instead of the *Unix*® binary file), which can be read and plotted by other graphic software such as *Igor*® or *Excel*® in the *Microsoft Office*® package.

The XMASS program is installed on a *UNIX*® platform, which is on a silicon graphic O_2 workstation operating under the *IRIX*® system.

2.4 Sample Preparation

The two FTICR mass spectrometers used in the experimental work both have sample inlet systems that allow solid, liquid or gas samples to be introduced into the ICR cell for mass analysis. A brief description of the sample preparation is presented here with focuses on the sample preparations for both laser ablation experiments and electrospray experiments. Detailed sample preparations will also be described in the later sections when the discussions become relevant to these details.

2.4.1 Sample Preparation for the Laser Ablation Experiments

Part of the laser ablation experiments described in this thesis was carried out on the CMS-47X FTICR mass spectrometer. Solid samples were used as the laser ablation targets. Sample powder was pressed into a stainless steel probe tip by a home-built press. The sample probe tip was mounted on a satellite, which screws onto the end of a suspended magnetic insertion arm (see Figure 2-01). The sample probe tip and the satellite were inserted into the ICR cell by the insertion arm and located on the one of the cell trapping plate, which was facing to the incoming laser beam.

The study of metallofullerenes and metal-carbon clusters that are described in Chapter Three and Four involve carbonaceous materials such as *carbon thermal black* or pyrolysed *Koppers coal-tar* pitch. The sample mixture comprised of carbonaceous materials and metal compounds at various carbon/metal ratios.

In the study of CID and ion-molecule reactions, argon collision gas or volatile chemical reagents such as methanol or benzene are introduced into the ICR cell via the molecular leak valve or the pulsed molecular valve.

As the CMS-47X FTICR-MS instrument was decommissioned during this project, further experimental work was undertaken on the BioAPEX II 70e FTICR mass spectrometer using a modified MALDI ion source. A new sample probe and sample press were designed by Adriana Dinca, a fellow postgraduate student at UNSW and this press was used for the laser ablation experiments (See Figure 2-14a).

2.4.2 Sample Preparation for the ESI Experiments

The ESI-FTICR mass spectrometry study of fullerene derivatives described in Chapter Five was mainly performed on the BioAPEX II 70e FTICR mass spectrometer. These experiments require the samples to be dissolved in organic solvents and for this instrument, preferably methanol. The fullerene derivative samples were either directly dissolved in methanol or first dissolved in organic solvents such as dicholoromenthane and then mixed with over 90% of methanol by volume.

The 1,6-methano[60]fullerene-61,61-dicarboxylic acid was synthesized by Prof. Liangbing Gan and his group from Beijing University using the method of Lamparth and Hirsch.[20] For the ESI-FTICR mass spectrometry experiments, the methanol solution has a concentration of 1.22×10^{-4} M (0.1 mg/ml). The solution was unstable and after one week, the molecular anion could no longer be detected by ESI-MS.

The fluorinated fullerenes were synthesized by Dr. Gerry Gadd from Australian Nuclear Science and Technology Organization (ANSTO). Fullerene C_{60} was used to react with SF_6 under high pressure (~ 200 bar) and the methanol soluble products were analyzed by the FTICR mass spectrometry using the ESI method.

The cyano-fullerenes were prepared by reacting fullerene C_{60} with NaCN and the water-soluble products were analyzed by the ESI-FTICR-MS. Detailed synthesis procedures can be found elsewhere.[21,22]

Other fullerene derivatives were synthesized and supplied by Dr. Paul Keller from Wollongong University.

2.5 The Operation of FTICR Mass Spectrometer and the Associated Pulse Sequences

The computer programs, I89 or *XMASS* that operate the FTICR mass spectrometers contain a sequence of pulse-delay events and each pulse-delay executes a specific operation on the FTICR mass spectrometer. Both CMS-47X and BioAPEX II FTICR mass spectrometers came with several standard pulse sequences and they can be easily modified to suit different experimental requirements.

2.5.1 Pulse Sequences for Simple Experiments

The basic elements in each pulse sequence include ion generation, ion trapping, ion excitation and ion detection. Figure 2-17a shows a pulse program containing all these elements. The event sequence is as follows: prior to the ion generation, a quench pulse-delay P_1/D_1 is applied to the one of the trapping plates, which effectively ejects all the ions from the ICR cell. An ion generation pulse-delay P_2/D_2 is then followed to produce ions from the ion source. The P_2 pulse can be applied in different ways depending on which ion source is used. In MALDI or LA experiments, the P_2 pulse triggers the laser for the laser desorption or laser ablation, and in the internal or external electron ionization source it switches on the electron emitter. In the external ESI ion source, the P_2 pulse is the ion accumulation time in the hexapole ion trap.

After ions are trapped in the ICR cell, a P_3 pulse applies rf potential (50-200 V peak-to-peak and 180° out of phase) to the two excitation-plates and excites ions whose natural cyclotron frequencies are resonant with the applied rf field. Ions of the same

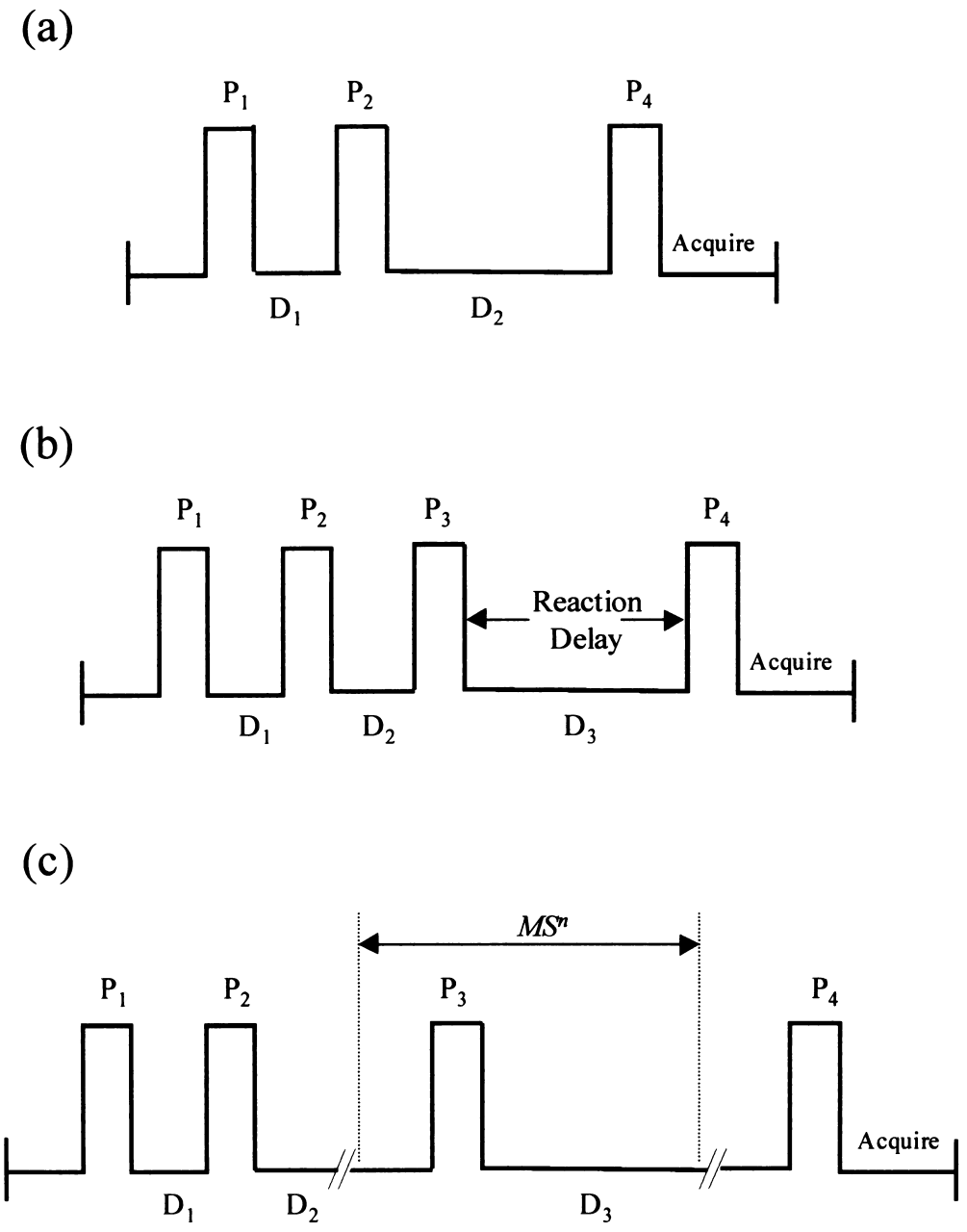

P_1 Quench Pulse; P_2 Ionization Pulse; P_3 Ion Selection Pulse; P_4 Excitation Pulse
$D_1 \sim D_3$ delays.

Figure 2-17 Pulse Sequences used by FT/ICR mass spectrometer, (a) for simple experiment (b) for a single stage ion-molecule reaction or CID experiment (c) for tandem mass spectrometry experiments.

mass that are generated randomly in time and space are now brought into phase coherent motion, effectively moving together in a packet. This phase coherent ion packet generates an ion-induced image current on the receiver plates, and this image current is passed to a differential amplifier circuit, which facilitates the detection and amplification of the signals.

If a single rf frequency is selected for the ion excitation, the result is defined mass detection, which is commonly referred to as 'narrow band' mass spectra. In contrast, the excitation and detection of ions can also be carried out in a wide mass range by sweeping the excitation frequency with a fast frequency chirp over a selected mass range. Ions in this mass range are excited into a phase coherent motion in less than a millisecond. This chirp excitation is often referred as 'broad band' mass spectra.

The amplitude of the rf excitation pulse P_3 can be varied by the attenuation parameter XA. The maximum rf potential (peak-to-peak) is 200 V for CMS-47X and 160 V for the BioAPEX II instrument with XA set equal to zero. The XA can be varied between 0 to 63 dB in steps of 1 dB.

2.5.2 Pulse Sequences for Tandem Mass Spectrometry Experiments

Based on the simple FTICR-MS experiments described above, tandem mass spectrometry experiments can also be performed by a pulse sequence with additional pulse-delay functions in the sequence. Tandem mass spectrometry experiments involve two or more steps of mass measurements such as those performed in the collision-induced dissociation and ion-molecule reaction experiments.

2.5.2.1 Collision-Induced Dissociation

The collision-induced dissociation is a very important technique in ion chemistry studies. It can provide structure information for the selected ion. The experiment is performed by introducing collision gas such as nitrogen or argon into the ICR cell either

mass that are generated randomly in time and space are now brought into phase coherent motion, effectively moving together in a packet. This phase coherent ion packet generates an ion-induced image current on the receiver plates, and this image current is passed to a differential amplifier circuit, which facilitates the detection and amplification of the signals.

If a single rf frequency is selected for the ion excitation, the result is defined mass detection, which is commonly referred to as 'narrow band' mass spectra. In contrast, the excitation and detection of ions can also be carried out in a wide mass range by sweeping the excitation frequency with a fast frequency chirp over a selected mass range. Ions in this mass range are excited into a phase coherent motion in less than a millisecond. This chirp excitation is often referred as 'broad band' mass spectra.

The amplitude of the rf excitation pulse P_3 can be varied by the attenuation parameter XA. The maximum rf potential (peak-to-peak) is 200 V for CMS-47X and 160 V for the BioAPEX II instrument with XA set equal to zero. The XA can be varied between 0 to 63 dB in steps of 1 dB.

2.5.2 Pulse Sequences for Tandem Mass Spectrometry Experiments

Based on the simple FTICR-MS experiments described above, tandem mass spectrometry experiments can also be performed by a pulse sequence with additional pulse-delay functions in the sequence. Tandem mass spectrometry experiments involve two or more steps of mass measurements such as those performed in the collision-induced dissociation and ion-molecule reaction experiments.

2.5.2.1 Collision-Induced Dissociation

The collision-induced dissociation is a very important technique in ion chemistry studies. It can provide structure information for the selected ion. The experiment is performed by introducing collision gas such as nitrogen or argon into the ICR cell either

provide structure information for the selected ion. On the other hand, CID product ions can also be selected to undergo ion-molecule reactions to reveal their gas-phase chemical reactivity.

2.6 Mass Calibration

For precise mass measurement, two factors must be taken into account, mass calibration and mass resolution.

The mass resolution is very much determined by the instrumental and experimental conditions such as the strength of the magnetic field and the pressure in the UHV chamber that houses the ICR cell.

The mass calibration is carried out by an automated function (MASSCAL for CMS-47X and MASSCALI for BioAPEXII) imbedded in the operation software I89 or *XMASS*. A mass calibration equation has been previously defined as:[12]

$$m = \frac{\gamma}{f_{obs}} + \frac{\beta}{f_{obs}^2} \qquad (2\text{-}01)$$

Where $\gamma = qB / 2\pi$ and $\beta = -2qG_TV_{eff} / 4\pi^2$

In which f_{obs} is the observed cyclotron frequency, G_T is the geometry factor for the ICR cell and V_{eff} is the effective cell trapping potential.

To calibrate the cell, a reference compound PFTBA (perfluorotertiarybutylamine) with well-identified EI spectrum is chosen and introduced into the FTICR-MS. Peaks over a wide mass range (e.g. m/z 18 - 650) are measured in the high-resolution mode. The mass calibration function in the FTICR-MS operating program then compares the measured frequencies (f_{obs}) with the expected frequencies (calculated) and adjusts the two calibration constants γ and β until the differences between the respective frequencies are minimized.

Table 2-02 shows the positive-ion masses of PFTBA and its fragments measured by BioAPEX II 70e FTICR mass spectrometer. Both measured and calculated masses are listed for these ions. The mass calibration results are shown in the right column.

Table 2-02 Mass calibration from PFTBA ions generated by electron ionization.

Calibration Points		Differences	
Obs. Mass	Assigned Mas	AMU	PPM
501.971098	501.970592	0.000506	1.0
413.976371	413.976977	0.000606	1.4
263.986332	263.986557	0.000225	0.8
218.985278	218.985081	0.000197	0.9
130.991523	130.991468	0.000055	0.4
68.994598	68.994661	0.000063	0.9

In the ESI-FICR-MS experiments on the BioAPEX II, many cluster ions have been used as references for mass calibration. Among these cluster ions, sodium iodide cluster ions are used in this study. The advantage of using this type of clusters as mass calibrant is that they are formed in both positive and negative ion mode covering a wide mass range typically from ~ 150 Da to ~ 2500 Da (m/z).

The mass calibration can also be performed with internal references, for which the analyzed sample is mixed with a reference chemical(s) that produces ions over the mass range including the sample ion(s). By calibrating the reference ion masses, the sample ion(s) may also be mass calibrated.

2.7 References

(1) Russell, D. H. *Mass Spectrom. Rev.* **1986**, *5*, 167.

(2) Derome, A. E. "*Modern NMR Techniques for Chemistry Research*" (Pergamon Press: Oxford), **1987**, 35.

(3) Comisarow, M. B. *Adv. Mass Spectrom.* **1980**, *8*, 1698.

(4) van der Hart, W. J.; van de Guchte, W. J. *Int. J. Mass Spectrom. Ion Proc.* **1988**, *82*, 17.

(5) Huang, S. K.; Rempel, D. L.; Gross, M. L. *Int. J. Mass Spectrom. Ion Proc.* **1986**, *72*, 15.

(6) Comisarow, M. B. *Int. J. Mass Spectrom. Ion Phys.* **1981**, *37*, 251.

(7) Dunbar, R. C.; Chen, J. H.; Hays, J. D. *Int. J. Mass Spectrom. Ion Phys.* **1984**, *57*, 39.

(8) Hunter, R. L.; Sherman, M. G.; McIver, R. T., Jr. *Int. J. Mass Spectrom. Ion Phys.* **1983**, *50*, 259.

(9) Lee, S.-H.; Wanczek, K.-P.; Hartmann, H. *Adv. Mass Spectrom.* **1980**, *8B*, 1645.

(10) Schweikhard, L.; Blundschling, M.; Jertz, R.; Kluge, H.-J. *Rev. Sci. Instrum.* **1989**, *60*, 2631.

(11) Rempel, D. L.; Ledford, E. B., Jr.; Huang, S. K.; Gross, M. L. *Anal. Chem.* **1987**, *59*, 2527.

(12) Jeffries, J. B.; Barlow, S. E.; Dunn, G. H. *Int. J. Mass Spectrom. Ion Proc.* **1983**, *54*, 169.

(13) Svelto, O. "*Principles of Lasers*" (Plenum: New York) **1982**, 22.

(14) Demtrodu, W. "*Laser Spectroscopy, Basic Concepts and Instrumentations*" (Springer-Verlag) **1982**, 12.

(15) Ready, J. F. "*Effects of High power Laser Radiation*" (Academic Press: New York) **1971**, 13.

(16) Andrews, D. L. "*Laser in Chemistry*" (Springer-Verlag) **1990**, 30.

(17) Rempel, D. L.; Huang, S. K.; Gross, M. L. *Int. J. Mass Spectrom. Ion Proc.* **1986**, *70*, 163.

(18) Beauchamp, J. L.; Armstrong, J. T. *Rev. Sci. Instrum.* **1969**, *40*, 123.

(19) Caravatti, P.; Allemann, M. *Org. Mass Spectrom.* **1991**, *26*, 514.

(20) Lamparth, I.; Hirsch, A. *J. Chem. Soc., Chem. Commun.* **1994**, *14*, 1727.

(21) Khairallah, G.; Peel, J. B. *J. Phys. Chem. A* **1997**, *101*, 6770.

(22) Khairallah, G.; Peel, J. B. *J. Chem. Soc., Chem. Commun.* **1997**, 253.

Chapter Three

Laser Ablation FTICR-MS Studies of Endohedral Metallofullerenes and Related Metal-Carbon Clusters

3.1 Introduction

The discovery of endohedral metallofullerenes has provoked much interest in the study of metal-carbon clusters. Several other types of metal-carbon clusters have also been extensively studied in recent years. These include small metal carbide clusters, metallocarbohedrenes[1] and metal/metal oxide encapsulated carbon nanotubes.[2-4] Laser ablation mass spectrometry has played a crucial role in most of these studies. As demonstrated by Smalley and coworkers in 1985, lanthano-fullerenes were first produced in their pulsed-molecular-valve (PMV) experiment by laser ablation, and confirmed to be endohedral in nature by a photodissociation mass spectrometry experiment.[5]

The observation of various metal carbon species has raised the question concerning metal carbon interaction at an atomic and molecular level, which is the essential knowledge for understanding the differences among various metal carbon species. Laser ablation FTICR-MS can provide defined conditions in the ICR cell to study gas-phase molecular species that are formed in the high temperature laser plume. The effect of carbon precursors and metals in the formation of different metal-carbon clusters also can be investigated.

The main reason to study endohedral metallofullerenes by laser ablation mass spectrometry is that macroscopic production of these cluster materials is still a difficult task and laboratory scale chemical studies of these materials are very limited. To date, the use of metal doped graphite rods with the arc vaporization[6] and the laser ablation-

furnace[7] represent the two major methods for metallofullerene production. It has been shown by many reports that metallofullerenes are formed in a much lower abundance then fullerenes, and they are mixed in the precursor product – carbon soot. The separation of metallofullerenes form fullerenes is a very low efficiency process. Even for the most abundant metallofullerene species $La@C_{82}$, only milligram quantity of this material is available at the moment.[8]

There are two important factors with regard to the formation of different type of metal-carbon clusters - the type of metal and the chemical form of carbon precursor used in the laser ablation target. It is well known that many transition metals possess catalytic properties for chemical bonding activation and transition metal compounds have been commonly used as catalysts in organic synthesis both in chemical laboratories and industries. In recent years, gas-phase studies have revealed much details about the mechanism of the catalytic process of transition metals. These gas-phase studies are not restricted to the normal laboratory conditions that are used for organic synthesis; they have also been applied to the extreme conditions such as in the high temperature arc plasma or laser plume. Smalley and Kroto groups have reported catalytic effect of some transition metals such as Ni and Co in carbon nanotube growth.[9-11] Ijima and coworkers have discussed the effect of several parameters in carbon nanotubes growth including the catalyst metals, carrier gas pressure, different types of laser and laser energies.[12-18]

On the other hand, the chemical forms of carbon precursors also have important bearings on the formation of metal-carbon clusters. Laser ablation mass spectrometry studies have shown that fullerenes can be produced from many carbonaceous materials other than graphite including coals,[19,20] coal coke,[21] meso-phase carbon,[22,23] kerogen,[24]

shungite,[25] humic substances,[26] polymers,[27] pyrolysed naphthalene.[28,29] or even 'Chinese ink'.[30] One major observation form these studies is that this type of materials generally require much less laser energy than graphite to form fullerenes, and the amount of laser energy required correlates to the aromaticity of the carbonaceous material used. These studies also imply that a way to obtain improved metallofullerene yields in arc or laser ablation experiments may lie in the choice of the carbon precursor and that precursors other than graphite may need to be discovered.

In this chapter, two carbonaceous materials namely carbon thermal black (CTB) and pyrolysed Koppers coal-tar (KCT) pitch are examined by LA-FTICR-MS. The study is focused on the effect of both carbonaceous materials in the formation of fullerenes, endohedral metallofullerenes and other metal-carbon clusters. A comparison is also made among various transition metals in regard to their characteristic interactions with carbon clusters.

3.2 Sample Preparation and Experimental Setup

While the laser ablation experiments were mainly carried out on the two FTICR mass spectrometers (CMX-47 and BioAPEX II), several other instruments were also used in this study for the sample preparation or product characterization. A brief description is given here of the experimental setups and the carbon precursor materials.

3.2.1 Carbon Thermal Black and Koppers Coal-Tar Pitch

There are several types of carbon blacks including carbon thermal black, furnace black, channel lamp black and acetylene black. Carbon blacks are colloidal size carbon particles that have coalesced into aggregates and agglomerates.[31] They are produced either by incomplete combustion or thermal decomposition of hydrocarbons depending on whether oxygen is presented. Thermal black is manufactured by thermal

decomposition of hydrocarbons in natural gas or oil in the absence of oxygen and has the largest particle sizes among all the carbon blacks, with particle sizes up to 500 nm. Electron microscopy studies by Hall[32,33] showed many parallel layer groups were orientated with the graphitic planes approximately parallel to the surface in thermal black and other large particle size carbon blacks. In this current study, carbon thermal black is used as a carbon precursor to generate fullerenes and endohedral metallofullerenes. The carbon thermal black sample was obtained from CanCarb (Medicine Hat, Alberta, Canada) and used as supplied. It is classified as a Thermax Floform Carbon Black-Grade N990 with PH value of 9-11.

Coal-tar pitches are complex mixtures of polycyclic aromatic hydrocarbons (PAHs) that are derived from high-temperature coal-tar or petroleum with molecular weight ranging from 200 ~ 2,000 Da. The chemical composition of coal-tar pitch can be altered by a pyrolysis process, which effectively removes the low molecular weight volatile species from the raw pitch. The coal-tar pitch sample used in this current study was obtained from Koppers Coal Tar Pitch Products, Mayfield, New South Wales, Australia, which was named Koppers coal-tar pitch (KCT-pitch). The chemical characterization of Koppers coal-tar pitch has been reported elsewhere.[34]

3.2.2 Pyrolysis of Koppers Coal-Tar Pitch

The pyrolysis of KCT-pitch was carried out on an apparatus illustrated in Figure 3-01. It consists of a cylindrical furnace for which the temperature can be raised to ~1,500 °C. A quartz tube sits inside the furnace with one end connects to a cold trap, and the other end connects to a T-switch which can turn to either the vacuum pump for evacuation or to helium gas cylinder to introduce the carrier gas. KCT-pitch samples are ground into a fine powder prior to the pyrolysis. The sample powder is placed in a 5

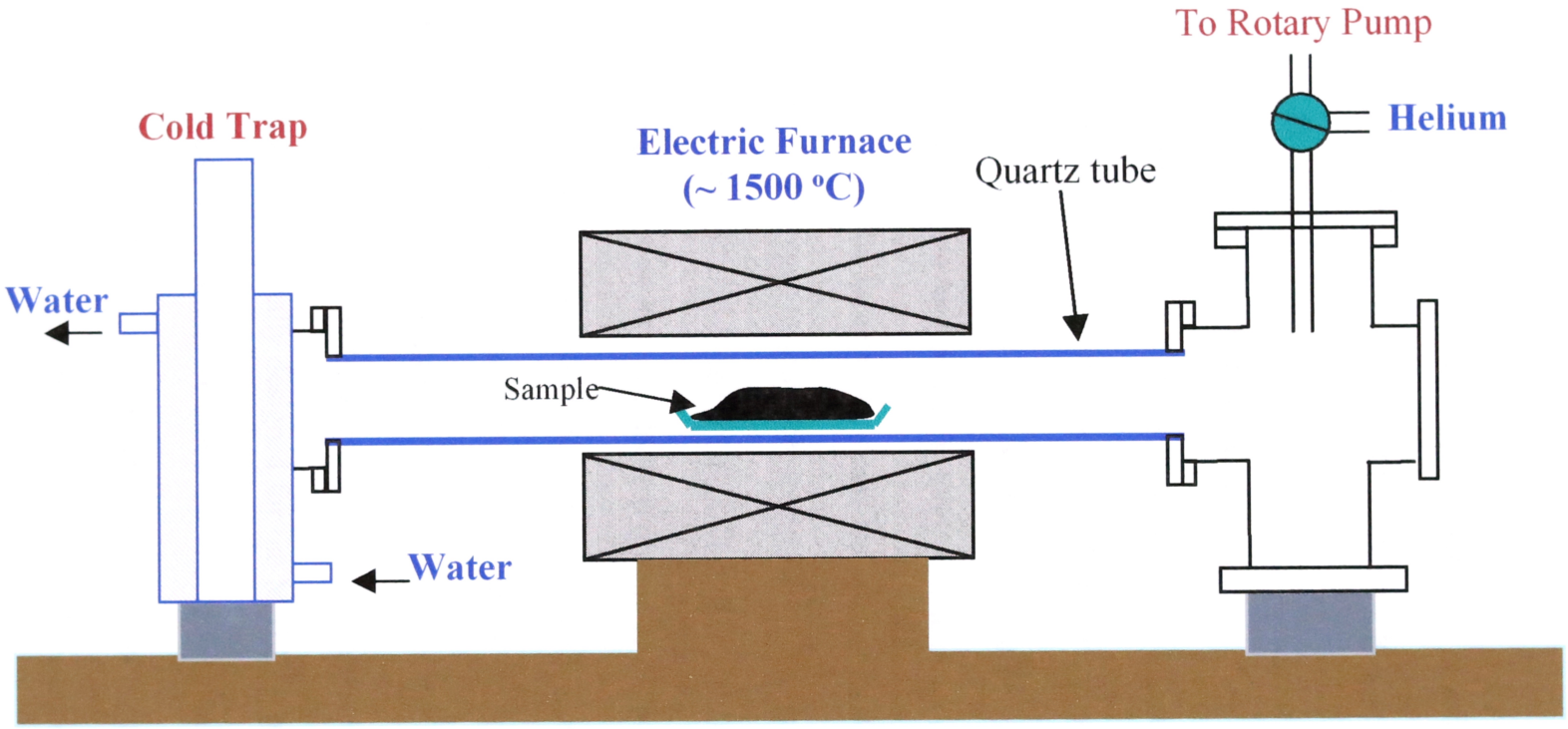

Figure 3-01 An apparatus for KCT-pitch pyrolysis.

cm long and 1 cm wide quartz boat, which sits inside the quartz tube. The pyrolysis is carried out at defined temperature and the pyrolysis duration is one hour for each sample.

In order to produce metal-doped carbon precursors for metallofullerene studies, metal compounds such as La_2O_3 are mixed with pitch sample and pyrolysed together under same pyrolysis conditions.

3.2.3 Laser Ablation Fullerene/Metallofullerene Generator

A laser ablation fullerene/metallofullerenes generator was built at UNSW by honors student Mr. Nathan Paris and modified by the author to carry out macroscopic production of endohedral metallofullerenes. As shown in Figure 3-02, this apparatus consists of a cylindrical furnace and a quartz tube, which sits in the center of the furnace. The temperature in the furnace can be as high as 1,500 ^{o}C, which helps the activation of carbon materials (such as graphite) in the laser ablation experiments. Two stainless-steel cross-chambers are mounted on each end of the quartz tube. A rotary arm with the sample target fitted at its end is located on one of the cross-chamber. The other cross-chamber is fitted with pumping/carrier gas inlet system and a quartz window. An optical lens (focus: 80 cm) mounted at about 20 cm from the quartz window focuses the laser beam onto the target. The Spectra Physics DCR 11 Nd-YAG laser was used for the laser ablation experiment. As shown in Figure 2-14a, a special laser ablation probe which was initially designed for the MALDI experiments are used to accommodate the sample material. Guided by the laser ablation FTICR mass spectrometry results, the metallofullerne production using pyrolysed KCT-pitch/La_2O_3 were carried at room temperature. The fullerene/metallofullerenes soot was collected on the inside of the quartz tube and extracted by toluene or CS_2.

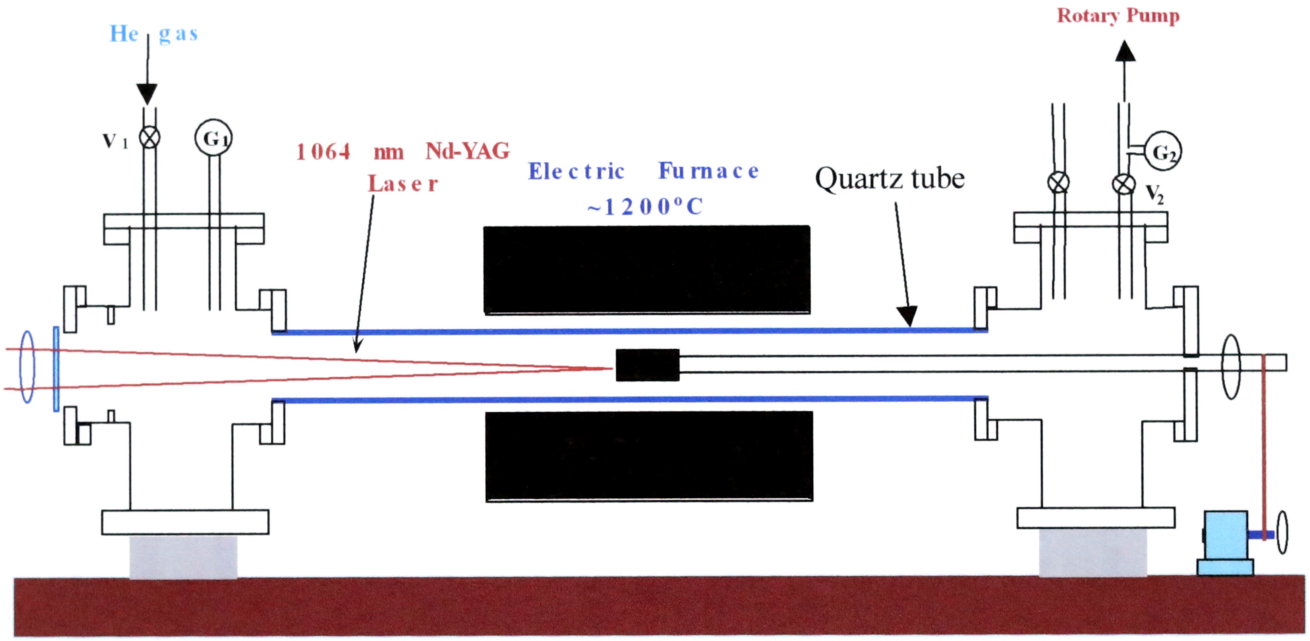

Figure 3-02 Laser ablation fullerene/endohedral metallofullerene generator (V1, V2: Variable valves; G1, G2: Pressure gauges)

Other instruments involved in this study include a home-built reflectron TOF mass spectrometer, which is located at Tokyo Metropolitan University, Japan. The description of this instrument can be found elsewhere.[35] This instrument was used to characterize pyrolysed KCT-pitch residues. A special kind of laser desorption ionization technique called graphite surface-assisted laser desorption ionization[50] was also used for the characterization of KCT-pitch residues using the FTICR instrument. In such experiments, fine graphite powder was mixed with the KCT-pitch pyrolysis residues then compressed into a MALDI probe tip. Graphite was used as a solid-matrix to assist the laser desorption.

A commercial MALDI-TOF mass spectrometer, *Kompact MALDI III* (Kratos Analytical) was used to characterize the metallofullerenes that were extracted from the laser ablation soot.

3.3 FTICR Mass Spectrometry of Carbon Thermal Black

3.3.1 Laser Ablation of Carbon Thermal Black

Laser ablation of CTB was carried out in both positive-ion and negative-ion mode. Laser irradiance at 1064 nm wavelength was applied in these experiments. Two pulses, 230 microsceonds for the long-pulse mode and 8 nanoseconds for the Q-switch mode were used. The laser ablation experiment was started with very low laser power (~ 0.5 $kWcm^{-2}$) in the long-pulse mode and slowly increased to the maximum power of ~ 2 $MWcm^{-2}$. In the Q-switch mode, the laser power was varied between 1-2,300 $MWcm^{-2}$. Different size carbon clusters were observed within these power ranges.

Laser ablation of a pressed CTB sample produced positive-ion mass spectra shown in Figure 3-03 ~ 3-05. In Figure 3-03, the laser power used was ~160 $kWcm^{-2}$. Carbon

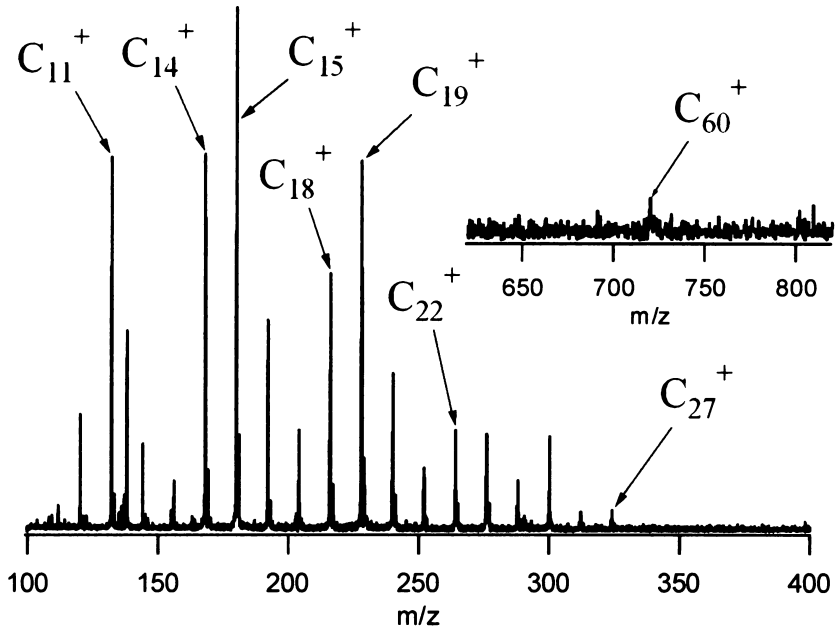

Figure 3-03 Positive-ion laser ablation FTICR mass spectrum of carbon thermal black at ~160 kWcm^{-2} (1064 nm, long pulse 230 μs).

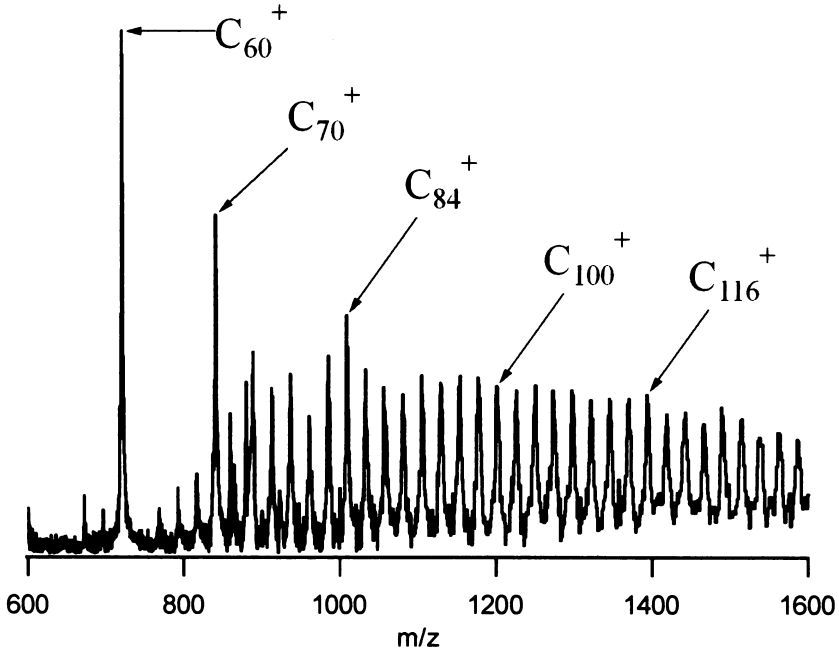

Figure 3-04 Positive-ion laser ablation FTICR mass spectrum of carbon thermal black at ~700 kWcm^{-2} (1064 nm, long pulse 230 μs).

cluster cations C_n^+ with n up to 27 could be observed in this mass spectrum. Close examination of this mass spectrum reveals that the laser power is close to the threshold energy for fullerene formation with only a small trace of C_{60}^+ observed (See figure 3-03, insert). Above this threshold energy, a broad range of fullerene ions are generated. Figure 3-04 shows fullerene ions are formed at a laser power density of ~700 $kWcm^{-2}$. C_{60}^+, C_{70}^+ and C_{84}^+ are the most abundant fullerene ions in this mass spectrum. This laser power is significantly lower than the laser power used for fullerene formation from graphite, which is generally on the order of many hundreds of $MWcm^{-2}$.

In the negative-ion mode, the 1064 nm laser ablation of CTB produced a range of small carbon cluster anions (See Figure 3-05). The number of carbon anions and the abundance of these ions can vary significantly with the laser power. No fullerene anions were observed over the available power range (0 ~ 2,300 $MWcm^{-2}$).

3.3.2 Laser Ablation of La_2O_3 Doped Carbon Thermal Black

Laser ablation experiments were also carried out with metal-doped CTB. A positive-ion laser ablation FTICR mass spectrum acquired at a laser irradiance of ~1,600 $kWcm^{-2}$ (1064 nm and 230 μs) is shown in Figure 3-06. The laser ablation target contained a mixture of La_2O_3 and CTB at a metal/carbon ratio of 1:50 (by weight). Although the base peak in the spectrum is assigned to the fullerene ion C_{60}^+, close inspection of the other peaks in this spectrum show that these consist of two series of peaks corresponding to the lanthanum carbon cluster ions and bare carbon cluster ions. Two series of cluster ions emerged from this mass spectrum with the first one, LaC_n^+, having two carbon atoms spacing between the peaks in the distribution (n is an even number between 44 and 98). The other series consists of positive-ion carbon clusters, C_n^+, of generally lower intensity (except for C_{60}^+ and C_{70}^+) and also with an m/z = 24 spacing

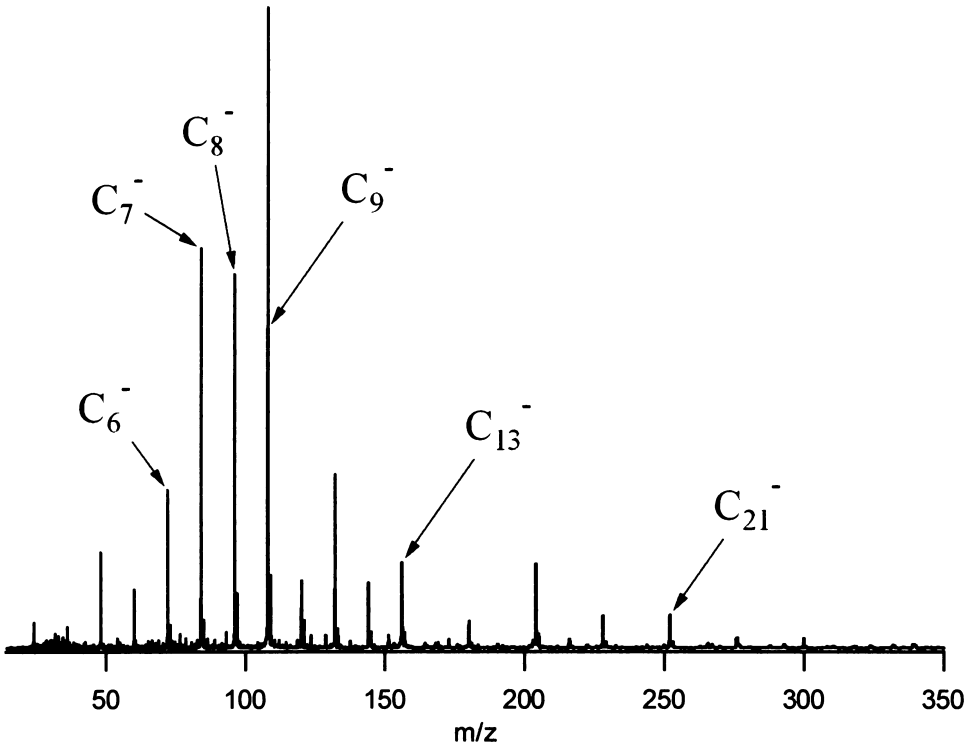

Figure 3-05 Negative-ion laser ablation FTICR mass spectrum of carbon thermal black at ~300 $kWcm^{-2}$ (1064 nm, long pulse 230 μs).

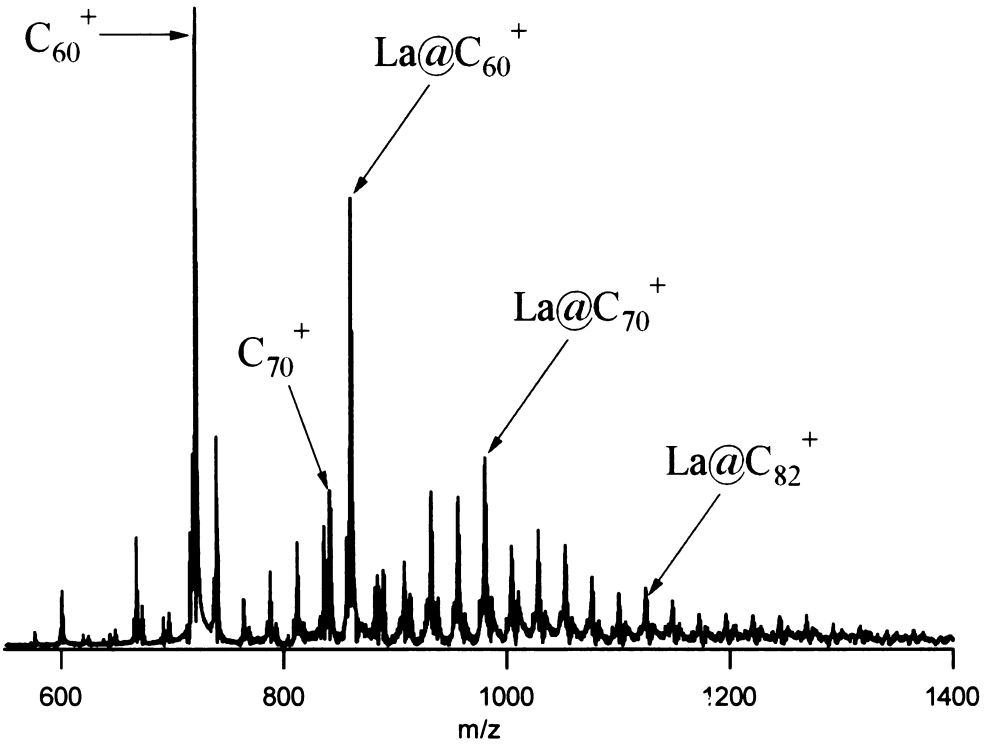

Figure 3-06 Positive-ion laser ablation FTICR mass spectrum of La_2O_3/CTB mixture at ~1,600 $kWcm^{-2}$ (1064 nm, long pulse 230 μs).

between peaks. The strongest metallofullerene ion peak is assigned as LaC_{60}^+ and confirmed by high-resolution mass measurements. LaO^+ and small amounts of La^+ were observed in the mass spectra acquired at lower m/z (not shown in this figure).

The detection of metallofullerene ions became increasingly difficult with successive laser shots at the same point on the sample. This was the same phenomenon as observed for fullerene ions from the laser ablation of pure thermal black. The ion signal diminished after repeated laser ablation at same energy and a higher energy laser pulse was required to regenerate the metallofullerene ion signal. This phenomenon made generation and isolation of ions in the ICR cell difficult and consequently hard to ascertain whether LaC_{60}^+ was either an endohedral or an exohedral fullerene. Previous CID and ion/molecule reaction studies using FTICR mass spectrometry on related metallofullerenes tend to suggest that these ions are most likely endohedral metallofullerenes.[35,36]

3.4 Mass Spectrometry Studies of Pyrolysed KCT-Pitch

3.4.1 Characterization of KCT-Pitch Pyrolysis Residues

KCT-pitch pyrolysis residues were collected at different temperatures in order to optimize the effect of this carbonaceous material for fullerene and metallofullerene production. Table 3-01 shows the yield and chemical compositions of pyrolysed KCT-pitch residues generated over the temperature range 200 - 600 °C. Note that the chemical analysis was only carried out for the 200 °C, 400 °C and 600 °C residues. The carbon to hydrogen ratio increases with temperature due to the carbonization of KCT-pitch. Pyrolysis temperature above 600 °C resulted in KCT-pitch weight loss over 80%. The material collected from the condensation of the evaporated KCT-pitch is a tar-like mixture which is presumably composed of various low molecular weight hydrocarbons.

Table 3-01. Measured chemical compositions of pyrolysed KCT-pitch residues

T(°C)	Residue (%)	C (%)	H (%)	N (%)
200	89.7	93.05	4.54	1.16
300	76.4	-	-	-
400	64.2	94.04	4.56	1.15
500	48.5	-	-	-
600	12.0	94.30	3.14	0.85

The KCT-pitch pyrolysis residues were analysed by laser desorption time-of-flight mass spectrometry. Figure 3-07 shows the positive-ion LD-TOF mass spectrum of the 450 °C KCT-pitch residue. A broad range of PAHs is detected but there are no fullerene or metallofullerene ions observed. The PAHs ions in this spectrum have a mass range of m/z = ~200 - ~600 and appeared with even or odd carbon numbers. The number of hydrogen atoms in these PAHs varies with the degree of unsaturation. For example, $C_{22}H_{14}^+$, $C_{23}H_{15}^+$ and other PAHs are observed with the number of carbon atoms up to ~50. Smaller PAHs are possibly lost in the original pyrolysis of the KCT-pitch.

FTICR mass spectrometry was also used to characterize pyrolysed KCT-pitch. Figure 3-08 is a positive-ion GSALDI-FTICR mass spectrum of the KCT-pitch pyrolysis residue (450 °C). A wide range of PAHs that are similar but larger than those observed in the LD-TOF-MS experiment, is observed in this spectrum. Again in this experiment there are no obvious traces of fullerene or metallofullerene ions. The PAHs detected in this experiment have a mass range of m/z = ~200 - ~900 and also appeared with even or odd numbers of carbons. Their corresponding hydrogen atom numbers vary with the degree of unsaturation. In Figure 3-08 ions such as $C_{60}H_{28}^+$ can be

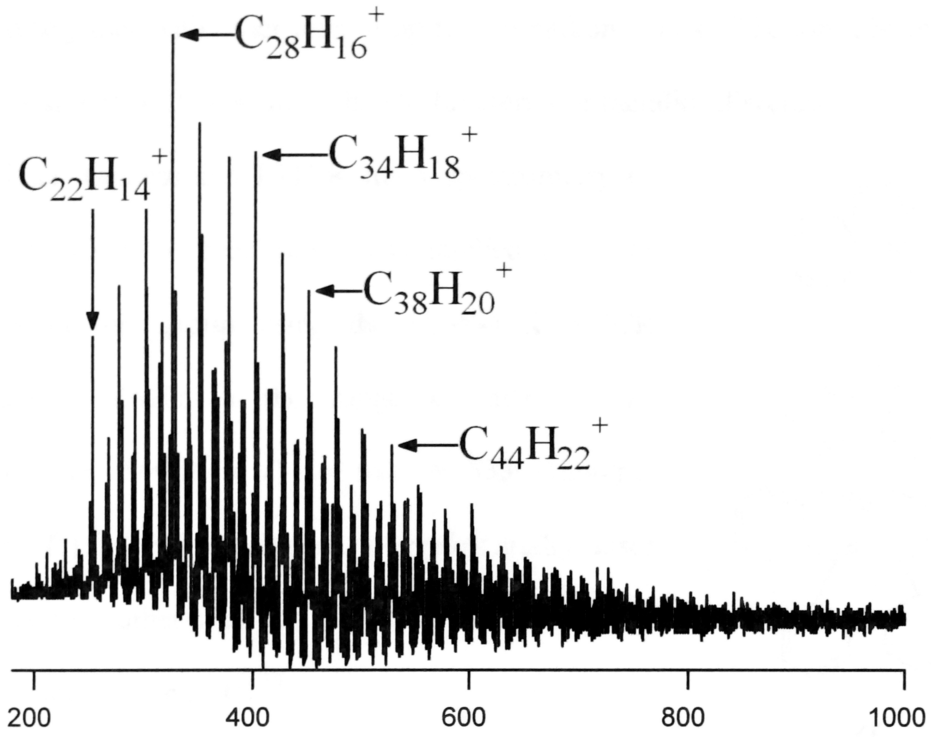

Figure 3-07 Positive-ion laser desorption time-of-flight mass spectrum of pyrolysed KCT-pitch (450 °C).

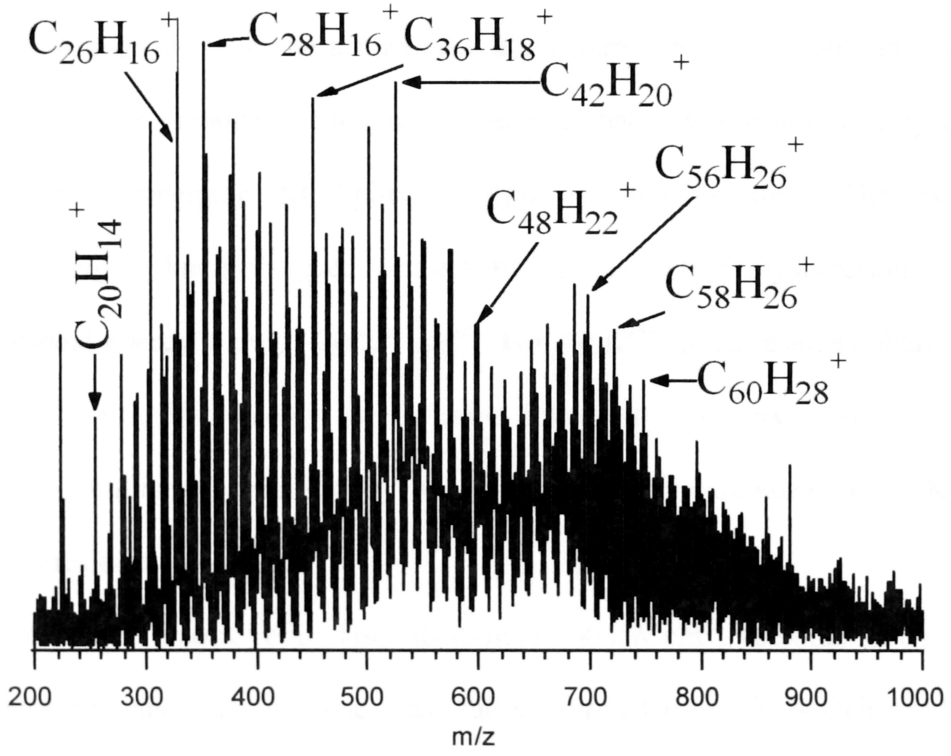

Figure 3-08 Positive-ion GSALDI-FTICR mass spectrum of pyrolysed KCT-pitch (450 °C) at a laser power density of ~200 $MWcm^{-2}$ (1064 nm, Q-switch 8 ns).

observed together with other ions of up to ~70 carbon atoms. The ions above m/z 700 are best assigned to PAHs rather than to fullerenes or metallofullerenes.

Direct laser vaporization FTICR mass spectrometry of selected PAHs have been previously studied by other members in this group using the CMS-47X FTICR instrument. PAHs in the range of m/z = 178 (phenanthrene, *Structure I*) to m/z = 533 (rubrene, *Structure II*) have been shown to preferentially laser desorb as $M^{+\cdot}$ rather than as $[M+Na]^+$, even when the sample is doped with NaCl.[19]

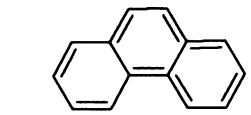

I

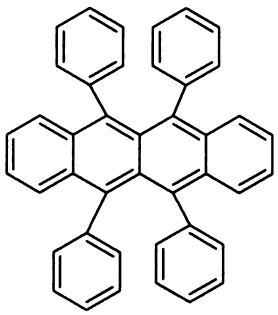

II

3.4.2 Laser Ablation of Pyrolysed KCT-Pitch

The laser ablation FTICR mass spectrometry shows that raw KCT-pitch can produce fullerene ions at a minimum laser energy of ~ 100 kW cm^{-2} (1064 nm, 230 μs). This threshold energy for fullerene formation is about three orders of magnitude lower than that required for graphite. It has been observed that this threshold energy decreases when higher temperature KCT-pitch pyrolysis residues are used. The lowest laser ablation energy value is observed for the 450 °C KCT-pitch pyrolysis residue, for which the threshold energy is only ~20 kW cm^{-2}. For the KCT-pitch residues obtained above 500 °C, the threshold energy for fullerene formation is observed to increases very rapidly, which may be caused by a higher degree of carbonization in KCT-pitch pyrolysis residue.

Figure 3-09 is a positive-ion laser ablation (1,700 kW cm^{-2}, 1064 nm, 230 μs) FTICR mass spectrum showing fullerene ions that are formed from KCT-pitch residues. An expansion of the spectrum between m/z = 200 and 700 is shown in Figure 3-09*a*. C_{60}^+

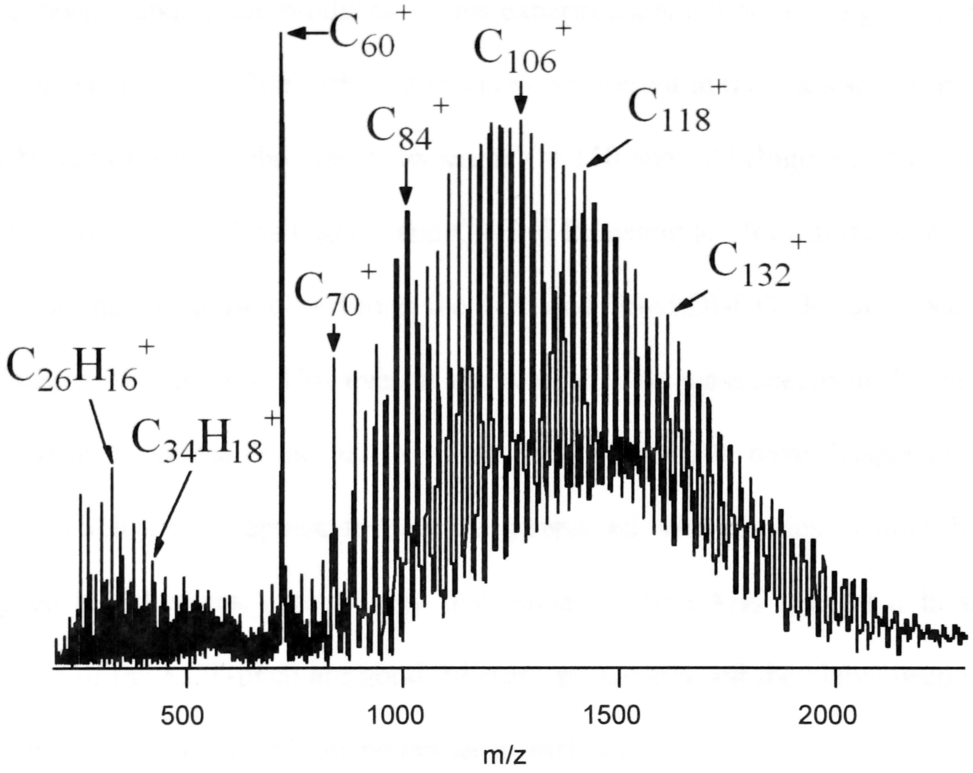

Figure 3-09 Positive-ion laser ablation FT/ICR mass spectrum of pyrolysed KCT-pitch (450 °C) at laser power density of ~700 kWcm^{-2} (1064 nm, long pulse 230 μs).

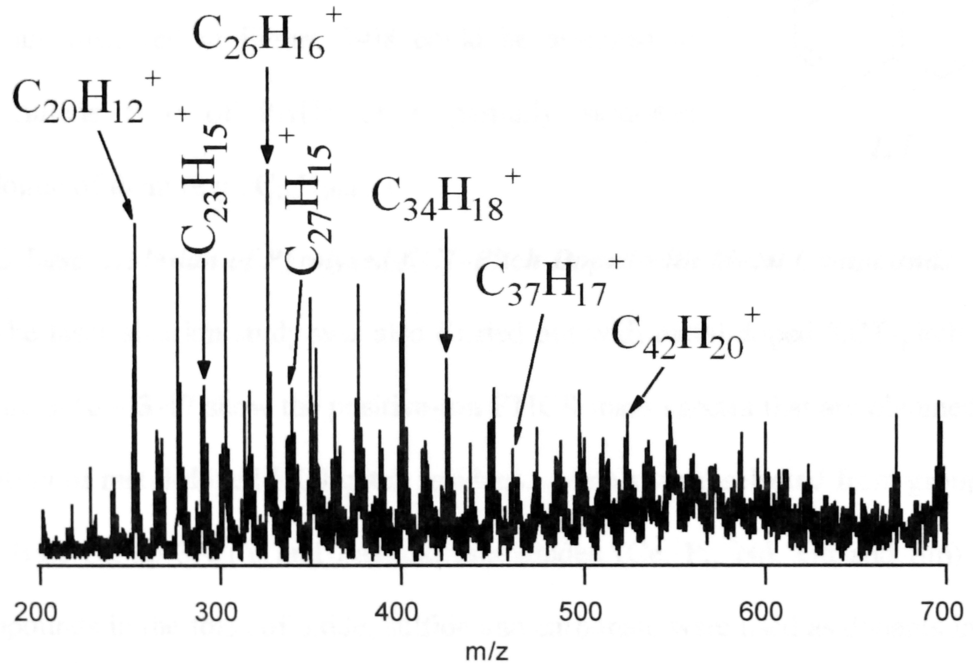

Figure 3-09a Expanded mass region of m/z 200 ~ 700 of Figure 3-09.

is the most abundant ion produced in this experiment and a broad range of higher mass fullerene ions of up to 200 carbon atoms are also present in the mass spectrum. Another distribution of ions is observed between m/z = 150 and 500 (Figure 3-09*a*) that can be assigned to PAHs such as $C_{26}H_{16}^{+}$ and $C_{27}H_{17}^{+}$ for example. Ions in this distribution are similar in mass to those observed in the TOF and GSALDI-FTICR mass spectra shown in Figure 3-07 and 3-08. However, in the laser ablation mass spectrum shown in Figure 3-09, what is noticeable is that the PAHs near m/z = 700 have disappeared or have reduced intensity and appear to have been replaced with a series of ions that can be assigned to fullerenes. It is likely that some of the PAHs generated in the initial pyrolysis of the KCT-pitch are good fullerene precursors and they have been converted into fullerenes by a kind of low power laser 'fusion'.

For example, corranulene, $C_{20}H_{10}$ (*Structure **III***), has a bowl shaped structure with a five-member carbon ring surrounded by five six-member carbon rings. Many ions that are observed in Figure 3-08 could be assigned to corranulene type of PAHs or a partially saturated analogue of them (e.g., $C_{20}H_{10\text{-}14}^{+}$).

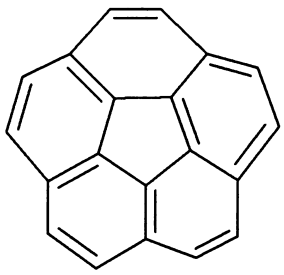

III

3.4.3 Laser Ablation of Pyrolysed KCT-Pitch Doped with Metal Compounds

The laser ablation study was also carried out with metal-doped KCT-pitch residues. Figure 3-10 ~ 3-17 show the positive-ion FTICR mass spectra that are obtained by laser ablation of metal-doped KCT-pitch residues. Metals were selected from group 2A (Ca and Ba), Group 3A (Y and La) and lanthanides (Ce, Pr, Nd, Gd and Sm). Metal compounds in the form of oxide, sulfide and carbonate were used as dopants in order to study their effect in the formation of metallofullerenes.

3.4.3.1 Pyrolysed KCT-Pitch Doped with CaO or $BaCO_3$

Among the group 2A metals, Ca and Ba were selected for the study of metallofullerenes. Figure 3-10 shows a positive-ion laser ablation FTICR mass spectrum of CaO doped KCT-pitch pyrolysis residue (450 °C). C_{60}^+ is assigned to the base peak in this mass spectrum with $Ca@C_{50}^+$, $Ca@C_{60}^+$ and C_{70}^+ present as the other major ions. A series of fullerenes ions are present in the high-mass region and are accompanied by a small amount of calcium-fullerenes. It is observed in the laser ablation experiments that the relative intensities of the carbon fullerenes and calcium-fullerenes remain almost unchanged under different laser ablation conditions. Calcium-fullerenes have been previously studied by Rose under similar conditions using a carbonaceous material coorongite as the carbon percursor.[37,38] Calcium was naturally occurred in these materials. Other Group 2A metals such as Sr and Ba were also studied by Rose using the laser ablation method, both strontium-fullerenes and barium-fullerenes were observed by FTICR mass spectrometry.[36]

In this present study, barium is also investigated by laser ablation using pyrolysed KCT-pitch as the carbon precursor. Figure 3-11 shows a positive-ion laser ablation FTICR mass spectrum of KCT-pitch containing barium salt, $BaCO_3$. Unlike the calcium-fullerenes presented in Figure 3-10 that are the minor ions, in Figure 3-11, the barium-fullerene ions appear as the predominant species. Two series of peaks are assigned to fullerene and barium-fullerene ions respectively. $Ba@C_{60}^+$ is assigned to the base peak in this mass spectrum with $Ba@C_{44}^+$, C_{60}^+, $Ba@C_{50}^+$, $Ba@C_{70}^+$ and $Ba@C_{82}^+$ assigned to other peaks in the spectrum. Most of the low intensity peaks are assigned to fullerene ions.

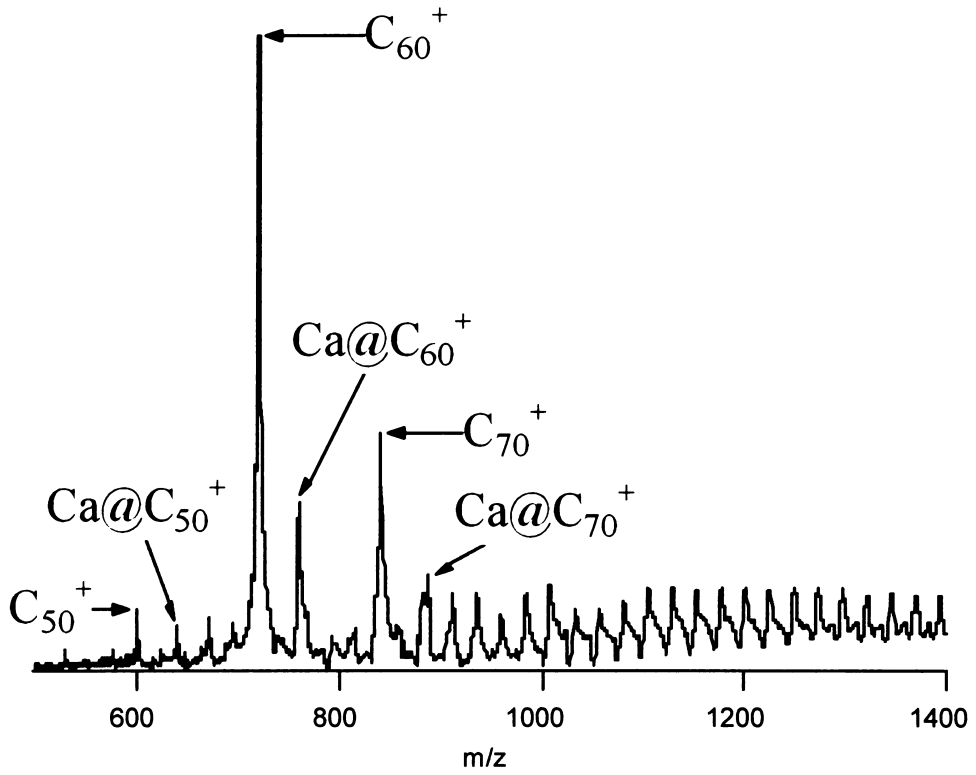

Figure 3-10 Positive-ion laser ablation FTICR mass spectrum of pyrolysed KCT-pitch (450 °C) doped with CaO at a laser power energy of ~ 500 $kWcm^{-2}$ (1064 nm, long pulse 230 μs).

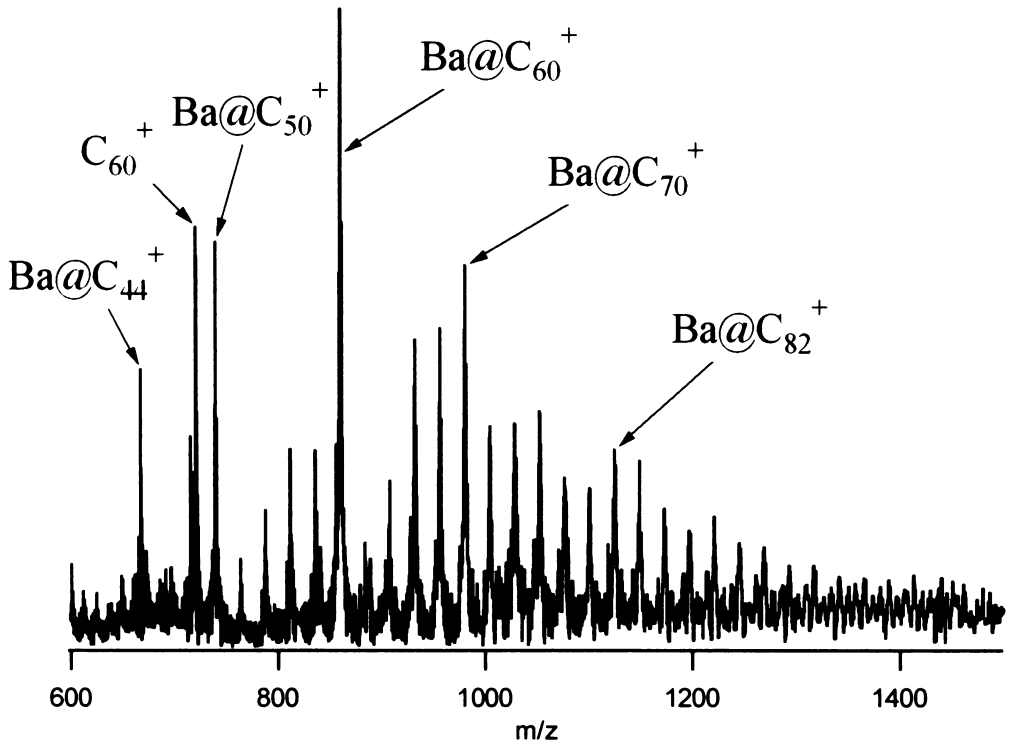

Figure 3-11 Positive-ion laser ablation FTICR mass spectrum of pyrolysed KCT-pitch (450 °C) doped with $BaCO_3$ at a laser power energy of ~500 $kWcm^{-2}$ (1064 nm, long pulse 230 μs).

3.4.3.2 Pyrolysed KCT-Pitch Doped with Y_2O_3 or Ln_2O_3/Ln_2S_3 (Ln=La, Ce, Pr, Nd, Gd and Sm)

Group IIIB metals have been the focus of endohedral metallofullerenes studies since the first metallofullerenes report by Smalley and coworkers.[5] Among these endohedral metallofullerenes, scandium-, yttrium- and lanthanum-fullerenes have been mostly studied. Much attention has been paid to scandium-fullerenes due to the fact that several multi-metal encapsulated scandium-fullerenes have been purified. These include, $Sc_2@C_{82}$, $Sc_3@C_{82}$, $Sc_2@C_{84}$, $Sc_2@C_{86}$, and a scandium dicarbide endohedral metallofullerene $(Sc_2C_2)@C_{86}$.[39] Spectroscopic analysis includes, C^{13}-NMR,[40,41] ESR or EPR,[42-44] far- and mid-infrared,[45] synchrotron X-ray diffraction[46] and high resolution ion-mobility measurements[47] have been carried out on these molecules.

Unlike the fullerenes where C_{60} and C_{70} are observed to be the most stable species in the series, endohedral metallofullerenes show different stabilities, with $M@C_{82}$ observed to be the most stable and extractable molecule of the series.

Similar to the study of calcium- and barium-fullerenes, the laser ablation FTICR mass spectrometry shows that, by using KCT-pitch residues, group IIIB metals and the lanthanides readily produce metallofullerenes ions by laser ablation. These experiments were carried out under same conditions in terms of sample composition and laser ablation energy. Figure 3-12 shows that yttrium-fullerene ions are formed along with fullerene ions. C_{60}^+ is assigned to the base peak in this spectrum with $Y@C_{60}^+$ and C_{70}^+ appear in similar abundance. A trace of diyttrium fullerenes ions such as $Y_2@C_{84}^+$ is also observed in this spectrum. In Figure 3-13, lanthanum-fullerene ions are the major species in the mass spectrum with $La@C_{60}^+$ is observed to be the most abundant ion.

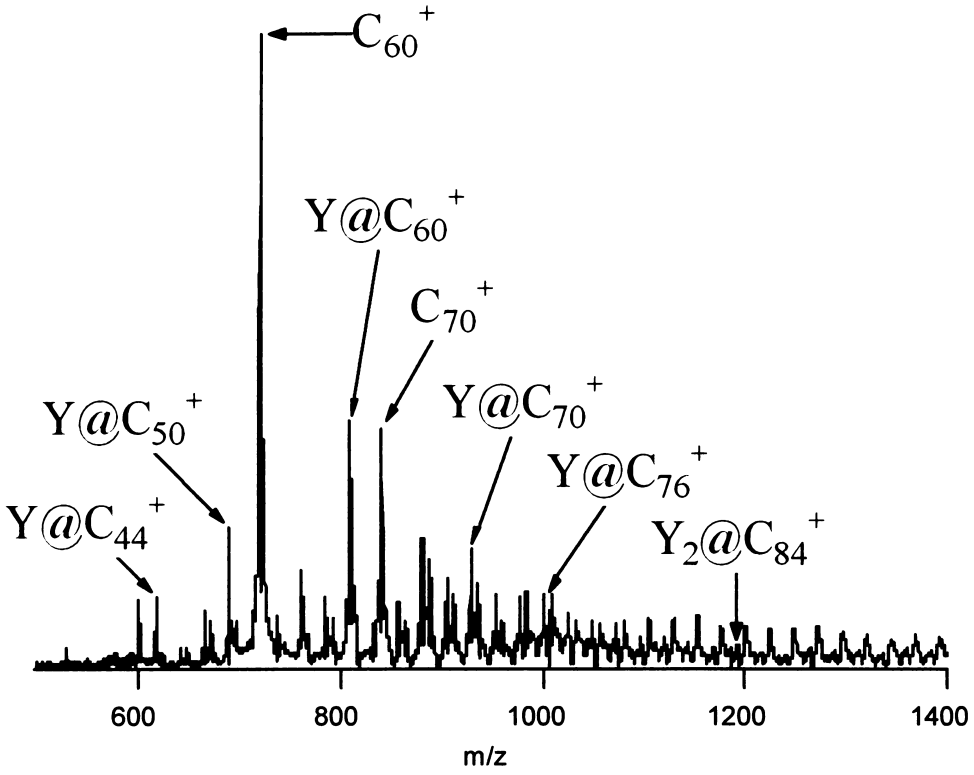

Figure 3-12 Positive-ion laser ablation FTICR mass spectrum of pyrolysed KCT-pitch (450 °C) doped with Y_2O_3 at a laser power density of ~700 $kWcm^{-2}$ (1064 nm, long pulse 230 μs).

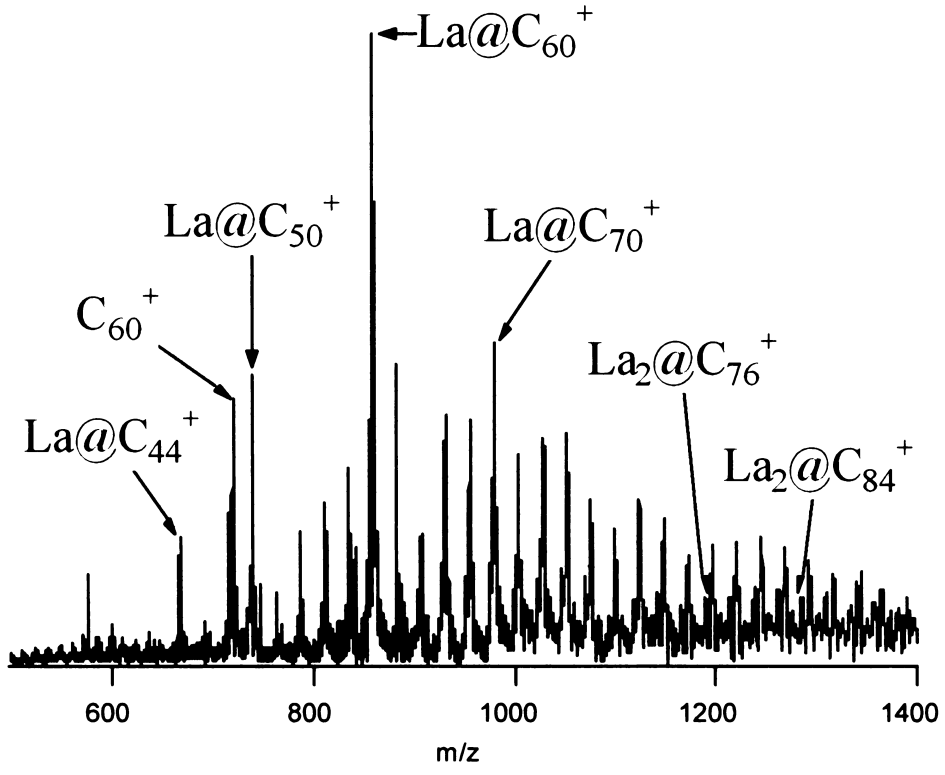

Figure 3-13 Positive-ion laser ablation FTICR mass spectrum of pyrolysed KCT-pitch (450 °C) doped with La_2O_3 at a laser power density of ~700 $kWcm^{-2}$ (1064 nm, long pulse 230 μs).

Note C_{60}^+ is not the predominant ion this spectrum. Dilanthanum fullerene ions are also present in this mass spectrum and begin with $La_2@C_{74}^+$.

Lanthanide metals are expected to show similarities in the formation of endohedral metallofullerenes because these they all have similar electronic structures and ionic radius. The laser ablation experiments carried out with some of the lanthanide metals have produced very similar species. Figure 3-14 ~ 3-17 show that metallofullerene ions containing Ce, Pr, Nd and Sm metals are assigned in LA-FTICR mass spectra.

For the mass spectra shown in Figure 3-12 ~ Figure 3-17, the laser energy used in the formation of endohedral metallofullerenes from KCT pitch residues is about 700 $kWcm^{-2}$, which is much lower than that required for graphite (on the order of hundreds of $MWcm^{-2}$). This can be explained if fullerenes or endohedral metallofullerenes are formed by dehydrogenation and annealing of large polycyclic aromatic hydrocarbons - the major constituents in KCT pitch pyrolysis residues. Higher energy is needed for graphite or carbon thermal black to break the C-C bonds in the massive graphitic hexagonal carbon sheets in order to produce small carbon clusters that are the precursors for fullerenes.

Ion mobility mass spectrometry experiments have shown that laser ablation of metal oxide/graphite mixtures generate a variety of LaC_{60}^+ isomers including some in which the lanthanum atom appears to be bound to polycyclic polyene rings. Upon heating (annealing) it was found that nearly all the different ring isomers converted spontaneously into metallofullerenes with an endohedral lanthanum which suggests that the lanthanum atom acts as a nucleation center and the carbon rings arrange themselves around the lanthanum before converting into a fullerene cage.[48-50] Given that large PAHs with up to 70 ~ 80 carbon atoms are present in the pyrolysed KCT-pitch sample

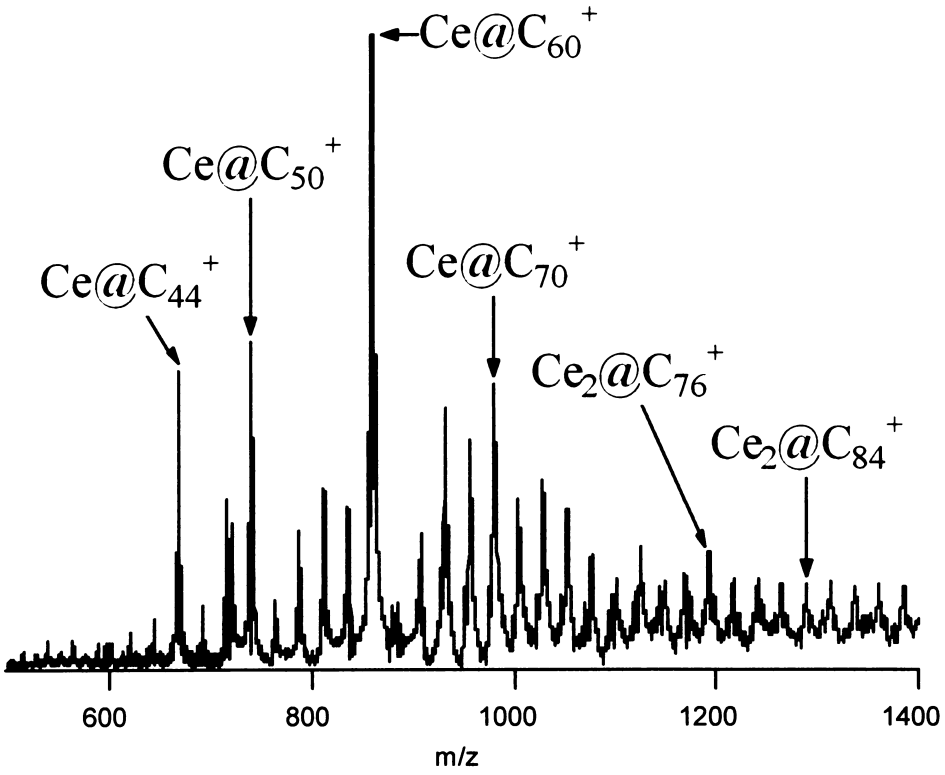

Figure 3-14 Positive-ion laser ablation FTICR mass spectrum of pyrolysed KCT-pitch (450 °C) doped with Ce_2O_3 at a laser power density of ~700 $kWcm^{-2}$ (1064 nm, long pulse 230 μs).

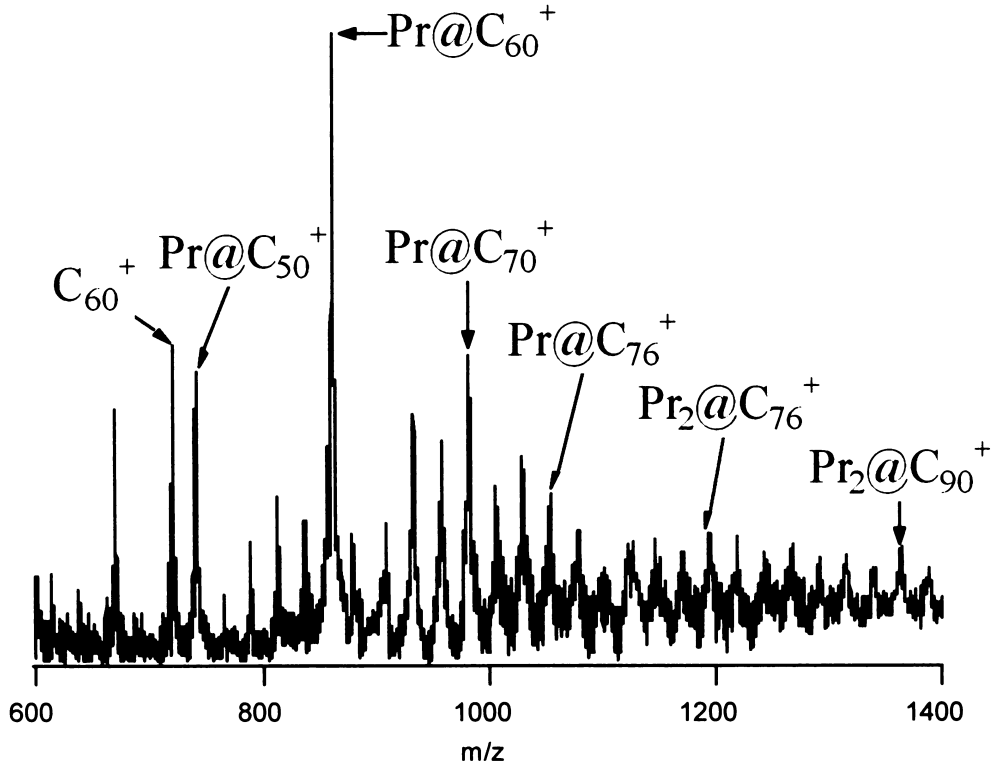

Figure 3-15 Positive-ion laser ablation FTICR mass spectrum of pyrolysed KCT-pitch (450 °C) doped with Pr_2O_3 at a laser power density of ~700 $kWcm^{-2}$ (1064 nm, long pulse 230 μs).

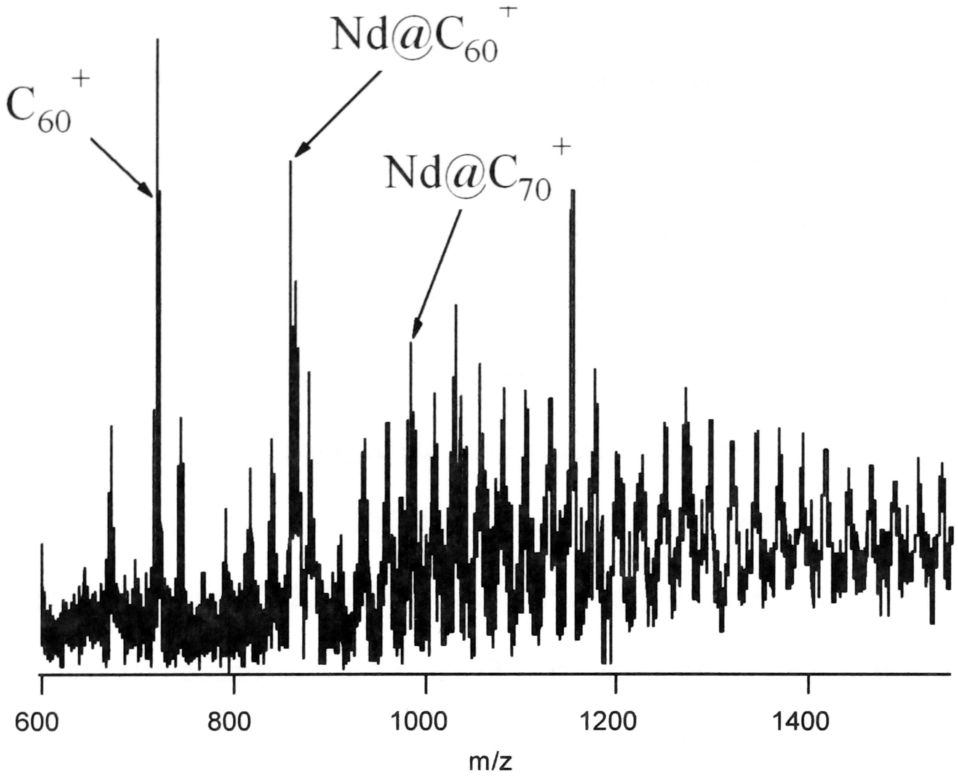

Figure 3-16 Positive-ion laser ablation FTICR mass spectrum of pyrolysed KCT-pitch (450 °C) doped with Nd_2O_3 at a laser power density of ~700 $kWcm^{-2}$ (1064 nm, long pulse 230 μs).

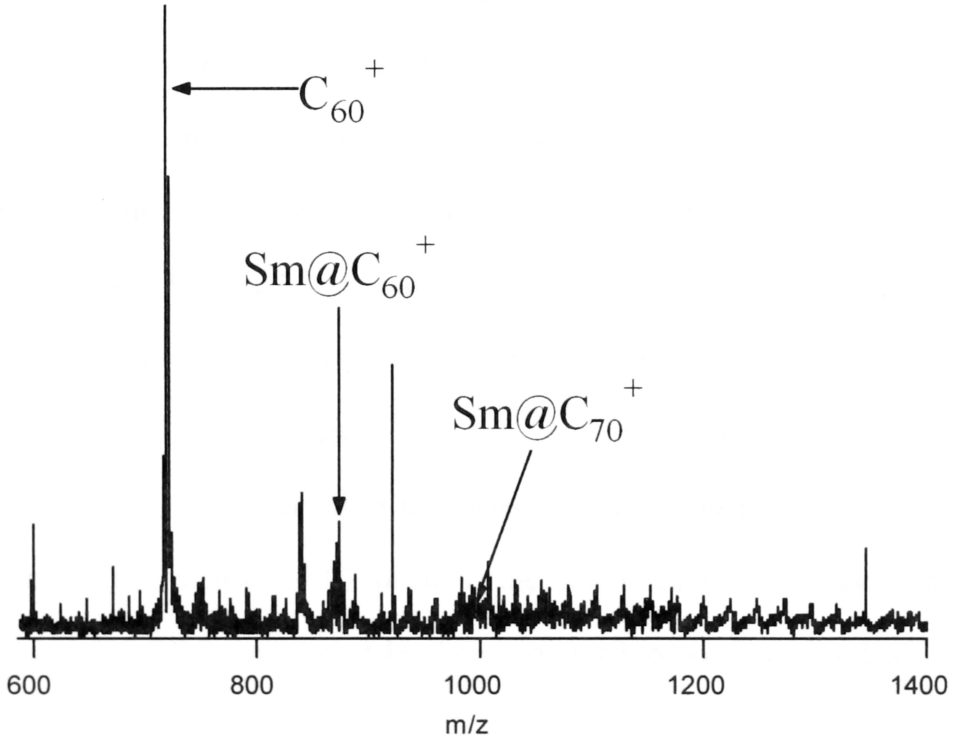

Figure 3-17 Positive-ion laser ablation FTICR mass spectrum of pyrolysed KCT-pitch (450 °C) doped with Sm_2O_3 at a laser power density of ~700 $kWcm^{-2}$ (1064 nm, long pulse 230 μs).

(Figures 3-07 and 3-08), if metal oxide or metal sulfide is reduced then only low laser powers might be expected to generate endohedral metallofullerenes.

An important observation made in the present laser ablation studies is that the laser pulse-width has a dramatic effect in metallofullerene formation. Metallofullerene ions were only formed with long-pulse (230 μs, 200-2,000 kW cm^{-2}) laser ablation of KCT-pitch pyrolysis residues containing metal compounds. When the Q-switch (8 ns) mode was used for laser ablation, metallofullerene ions were not observed over any of the available power densities (1-2,300 MW cm^{-2}) although, in some cases, fullerene ions were generated. By comparison, when the Q-switch laser power density was set close to the upper limit of the long-pulse laser power density range (~ 2,000 kW cm^{-2}), there were no ions observed. This last observation suggests that in such laser ablation experiments, the laser pulse width rather than the laser power density is a key variable for gas-phase endohedral metallofullerene formation.

Besides the difference between the Q-switch and long-pulse laser ablation that is observed at the high m/z end in the mass spectra, there are also differences in the spectra at the low m/z end, in particular, the observation of small metal-carbide cluster ions. For example, Figures 3-18*a* shows a low m/z region of a positive-ion laser ablation FTICR mass spectrum (Q-switch, 1064 nm, 500 MW cm^{-2}) of a 450 °C pyrolysed La_2O_3 / KCT-pitch residue. La^+, LaO^+ and small lanthanum carbon cluster ions, LaC_n^+, (n=2-10) are observed in this mass spectrum, together with some PAHs ions that may be the residues of KCT-pitch. In the experiment when the laser is used in the long-pulse mode, the same target has been observed to produce only LaO^+ in the low m/z region.

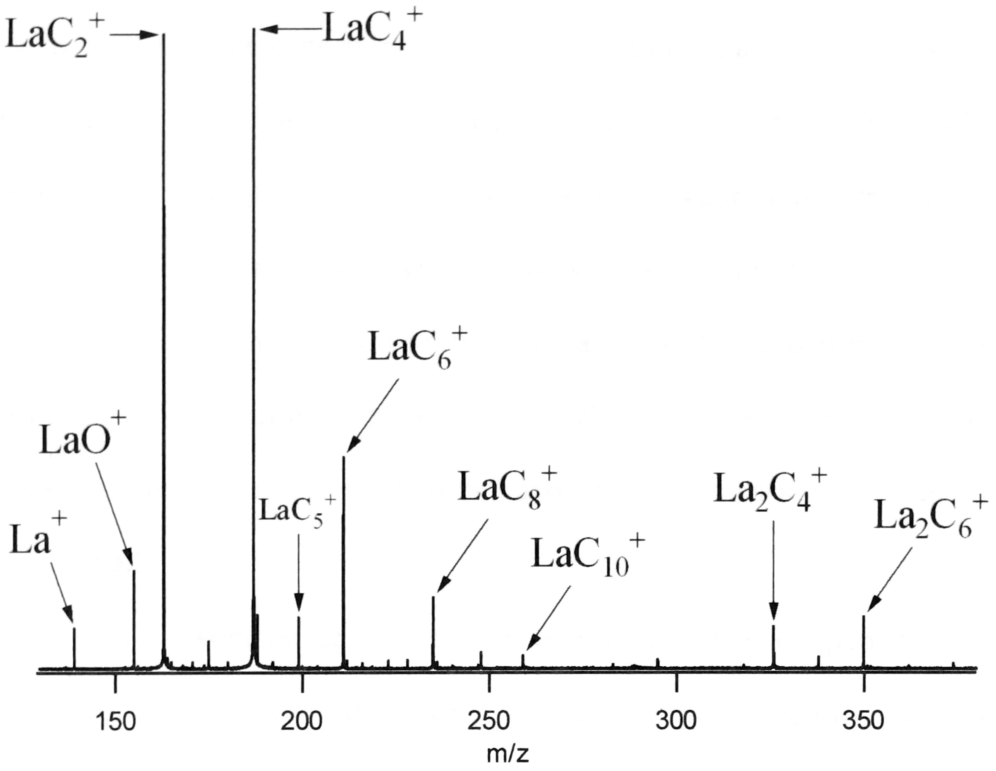

Figure 3-18a Positive-ion laser ablation (1064 nm, long pulse 230 μs) FTICR mass spectrum of pyrolysed KCT-pitch (450 °C) doped with La_2O_3 at a laser power density of ~500 $MWcm^{-2}$ (m/z 130 ~ 380).

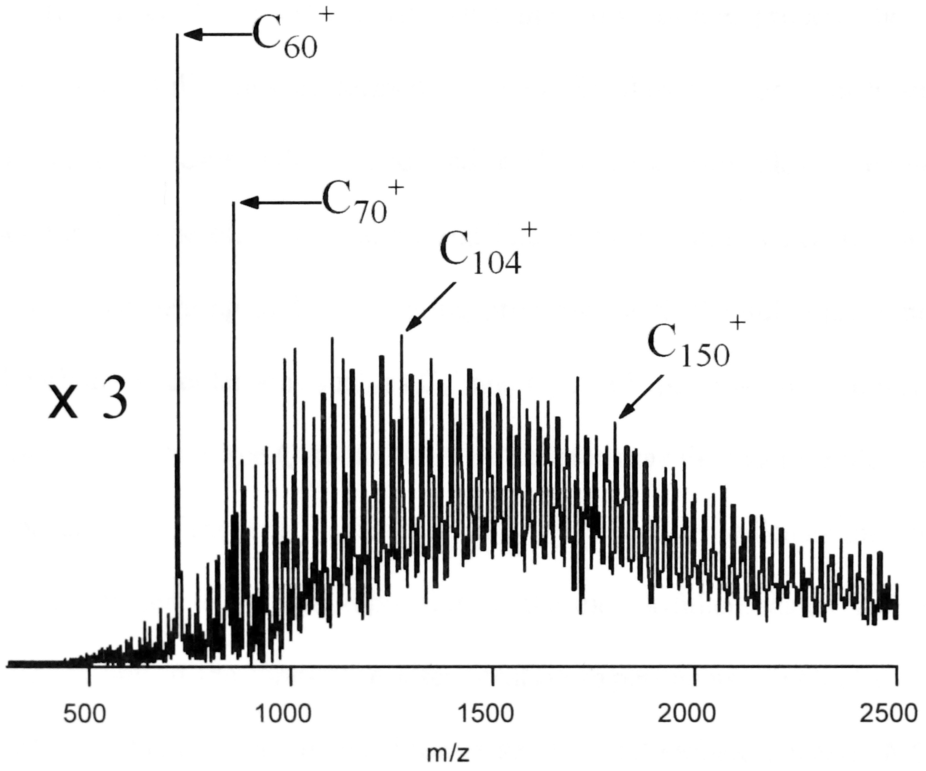

Figure 3-18b Positive-ion laser ablation (1064 nm, long pulse 230 μs) FTICR mass spectrum of pyrolysed KCT-pitch (450 °C) doped with La_2O_3 at a laser power density of ~500 $MWcm^{-2}$ (m/z 400 ~ 2500).

In Figure 3-18*a*, the lanthanum carbide ions with even numbers of carbon atoms are more abundant than those with odd numbers of carbon atoms. Small dilanthanum carbon cluster ions $La_2C_m^+$ (m = 4 - 8) also appear in this part of the mass spectrum.

The high m/z section of the mass spectrum is shown in Figure 3-18*b*. Only fullerene ions are observed in this mass spectrum. Metallofullerene ions were not observed at any of the Q-switch laser powers. In the Q-switch laser power range (2 ~ 2,300 $MWcm^{-2}$), these fullerene ions appeared with variable peak intensities and are often not observed at all.

Láska and co-workers reported that surface vaporization of graphite in the laser ablation process is determined not only by the laser power density, but also by the duration of laser interaction with the target material.[51] One consequence of a longer laser pulse (μs) when compared to a Q-switch pulse (ns) is that a larger amount of evaporated material is produced and with the slow cooling process the large carbon clusters such as fullerenes are formed. Curl and Smalley have previously suggested that C_{60} appears to result when vaporized carbon condenses slowly enough at high temperature.[52] The effect of a short and intense laser pulse is that the target material undergoes fast heating and fast cooling processes with the subsequent production of small carbon molecular ions such as C_2^+ and C_3^+. It is possible that the fast heating and fast cooling effects of the Q-switch laser pulse interrupts the metallofullerene formation. The appearance of the small lanthanum-carbon cluster ions indicates that these ions are most likely linked to the decomposition of the metallofullerenes as such ions are not observed in any of the long-pulse laser ablation experiments which also clearly ablate the surface at high temperatures. Similar small metal carbide clusters, MC_x^+ (M= La, Gd; x = 2-10), have been observed in high-energy collisions (160 keV) of LaC_{82}^+ and

GdC_{82}^+ with target atoms such as H_2 and Ne.[53] In these experiments a range of fullerene ions was also observed. These observations suggest that the bonding in the small metal carbides may hold important clues for understanding the formation and growth mechanism of the endohedral metallofullerenes. It also implies that long-pulse laser irradiation may be advantageous for fullerene or metallofullerene production while the Q-switched short pulse high-power laser is more advantageous for the formation of small carbon or metal carbide clusters.

3.4.3.3 Pyrolysed KCT-Pitch Doped with Nb_2O_5 or Ta_2O_5

As a general conclusion from many endohedral metallofullene studies that have been reported, the formation of endohedral metallofullerenes is known to be metal-selective. This selectivity reflects the intrinsic difference among the metallic elements in the periodic table in terms of their bonding characters. Besides the metals that have been discussed above, several metals from other groups in the periodic table (Nb, Ta, Mn, Fe, Co, Ni, Cu and Zn) were also studied by laser ablation experiments. Among these metals, only Nb and Ta are observed to form metal-carbon cluster ions, therefore, the following discussion will be focused on the niobium-carbon clusters and tantalum-carbon cluster ions.

Figure 3-19 is a positive-ion FTICR mass spectrum of laser ablation of carbon thermal black containing Nb_2O_5. Niobium-carbon cluster ions, $Nb_xC_y^+$ (x= 0-8, y=0-12) are observed in this mass spectrum with Nb^+ is assigned to the base peak. Unlike the small lanthanum-carbon clusters that were discussed in the previous section (see discussion on Figure 3-18a), these niobium-carbon clusters do not show the intensity alternation between the even and odd carbon number clusters. The most abundant group of cluster ions is assigned to the $Nb_4C_y^+$, where y ranges from 0 to 7. The

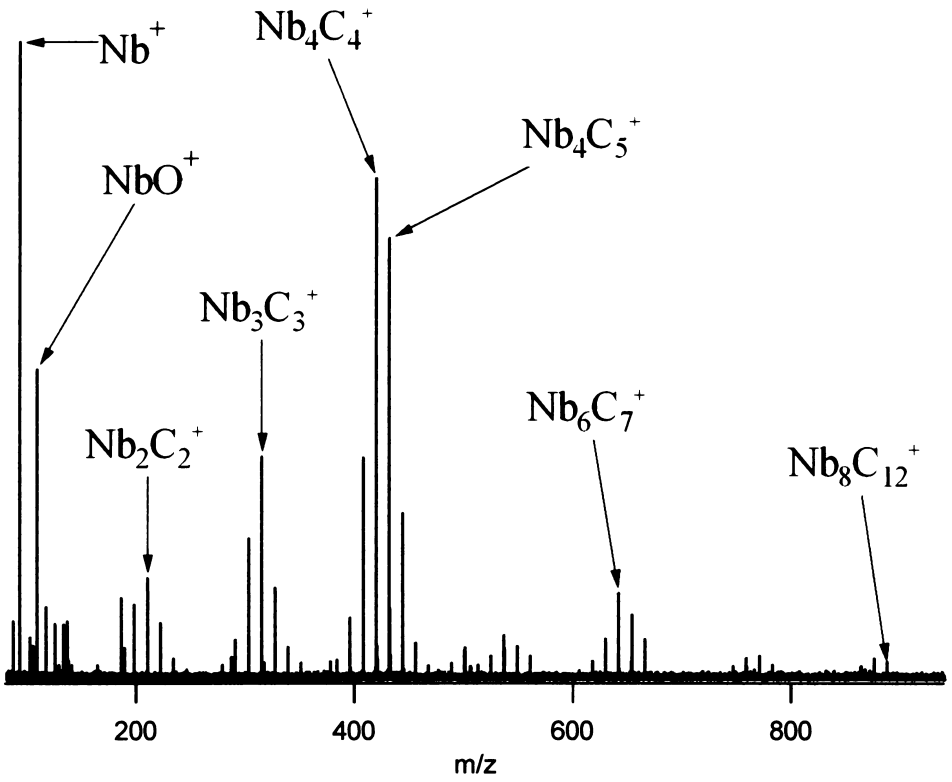

Figure 3-19 Positive-ion laser ablation FTICR mass spectrum of Nb_2O_5/carbon thermal black (atomic ratio 1:1) at a laser power density of 500 $kWcm^{-2}$ (1064 nm, long pulse 230 μs).

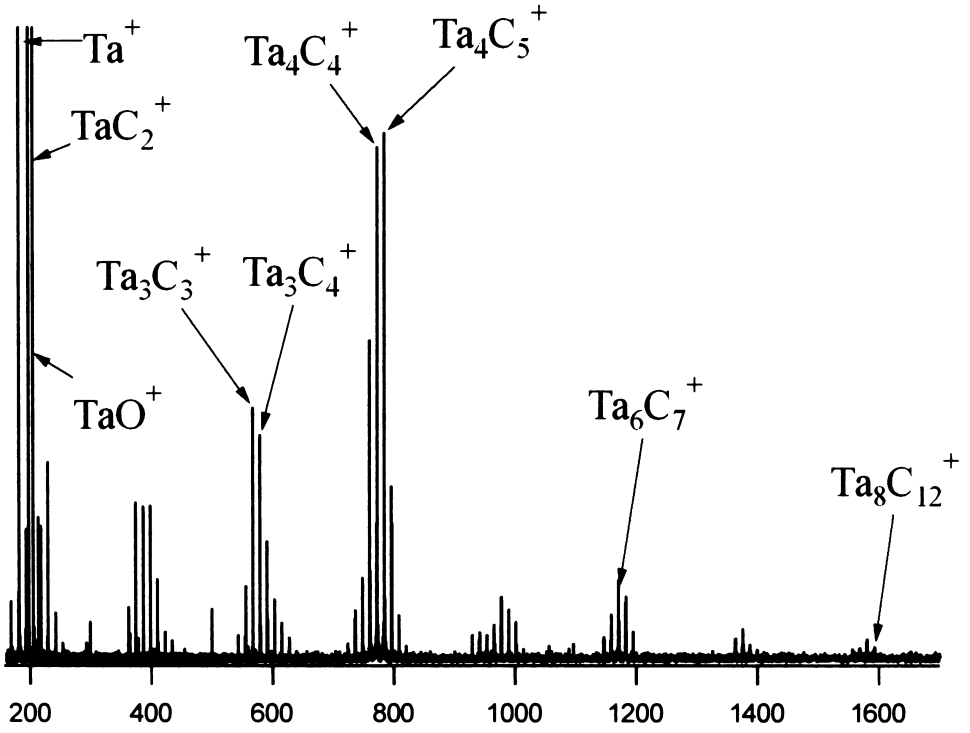

Figure 3-20 Positive-ion laser ablation FTICR mass spectrum of Ta_2O_5/graphite (atomic ratio 1:1) at a laser power density of 700 $kWcm^{-2}$ (1064 nm, long pulse 230 μs).

formation of these clusters requires a high metal concentration in the target; a niobium/carbon atomic ratio of 1:1 (by weight) is used. With low metal concentration, for example < 5%, only Nb^+ and sometimes fullerene ions were observed. Various carbonaceous materials including graphite, carbon thermal black, kerogen and pyrolysed KCT-pitch have been used in the laser ablation studies, and similar cluster patterns are observed in these experiments. The laser energy was optimized for the ion production with different carbonaceous materials. Carbonaceous material with high contents of PAHs also show a wide range of PAHs ions in the mass spectrum that are sometimes interfere with the observation of metal-carbon clusters.

Figure 3-20 is a positive-ion FTICR mass spectrum obtained by laser ablation of graphite containing Ta_2O_5. $Ta_xC_y^+$ (x= 0-8, y=0-13) cluster ions are observed in this mass spectrum. It shows a similar cluster pattern to that observed for $Nb_xC_y^+$ clusters. In this case, the Ta^+, TaO^+ and TaC_2^+ are the most abundant ions with $Ta_4C_y^+$ (y = 0 - 7) being the most abundant group of tantalum-carbon cluster ions.

An important observation from both mass spectra, as shown in Figure 3-19 and Figure 3-20, is the low abundance of the cluster ions $Nb_8C_{12}^+$ and $Ta_8C_{12}^+$. According to the reports by Castleman, Duncan and coworkers, metal-carbon clusters $M_8C_{12}^+$ (M= Ti, Zr, Hf, V and Nb), the so-called metallocarbohedrenes or metcars are expected to be very stable and show outstanding abundance in the mass spectra obtained in the pulsed-molecular-valve TOF experiments.[54] Also, tantalum was excluded in their reports and tantalum-carbon clusters Ta_xC_y with only x= 4 and y= 8 have been reported so far. In contrast, this current LA-FTICR-MS study tends to suggest that $M_8C_{12}^+$ are not unique species and tantalum is also capable of forming this type of clusters. What is different between the experiments carried out by the Castleman or Duncan groups and the present

work is that the metal-carbon clusters were generated using very different methods. While the direct laser ablation method is adopted by this current study, the experiments carried out by the Castleman or Duncan groups were accomplished by ion-molecule reactions between the supersonically cooled laser ablated metal ions and gaseous alkanes such as methane. It is possible that the metal-carbon clusters observed in the current experiments may have different structures from the ones that were observed by Castleman or Duncan groups.

According to the structure proposed by Dance and many other theoretical studies, metcars are reactive species due to the fact that metal atoms in these structures are exposed and can be easily oxidized.[55] Metcars are therefore air-sensitive molecules and there has been no report on successful production of its bulk material. On the other hand, the high reactivity of metcars has made them good precursors for the gas-phase ion-molecule reaction studies. A preliminary investigation in this aspect has been attempted with cluster ions $Nb_xC_y^+$ and $Ta_xC_y^+$ in this current study. Ions of both clusters were reacted with methanol without ion selection, and complicated product ions were formed. Further study is needed if the bonding and energy of these product ions are to be revealed.

Several other first-row transition metals including Mn, Fe, Co, Ni, Cu and Zn were also studied by direct laser ablation method. In all these cases, there were no metal-carbon clusters observed, fullerene carbon clusters were the main product ions for the low metal concentrations samples (less than 5%, molar ratio). With high metal contents in the target (equal or greater than 1:1, molar ratio), only bare metal ions M^+ or metal oxide ions MO^+ are observed. This observation confirms what Smalley, Kroto and coworkers have proposed, that metals such as Co and Ni can be used as catalysts to

enhance the carbon network growth, which leads to the formation of carbon nanotubes.[56]

3.5 CID of Endohedral Metallofullerenes and Metal Carbide Cluster Ions

3.5.1 CID of $La@C_{60}^+$

The dissociation of gas-phase fullerene / metallofullerene ions has been previously studied by several research groups, with the loss of C_2 units observed to be the primary dissociation pathway. A variety of dissociation methods have been employed in these studies including photodissociation and CID with ions, atoms, molecules and surfaces.[35,53,57-67] These experiments have shown that at least 20 eV of excitation energy is required to initiate the first C_2-loss from the fullerenes. Smalley and co-workers originally used photodissociation via the so-called "shrink-wrap" mechanism to confirm that metals can be encapsulated by the C_{60} cage in metallofullerenes such as MC_{60} (M = K and Cs).[57,68]

As noted on page 150, CID-FTICR mass spectrometry has also been used to demonstrate that calcium and barium metallofullerenes produced by the laser ablation of coorongite[37] or $BaSO_4$ / kerogen[36] are endohedral in structure. Freiser also used this technique to demonstrate that Ni, Co and Fe metallofullerenes produced from the gas-phase ion molecule reactions between fullerenes and metal ions were exohedral metallofullerenes.[69,70]

The high mass-selectivity of the FTICR mass spectrometer enables the mass selection of metallofullerene ions that subsequently undergoes collisions with inert gases or react with different chemical reagents in the gas-phase. With the use of a pulse sequence such as that shown in Chapter Two (Figure 2-17), $La@C_{60}^+$ is selected (Figure 3-21*a*), and allowed to undergo dissociation after a collision with argon gas at a static

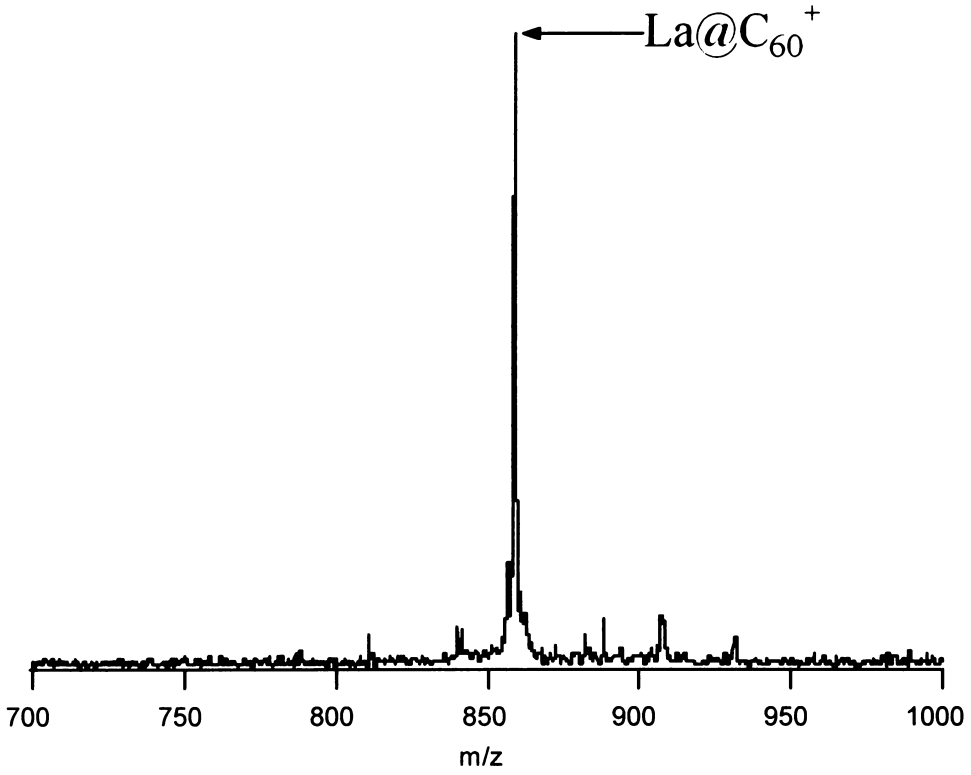

Figure 3-21a An FTICR mass spectrum of the isolated endohedral metallofullerene ion $La@C_{60}^{+}$.

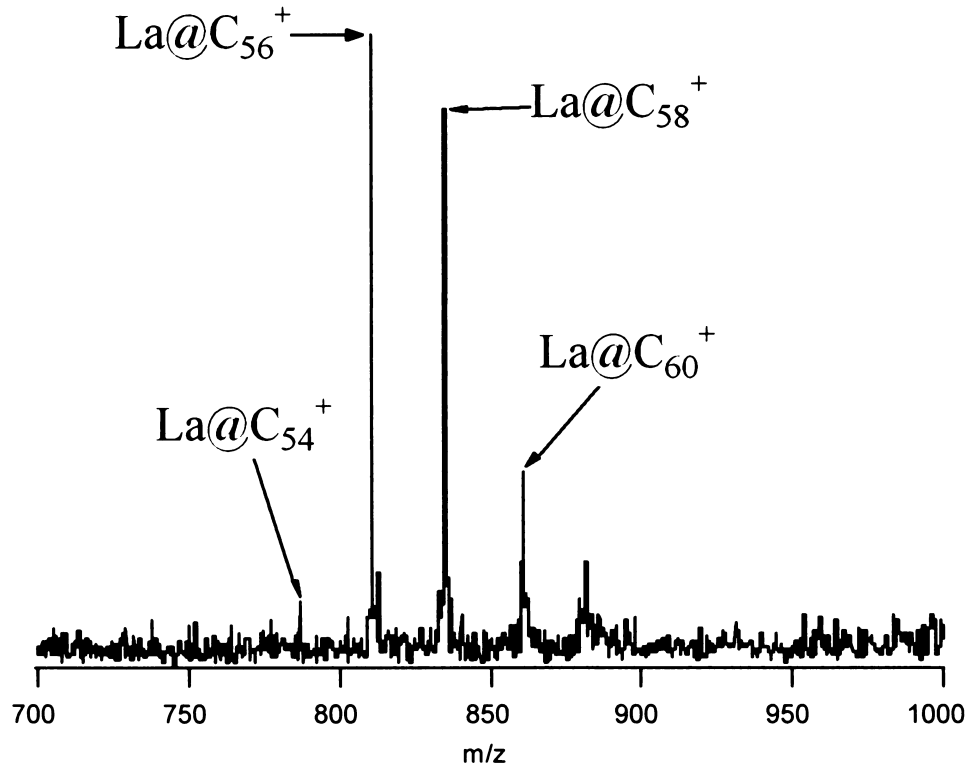

Figure 3-21b Collision-induced-dissociation FTICR mass spectrum of $La@C_{60}^{+}$.

pressure of $1x10^{-9}$ mbar. Figure 3-21*b* is the positive-ion CID-FTICR mass spectrum of $La@C_{60}^+$. $La@C_{60}^+$ is observed to dissociate by losses of C_2 units with $La@C_{58}^+$ and $La@C_{56}^+$ observed as the major product ions. The C_2 losses from $La@C_{60}^+$ are observed to increase progressively as the $La@C_{60}^+$ ion excitation energy is increased.

The center-of-mass translational kinetic energy (in eV) of $La@C_{60}^+$, E_k^{com} can be calculated using equation 2-01. For m_t is the argon target ion mass (40 Da); m_p is 859 Da (m/z) for $La@C_{60}^+$; S_e is 0.81 for cylindrical ICR cell; V_{pp} is 165 V; d is 6 cm. For the CID-FTICR experiment shown in Figure 3-21*b*, $La@C_{60}^+$ was accelerated for 380 μs, and according to equation 2-01, its E_k^{com} = 430 eV.

The ion collision frequency during the ion activation N_c can be calculated by equation 2-02, here r_t is the average radius of the target molecule (argon r_t is 0.94 Å); r_p is the average collision radius of the parent ion ($La@C_{60}^+$ is ~6 Å); C_n is the number density of the target gas and in this experiment the argon gas number density is C_n = 2.2×10^{15} atoms/m^3 at a corrected pressure of 9 x 10^{-8} mbar. A calculation using equation 2-02 reveals that the CID experiment performed with $La@C_{60}^+$ in this experiment occurs in the single collision regime. Figure 3-21*b* reveals that neither C_{60}^+ nor La^+ or LaO^+ were observed during the CID-FTICR experiment. This result suggests that the lanthanum atom was encapsulated by the fullerene carbon-cage.

Gas-phase ion-molecule reactions between $La@C_{60}^+$ and organic reagents including methanol, benzene and carbon disulfide were also attempted, but in each case no reaction product was observed. The lack of reactivity of $La@C_{60}^+$ provides additional evidence that the metallofullerenes observed in the LA-FTICR-MS experiments are endohedral in nature.

One of the puzzling questions about metallofullerene formation is why only some of the metals in the periodic table can form endohedral metallofullerenes. So far only some of the group IIA, IIIB and lanthanide metals appear to form endohedral metallofullerenes.

It has been assumed that the similar ionic radii and first ionization energies of these metals account for the stability of the corresponding metallofullerenes.[36] Wang et al.[71] have presented a thermodynamic calculation of the stability of endohedral metallofullerene $M@C_{60}$, and they claim that the formation energy of $M@C_{60}$ depends crucially on the ionization energy of the metal atom and on the electron affinity of the C_{60} molecule. However, from these thermodynamic studies we cannot obtain detailed information on how metallofullerenes are formed.

One possible path for fullerene formation in the gas-phase is through a growth process beginning with a small carbon ring structure.[72] It follows that the formation of endohedral metallofullerenes may involve the metal atoms interacting with the carbon rings prior to encapsulation into the metallofullerene. This metal-carbon interaction has to be strong enough to sustain the metals on the carbon network during the fullerene growth.

Several experimental and theoretical studies have been undertaken on small metal-carbide clusters such as ScC_n, YC_n, LaC_n, ($n<10$), and a general conclusion is that a *'fan structure'* in which the metal atom sits above the carbon chain and bonds to each carbon is the most stable structure for those metals that form endohedral metallofullerenes.[73-78] For example, Suzuki et al. have also shown that there is a correlation between the formation of MC_n^+ ($n \leq 6$) and the formation of MC_{82}^+, which indicates that these very small metal carbides are possibly the precursor for $M@C_{82}^+$.[78-80]

3.5.2 CID of LaC_4^+

Figure 3-22 shows the CID-FTICR mass spectrum of LaC_4^+ with argon as the collision gas and this spectrum reveals that these ions fragment through a loss of C_2 or C_4 radicals. The center-of-mass translational kinetic energy LaC_4^+, E_k^{com} is calculated to be ~ 20 eV. It is difficult to reveal the structure of LaC_4^+ by CID experiments alone; more sophisticated spectroscopic experiments or theoretical studies are needed in order to probe its bonding and energy. A theoretical approach on metal-carbon clusters will be presented in Chapter Four.

3.6 Macroscopic Production of Endohedral Metallofullerenes Using Pyrolysed KCT-Pitch as a Carbon Precursor

Based on the LA-FTICR-MS study results, the production of endohedral metallofullerenes was attempted using the home-built laser ablation fullerene / metallofullerene generator with metal containing KCT-pitch pyrolysis residue as the laser ablation target. Unlike the experimental conditions used by some of other research groups that applied high temperature (over 1,200 °C) to the metal-doped graphite target during the laser ablation, in this current laser ablation studies, it was found that metallofullerene could be produced at room temperature by laser ablation. The variables in this experiment are found to be mainly the laser ablation energy and carrier gas pressure.

Preliminary results have been obtained, nevertheless, they are encouraging. Figure 3-23 shows the negative-ion MALDI-TOF mass spectrum of the CS_2 extraction of laser ablation soot, which is produced by laser ablation of a target containing 450 °C KCT-pitch prolysis residue doped with 1% of La_2O_3. The laser energy used is about 700 kW

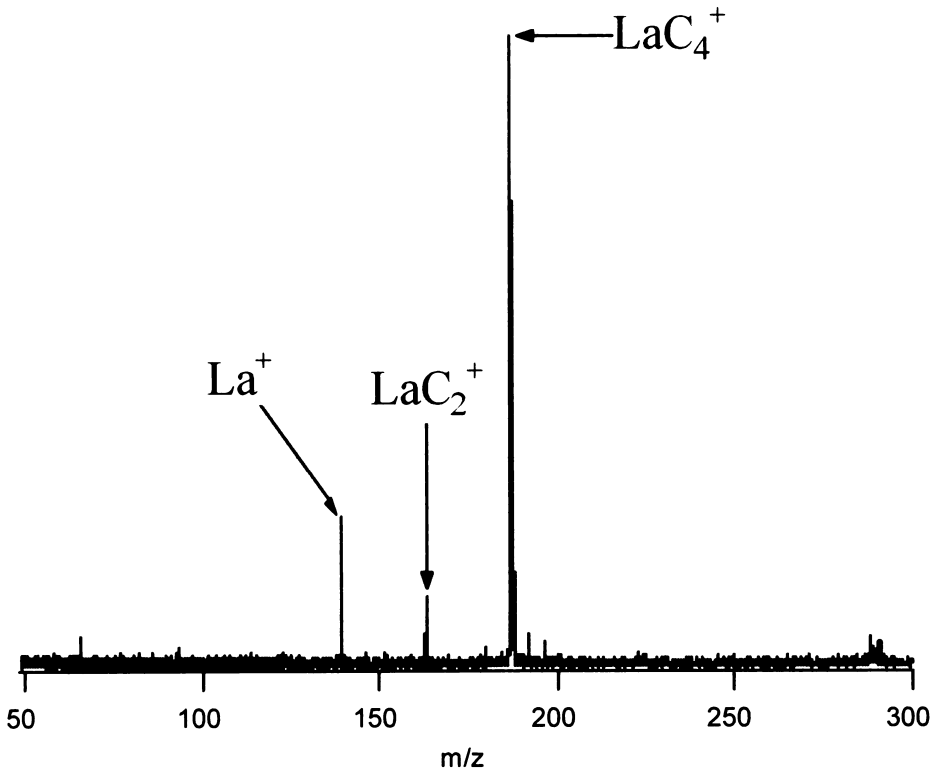

Figure 3-22 Collision-induced-dissociation FTICR mass spectrum of LaC_4^+.

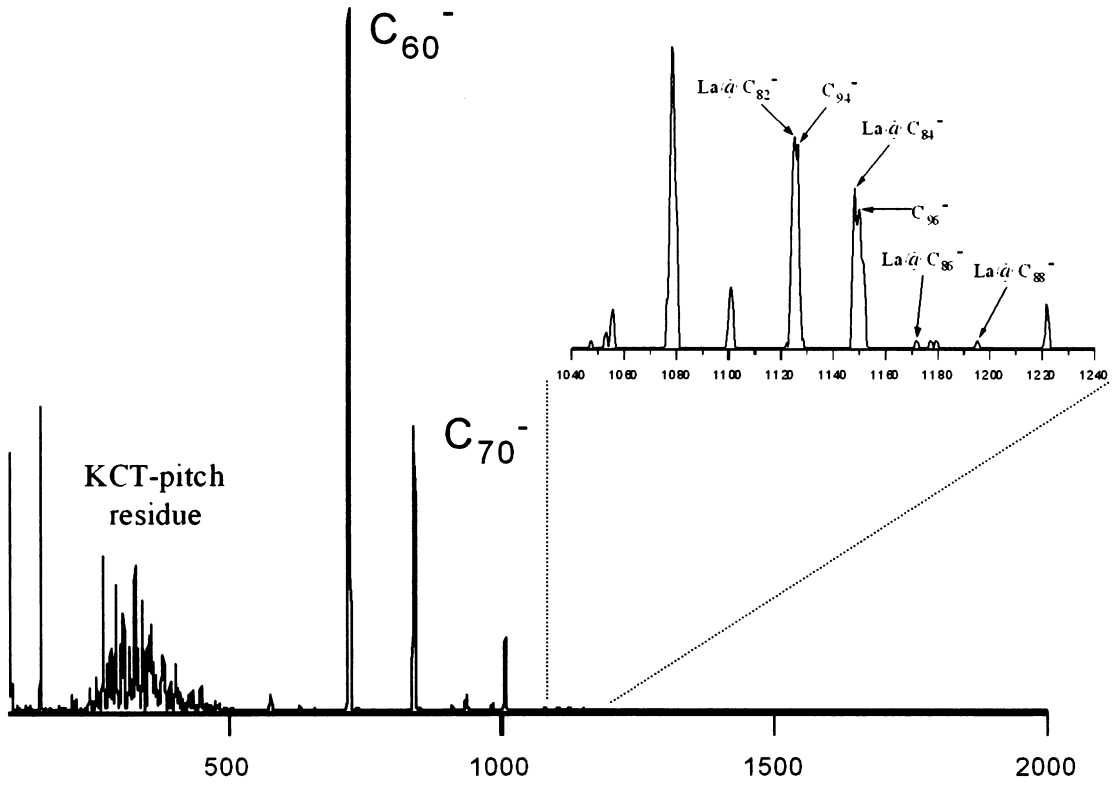

Figure 3-23 Negative-ion laser desorption time-of-flight mass spectrum of the CS_2 soot extraction which is generated by laser ablation of pyrolysed mixture of KCT-pitch and La_2O_3 (laser ablation condition: laser power density, ~800 $kWcm^{-2}$; helium buffer gas pressure, 400 torr; room temperature 25 °C).

cm^{-2} and with ~ 400 mbar helium carrier gas. Several lanthano-fullerene ions including $La@C_{82}^-$ and $La@C_{84}^-$ are identified in the mass spectrum.

3.7 Conclusions

Laser ablation FTICR mass spectrometry shows that the formation of certain type of metal-carbon clusters is determined by the intrinsic property of the corresponding metal used in the laser ablation target. Studies on carbonaceous materials including carbon thermal black and pyrolysed KCT-pitch indicate that disordered carbons such as PAHs require much less laser ablation energy than graphite to form metal-carbon clusters such as endohedral metallofullerenes.

Laser desorption TOF- and FTICR-mass spectrometry of pyrolysed (450 °C) KCT-pitch shows the presence of a range of PAHs with various degrees of unsaturation incorporating up to 70 carbon atoms. Laser ablation FTICR mass spectrometry studies on KCT-pitch pyrolysis residues show this material is potentially a good precursor for macroscopic metallofullerenes production.

Metal compounds of Ca, Ba, Y, La, Ce, Pr, Nd, Gd and Sm when pyrolysed in KCT-pitch all form a range of gas-phase metallofullerene ions using low-power (200-1000 kW cm^{-2}) long-pulse (230 μs) laser ablation. The CID-FTICR experiments on $La@C_{60}^+$ and its lack of reactivity towards chemical reagents such as methanol, benzene and carbon disulfide indicate that the lanthanum metal atom is encapsulated in the fullerene cage. This result also suggests that the metal atoms of Ca, Ba, Y, Ce, Pr, Nd, Gd and Sm in the corresponding metallofullerene cations are endohedral to the fullerene cage. Experimentation with two different laser pulse widths of 230 μs and 8 ns, shows that only the 230 μs pulse laser ablation forms metallofullerene whilst fullerenes are produced with both laser pulse widths.

Small metal-carbide cluster ions such as LaC_n^+ (n = 2 - 10) and $La_2C_m^+$ (m = 4 - 9) were observed as the main product ions from the high-power Q-switch (8 ns) laser ablation of pyrolysed KCT-pitch/metal compound mixtures.

Laser ablation studies of carbon material containing Nb_2O_5 and Ta_2O_5 show that a range of metal-carbon clusters in the form of $M_xC_y^+$ (x= 0-8, y=0-13) is formed. Similar studies with late first-row transition metals Mn, Fe, Co, Ni, Cu and Zn show neither metallofullerene ions nor metallocarbohedrenes ions in mass spectra. With low concentration of these metals only bare metal ions and fullerene ions were observed.

Macroscopic production of metallofullerenes was carried out at room temperature using a home-built laser ablation fullerene/metallofullerenes generator. The MALDI-TOF mass spectrum of CS_2 extracted soot collected from the laser ablation of pyrolysed KCT-pitch/La_2O_3 target show several metallofullerene ions including $La@C_{82}^-$ and $La@C_{84}^-$.

3.8 References

(1) Wei, S.; Guo, B. C.; Purnell, J.; Buzza, S.; Castleman, A. W., Jr. *J. Phys. Chem.* **1992**, *96*, 4166.

(2) Terrones, M.; Hsu, W. K.; Schilder, A.; Terrones, H.; Grobert, N.; Hare, J. P.; Zhu, Y. Q.; Schwoerer, M.; Prassides, K.; Kroto, H. W.; Walton, D. R. M. *Appl. Phys. A: Mater. Sci. Proc.* **1998**, *A66*, 307.

(3) Lago, R. M.; Tsang, S. C.; Lu, K. L.; Chen, Y. K.; Green, M. L. H. *J. Chem. Soc., Chem. Commun.* **1995**, 1355.

(4) Liu, M.; Cowley, J. M. *Carbon* **1995**, *33*, 749.

(5) Heath, J. R.; O'Brien, S. C.; Zhang, Q.; Liu, Y.; Curl, R. F.; Tittel, F. K.; Smalley, R. E. *J. Am. Chem. Soc.* **1985**, *107*, 7779.

(6) Krätschmer, W.; Lamb, L. D.; Fostiropoulos, K.; Huffman, D. R. *Nature* **1990**, *347*, 354.

(7) Iijima, S.; Wakabayashi, T.; Achiba, Y. *J. Phys. Chem.* **1996**, *100*, 5839.

(8) Kikuchi, K.; Suzuki, S.; Nakao, Y.; Nakahara, N.; Wakabayashi, T.; Shiromaru, H.; Saito, K.; Ikemoto, I.; Achiba, Y. *Chem. Phys. Lett.* **1993**, *216*, 67.

(9) Guo, T.; Nikolaev, P.; Thess, A.; Colbert, D. T.; Smalley, R. E. *Chem. Phys. Lett.* **1995**, 246, 49.

(10) Wallis, D. J.; Grobert, N.; Reeves, C. L.; Pidduck, A. J.; Walton, D. R. M.; Hare, J. P.; Hsu, W. K.; Terrones, M.; Kroto, H. W.; Wright, P. J.; Vizard, C. *Proc. 14th Int. Congr. Electron Microsc.* (American Institute of Physics) **1998**, *3*, 129.

(11) Birkett, P. R.; Cheetham, A. J.; Eggen, B. R.; Hare, J. P.; Kroto, H. W.; Walton, D. R. M. *Chem. Phys. Lett.* **1997**, *281*, 111.

(12) Yudasaka, M.; Komatsu, T.; Ichihashi, T.; Iijima, S. *Chem. Phys. Lett.* **1997**, *278*, 102.

(13) Yudasaka, M.; Komatsu, T.; Ichihashi, T.; Achiba, Y.; Iijima, S. *J. Phys. Chem. B* **1998**, *102*, 4892.

(14) Yudasaka, M.; Ichihashi, T.; Iijima, S. *J. Phys. Chem. B* **1998**, *102*, 10201.

(15) Yudasaka, M.; Sensui, N.; Takizawa, M.; Bandow, S.; Ichihashi, T.; Iijima, S. *Chem. Phys. Lett.* **1999**, *312*, 155.

(16) Yudasaka, M.; Yamada, R.; Sensui, N.; Wilkins, T.; Ichihashi, T.; Iijima, S. *J. Phys. Chem. B* **1999**, *103*, 6224.

(17) Yudasaka, M.; Kokai, F.; Takahashi, K.; Yamada, R.; Sensui, N.; Ichihashi, T.; Iijima, S. *J. Phys. Chem. B* **1999**, *103*, 3576.

(18) Yudasaka, M.; Kasuya, Y.; Takizawa, M.; Bandow, S.; Takahashi, K.; Kokai, F.; Iijima, S. *AIP Conf. Proc.* (American Institute of Physics) **2000**, *544*, 217.

(19) Greenwood, P. F.; Strachan, M. G.; Willett, G. D.; Wilson, M. A. *Org. Mass Spectrom.* **1990**, *25*, 353.

(20) Pang, L. S. K.; Vassallo, A. M.; Wilson, M. A. *Ener. Fuels* **1992**, *6*, 176.

(21) Greenwood, P. F.; Dance, I. G.; Fisher, K. J.; Willett, G. D.; Pang, L. S. K.; Wilson, M. A. *Org. Mass Spectrom.* **1991**, *26*, 920.

(22) Dance, I. G.; Fisher, K. J.; Willett, G. D.; Wilson, M. A. *J. Phys. Chem.* **1991**, *95*, 8425.

(23) Tohji, K.; Saito, K.; Matsuoka, I.; Sogabe, T.; Nagasawa, K. *Fullerenes - Recent Advances in the Chemistry and Physics of Fullerenes and Related Materials* Ed. Ruoff, R. S. (Electrochemical Society) **1994**, *1*, 132.

(24) Rose, H. R.; Smith, D. R.; Fisher, K. J.; Dance, I. G.; Willett, G. D.; Wilson, M. A. *Org. Mass Spectrom.* **1993**, *28*, 825.

(25) Gu, Y.; Wilson, M. A.; Fisher, K. J.; Dance, I. G.; Willett, G. D.; Ren, D.; Volkova, I. B. *Carbon* **1995**, *33*, 862.

(26) Lu, X. Q.; Smith, D. R.; Johnson, D. W.; Rose, H. R.; Wilson, M. A. *Carbon* **1996**, *34*, 1145.

(27) Feld, H.; Zurmühlen, R.; Leute, A.; Benninghoven, A. *J. Phys. Chem.* **1990**, *94*, 4595.

(28) Taylor, R.; Langley, G. J.; Kroto, H. W.; Walton, D. R. M. *Nature* **1993**, *366*, 728.

(29) Taylor, R.; Langley, J. *Fullerenes - Recent Advances in the Chemistry and Physics of Fullerenes and Related Materials* Ed. Ruoff, R. S. (Electrochemical Society) **1994**, *1*, 68.

(30) Yamasaki, A.; Iizuka, T.; Osawa, E. *Fullerene Sci. & Tech.* **1995**, *3*, 529.

(31) Donnet, J.-B. *Carbon* **1994**, *32*, 1305.

(32) Hall, C. E. *J. Appl. Phys.* **1948**, *19*, 271.

(33) Hall, C. E. *J. Appl. Phys.* **1948**, *19*, 198.

(34) Loustalet, D.; Oberlin, A.; Moreau, A. *Carbon* **1994**, *32*, 1384.

(35) Wakabayashi, T.; Shiromaru, H.; Suzuki, S.; Kikuchi, K.; Achiba, Y. *Surf. Rev. Lett.* **1996**, *3*, 793.

(36) Rose, H. R.; Dance, I. G.; Fisher, K. J.; Smith, D. R.; Willett, G. D.; Wilson, M. A. *J. Chem. Soc., Chem. Commun.* **1993**, 1361.

(37) Rose, H. R.; Dance, I. G.; Fisher, K. J.; Smith, D. R.; Willett, G. D.; Wilson, M. A. *J. Chem. Soc., Chem. Commun.* **1993**, 941.

(38) Rose, H. R.; Dance, I. G.; Fisher, K. J.; Smith, D. R.; Willett, G. D.; Wilson, M. A. *Org. Mass Spectrom.* **1994**, *29*, 470.

(39) Wang, C.-R.; Kai, T.; Tomiyama, T.; Yoshida, T.; Kobayashi, Y.; Nishibori, E.; Takata, M.; Sakata, M.; Shinohara, H. *Angew. Chem., Int. Ed.* **2001**, *40*, 397.

(40) Shinohara, H.; Yamamoto, E.; Tomiyama, T.; Kobayashi, Y.; Takata, M.; Sakata, M. *Proc. Electrochem. Soc.* **1996**, *96-10*, 549.

(41) Yamamoto, E.; Tansho, M.; Tomiyama, T.; Shinohara, H.; Kawahara, H.; Kobayashi, Y. *J. Am. Chem. Soc.* **1996**, *118*, 2293.

(42) Inakuma, M.; Shinohara, H. *J. Phys. Chem. B* **2000**, *104*, 7595.

(43) Kato, T.; Suzuki, S.; Kikuchi, K.; Achiba, Y. *J. Phys. Chem.* **1993**, *97*, 13425.

(44) Shinohara, H.; Sato, H.; Saito, Y.; Ohkohchi, M.; Ando, Y. *J. Phys. Chem.* **1992**, *96*, 3571.

(45) Hulman, M.; Inakuma, M.; Shinohara, H.; Kuzmany, H. *AIP Conf. Proc.* (American Institute of Physics) **1998**, *442*, 379.

(46) Takata, M.; Nishibori, E.; Sakata, M.; Shinohara, H. *Proc. Electrochem. Soc.* **1997**, *97-14*, 457.

(47) Sugai, T.; Inakuma, M.; Hudgins, R.; Dugourd, P.; Fye, J. L.; Jarrold, M. F.; Shinohara, H. *J. Am. Chem. Soc.* **2001**, *123*, 6427.

(48) Clemmer, D. E.; Shelimov, K. B.; Jarrold, M. F. *Nature* **1994**, *367*, 718.

(49) Shelimov, K. B.; Clemmer, D. E.; Jarrold, M. F. *J. Phys. Chem.* **1995**, *99*, 11376.

(50) Shelimov, K. B.; Clemmer, D. E.; Jarrold, M. F. *Proc. Electrochem. Soc.* **1995**, *95-10*, 1437.

(51) Laska, L.; Krasa, J.; Juha, L.; Hamplova, V.; Soukup, L. *Carbon* **1996**, *34*, 363.

(52) Curl, R. F.; Smalley, R. E. *Sci. Amer.* **1991**, 5, 32.

(53) Lorents, D. C.; Yu, D. H.; Brink, C.; Jensen, N.; Hvelplund, P. *Chem. Phys. Lett.* **1995**, *236*, 141.

(54) Guo, B. C.; Wei, S.; Purnell, J.; Buzza, S.; Castleman, Jr. A. W. *Science* **1992**, *256*, 515.

(55) Dance, I. *J. Chem. Soc., Chem. Commun.* **1998**, 523.

(56) Bethune, D. S.; Kiang, C. H.; DeVries, M. S.; Gorman, G.; Savoy, R.; Beyers, R. *Nature* **1993**, *363*, 605.

(57) Weiss, F. D.; Elkind, J. L.; O'Brien, S. C.; Curl, R. F.; Smalley, R. E. *J. Am. Chem. Soc.* **1988**, *110*, 4464.

(58) Beck, R. D.; John, P. S.; Alvarez, M. M.; Diederich, F.; Whetten, R. L. *J. Phys. Chem.* **1991**, *95*, 8402.

(59) Christian, J. F.; Wan, Z.; Anderson, S. L. *Chem. Phys. Lett.* **1992**, *199*, 373.

(60) Christian, J. F.; Wan, Z.; Anderson, S. L. *J. Phys. Chem.* **1992**, *96*, 3574.

(61) Busmann, H. G.; Lill, T.; Reif, B.; Hertel, I. V. *Surf. Scien.* **1992**, *272*, 146.

(62) Caldwell, K. A.; Giblin, D. E.; Gross, M. L. *J. Am. Chem. Soc.* **1992**, *114*, 3743.

(63) Foltin, M. *J. Chem. Phys.* **1997**, *16*, 6246.

(64) Foltin, M.; Lezius, M.; Scheier, P.; Mark, T. D. *J. Chem. Phys.* **1993**, *98*, 9624.

(65) Yoo, R. Y.; Ruscic, B.; Berkowitz, J. *J. Chem. Phys.* **1992**, *96*, 911.

(66) Wurz, P.; Lykke, K. R. *J. Chem. Phys.* **1992**, *96*, 10129.

(67) Campbell, E. E. B.; Ulmer, G.; Hertel, I. V. *Z. Phys. D* **1992**, *24*, 81.

(68) O'Brien, S. C.; Heath, J. R.; Curl, R. F.; Smalley, R. E. *J. Chem. Phys.* **1988**, *88*, 220.

(69) Huang, Y.; Freiser, B. S. *J. Am. Chem. Soc.* **1991**, *113*, 8186.

(70) Huang, Y.; Freiser, B. S. *J. Am. Chem. Soc.* **1991**, *113*, 9418.

(71) Wang, Y.; Tomanek, D.; Ruoff, R. S. *Chem. Phys. Lett.* **1993**, *208*, 79.

(72) Goroff, N. S. *Acc. Chem. Res.* **1996**, *29*, 77.

(73) Wu, Z. J.; Meng, Q. B.; Zhang, S. Y. *Chem. Phys. Lett.* **1997**, *281*, 233.

(74) Roszak, S.; Balasubramanian, K. *Chem. Phys. Lett.* **1995**, *246*, 20.

(75) Strout, D. L.; Hall, M. B. *J. Phys. Chem.* **1996**, *100*, 18007.

(76) Roszak, S.; Balasubramanian, K. *J. Chem. Phys.* **1997**, *106*, 158.

(77) Ayuela, A.; Seifert, G.; Schmidt, R. *Z. Phys. D.* **1997**, *41*, 69.

(78) Suzuki, S.; Torisu, H.; Kubota, H.; Wakabayashi, T.; Shiromaru, H.; Achiba, Y. *Int. J. Mass Spectrom. Ion Proc.* **1994**, *138*, 297.

(79) Suzuki, T.; Maruyama, Y.; Kato, T.; Kikuchi, K.; Achiba, Y. *J. Am. Chem. Soc.* **1993**, *115*, 11006.

(80) Suzuki, S.; Wakabayashi, T.; Achiba, Y. *Proceedings of the Symposium on Recent Advances in the Chemistry and Physics of Fullerenes and Related Materials* Ed. Ruoff, R. S. (Electrochemical Society) **1995**, *95-10*, 740.

Chapter Four

Studies of Endohedral Metallofullerene Related Small Metal-Carbon Clusters by Gas-phase Ion-molecule Reactions and Density Functional Theory Quantum Chemical Calculations

4.1 Introduction

The laser ablation studies described in the last chapter show the characteristic interactions between various metals and carbon clusters. The observation of endohedral metallofullerenes and small metal-carbon clusters such as YC_n^+ and LaC_n^+ under different laser ablation conditions indicate a correlation between the small and large metal-carbon clusters. Some researchers have suggested that endohedral metallofullerene related small metal-carbon clusters tend to form specific structures that result in the encapsulation of metals in the fullerene cage.[1-3] It is therefore important to study the electronic structures of the small metal-carbon clusters in order to understand their relationship to larger metal-carbon clusters such as endohedral metallofullerenes. In this chapter, both gas-phase ion chemistry studies and quantum chemical calculations using density functional theory are employed to investigate small yttrium- and lanthanum-carbide cluster cations, YC_n^+ and LaC_n^+ ($n<10$).

It should be noted that the gas-phase study of metal-carbon clusters is not only of the interest in endohedral metallofullerene formation, but also to studies involving metal-carbon clusters in chemical catalytic processes. It is well known that bare or ligated transition metals can activate C-H or C-C bond in hydrocarbons such as alkanes and this catalytic property possess huge potentials in the petrochemical industry.[4] It is of importance to realize, however, that the C-H and C-C bond activation by transition metals can be considered via two mechanisms - bond formation and bond cleavage.

Several books and review articles are available for comprehensive and detailed discussions on this subject.[5-13] One interesting fact is that, in recent years, the catalytic properties of transition metals has also been demonstrated in the studies of carbon nanotubes, for which the catalytic process for C-C bond formation was accomplished under some extreme conditions such as a high-temperature laser plume. Several transition metals including Fe, Co and Ni have been used to promote carbon nanotubes growth in the laser ablation process.[14-18]

Gas-phase ion-molecule reactions between bare transition metal ions (cations or anions) and organic reagents produce unusual organometallic complexes that are difficult to observe in the condensed phase. Gas-phase studies eliminate the interferences of solvent effect or ion pair attractions, and the chemical reactivity of the studied ions can be revealed in detail at the atomic/molecular level. Species that are formed by weak interactions can be easily manipulated in the gas-phase. For example, many transition metal ions have been studied in the reaction with benzene. The early transition metals such as Sc can form product $[M\text{-}C_6H_4]^+$ by H_2 elimination.[19,20] The electronic charge on the metal cation remains as a reactive site for further electrostatic interactions. Freiser and co-workers reported that $Sc(C_6H_4)^+$ continued to react with benzene to form condensation products $M(C_6H_4)(C_6H_6)_n^+$ (n= 1-2).[21] Studies of the first-row transition metal cations reacting with cyclohexane have shown that the early transition metal cations such as Sc^+, Ti^+ and V^+ are capable of multiple dehydrogenation to yield M^+/benzene(s) complexes.[22] Other reports on the reactions of transition metal cluster ions with benzene show that multi-nuclear multi-benzene complexes are formed.[23-25]

In general, most of the gas-phase studies mentioned above were carried out with bare metal or metal oxide ions, little is known of the gas-phase reactivity of metal-carbon

cluster ions. In this chapter, yttrium- and lanthanum-carbide cluster cations YC_n^+ and LaC_n^+ (n <10) are studied with a focus on their reactions with several chemical reagents including methanol, H_2S, benzenethiol, benzene and cyclohexane. Collision-induced-dissociation is used to assist the investigation of the structures of gas-phase ion-molecule reaction products.

4.2 Generation of Small Metal-Carbon Cluster Ions MC_n^+ (M=Y, La; n <10)

As shown in the Chapter Three, laser ablation of pyrolysed mixtures of KCT-pitch and Y_2O_3 or La_2O_3 produces either endohedral metallofullerenes or small metal-carbon cluster depending on the laser pulse used. Here the focus is on small yttrium- and lanthanum-carbon clusters that are generated by the Q-switch laser. Figure 4-01 and 4-02 show positive-ion laser ablation FTICR mass spectra of pyrolysed KCT-pitch containing Y_2O_3 and La_2O_3 respectively. In Figure 4-01, the major peaks are assigned to YC_n^+ (n <10). The peak assigned to YC_2^+ is the base peak in this spectrum with Y^+ and YC_4^+ being the other two major ions observed. Minor peaks are assigned to YO^+, YC_3^+ and YC_6^+ in this mass spectrum. In Figure 4-02, LaC_2^+ and LaC_4^+ are shown as the most abundant ions and cluster ions up to LaC_{10}^+ can be observed. La^+ and LaO^+ have low intensities. Some dilanthanum-carbon cluster ions such as $La_2C_4^+$ and $La_2C_6^+$ are also assigned in this mass spectrum.

Based on the relative intensities, the cluster ions containing even numbers of carbon atoms are more abundant than those with odd numbers of carbon atoms. One possibility is that the ion intensity variation is caused by the different ionization energies (IE) of these cluster ions. Ayuela[26] and co-workers reported the electronic structure of lanthanum-carbon clusters, and they have shown that the calculated IE for LaC_n (n= 1-6) versus carbon numbers have an even-odd alternation with the IE for the even carbon number clusters much lower than the ones for the odd carbon number

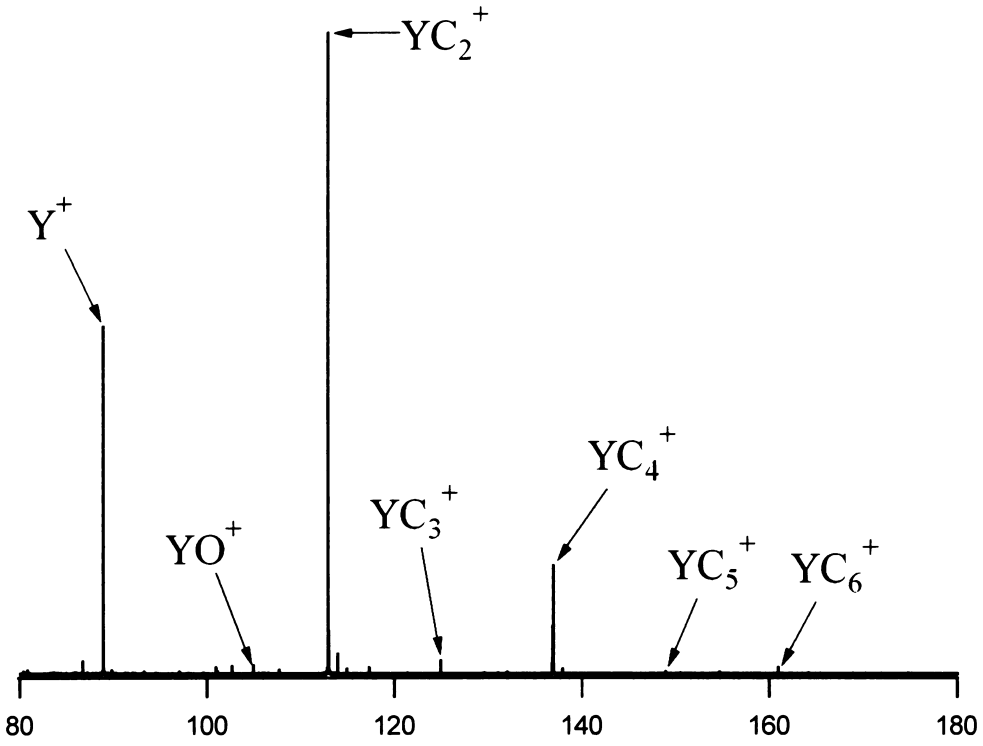

Figure 4-01 Positive-ion LA-FTICR mass spectrum of pyrolysed mixture of KCT-pitch (450 °C) and Y_2O_3 at a laser power density of ~ 700 $MWcm^{-2}$. (1064 nm, Q-switch, 8 ns).

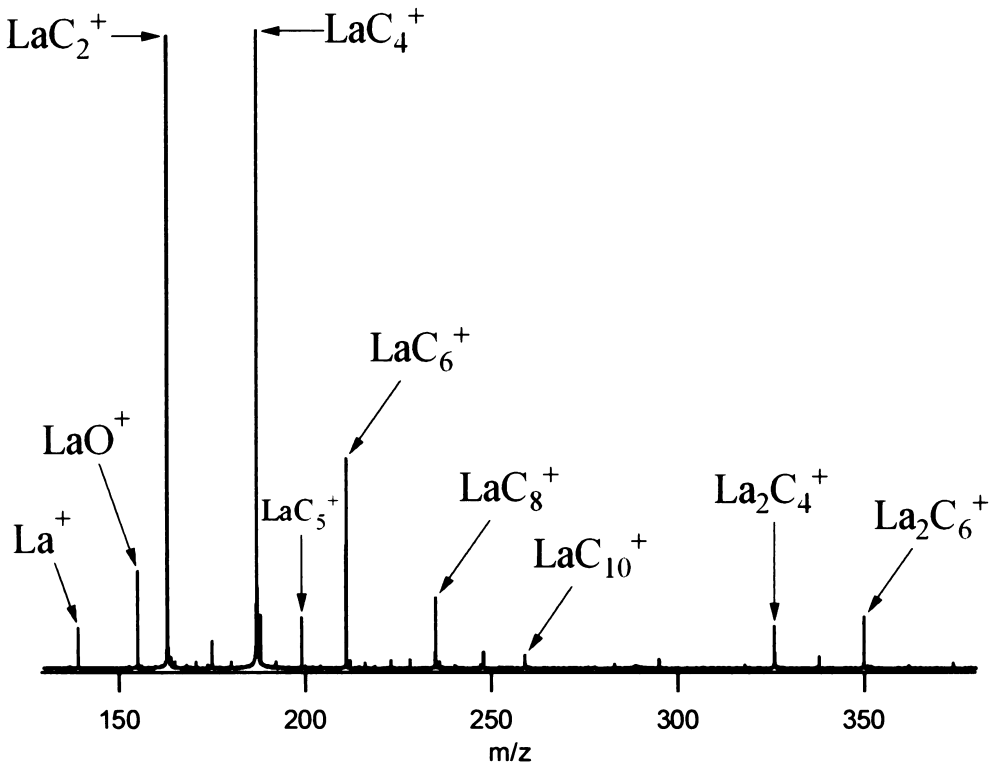

Figure 4-02 Positive-ion LA-FTICR mass spectrum of pyrolysed mixture of KCT-pitch (450 °C) and La_2O_3 at a laser power density of ~ 700 $MWcm^{-2}$ (1064 nm, Q-switch, 8 ns).

clusters. As fullerene or endohedral metallofullerenes are observed as even carbon clusters, the outstanding intensity of small even carbon numbers of yttrium- and lanthanum-carbon clusters may also bear some links to the endohedral metallofullerenes.

Another possible explanation for the even-odd ion-intensity alternation is that such ion distribution reflects the neutral abundance of the cluster ions in the laser ablation plume. In this case, the abundance of cluster ions indicates their relative stability in the gas-phase; in other words, the even carbon number cluster ions are more stable than the odd carbon number clusters. An interesting fact related to this is that for endohedral metallofullerenes, both mass spectrometric results and macroscopic production show only those with even number of carbons are observed so far.

4.3 Gas-phase Ion-molecule Reactions of MC_n^+ (M=Y, La; n =2, 4, 6)

4.3.1 The Reactions of LaC_2^+ and LaC_4^+ with Methanol

Figure 4-03 shows the result of the reaction between LaC_2^+ and methanol at a reaction delay of 5 seconds. The lanthanum carbon bonds are cleaved and the carbon group C_2 is replaced by two methoxide groups to form a product ion $La(CH_3O)_2^+$. This reaction occurs in two steps as indicated by Equation 4-01 and 4-02. The first reaction (Equation 4-01) is observed as a fast intermediate step, which completes in less then 100 ms. The second step is much slower and it forms reaction product ion $La(CH_3O)_2^+$. This product is fairly stable.

$$LaC_2^+ + CH_3OH \longrightarrow LaC_2(CH_3OH)^+ \qquad (4\text{-}01)$$

$$LaC_2(CH_3OH)^+ + CH_3OH \longrightarrow La(CH_3O)_2^+ + C_2H_2 \qquad (4\text{-}02)$$

$$LaC_4^+ + CH_3OH \longrightarrow LaC_2(CH_3OH)^+ + C_2 \qquad (4\text{-}03)$$

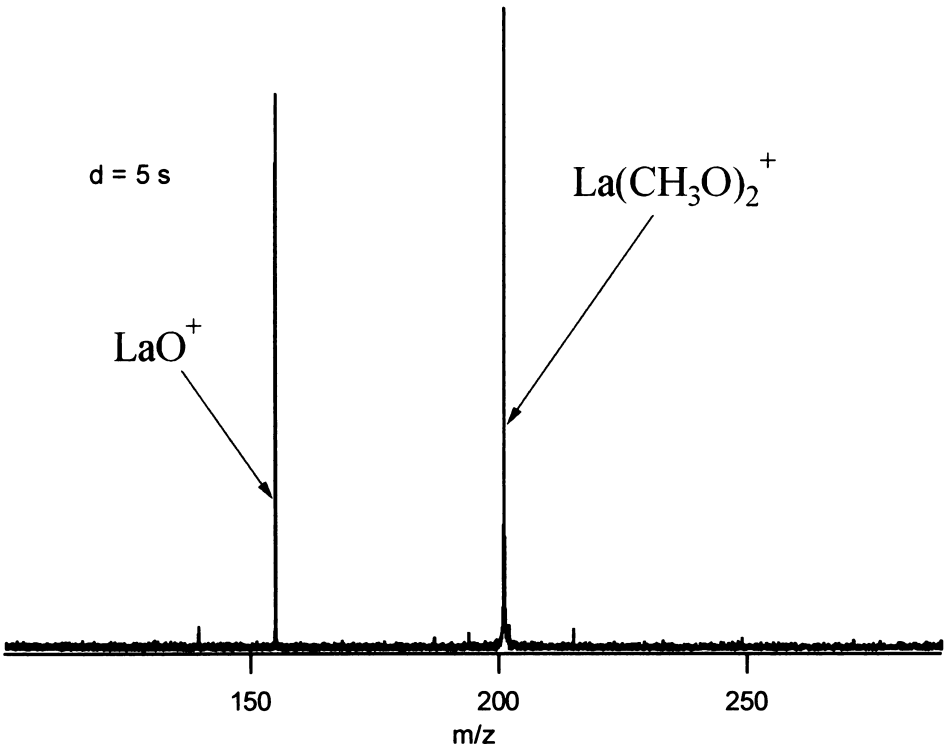

Figure 4-03 Positive-ion FTICR mass spectrum of the gas-phase ion-molecule reaction of LaC_2^+ with methanol after 5 seconds of reaction delay.

The reaction of LaC_4^+ with methanol also yields the product ion $La(CH_3O)_2^+$ as indicated by Equation 4-03 and 4-02, but the reaction is slower. LaO^+ was also observed as a reaction product possibly due to the reaction of LaC_2^+ / LaC_4^+ with background water (Equation 4-04 and 4-05). LaO^+ appears to be more stable than $La(CH_3O)_2^+$, and with long reaction delays (d > 10 s), all the product ions are converted into LaO^+ (Equation 4-06).

$$LaC_2^+ + H_2O \longrightarrow LaO^+ + C_2H_2 \qquad (4\text{-}04)$$

$$LaC_4^+ + H_2O \longrightarrow LaO^+ + C_4H_2 \qquad (4\text{-}05)$$

$$La(CH_3O)_2^+ + H_2O \longrightarrow LaO^+ + 2CH_3OH \qquad (4\text{-}06)$$

Many bare transition metal ions have been studied by gas-phase ion-molecule reactions with methanol or alcohol type of small organic molecules.[27-33] In these reactions, transition metals activate the C-H bonds in organic molecules and eliminate single or several hydrogens. Azzaro and coworkers reported their FTICR mass spectrometry studies of isovalent metal cations Sc^+, Y^+ and Lu^+ reacting with methanol.[34] They claim that M^+ (M= Sc, Y and Lu) reacting with methanol first form an intermediate product $M\text{-}CH_3OH^+$, and then through C-O, O-H bond insertion or 'direct' hydrogen extraction this intermediate product gives many different dissociation products depending on the dissociation energy in the different reaction channels. Subsequent reactions of these dissociation products with methanol all terminated by the formation of $M(CH_3O)_2^+$. The gas-phase ion-molecule reactions of LaC_2^+ and LaC_4^+ with methanol present many similarities to the reactions of bare metal ions. The main difference is that the intermediate product formed from LaC_2^+ or LaC_4^+ has a carbon group attached, but the reactions seem to follow a similar pathway which all starts with the cleavage of the carbon ligands from the primary ions and followed by releases H_2 from the reagent molecule, methanol in this case.

4.3.2 The Reactions of LaC_2^+ and LaC_4^+ with H_2S

Figures 4-04*a* and 4-04*b* show the reaction results for LaC_4^+ with H_2S at 1 second and 5 seconds of the reaction delay respectively. LaO^+ appears to be more stable than LaS^+, and after 5 seconds of the reaction delay, the intensity of LaS^+ is significantly reduced and LaO^+ is assigned to the base peak in the mass spectrum. In a separated experiment, LaO^+ is also isolated to react with H_2S, but no reaction products are observed.

The reactions of LaC_2^+ or LaC_4^+ with H_2S both yield the product ion LaS^+ as shown in by Equation 4-07 and 4-08. The observation of LaO^+ is probably due to the reaction between LaC_n^+ and background water in the ICR cell (Equation 4-04, 4-05 and 4-09). The carbon groups in LaC_2^+ and LaC_4^+ are completely depleted in these reactions. For LaC_4^+, no intermediate product such as LaC_2S^+ is observed which indicates the cleavage of carbon ligands is the early steps in these reactions.

$$LaC_2^+ + H_2S \longrightarrow LaS^+ + C_2H_2 \qquad (4\text{-}07)$$

$$LaC_4^+ + H_2S \longrightarrow LaS^+ + C_4H_2 \qquad (4\text{-}08)$$

$$LaS^+ + H_2O \longrightarrow LaO^+ + H_2S \qquad (4\text{-}09)$$

4.3.3 The Reactions of LaC_2^+ and LaC_4^+ with Benzenethiol

The reaction between LaC_2^+ or LaC_4^+ with benzenethiol shows that both ions yield the product ions, La^+, LaO^+ and LaS^+, in the initial stage. These ions continue to react with benzenethiol to form product ions $La(C_6H_3SH)^+$, $LaS(C_6H_3SH)^+$ and $LaO(C_6H_5SH)^+$. Unlike the reaction with methanol or H_2S in which LaO^+ was non-reactive towards both reagents, LaO^+ reacts with benzenethiol to form $LaO(C_6H_3SH)^+$. LaS^+ is also reactive towards benzenethiol, and it produces the product ion $LaS(C_6H_3SH)^+$, but no further reaction is observed with benzenethiol.

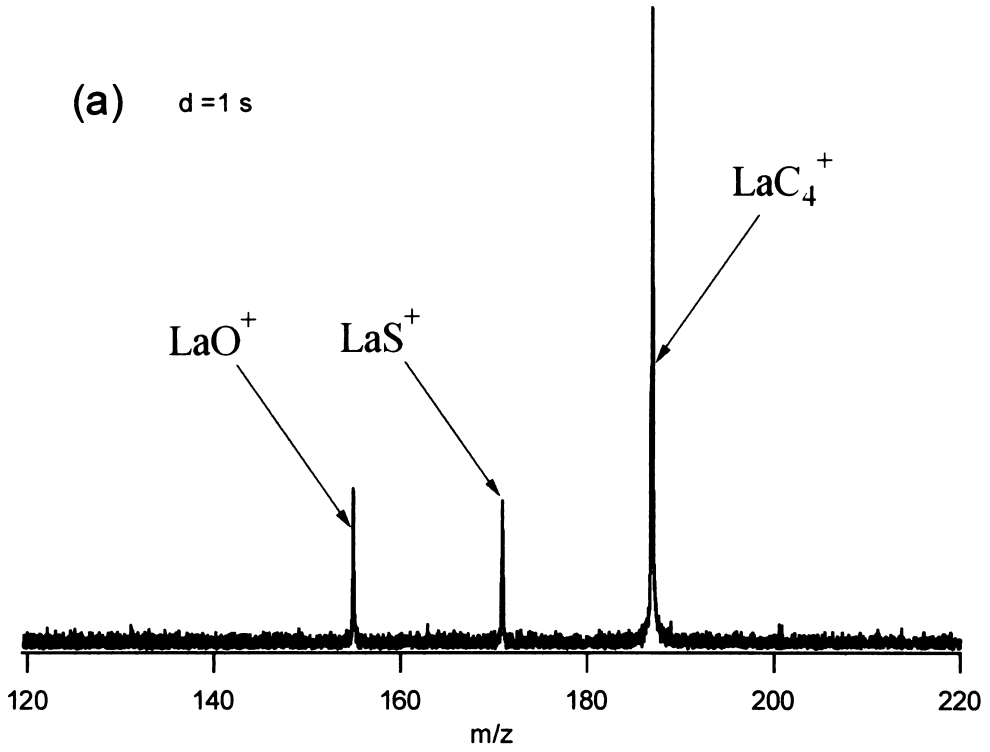

Figure 4-04a Positive-ion FTICR mass spectrum of the gas-phase ion-molecule reaction of LaC_4^+ with H_2S after 1 second of reaction delay.

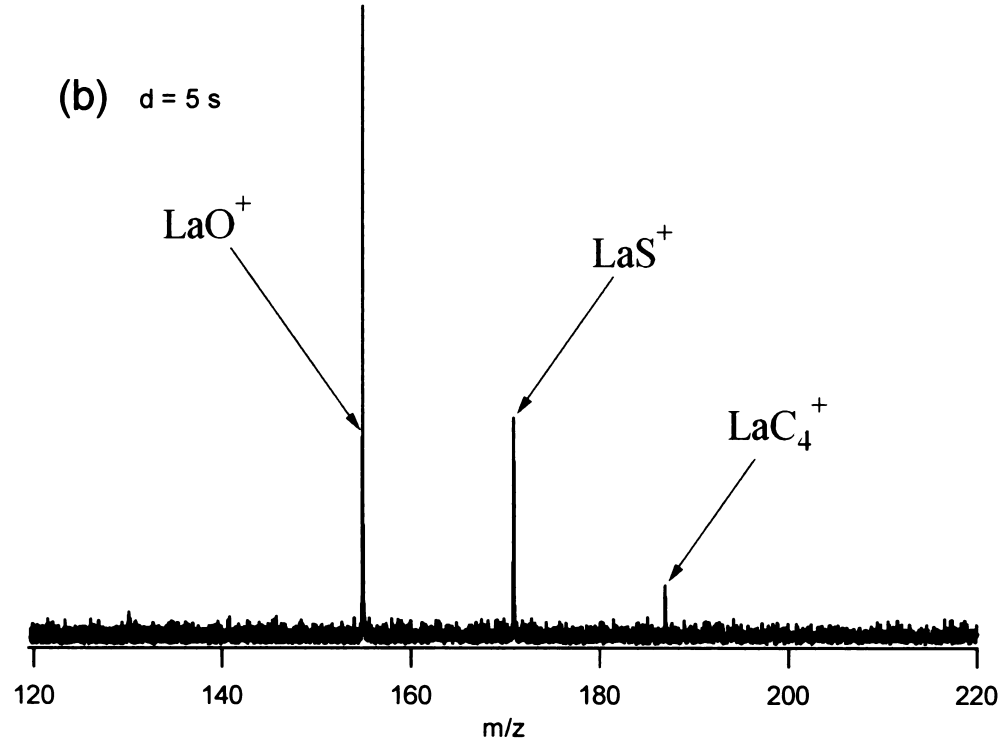

Figure 4-04b Positive-ion FTICR mass spectrum of the gas-phase ion-molecule reaction of LaC_4^+ with H_2S after 5 seconds of reaction delay.

4.3.4 The Reactions of YC_n^+ and LaC_n^+ with Benzene

As YC_n^+ and LaC_n^+ are isovalent species, the reactions of YC_n^+ with benzene are expected to be similar to the reaction of LaC_n^+ with benzene. Such an expectation is confirmed by seemingly identical reaction pathways for the two groups of cluster ions. For simplicity of the description, only the reactions with LaC_n^+ will be discussed below. It is also important to note that the formulae refer to the product ions in this part of the discussion are postulated. Confirmation of these formulae will be presented in the later section.

4.3.4.1 The Reaction of LaC_2^+ with Benzene

In the reaction of LaC_2^+ with benzene, the initial product ions formed after 0.5 s reaction delay are $La(C_6H_4)^+$, $La(C_8H_4)^+$ and a small amount of $La(C_8H_6)^+$. LaO^+ is also observed due to the reaction of LaC_2^+ with background water molecule. Except for LaO^+, the three cluster ions $La(C_6H_4)^+$, $La(C_8H_4)^+$ and $La(C_8H_6)^+$ continue to react with benzene or background water through three main pathways and side-pathways as shown in Figure 4-05. In the pathway ***I***, the lanthanum-benzyne cation $La(C_6H_4)^+$ adds on three benzene molecules to form complex cluster ions $La(C_6H_4)(C_6H_6)_n^+$ (where n= 1-3). This addition of benzene molecules probably occurs successively since the larger cluster ions such as $La(C_6H_4)(C_6H_6)_3^+$ is only observed with long reaction delays (> 10 s). Some of the cluster ion $La(C_6H_4)(C_6H_6)_n^+$ (for n= 0-2) also react with background water to form $LaO(C_6H_6)_n^+$, where n= 1-3. With long reaction delays (over 15 s), water addition to $LaO(C_6H_6)_n^+$ (n= 1-2) yields product ions $LaO(C_6H_6)_n(H_2O)^+$ (where n= 1-2). In the pathway ***II***, $La(C_8H_4)^+$ adds on three benzene molecules successively to form $La(C_8H_4)(C_6H_6)_n^+$ (where n= 1-3). Further reactions of $La(C_8H_4)(C_6H_6)_n^+$ with background water produces the complex species $LaO(C_8H_6)(C_6H_6)_n^+$ (n= 0-2). In reaction the pathway ***III***, $La(C_8H_6)^+$ is observed to react with two benzene molecules to

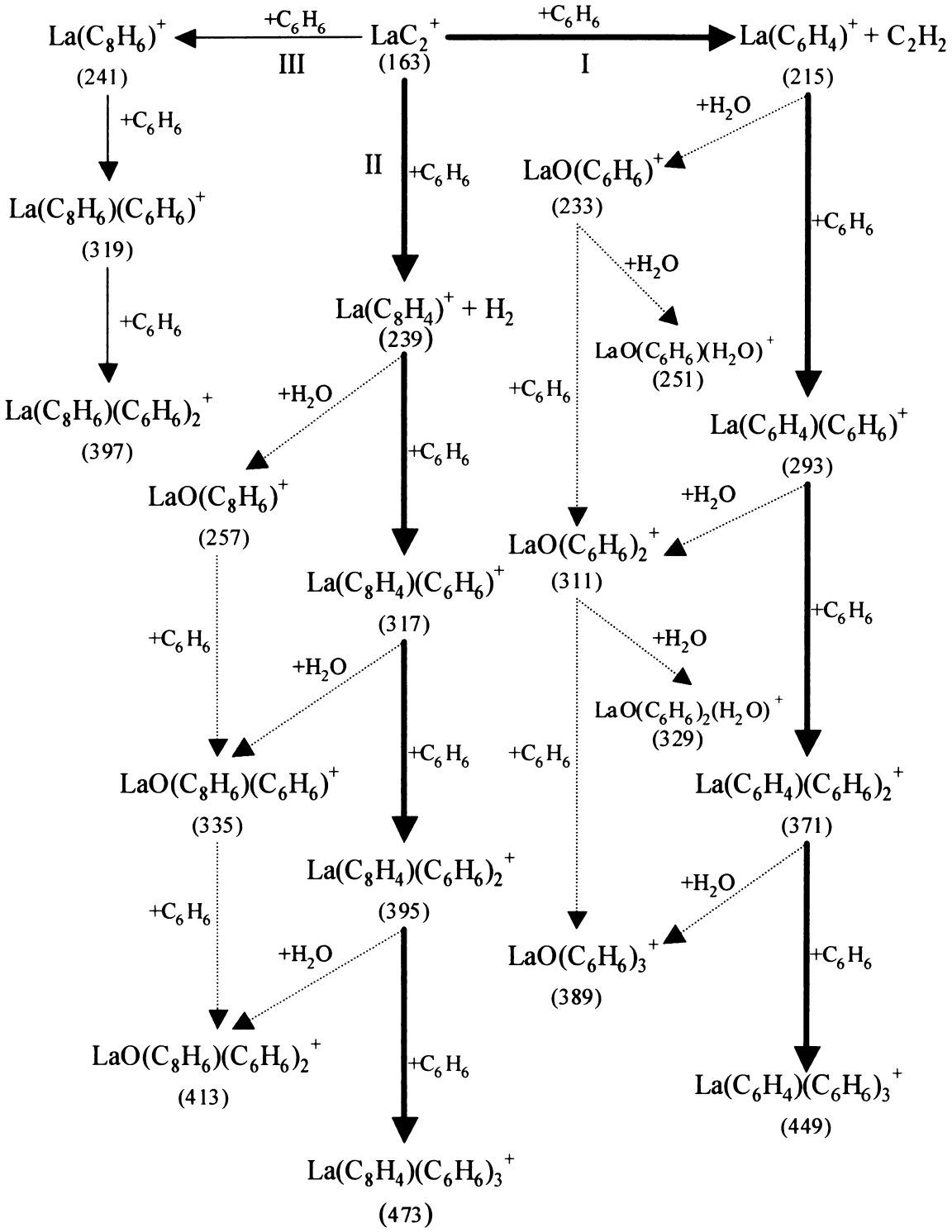

Figure 4-05 Proposed reaction pathways for LaC_2^+ reactions with benzene (and background water).

form $La(C_8H_6)(C_6H_6)_n^+$ (n= 1-2). The abundance of these product ions reveals that the formation of $La(C_6H_4)(C_6H_6)_n^+$ series is the dominant reaction route, followed by $La(C_8H_4)(C_6H_6)_n^+$ and $La(C_8H_6)(C_6H_6)_n^+$ series. As the background water only exists at an extremely low concentration (less than $1x10^{-9}$ mbar), all the product ions formed from the reaction with water are observed in a low abundance.

Figure 4-06 is the reaction profile showing the three major reaction pathways for LaC_2^+. They are plotted as the product ion intensities versus the reaction delay time. These plots indicate the clustering process progressing with extended reaction delays. It is observed that by increasing the reactant concentration in the ICR cell this clustering process can be accelerated. With a pulse valve gas inlet, the pressure of benzene can be raised as high as $1x10^{-6}$ mbar within a very short period of time (< 5 ms). Under such conditions, the formation of large cluster ions such as $La(C_6H_4)(C_6H_6)_3^+$ is possible even when the reaction delay is three or four times shorter than the one with a static low pressure of benzene.

4.3.4.2 The Reactions of LaC_4^+ / LaC_6^+ with Benzene

Reactions of LaC_4^+ and LaC_6^+ with benzene appear to be straight forward. No dehydrogenated products are observed for both ions, instead, only benzene addition products are observed in the form of $LaC_4(C_6H_6)_n^+$ and $LaC_6(C_6H_6)_n^+$ (n= 1-2) respectively. Water addition products $LaC_4(C_6H_6)(H_2O)^+$ and $LaC_6(C_6H_6)(H_2O)^+$ are observed as minor product ions. These results suggest that the increasing number of carbon atoms in lanthanum-carbide clusters can reduce the ion reactivity towards benzene. This might occur because the extra carbon atoms tie up all the available lanthanide valence electrons, which results in the decline of their reactivity. The reaction profiles also show that these reactions are slower than the reaction of LaC_2^+ with benzene (See Figure 4-07).

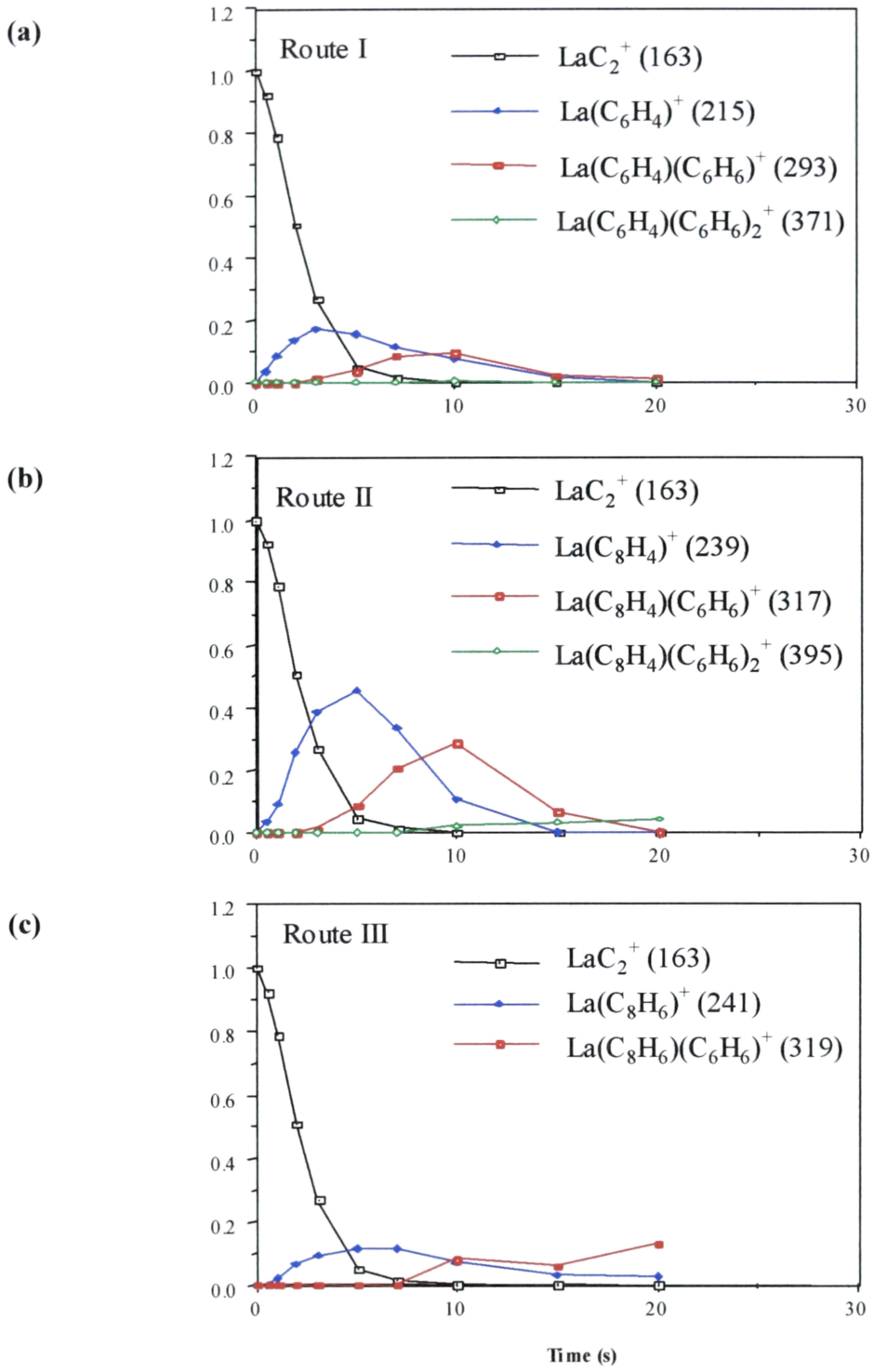

Figure 4-06 Reaction profiles of the three major reaction routes in the reaction of LaC_2^+ with benzene.

(a)

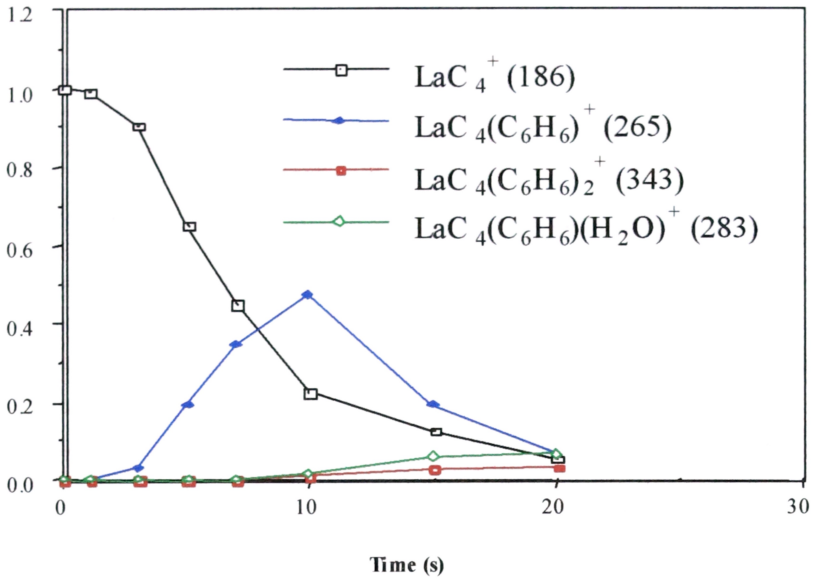

(b)

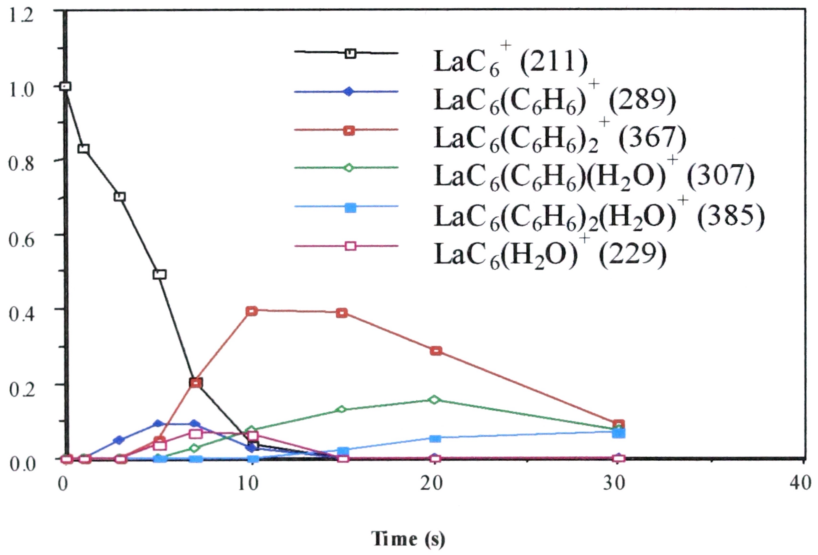

Figure 4-07 Reaction profiles of the reactions of LaC_4^+/LaC_6^+ with benzene.

4.3.4.3 The Reaction of YC_n^+ (n= 2, 4 and 6) with Benzene

The reactions of YC_n^+ (n = 2, 4 and 6) with benzene were carried out without any ion selection. The product ions are comparable to the reactions with LaC_n^+, except for YC_6^+, which was produced at extremely low abundance in the initial laser ablation step, and no corresponding reaction product ions are observed for this ion.

4.3.5 The Reactions of YC_n^+ and LaC_n^+ (n= 2, 4 and 6) with Cyclohexane

YC_n^+ or LaC_n^+ (n = 2, 4 and 6) are also reacted with cyclohexane as shown in Figures 4-08 and 4-09. In both cases, multiple dehydrogenation of the cyclohexane occurred. Metal-benzene complexes $M(C_6H_6)_n^+$ (M=Y or La; n= 1-3) are found to be the major product ions. Minor products such as $M(C_8H_8)(C_6H_6)_n^+$ (where n= 0-1) are also observed which suggests that the C_2 group in MC_2^+ may have been involved in the reaction. For MC_4^+, the aromatization of cyclohexane occurs with C_4 remaining on the M^+. $MC_4(C_6H_6)_n^+$ (n= 1-2) are also observed as minor product ions.

Reactions of MC_n^+ with benzene and cyclohexane show different reactivity among these metal-carbide cluster ions. MC_2^+ behaves similar to the corresponding bare metal ions and they are capable of multiple dehydrogenation of saturated hydrocarbon molecules such as cyclohexane. For MC_4^+ and MC_6^+, their lack of reactivity suggests that C_4 and C_6 groups have stronger interaction with the metal ion than the C_2 group. The speculation of these cluster ions is that if MC_n^+ has the linear structure that is commonly agreed for small pure carbon clusters C_n (n<10),[35,36] the extension of the carbon chain should have minor effect on the metal ions' reactivity because the metal is the reactive site. The weaker reactivity shown by MC_4^+ and MC_6^+ towards benzene seems to suggest structure other than linear for these cluster ions. In the later discussion in this chapter, DFT calculation will be employed to reveal the energy minimized structures for these MC_n^+.

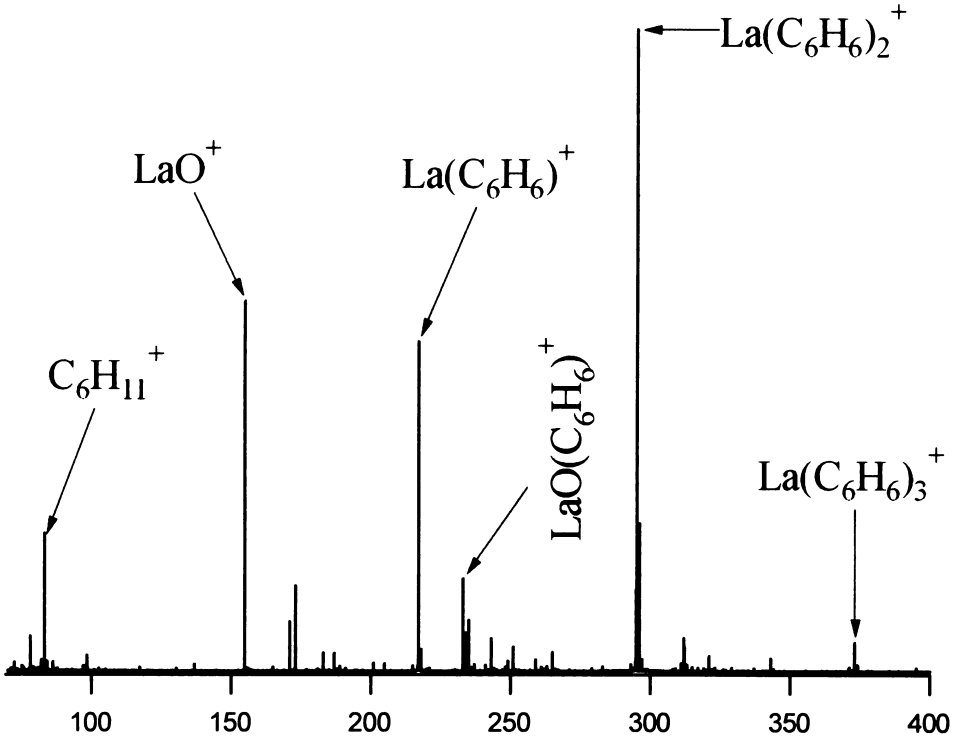

Figure 4-08 Positive-ion FTICR mass spectrum of gas-phase ion-molecule reactions of LaC_n^+ reacting with cyclohexane for 24 seconds.

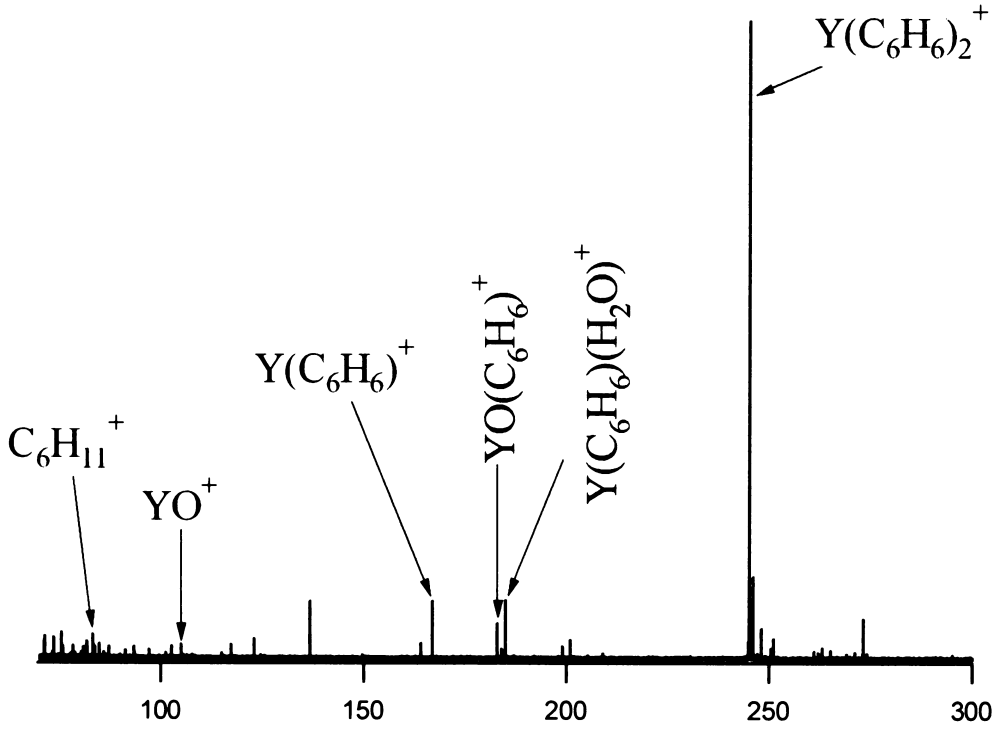

Figure 4-09 Positive-ion FTICR mass spectrum of gas-phase ion-molecule reactions of YC_n^+ reacting with cyclohexane for 12 seconds.

4.4 Collision-Induced Dissociation of the Ion-Molecule Reaction Products

The ion-molecule reaction of YC_n^+ and LaC_n^+ with benzene and cyclohexane also raise many questions about the nature of the interactions between the ligated transition metal ions and the reactant molecules. On the whole, mass spectrometry results provide little knowledge of the structure and bonding for the product ions. More sophisticated mass spectrometry experiments are needed to reveal detailed structure information of such product ions. This has made the collision-induced-dissociation technique very useful in such circumstances. Note that all the CID experiments describing in the following text are performed with on-resonance irradiation.

As shown above, in the reaction of LaC_2^+ with benzene, three major series of product ions are formed. The formula assigned for these product ions may appear to be ambiguous. For example, the core-ion of the $La(C_8H_6)(C_6H_6)_n^+$ series, which is $La(C_8H_6)^+$, can also be considered as $LaC_2(C_6H_6)^+$, for which the LaC_2^+ unit remains intact. The CID results from a related ion in this series, $La(C_8H_6)(C_6H_6)^+$ shows that the fragmentation of this ion begins with the dissociation of a benzene molecule producing a high abundance of $La(C_8H_6)^+$ (See Figure 4-10). The dissociation of $La(C_8H_6)^+$ occurs via several steps with triple losses of C_2H_2 followed by the loss of a C_2 group that yield the final product ion La^+. These steps require more CID energy than the dissociation of the benzene molecule in the first step, and all the fragment ions were produced in low abundance, which suggests that C_8H_6 exists as a strong covalent unit in the complex.

Figure 4-11 is a CID-FTICR mass spectrum of $La(C_6H_4)(C_6H_6)_3^+$. It shows that three benzene molecules are successively dissociated from the parent ion and produce three intense fragment ions $La(C_6H_4)(C_6H_6)_2^+$, $La(C_6H_4)(C_6H_6)^+$ and $La(C_6H_4)^+$. Further dissociation of $La(C_6H_4)^+$ shows two successive losses of C_2H_2 and the loss of a C_2

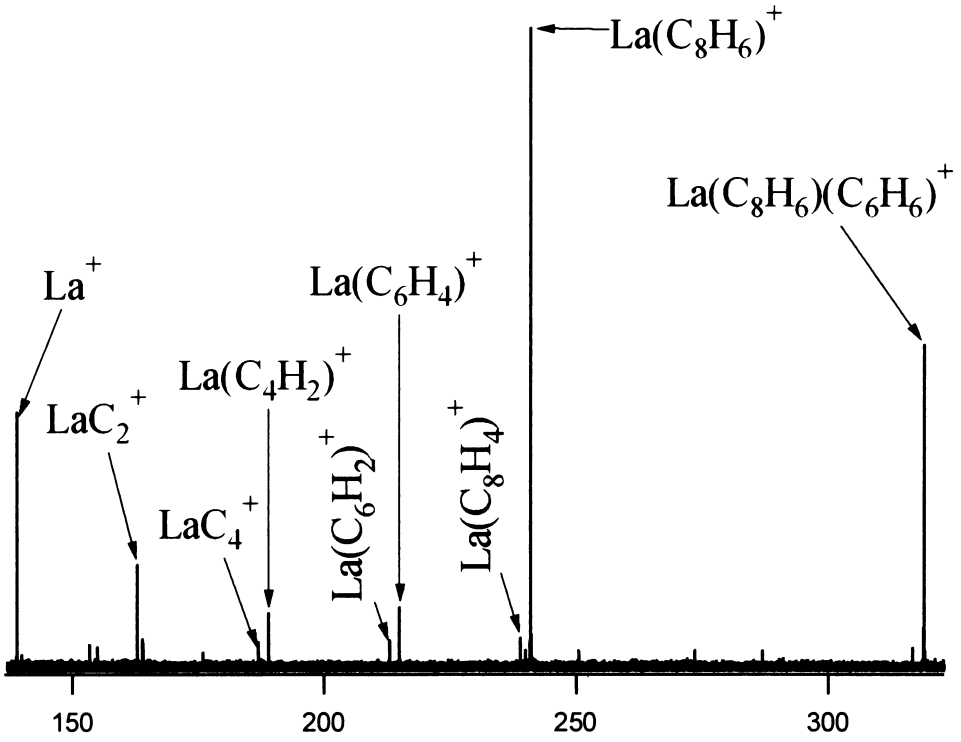

Figure 4-10 ORI-CID-FTICR mass spectrum of $La(C_8H_6)(C_6H_6)^+$.

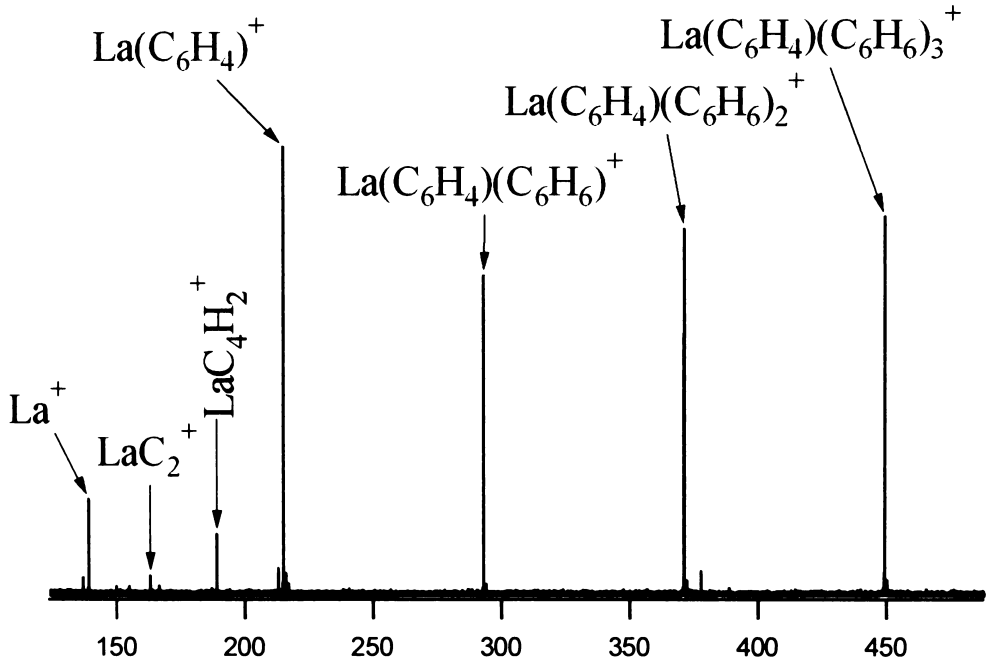

Figure 4-11 ORI-CID-FTICR mass spectrum of $La(C_6H_4)(C_6H_6)_3^+$.

group to yield the bare metal cation La^+ as the end product. The dissociation of $La(C_6H_4)^+$ appears to be a high-energy process, all the dissociation products from $La(C_6H_4)^+$ are produced in low abundance. For the three benzene molecules in $La(C_6H_4)(C_6H_6)_3^+$, they are most likely to be bond by electrostatic attraction from La^+. The relative low intensity of the fragment ions from $La(C_6H_4)^+$ indicates strong covalent interaction between La^+ and the ortho-benzyne group.

For the $La(C_8H_4)(C_6H_6)_n^+$ series, $La(C_8H_4)(C_6H_6)_2^+$ was selected to undergo the CID process. Figure 4-12 shows a CID-FTICR mass spectrum of $La(C_8H_4)(C_6H_6)_2^+$. Two benzene molecules are readily removed from the parent ion to produce $La(C_8H_4)^+$ in high abundance. The dissociation of $La(C_8H_4)^+$ shows loss of two C_2H_2 groups and two C_2 groups. This CID result also indicates that C_8H_4 exist as an entity in the complex. Similar product ions from the reaction of YC_2^+ with benzene are also investigated by a CID experiment. Figure 4-13 shows the CID result for $Y(C_8H_4)(C_6H_6)_2^+$. An almost identical fragmentation pattern to $La(C_8H_4)(C_6H_6)_2^+$ is shown in this mass spectrum.

Among the LaC_4^+ reaction products, $LaC_4(C_6H_6)_2^+$ was examined by a CID experiment. As shown in Figure 4-14, two benzene molecules are removed from this ion followed by two C_2 losses to yield La^+. A comparison can be made to $YC_4(C_6H_6)_2^+$ (Figure 4-15), for which the two benzene molecules are also removed from the parent ion with further dissociation of two C_2 groups.

Many minor product ions containing oxygen atoms are observed in the YC_n^+ and LaC_n^+ reactions. Although the relative intensities of these by-product ions are insignificant compared to those main-stream benzene product ions, the structure of these ions is equally important in revealing the intrinsic properties of metal carbon interactions. For this reason, a few of these minor product ions such as $YO(C_6H_6)_3^+$, $YO(C_6H_6)_2^+$, $LaO(C_6H_6)_2^+$, $LaO(C_6H_6)^+$, $YO(C_6H_6)(H_2O)^+$, $LaO(C_6H_6)(H_2O)^+$,

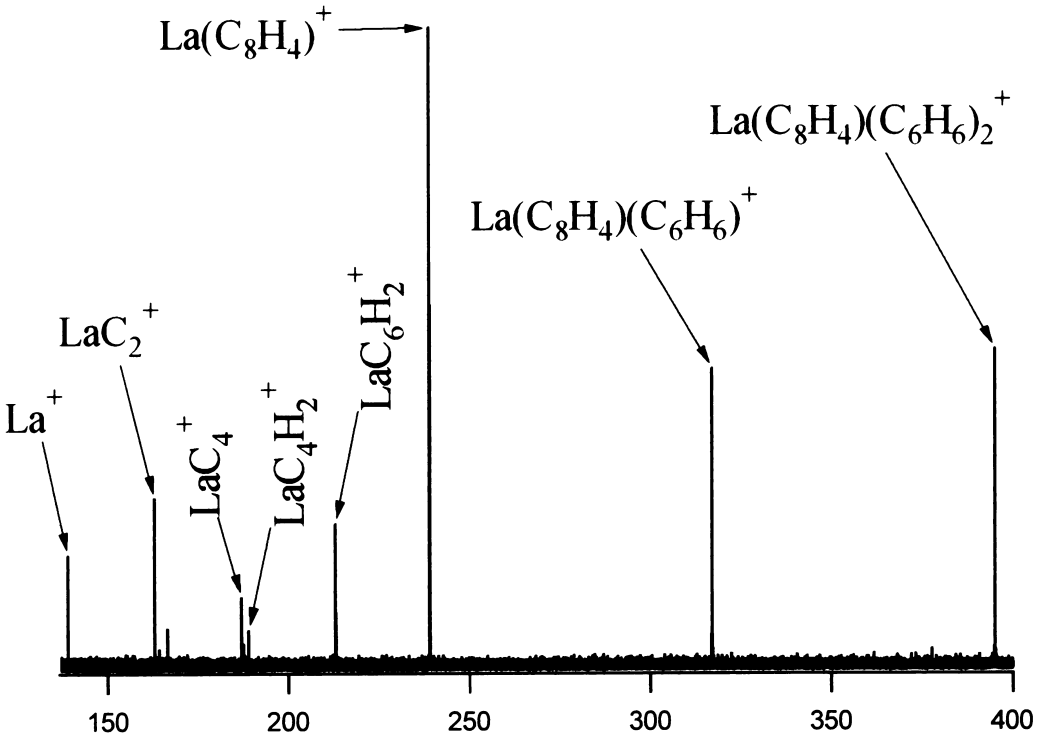

Figure 4-12 ORI-CID-FTICR mass spectrum of $La(C_8H_4)(C_6H_6)_2^+$.

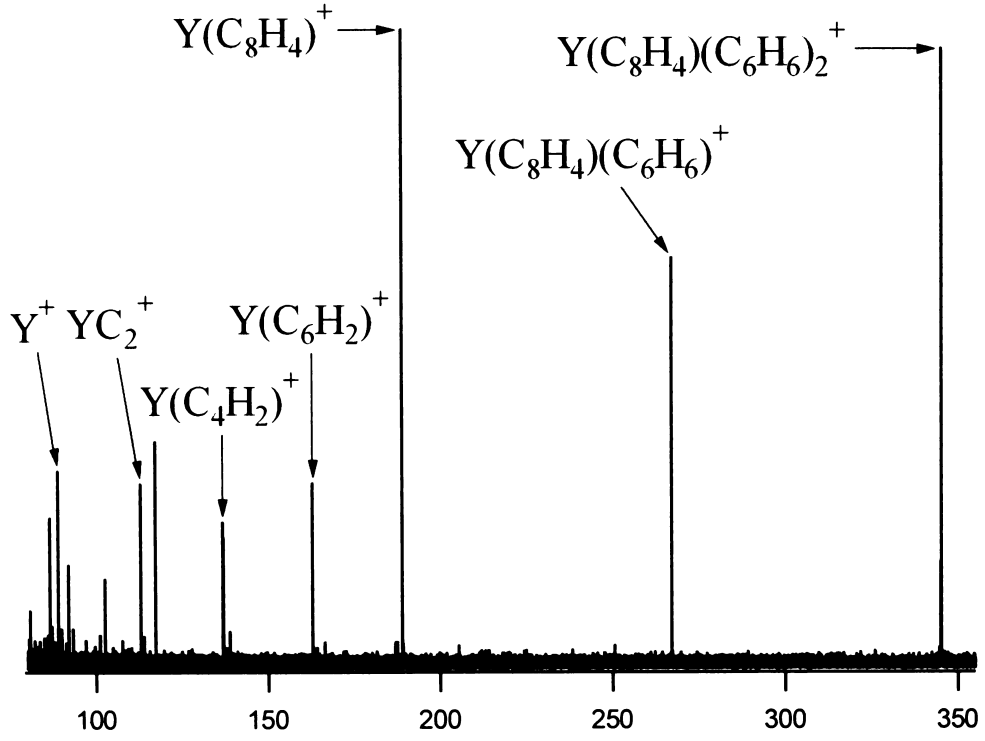

Figure 4-13 ORI-CID-FTICR mass spectrum of $Y(C_8H_4)(C_6H_6)_2^+$.

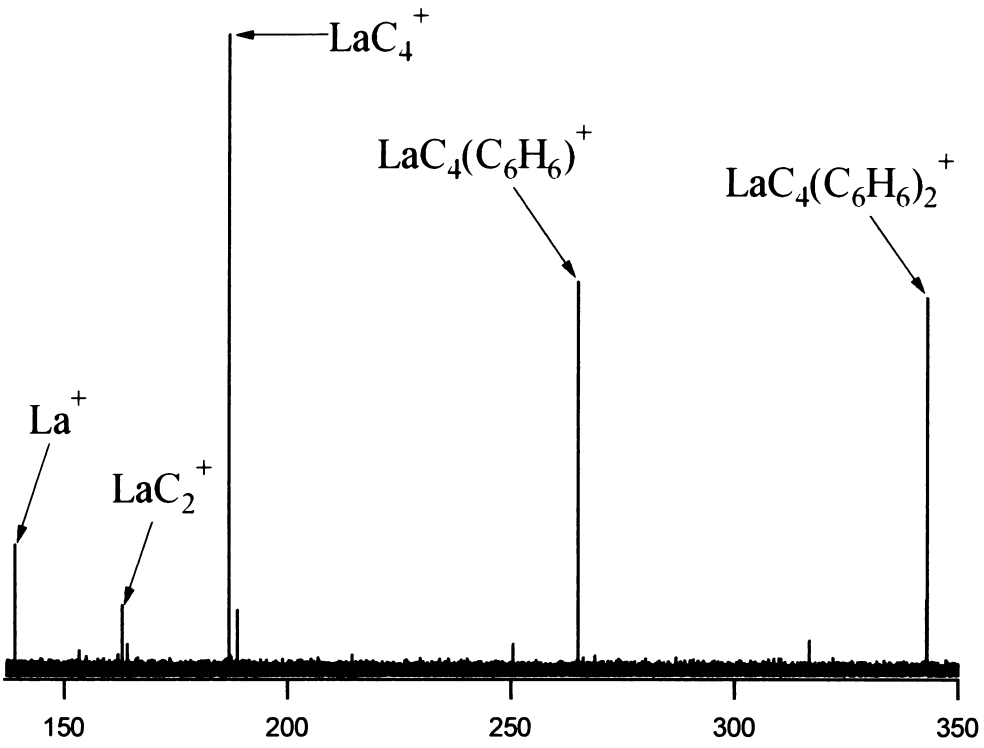

Figure 4-14 ORI-CID-FTICR mass spectrum of $LaC_4(C_6H_6)_2^+$.

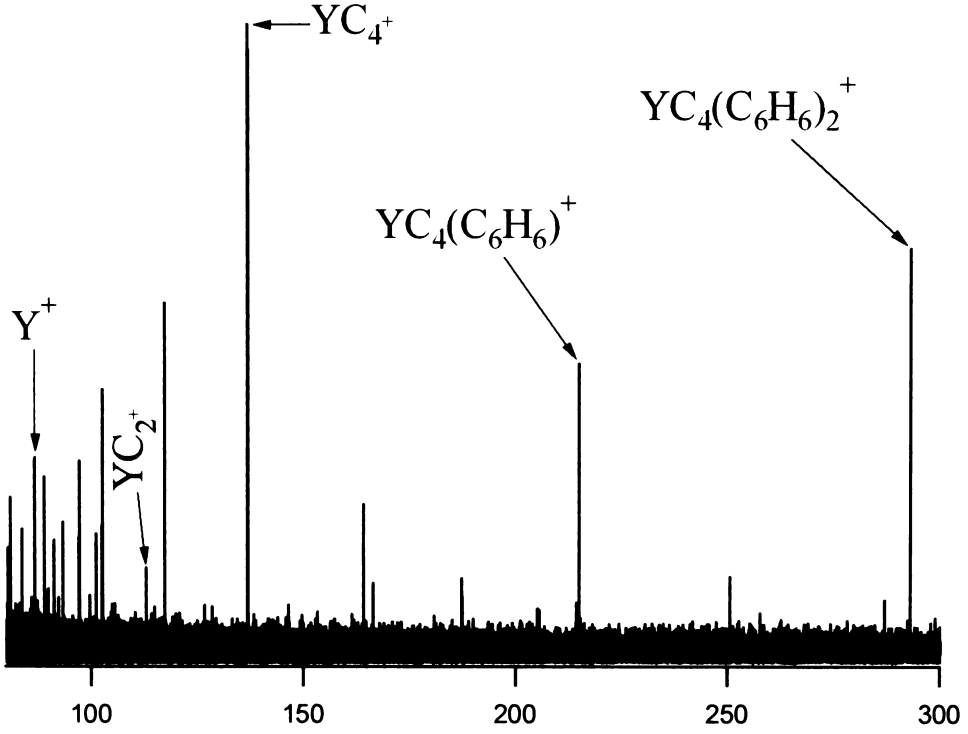

Figure 4-15 ORI-CID-FTICR mass spectrum of $YC_4(C_6H_6)_2^+$.

$YO(C_8H_6)(C_6H_6)^+$, $LaO(C_8H_6)^+$ and $LaO(C_8H_6)(C_6H_6)^+$ are investigated by CID experiments. Since both YO^+ and LaO^+ are not reactive towards benzene, these oxygen containing species are most likely formed from the ion-molecule reactions with water. The analysis of these CID results suggest that for species such as $M(C_6H_4)^+$ and $M(C_8H_4)^+$, their reaction with water effectively hydrogenates the C_6H_4 and C_8H_4 to form $MO(C_6H_6)^+$ and $MO(C_8H_6)^+$ respectively. The oxygen atom is strongly bonded to the metal ion and attracts the electronic charge from the metal, which weakens the interaction between the metal and the other ligands. This weakening effect has been reflected by the CID results of $MO(C_8H_6)(C_6H_6)^+$. In this case, after the initial lost of a benzene molecule, the following dissociation occurs via the loss of C_8H_6 as a whole unit (see Figure 4-16) no intermediate products are observed in this step, whereas in the CID of $M(C_8H_6)(C_6H_6)^+$, the $M(C_8H_6)^+$ fragmented in many steps and required much higher energy (See Figure 4-10) for dissociation.

In the reaction of YC_n^+ and LaC_n^+ with cyclohexane, the product ion, metal-benzene complex $M(C_6H_6)_n^+$ (M=Y and La; n= 1-3) and the minor product ions $M(C_8H_8)(C_6H_6)^+$ are not observed in the reactions with benzene. The CID result of $La(C_6H_6)_2^+$ (See Figure 4-17) suggests that after the initial lost of a benzene molecule, further dissociation of $M(C_6H_6)^+$ involves H_2 elimination to produce $M(C_6H_4)^+$ and a trace of $M(C_6H_2)^+$. Further dissociation of $M(C_6H_4)^+$ shows losses of two C_2H_2 groups and a C_2 group. In the case of $La(C_8H_8)^+$ (see Figure 4-18), the fragmentation first produced $La(C_6H_6)^+$, with further fragmentation follows similar dissociation channels as $M(C_6H_6)^+$.

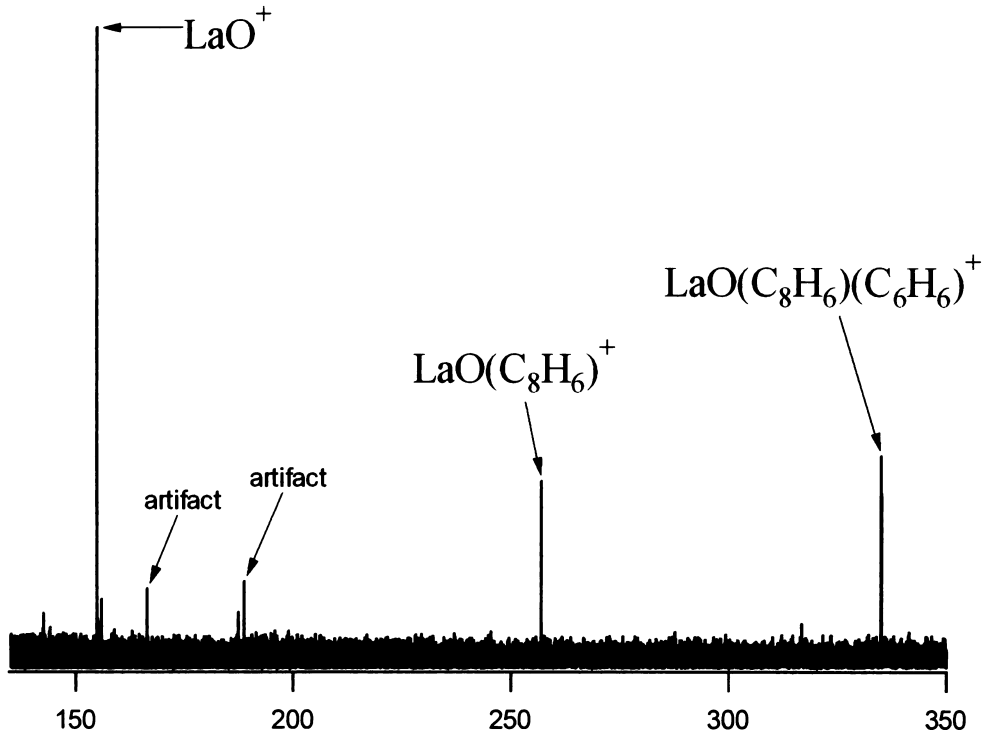

Figure 4-16 ORI-CID-FTICR mass spectrum of $LaO(C_8H_6)(C_6H_6)^+$.

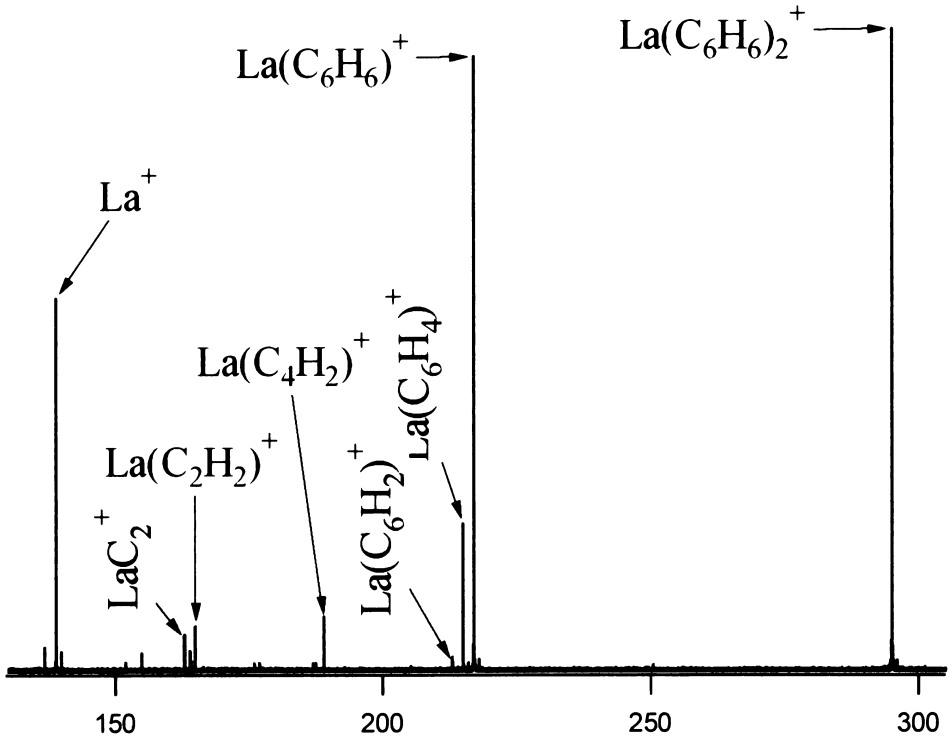

Figure 4-17 ORI-CID-FTICR mass spectrum of $La(C_6H_6)_2^+$.

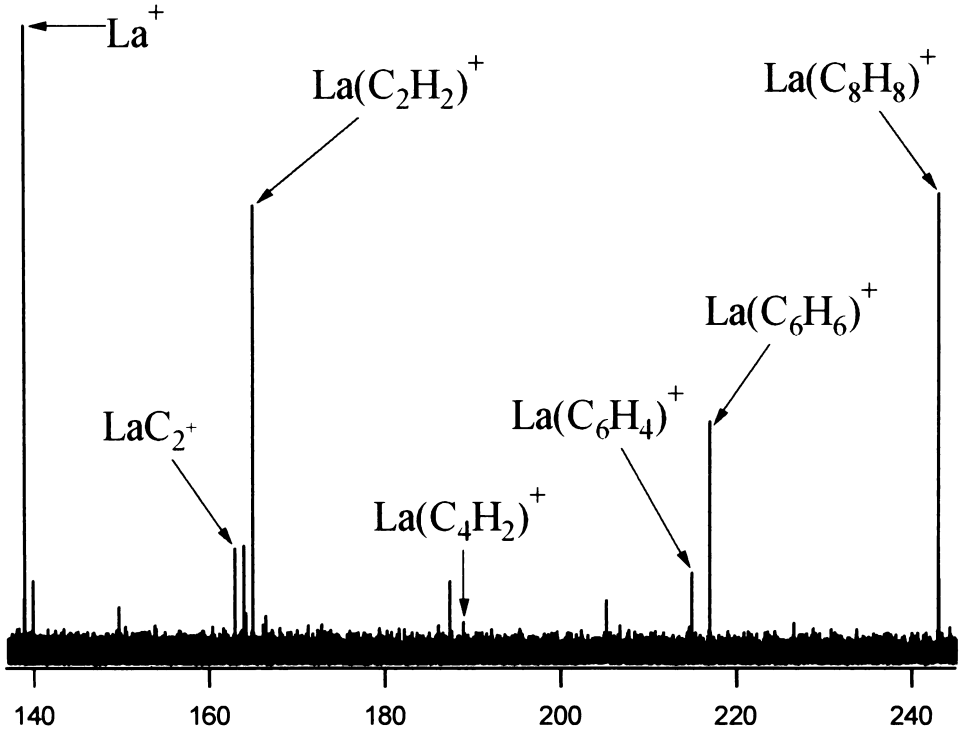

Figure 4-18 ORI-CID-FTICR mass spectrum of $La(C_8H_8)^+$.

4.5 DFT Quantum Chemical Calculations of Selected Metal-carbon Clusters and Its Gas-phase Ion Molecule Reaction Products

4.5.1 Gaussian 98W® Quantum Chemical Calculations Package

4.5.1.1 The Calculation Algorithm

In general, DFT calculations proceed in the same way as Hartree-Fock calculations, with addition of the evaluation of an extra term, the electron exchange energy E^{XC}. This term cannot be evaluated analytically for DFT methods, so it is computed via numerical integration. These calculations employ a grid of points in space in order to perform the numerical integration. Grids are specified as number of radial shells around each atom, each of which contains a set number of integration points. For example, in the (75,302) grid, 75 radial shells each contain 302 points, resulting in a total of 22,650 integration points. Uniformed and pruned versions of many grids have been defined. Uniformed grids contain the same number of angular points at each radial distance, while pruned grids are reduced from their full form so that fewer points are used on the shells near the core and far from the nucleus, where less density is needed for a given level of computational accuracy. Put another way, pruned grids are designed to be densest in the region of the atom where properties are changing most rapidly.

For the *Gaussian98W®*[37] quantum chemical calculation package used in this present study, the pruned grid (75,302)p has been set as the default for all but single point calculations using standard SCF convergence. The SG1 grid, a pruned (50,194) grid containing about 3,600 points per atom is used for lower-accuracy single point calculations.

4.5.1.2 Basis Sets Used in Calculations

The *Gaussian 98W®* program adopts gaussian-type atomic functions as *basis functions*. Gaussian functions have the general form:

$$g(\alpha,\vec{r}) = cx^n y^m z^l e^{-\alpha r^2} \tag{4-10}$$

where $\vec{r}$ is composed of x, y and z. α is a constant determining the size (radial extent) of the function. In a gaussian function, $e^{-\alpha r^2}$ is multiplied by powers (possibly 0) of x, y and z, and a constant for normalization, so that

$$\int_{all-space} g^2 = 1 \tag{4-11}$$

thus, c depends on l, m and n. Linear combination of primitive gaussians forms the actual basis function which are called contracted gaussians:

$$\chi_\mu = \sum_p d_{\mu p} g_p \tag{4-12}$$

where there are fixed constants within a given basis set. The contracted functions are also normalized. Molecular orbitals are therefore expressed as:

$$\phi_i = \sum_\mu c_{\mu i} \chi_\mu = \sum_\mu c\mu i \left(\sum_p d_{\mu p} g_p \right) \tag{4-13}$$

In this present study, most of the species studied by the quantum chemical calculation involve the third-row transition metal, lanthanum. The chosen basis set must take into account the effective core potentials (ECPs) and relativistic effects in order to produce more accurate results. LanL2DZ and SDD are the two basis sets used in all the calculations. The LanL2DZ basis set uses D95[38] (Duning/Huzinaga full double-zeta (DZ)) basis functions for the first row elements, and Los Alamos ECP plus DZ functions on Na-Bi.[39-41] The SDD basis set uses D95V[38] (Duning/Huzinaga valence DZ) for the first row elements and Stuttgart/Dresden ECP's for the rest of the periodic table.[42-64] For both basis sets, the ECP treatment has taken into account some degree of relativistic effect for large nuclei.

4.5.2 DFT Calculation of LaC_n^+ (n = 2, 4 and 6) Clusters

The ion-molecule reactions that were discussed earlier in this chapter involve metal-carbon cluster ions YC_n^+ and LaC_n^+ (n =2, 4, 6). In order to understand their reaction dynamics, it is helpful to know something about the geometric and electronic structures of these cluster ions and their associated electronic energies.

The DFT calculation of the energy minimal structure of LaC_2^+ was carried out on several possible geometries including linear, lanthanum-bridged ring and dumbbell (Figure 4-19). The linear structure has lanthanum bonded to the one end of the C-C bond, which has a double bond character. Electron spin states of singlet, triplet and quintet are investigated for all these structures. The ground state structure is the lanthanum-bridged isomer in the singlet state. Calculations using two different basis sets, LanL2DZ and SDD give similar results for these isomers. The total energy differences between these isomers are shown in Table 4-01.

Table 4-01 Calculated relative energies (in kcal/mol) for three LaC_2^+ isomers.

Basis set	Ring*	Linear	Dumbbell
LanL2DZ	0.000	7.629	165.741
SDD	0.000	8.498	169.332

* Calculated ring structure energy used as energy minimal for comparison

All structures are optimized with respect to the geometry and frequencies. Positive frequencies are obtained for all these structures. It shows that the La-C bond in the ring is the longest one. The C-C bond in this structure has a double bond character. The La-C bond length in the linear structure is the shortest with the connecting C-C bond slightly longer than the one in the ring structure. The C-La-C bond angle is 32.4°.

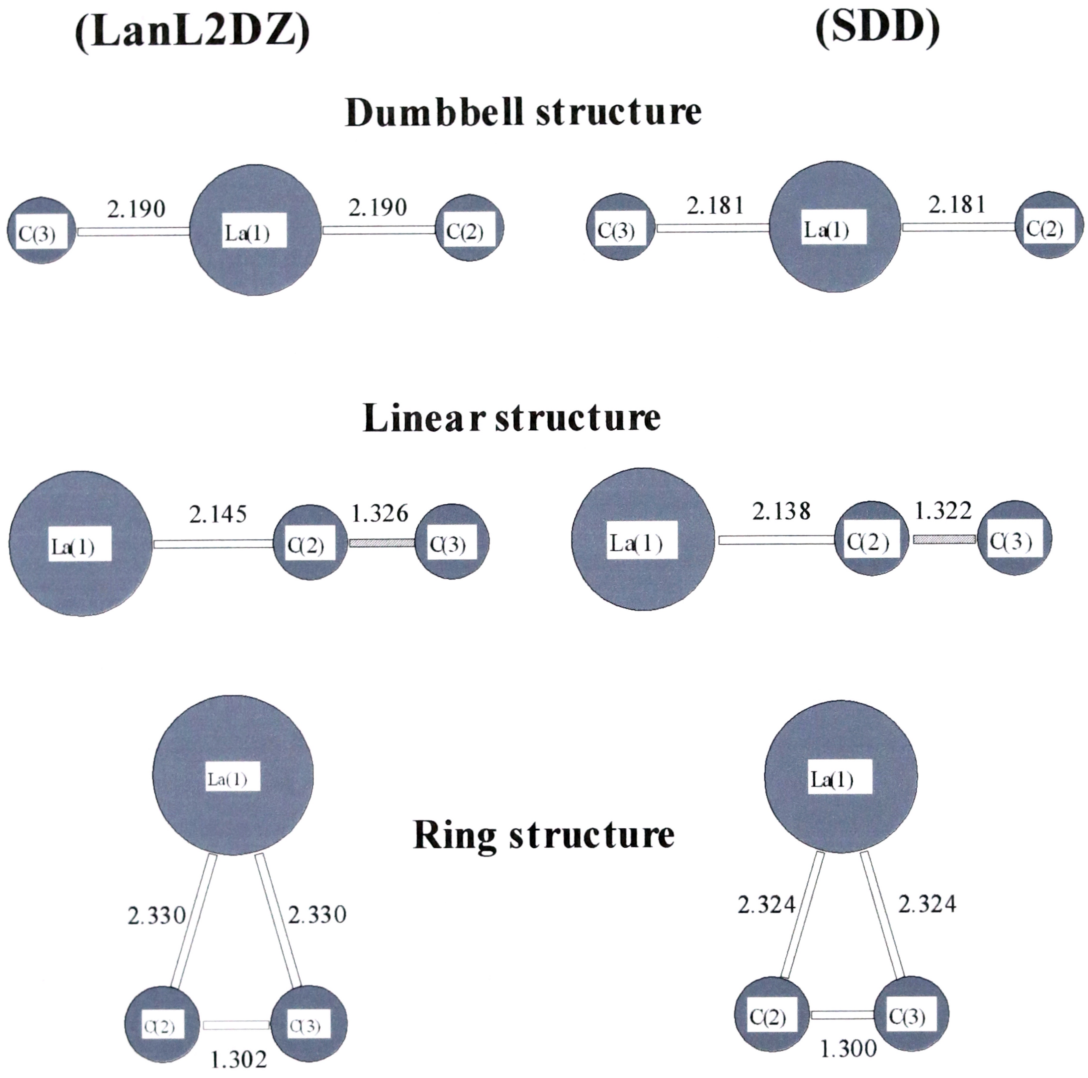

Figure 4-19 Optimized structures (DFT) for three LaC_2^+ isomers in the singlet state (Bond length in Angstroms).

For LaC_4^+ isomers, linear, ring, tetrahedral and fan geometries are investigated for singlet, triplet and quintet electronic states using the B3LYP/SDD method. The calculated ground-state structure has a fan-shape geometry (Figure 4-20). The bond length and bond angles are listed in Table 4-02.

Table 4-02 Bond length and bond angles of ground-state LaC_4^+.

Bond	Bond Length (Å)	Bond Angle
La(1)-C(2)	2.176	C(2) -La(1)-C(3) 34.6°
La(1)-C(3)	2.229	C(3) -La(1)-C(4) 34.9°
La(1)-C(4)	2.229	C(4) -La(1)-C(5) 34.6°
La(1)-C(5)	2.176	
C(2)-C(3)	1.312	La(1)- C(2) - C(3) 74.9°
C(3)-C(4)	1.337	La(1)- C(3) - C(4) 72.6°
C(4)-C(5)	1.312	La(1)- C(4) - C(5) 70.5°

Quantum chemical calculations on metal-carbide cluster neutrals and cations $MC_n^{0/+}$ (M=Y and La; n < 10) have been reported by several research groups.[1,65-67] In general, they claim that the ground-state structure for these clusters is the 'fan' structure, for which the lanthanum atom or cation bond to each carbon atom on a curved carbon chain. The singlet state was found to be the ground state for cations. Current calculations on both linear and 'fan' isomers for LaC_n^+ (n= 2, 4 and 6) are in a good agreement with these reports except for LaC_6^+, this current study shows that it is not co-planer but being a 'shell' shaped structure (Figure 4-20).

Analysis of computed Mulliken population charges for LaC_n^+ (n=2, 4 and 6) show that the La-C bonds are strongly ionic (Table 4-03). The electronic charge is transferred

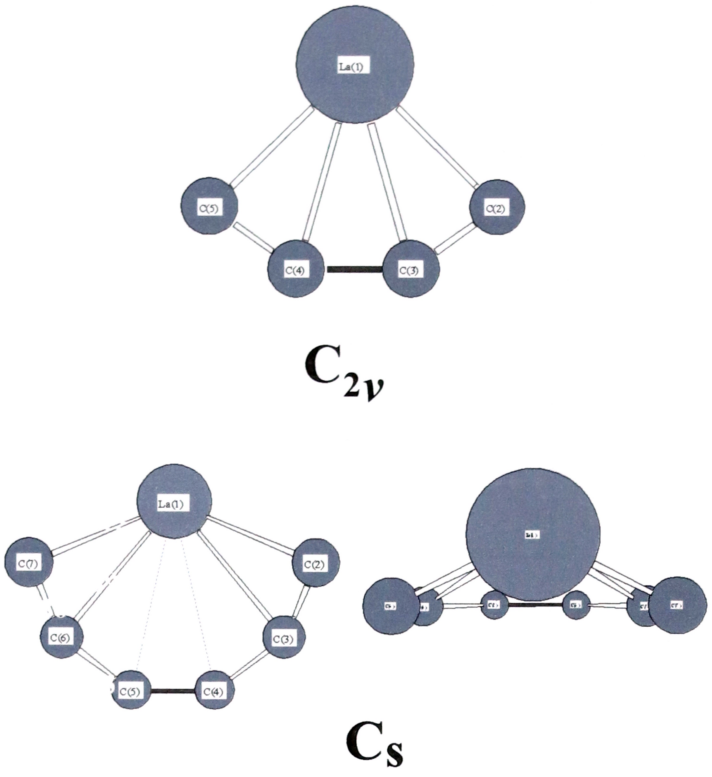

Figure 4-20 Fully optimized ground-state structures for LaC_4^+ and LaC_6^+ in the singlet state calculated by DFT method (B3LYP/SDD).

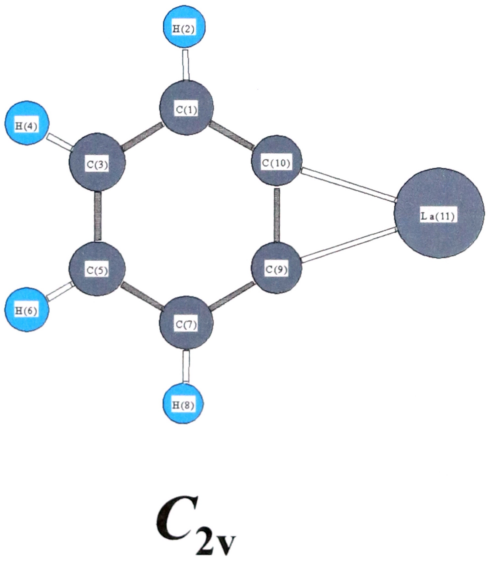

Figure 4-21 Fully optimized ground-state structure for $LaC_6H_4^+$ in the singlet state calculated by DFT method (B3LYP/SDD).

from lanthanum to carbon atoms.[65] As the number of carbon atoms increases, the electron density on lanthanum is largely reduced and this has compromised its capability for bond activation in the reaction with organic molecules.

Table 4-03 Atomic Charges on LaC_2^+, LaC_4^+ and LaC_6^+.

Ion	Atom	Atomic Charge
LaC_2^+	La(1)	**1.189705**
	C(2)	-0.094853
	C(3)	-0.094853
LaC_4^+	La(1)	**1.352253**
	C(2)	-0.174581
	C(3)	-0.001446
	C(4)	-0.001446
	C(5)	-0.174581
LaC_6^+	La(1)	**1.499610**
	C(2)	-0.134707
	C(3)	-0.158885
	C(4)	0.043787
	C(5)	0.043787
	C(6)	-0.158885
	C(7)	--0.134707

4.5.3 Calculation of Gas-Phase Ion-Molecule Reaction Products

Although the CID studies described earlier in this chapter clarify many ambiguities concerning the product ion structures, questions still remain as what is the minimal energy structure for a particular ion. The mass spectrometry method has reached its limit to provide further information at this point. The quantum chemical calculation therefore becomes a necessary and complementary method to reveal the underlying physical and chemical properties of these cluster ions.

In the reactions with benzene, the main concern is to reveal the ground-state structures for $La(C_6H_4)^+$, $La(C_8H_4)^+$ and $La(C_8H_6)^+$ as they are the 'core' ions for the clustering reaction. As shown in Figures 4-21 ~ 4-23, in all three cases, charged lanthanum metal forms two covalent bonds with their organo-ligands. These structures satisfy the s^1d^1 configuration for La^+. In the case of $La(C_8H_6)^+$, an isomer built by LaC_2^+ absorbed on to the benzene ring is also calculated. The computed energy difference between the two isomers of $La(C_8H_6)^+$ is 36.4 kcal/mol.

The calculations of larger cluster ions containing more than one benzene molecules are time-consuming tasks. Currently only preliminary results are obtained for some of these organometallic complexes. Figure 4-24 shows the fully optimized structure for $La(C_6H_4)(C_6H_6)^+$. The important feature of this structure is the angle formed between C_6H_6 and $La(C_6H_4)$ planes, and for this cluster ion the angle is about 12°. It has been observed during the calculation when the two planes reach to this angle, the rotation of the benzene molecule in the plane has made little change in the total energy. It is therefore difficult to determine the correct symmetry for the energy minimal structure for this type of the cluster ions. The fully optimized structure for $La(C_6H_4)(C_6H_6)_2^+$ shows that a tilted 'sandwich' type of structure can be formed (Figure 4-25), with the angles between the center ion and the two benzene molecules similar to

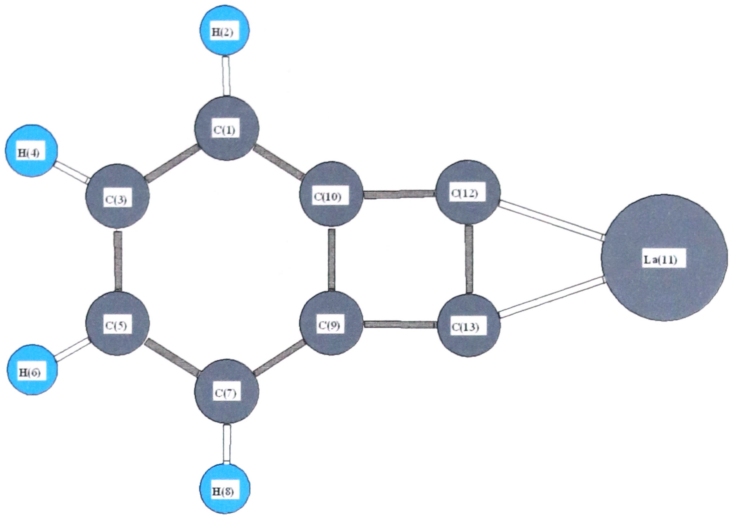

C_{2v}

Figure 4-22 Fully optimized ground-state structure for $LaC_8H_4^+$ in the singlet state calculated by DFT method (B3LYP/LanL2DZ).

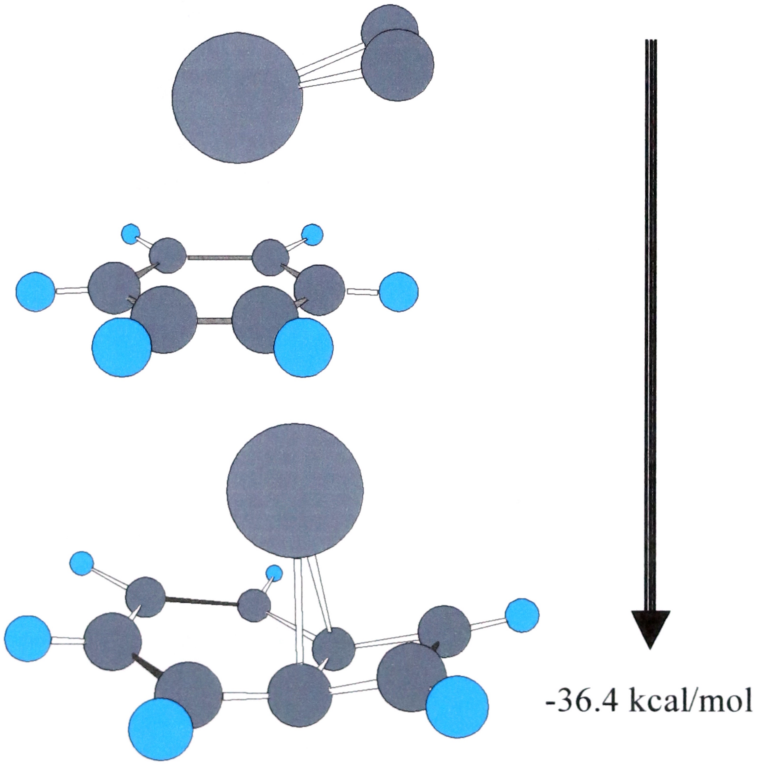

Figure 4-23 Fully optimized ground-state structures for $LaC_8H_4^+$ isomers in the singlet state calculated by DFT method (B3LYP/LanL2DZ).

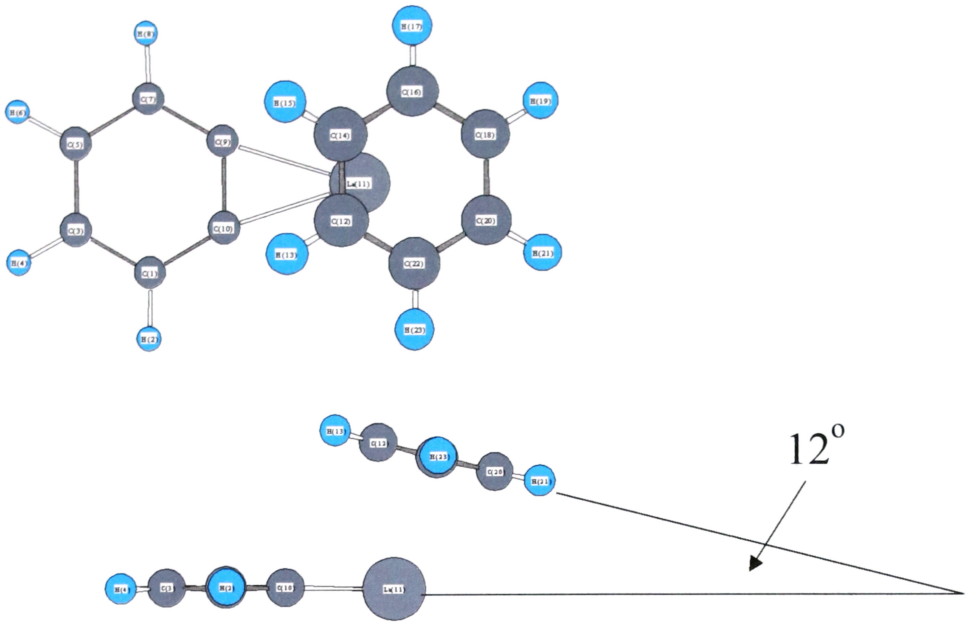

Figure 4-24 Fully optimize ground-state structure for $La(C_6H_4)(C_6H_6)^+$ calculated by DFT method (B3LYP/LanL2DZ).

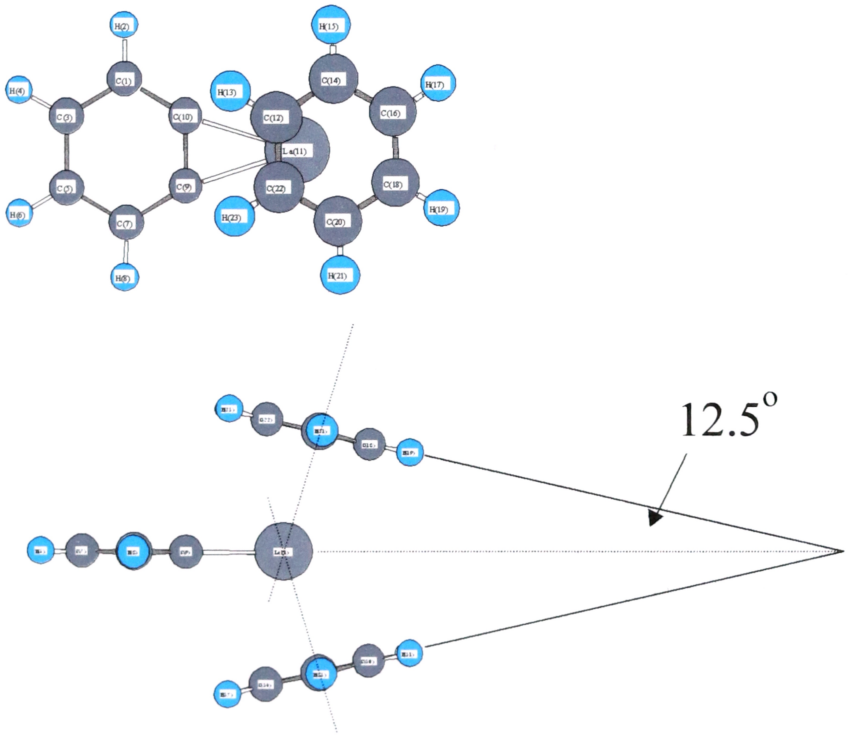

Figure 4-25 Fully optimize ground-state structure for $La(C_6H_4)(C_6H_6)_2^+$ calculated by DFT method (B3LYP/LanL2DZ).

$La(C_6H_4)(C_6H_6)^+$. Inspired by the optimized structures of $La(C_6H_4)(C_6H_6)^+$ and $La(C_6H_4)(C_6H_6)_2^+$, a geometry for $La(C_6H_4)(C_6H_6)_3^+$ is proposed and yet to be confirmed by the DFT calculation (Figure 4-26).

Geometrically optimized structures for $La(C_8H_4)(C_6H_6)^+$ and $LaC_4(C_6H_6)^+$ show their angles are about 10.5° and 15° respectively (Figure 4-27 and Figure 4-28). The greater angle in $LaC_4(C_6H_6)^+$ suggests that the closely bonded carbon atoms C_4 on lanthanum has increased the Coulomb repulsion between the absorbed benzene molecule and the carbon chain on LaC_4^+.

4.6 Conclusions

Yttrium- and Lanthanum-carbide cluster cations YC_n^+ and LaC_n^+ ($n<10$) are generated by laser ablation of targets containing carbonaceous material and Y_2O_3 or La_2O_3. YC_2^+, YC_4^+, LaC_2^+, LaC_4^+ and LaC_6^+ are selected to undergo gas phase ion-molecule reactions with benzene and cyclohexane. FTICR mass spectrometry studies of the reactions of YC_2^+ and LaC_2^+ with benzene show three main series of cluster ions are formed. They are in the form of $M(C_6H_4)(C_6H_6)_n^+$, $M(C_8H_4)(C_6H_6)_n^+$ and $M(C_8H_6)(C_6H_6)_m^+$ (M=Y and La; n= 0-3; m= 0-2). For YC_4^+, LaC_4^+ and LaC_6^+, only benzene addition products in the form of $MC_n(C_6H_6)_m^+$ (M=Y and La; n= 4, 6; m= 1, 2) are observed. In the reaction with cyclohexane, all the metal-carbide cluster ions results in a similar series of product ions in the form of $M(C_6H_6)_m^+$ (M=Y and La; m= 1, 2).

Collision-induced-dissociation results on the complex product ions indicate that both covalent and non-covalent interactions are involved in their formation. DFT calculation on the major product ions confirmed the ground-state for LaC_n^+ (n= 2, 4 and 6) is the singlet state with a 'fan' structure. LaC_6^+ has a non-coplanar shell shaped 'fan' structure.

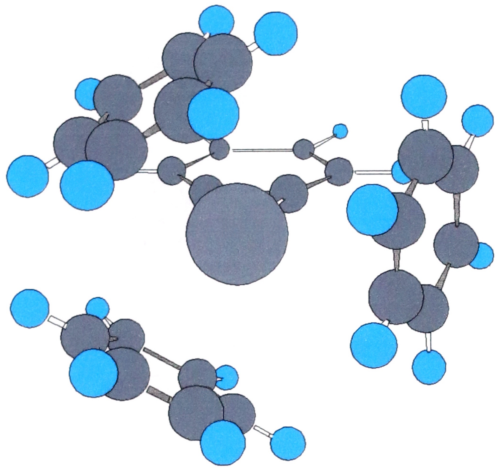

Figure 4-26 The proposed structure for $La(C_6H_4)(C_6H_6)_3^+$.

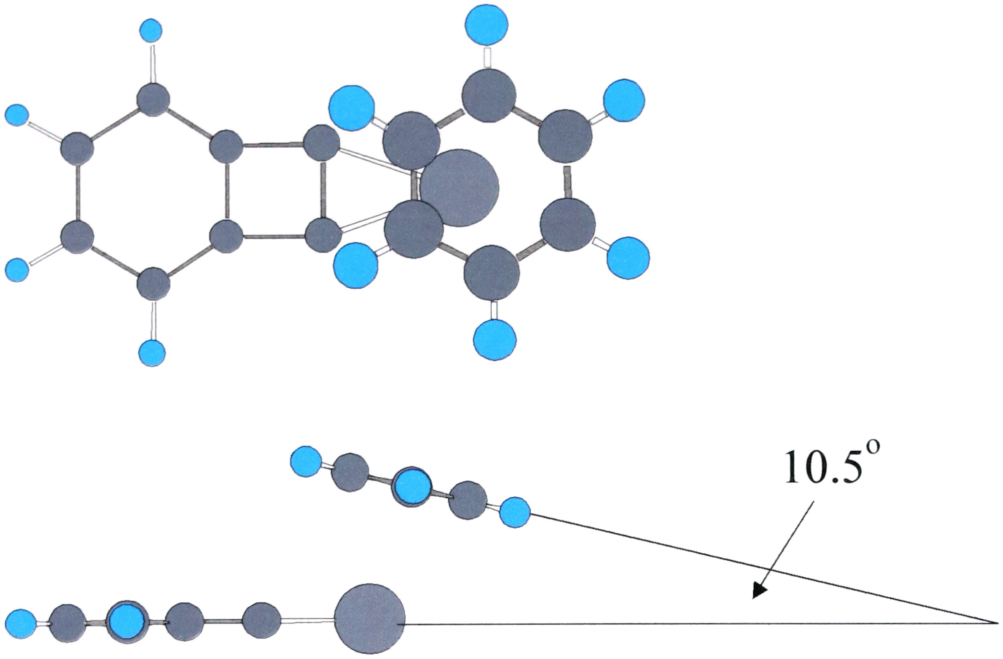

Figure 4-27 Fully optimized ground-state structure for $La(C_8H_4)(C_6H_6)^+$ calculated by DFT method (B3LYP/LanL2DZ).

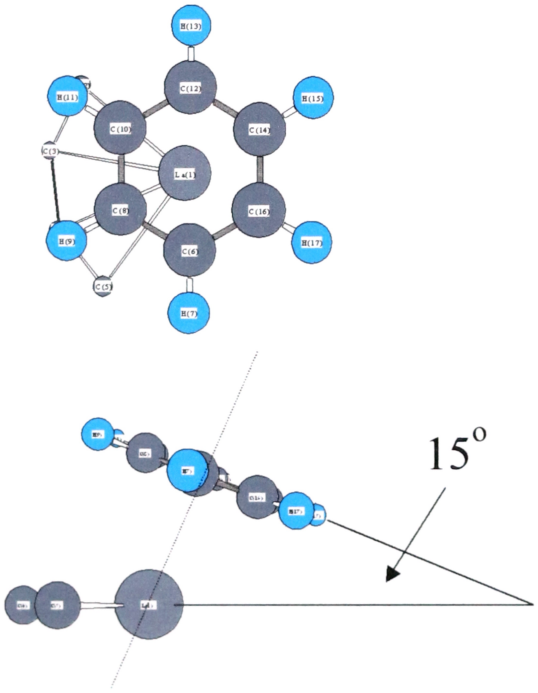

Figure 4-28 Fully optimized ground-state structure for $LaC_4(C_6H_6)^+$ calculated by DFT method (B3LYP/LanL2DZ).

The calculation on the complex product ions revealed that the plane of the initial core-ion in each complex forms different angles with the absorbed benzene molecular plane(s) and such angles are important in stabilizing the complex products.

4.7 References

(1) Suzuki, S.; Torisu, H.; Kubota, H.; Wakabayashi, T.; Shiromaru, H.; Achiba, Y. *Int. J. Mass Spectrom. Ion Proc.* **1994**, *138*, 297.

(2) Clemmer, D. E.; Jarrold, M. F. *Proc. SPIE-Int. Soc. Opt. Eng.* **1994**, *2124*, 400.

(3) Clemmer, D. E.; Shelimov, K. B.; Jarrold, M. F. *Nature* **1994**, *367*, 718.

(4) Eller, K.; Schwarz, H. *Chem. Rev.* **1991**, *91*, 1121.

(5) Schroeder, D.; Schwarz, H. *Angew. Chem., Int. Ed. Engl.* **1995**, *34*, 1973.

(6) Eller, K.; Schwarz, H. *Ber. Bunsenges. Phys. Chem.* **1990**, *94*, 1339.

(7) Freiser, B. S. *Organometallic Ion Chemistry (Understanding Chemical Reactivity, Vol. 15) Ed.* Freiser, B. S. (Kluwer Academic) ***1996***, *1.*

(8) Leary, J. A.; Armentrout, P. B. *Int. J. Mass Spectrom. Ion Proc.* ***2001***, *204,* 1.

(9) Schwarz, H. *Chem. Unserer Zeit* **1991**, *25*, 268.

(10) Schwarz, H.; Schroeder, D. *Proc. 38th Robert A. Welch Found. Conf. Chem. Res.* **1994**, 287.

(11) Schwarz, H.; Schroder, D. *Pure Appl. Chem.* **2000**, *72*, 2319.

(12) Eller, K.; Zummack, W.; Schwarz, H. *J. Am. Chem. Soc.* **1990**, *112*, 621.

(13) Eller, K.; Karrass, S.; Schwarz, H. *Ber. Bunsen-Ges. Phys. Chem.* **1990**, *94*, 1201.

(14) Smalley, R. E.; Hafner, J. H.; Colbert, D. T.; Smith, K. *PCT Int. Appl.* **2000**, 33.

(15) Grobert, N.; Terrones, M.; Trasobares, S.; Kordatos, K.; Terrones, H.; Olivares, J.; Zhang, J. P.; Redlich, P.; Hsu, W. K.; Reeves, C. L.; Wallis, D. J.; Zhu, Y. Q.; Hare, J. P.; Pidduck, A. J.; Kroto, H. W.; Walton, D. R. M. *Appl. Phys. A: Mater. Sci. Proc.* **2000**, *70*, 175.

(16) Nikolaev, P.; Bronikowski, M. J.; Bradley, R. K.; Rohmund, F.; Colbert, D. T.; Smith, K. A.; Smalley, R. E. *Chem. Phys. Lett.* **1999**, *313*, 91.

(17) Dai, H.; Rinzler, A. G.; Nikolaev, P.; Thess, A.; Colbert, D. T.; Smalley, R. E. *Chem. Phys. Lett.* **1996**, *260*, 471.

(18) Bronikowski, M. J.; Willis, P. A.; Colbert, D. T.; Smith, K. A.; Smalley, R. E. *J. Vac. Sci. Technol., A* **2001**, *19*, 1800.

(19) El-Nakat, J. H.; Dance, I. G.; Fisher, K. J.; Willett, G. D. *Polyhedron* **1993**, *12*, 2477.

(20) El-Nakat, J. H.; Dance, I. G.; Fisher, K. J.; Willett, G. D. *Polyhedron* **1994**, *13*, 409.

(21) Huang, Y.; Hill, Y. D.; Sodupe, M.; C. W. Bauschlicher, J.; Freiser, B. S. *Inorg. Chem.* **1991**, *30*, 3822.

(22) Seemeyer, K.; Schroeder, D.; Kempf, M.; Lettau, O.; Mueller, J.; Schwarz, H. *Organometallics* **1995**, *14*, 4465.

(23) Kurikawa, T.; Takeda, H.; Nakajima, A.; Kaya, K. *Z. Phys. D* **1997**, *40*, 65.

(24) Yasuike, T.; Nakajima, A.; Yabushita, S.; Kaya, K. *J. Phys. Chem.* **1997**, *101*, 5360.

(25) Berg, C.; Beyer, M.; Schindler, T.; Niedner-Schatteburg, G.; Bondybey, V. E. *J. Chem. Phys.* **1996**, *104*, 7940.

(26) Ayuela, A.; Seifert, G.; Schmidt, R. *Z. Phys. D.* **1997**, *41*, 69.

(27) Jackson, P.; Fisher, K. J.; Willett, G. D. *J. Chem. Phys.* **2000**, *262*, 179.

(28) Oiestad, A. M. L.; Uggerud, E. *J. Chem. Phys.* **2000**, *262*, 169.

(29) Guo, B. C.; Kerns, K. P.; Castleman, A. W., Jr. *J. Phys. Chem.* **1992**, *96*, 4879.

(30) Blum, O.; Stockigt, D.; Schroder, D.; Schwarz, H. *Angew. Chem. Int. Ed. Engl.* **1992**, *31*, 603.

(31) Karrass, S.; Pruesse, T.; Eller, K.; Schwarz, H. *J. Am. Chem. Soc.* **1989**, *111*, 9018.

(32) Wise, M. B.; Jacobson, D. B.; Freiser, B. S. *J. Am. Chem. Soc.* **1985**, *107*, 1590.

(33) Weil, D. A.; Wilkins, C. L. *J. Am. Chem. Soc.* **1985**, *107*, 7316.

(34) Azzaro, M.; Decouzon, B. M.; Geribaldi, S. *Int. J. MAss Spectrom. Ion Proc.* **1993**, *128*, 1.

(35) Raghavachari, K.; Binkley, J. S. *J. Chem. Phys.* **1987**, *87*, 2191.

(36) Martin, J. M. L.; Francois, J. P.; Gijbels, R. *J. Chem. Phys.* **1990**, *93*, 8850.

(37) *Gaussian 98* Revision A.7, Frisch, M. J.; Trucks, G. W.; Schlegel, H. B.; Scuseria, G. E.; Robb, M. A.; Cheeseman, J. R.; Zahrzewski, V. G.; Montgomery, J. A.; Stratmann, R. E.; Burant, J. C.; Dapprich, S.; Millam, J. M.; Daniels, A. D.; Kudin, K. N.; Strain, M. C.; Farkas, O.; Tomasi, J. Barone, V.; Cossi, M.; Cammi, R.; Mennucci, B.; Pomelli, C.; Adamo, C.; Clifford, S.; Ochterski, J.; Petersson, A. G.; Ayala, P. Y.; Cui, Q.; Morokuma, K.; Malick, D. K.; Rabuck, A. D.; Raghavachari, K.; Foresman, J. B.; Cioslowski, J.; Ortiz, J. V.; Stafanov, B. B.; Liu, G.; Liashenko, A.; Piskorz, P.; Komaromi, I.; Gomperts, R.; Martin, R. L.; Fox, D. J.; Keith, T.; Al-Laham, M. A.; Peng, C. Y.; Nanayakkara, A.; Gonzalez, C.; Challacombe, M.; Gill, P. M. W.; Johnson, B. G.; Chen, W.; Wang, M. W.; Andres, J. L.; Head-Gordon, M. Replogle, E. S.; Pople, J. A. Gaussian, Inc., Pittsburgh PA, 1998.

(38) Dunning Jr. T. H.; Hay, P. J. "Modern Theoretical Chemistry", Ed. Schaefer, III (Plenum, New York) **1976**, 3, 1.

(39) Hay, P. J,; Wadt, W. R. *J. Chem. Phys.* **1985,** *82,* 270.

(40) Wadt, W. R.; Hay, P. J. *J. Chem. Phys.* **1985,** *82,* 284.

(41) Hay, P. J,; Wadt, W. R. *J. Chem. Phys.* **1985,** *82,* 299.

(42) Fuentealba, P.; Preuss, H.; Stroll, H.; Szentpaly, L. v. *Chem. Phys. Lett.* **1989,** *89,* 418.

(43) Szentpaly, L. v.; Fuentealba, P.; Preuss, H.; Stroll, H.; *Chem. Phys. Lett.* **1982,** *93,* 555.

(44) Fuentealba, P.; Stroll, H.; Szentpaly, L. v.; Schwerdtfeger, P.; Preuss, H. *J. Phys. B* **1983,** *16,* 1323.

(45) Stroll, H.; Fuentealba, P.; Schwerdtfeger, P.; Flad, J.; Szentpaly, L. v.; Preuss, H. *J. Chem. Phys.* **1984,** *81,* 2732.

(46) Fuentealba, P.; Szentpaly, L. v.; Preuss, H.; Stroll, H.; *J. Phys. B* **1985,** *18,* 1287.

(47) Wedig, U.; Dolg, M.; Stroll, H.; Preuss, H. *"Quantum Chemistry: The Challenge of Transition Metals and Coordination Chemistry"* Ed. Veillard, A., (Reidel and Dodrecht) **1986**, 79.

(48) Dolg, M.; Wedig, U.; Stroll, H.; Preuss, H. *J. Chem. Phys.* **1987,** *86,* 866.

(49) Igel-Mann, G.; Stroll, H.; Preuss, H. *Mol. Phys.* **1988,** *65,* 1321.

(50) Dolg, M.; Stroll, H.; Preuss, H. *J. Chem. Phys.* **1989,** *90,* 1730.

(51) Schwerdtfeger, P.; Dolg, M.; Schwarz, W. H. E.; Bowmaker, G. A.; Boyd, P. D. W. *J. Chem. Phys.* **1989,** *91,* 1762.

(52) Dolg, M.; Stroll, H.; Savin, A.; Preuss, H. *Theor. Chim. Acta* **1989,** *75,* 173.

(53) Andrae, D.; Haeussermann, U.; Dolg, M.; Stroll, H.; Preuss, H. *Theor. Chim. Acta* **1990,** *77,* 123.

(54) Kaupp, W.; Schleyer, P. v. R.; Stroll, H.; Preuss, H. *J. Chem. Phys.* **1991,** *94,* 1360.

(55) Kuechle, W.; Dolg, M.; Stroll, H.; Preuss, H. *Mol. Phys.* **1991,** *74,* 1245.

(56) Dolg, M.; Fulde, P.; Kuechle, W.; Neumann, C. -S.; Stroll, H. *J. Chem. Phys.* **1991,** *94,* 3011.

(57) Dolg, M.; Stroll, H.; Flad, H. -J.; Preuss, H. *J. Chem. Phys.* **1992,** *97,*1162.

(58) Bergner, A.; Dolg, M.; Kuechle, W.; Stroll, H.; Preuss, H. *Mol. Phys.* **1993,** *80,* 1431.

(59) Dolg, M.; Stroll, H.; Preuss, H. *Theor. Chim. Acta* **1993,** *85,* 441.

(60) Dolg, M.; Stroll, H.; Preuss, H.; Pitzer, R. M. *J. Chem. Phys.* **1993,** *97,* 5852.

(61) Haeussermann, U.; Dolg, M.; Stroll, H.; Preuss, H. *Mol. Phys.* **1993,** *78,* 1211.

(62) Kuechle, W.; Dolg, M.; Stroll, H.; Preuss, H. *J. Chem. Phys.* **1994,** *100,* 7535.

(63) Nicklass, A.; Dolg, M.; Stroll, H.; Preuss, H. *J. Chem. Phys.* **1995,** *102,* 8942.

(64) Leininger, T.; Nicklass, A.; Stroll, H.; Dolg, M.; Schwerdtfeger, P. *J. Chem. Phys.* **1996,** *105,* 1052.

(65) Roszak, S.; Balasubramanian, K. *J. Chem. Phys.* **1997**, *106*, 158.

(66) Strout, D. L.; Hall, M. B. *J. Phys. Chem.* **1996**, *100*, 18007.

(67) Jackson, P.; Gadd, G. E.; Mackey, D. W.; Van der Wall, H.; Willett, G. D. *J. Phys. Chem. A* **1998**, *102*, 8941.

Chapter Five

ESI-FTICR-MS Studies of Fullerene Derivatives

5.1 Introduction

Fullerenes are highly unsaturated carbon molecules that behave like electron-deficient poly-alkenes in chemical reactions. Fullerene derivatizations are prepared mostly through addition reactions including cycloaddition,[1-3] nucleophilic addition,[4-6] radical addition,[7-9] transition metal complex formation,[10-12] hydrogenation[13-15] and halogenation.[16-20] Many functionalized fullerene derivatives possess interesting properties such as biological activity[21-23] and some may be used as intermolecular electron-transfer devices.[24]

Many fullerene derivatives are non-volatile and chemically labile compounds. The mass spectrometry studies of these compounds therefore require an ionization method, which can transfer ionized molecules into the gas phase with minimal fragmentation. For this reason, ESI mass spectrometry has been regarded as a promising method for fullerene derivative studies because of the soft-ionization nature of this method. Several types of fullerene derivatives have been investigated by ESI mass spectrometry using different organic solvents including toluene,[25] toluene/methanol[26-30] and anhydrous CH_2Cl_2.[31] Wilson and Wu have studied methoxide addition to C_{60}/C_{70}[26] and polyamines derived from C_{60} using a single quadrupole instrument;[32] Khairallah and Peel observed cyano-adduct anions of fullerene C_{60} and C_{70} using a triple-quadrupole system;[28-30] Grayson and co-workers studied malonic acid fullerene derivatives by a sector and ion trap mass spectrometry.[33] Among the fullerene derivatives, malonic acid fullerene derivatives are important fullerene compounds and they have been used in several

biological activity studies.[21,34] Also, a water-soluble fullerene malonic acid derivative was found to be a competitive inhibitor of HIV-1 protease.[35,36]

In this chapter, the ESI-FTICR mass spectrometry study of several types of fullerene derivatives will be presented. These fullerene derivatives include a malonic acid fullerene derivative, several amino acid fullerene derivatives, cyano-fullerenes and fluorinated fullerenes. The electrospray ionization method combined with FTICR mass spectrometry is used in the study of these fullerene derivatives. In many cases, ESI can produce both cationic and anionic ions of fullerene derivatives or their related species, and the high resolution of FTICR mass spectrometry provides unambiguous mass assignment for various ions produced. The high resolution of the FTICR method is especially useful in distinguish ions with close m/z values.

5.2 ESI-FTICR Mass Spectrometry Experimental Conditions

Prior to the mass analysis of the fullerene derivatives, the FTICR mass spectrometer was mass-calibrated using sodium iodide cluster ions formed by ESI from a sodium iodide methanol solution at a concentration of 6.7×10^{-4} M (0.1 mg/ml). In the positive-ion mode, ions over the mass range of m/z 173.7993 $(NaI)Na^+$ to m/z 2974.8956 $(NaI)_{19}Na^+$ were assigned to within 2.8 ppm (average) of their correct value. In the negative-ion mode, ions over the mass range of m/z 277.7993 $(NaI)I^-$ to m/z 2870.9805 $(NaI)_{19}I^-$ were assigned to within 3.3 ppm (average) of their correct value. In favorable circumstances sodium iodide solutions can produce clusters ions that cover the mass region up to 4369.9229 Da $[(NaI)_{29}Na^+]$ and 4473.8387 Da $[(NaI)_{29}I^-]$.

For the ESI-FTICR mass spectrometry experiments, the fullerene derivative samples were either directly dissolved in methanol, or first dissolved in the dichloromethane and then mixed with over 95 % (by volume) of methanol.

5.2.1 Fullerene Derivative I

5.2.1.1 Sample Preparation

A malonic acid fullerene derivative (1,6-methano[60]fullerene-61,61-dicarboxylic acid) and two amino acid type of fullerene derivatives (Structures ***I*** ~ ***III***) were synthesized by the method of Lamparth and Hirsch.[37]

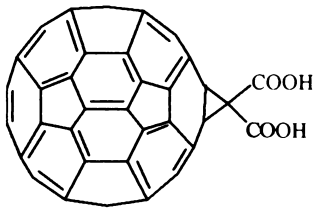

Structure I

The synthesis work was undertaken by Prof. Liangbing Gan's group from Peking University. Details of the synthesis and the chemical characterization can be found elsewhere.[7,38,39]

5.2.1.2 ESI-FTICR Mass Spectrometry Studies of Fullerene Derivative I

Although attempts were made to observe positive ions arising from the 1,6-methano[60]fullerene-61,61-dicarboxylic acid none were found. Only negative-ion species were observed for this compound. The ESI spray solution was also modified by adding a few drops of acetic acid methanol solution (concentration of 1.4×10^{-3} M), or sodium iodide methanol solution (concentration of 6.7×10^{-4} M), but no proton or sodium adduct ions were observed. For comparison, two other dicarboxylic acids, malonic acid $CH_2(COOH)_2$ and succinic acid $C_2H_4(COOH)_2$ in methanol solution were studied under the same condition. The results for these compounds show that only positive ions were observed and, for such ions, no monomolecular adduct cation $[M+Na]^+$ was observed for either of dicarboxylic acids. A significant difference in the behavior of these acids as compared to that of the dicarboxylic methano[60]fullerene, was that sodiated cluster cations were formed from both malonic acid and succinic acid with the general formula of $[M_n+Na]^+$ (n = 2-3) where M is the dicarboxylic molecule.

It is possible that the electron deficiency of fullerene C_{60} molecule has an effect on the attached malonic acid, which increases its acidity. As the result of such a change, the anions of this species might expect to be formed, especially the deprotonated carboxylic anions.

The negative-ion species that are formed from 1,6-methano[60]fullerene-61,61-dicarboxylic acid were first observed at a capillary/skimmer (C/S) potential difference of 45 V. As shown in Figure 5-01, the most abundant ion is that with m/z 820.988. This ion is assigned to the deprotonated molecule $C_{60}C(COOH)COO^-$ (δ(m/z) ~3 ppm). Another major ion observed at m/z 776.988 is assigned to $C_{60}CHCOO^-$ (δ(m/z) ~5 ppm). This ion could result from the loss of a COOH group from the molecular anion. Ions appearing at m/z 854.994 and 811.004 are possible by-products that can be assigned to the dihydroxylated fullerene derivative species, $(OH)_2C_{60}C(COOH)COO^-$ and $(OH)_2C_{60}CHCOO^-$ to within δ(m/z) = 4 ppm and 3 ppm, respectively.

ESI is a sensitive technique in which the observed ion distributions are very much dependent upon the spray conditions. For example, the voltages applied at the exit-end of capillary and skimmer has a significant effect on the ion distribution. This is possibly because the potential difference between capillary and skimmer determines the translational energy of the ions passing out of the capillary. By increasing this potential difference, higher energy collisions between ions and neutral molecules may occur, thereby leading to increased ion fragmentation. This capillary/skimmer collision-induced-dissociation (C/S-CID) is an effective way to obtain structural information of ions even though ions cannot be individually isolated.

In this present study, the ion intensity of the deprotonated molecule $C_{60}C(COOH)COO^-$ was observed to decrease when the C/S potential difference was raised, and correspondingly the fragment ions became more abundant. Figure 5-02 is a

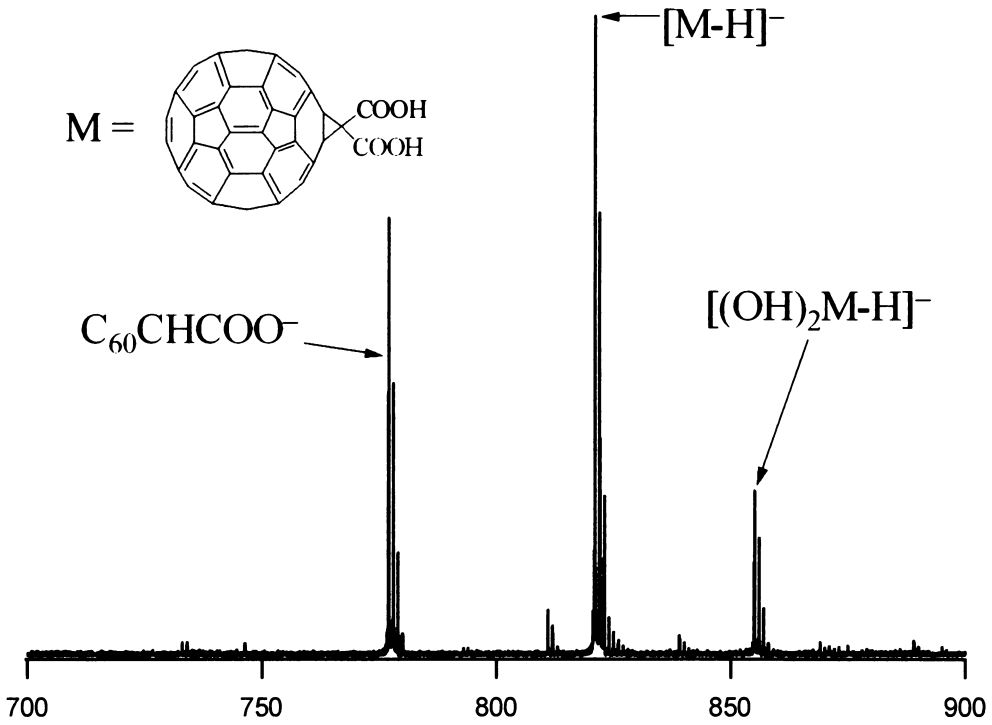

Figure 5-01 Negative-ion ESI-FTICR mass spectrum of fullerene derivative ***I*** at a capillary voltage of 50 V.

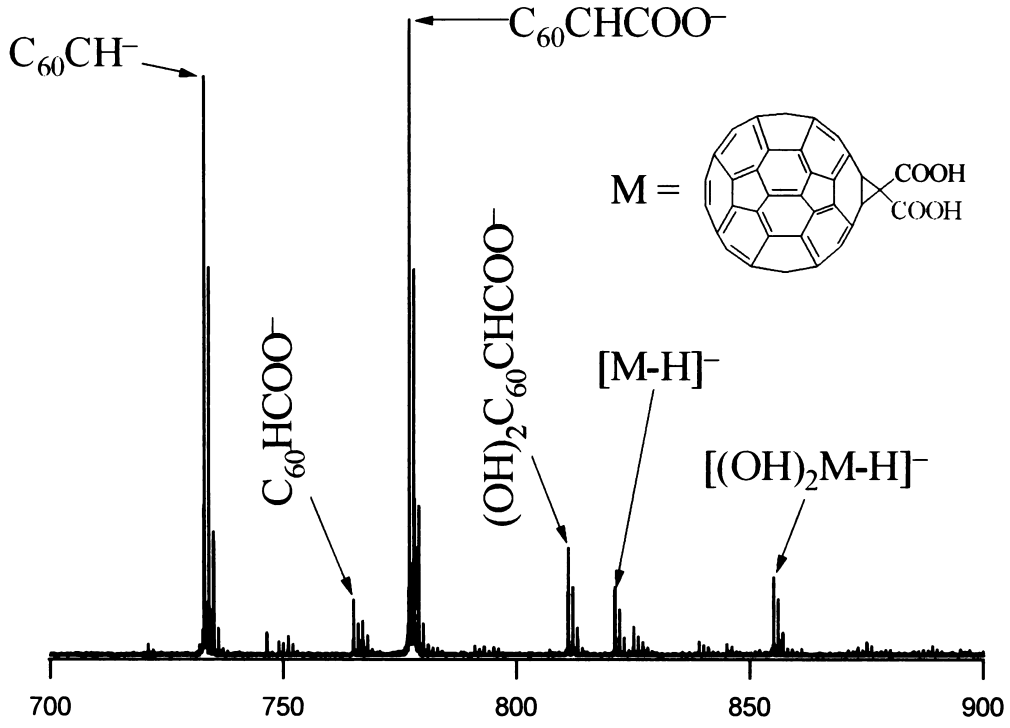

Figure 5-02 Negative-ion ESI-FTICR mass spectrum of fullerene derivative ***I*** at a capillary voltage of 150 V.

negative-ion ESI-FTICR mass spectrum of 1,6-methano[60]fullerene-61,61-dicarboxylic acid at a C/S potential difference of 150 V with an ion accumulation delay in the rf/dc hexapole of d_1 = 0.5 s. This figure shows that during C/S-CID, the dicarboxylic acid groups not only fragment but also possibly rearrange to produce product ions that include $C_{60}CHCOO^-$ (observed m/z 776.998), $C_{60}HCOO^-$ (observed m/z 764.998) and $C_{60}CH^-$ (observed m/z 733.008). With the maximum available C/S potential difference applied (400 V), $C_{60}CH^-$ (m/z 733.001) became the most abundant ions observed (Figure 5-03).

Since ions can be trapped in the rf/dc hexapole for periods of up to several seconds, the collisions between the ions and neutral molecules may also facilitate gas phase ion/molecule chemistry. The results of such reactions are shown in Figure 5-04 which is a negative-ion ESI-FTICR mass spectrum obtained at a C/S potential difference of 195 V and ion accumulation delay in the rf/dc hexapole of 2 seconds. The three major ionic species can be assigned to the cluster ions $[C_{60}C(COOH)_2]_nC_{60}CH^-$ (n = 0 - 2). The abundance of these ions is sensitive to the ion accumulation time in the rf/dc hexapole ion trap, which indicates that these cluster ions may form in the hexapole ion accumulation region by the trapped-ions reacting with neutral molecules. With short delay times (d_1 < 0.5 s), the abundance of these cluster ions markedly decreased.

In order to probe the structures of the ionic species that are observed in the ESI FTICR mass spectrometry experiments, SORI-CID was carried out with selected ionic species. A SORI-CID FTICR mss spectrum shows the dissociation of the deprotonated molecule $C_{60}C(COOH)COO^-$ (Figure 5-05). This anion is observed to lose up to two CO_2 groups to produce product ions $C_{60}CHCOO^-$ and $C_{60}CH^-$. A trace of C_{60}^- is also observed in this mass spectrum. The formation of $C_{60}CHCOO^-$ from

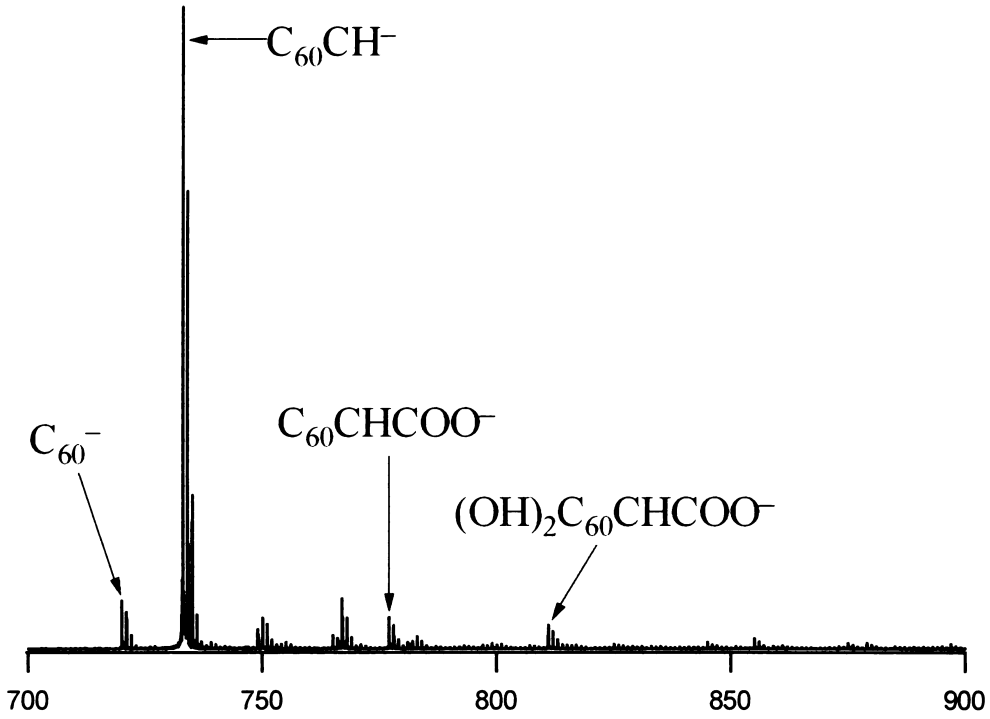

Figure 5-03 Negative-ion ESI-FTICR mass spectrum of fullerene derivative ***I*** at a capillary voltage of 400 V with 0.2 s of ion accumulation in the hexapole.

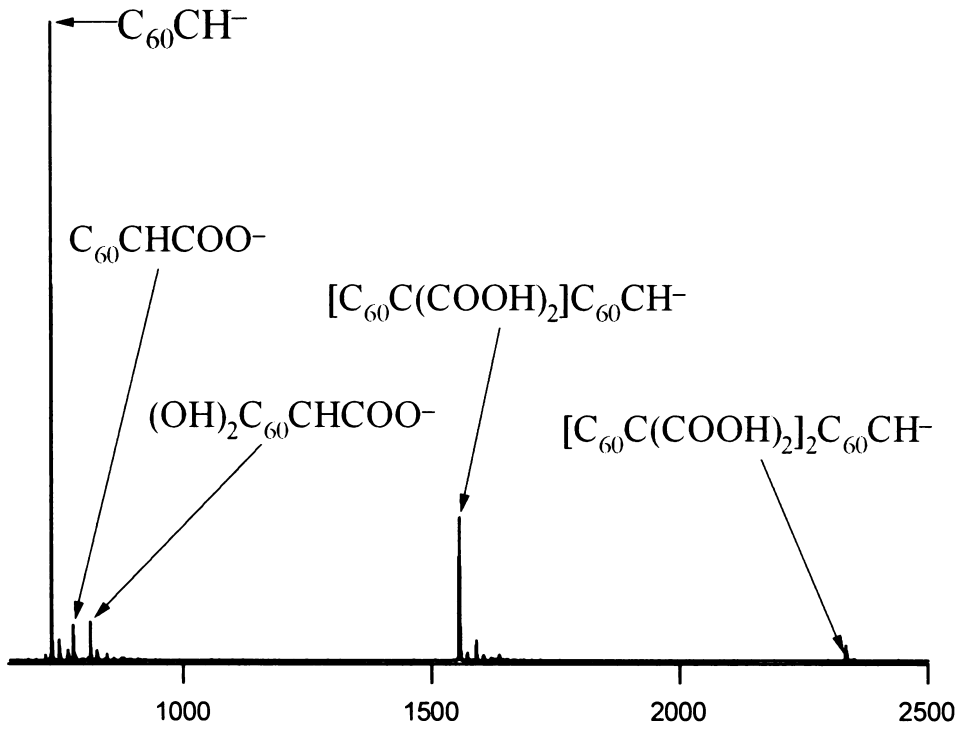

Figure 5-04 Negative-ion ESI-FTICR mass spectrum of fullerene derivative ***I*** at a capillary voltage of 195 V and with 2 s of ion accumulation in the hexapole.

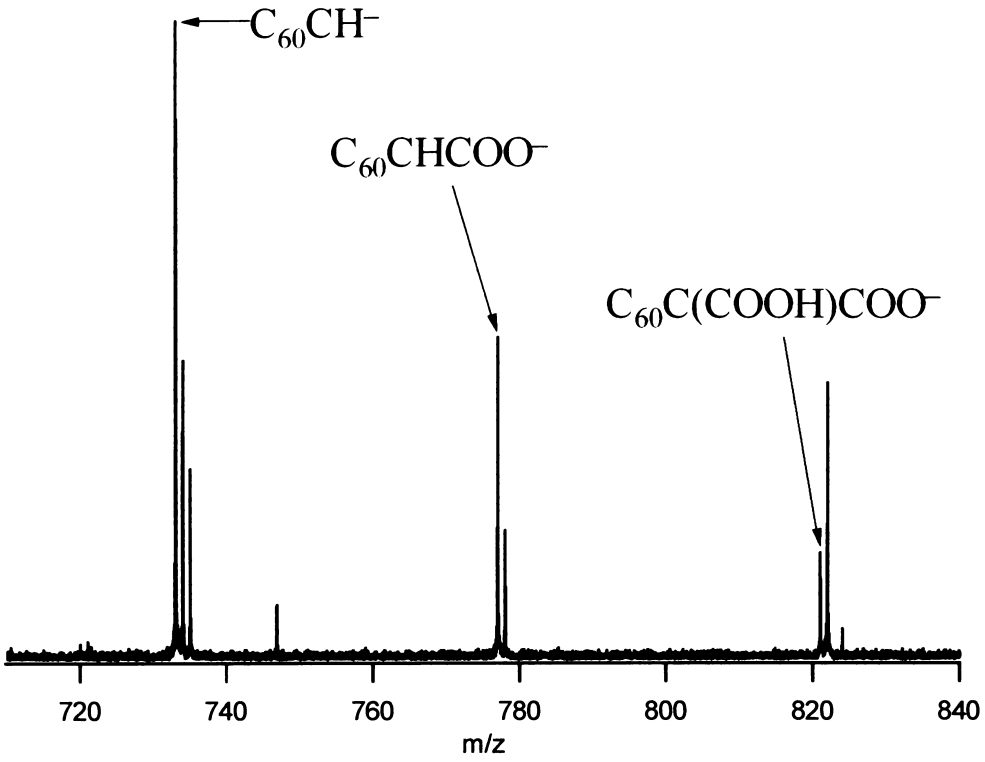

Figure 5-05 SORI-CID-FTICR mass spectrum of deprotonated fullerene derivative ***I*** anion.

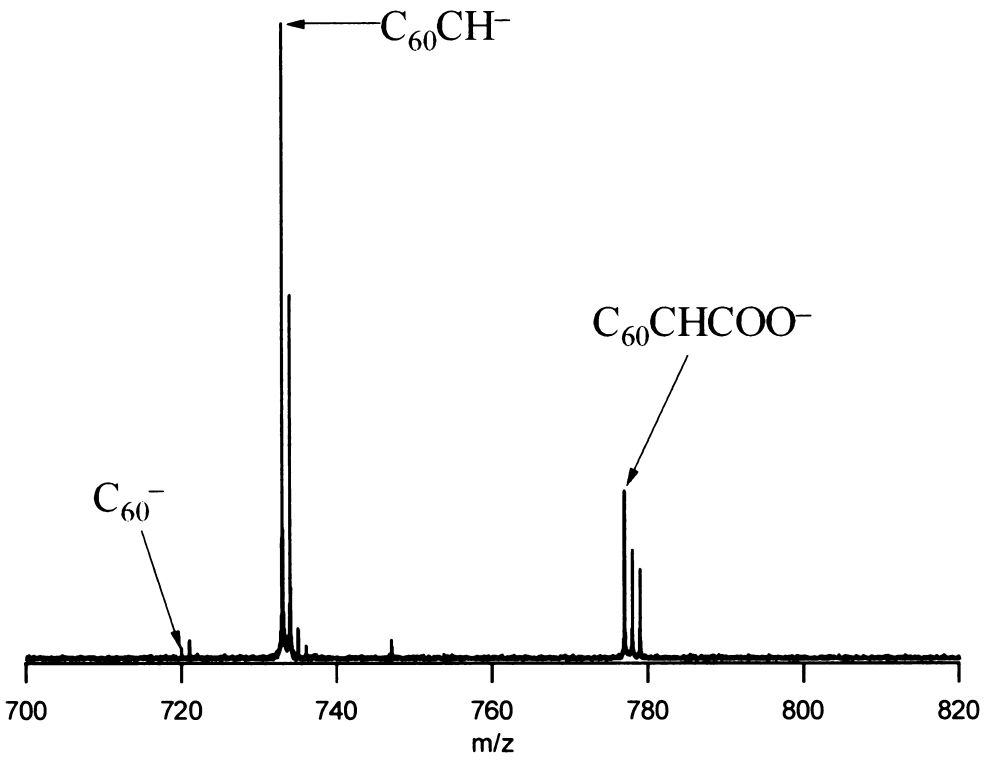

Figure 5-06 SORI-CID-FTICR mass spectrum of $C_{60}CHCOO^-$.

$C_{60}C(COOH)COO^-$ involves proton transfer from the carboxylic group to the methano-carbon on the C_{60} frame.

It is worthwhile to note that in Figure 5-05, the isotope pattern of the ions appears distorted. This is because in SORI-CID experiments, ion excitation was carried out using the correlated sweep pulse program in which the frequency pulse applied for the ion excitation is very narrow and it may only cover a single isotope peak region. This mass correlation minimizes any off-resonance excitation of the unwanted ions, but it also cause distortion of the ion isotope pattern.

During the SORI process, the average kinetic energy KE_{av} of the ions over long periods in the absence of collisions is described by equation 2-03. For the SORI-CID of $C_{60}C(COOH)COO^-$ experiment, the irradiation is applied with E_o = 44 Vm^{-1} and frequency offset was set at 500 Hz. Under such conditions, this ion is calculated to obtain an average kinetic energy of 12 eV in the absences of collision gas. Using argon as the collision gas, an average centre-of-mass kinetic energy of this ion is about 0.6 eV. During the SORI-CID, the excitation pulse was sustained for 0.3 second.

In another experiment, $C_{60}CHCOO^-$ was also studied by SORI-CID (see Figure 5-06). It is observed that $C_{60}CHCOO^-$ loses a CO_2 group to produce $C_{60}CH^-$. Interestingly, the ion $C_{60}HCOO^-$, that was observed in the ESI at the capillary/skimmer potential difference of 275 V was not present as a SORI-CID product. $C_{60}CH^-$ appears to be a very stable ion, even when the C/S potential difference was raised as high as 400 V, it still remained with high intensity. The apparent stability of $C_{60}CH^-$ is probably related to increased delocalization (aromatic in nature, 4n+2 with n = 0) of the electron pair on the cyclopropyl methano-carbon as it interacts with the carbon bonds in the C_{60}. A separate CID experiment was performed with $C_{60}CH^-$ using the SORI technique. Figure 5-07 shows the result of this experiment in which $C_{60}CH^-$ produces $C_{60}H^-/C_{60}^-$.

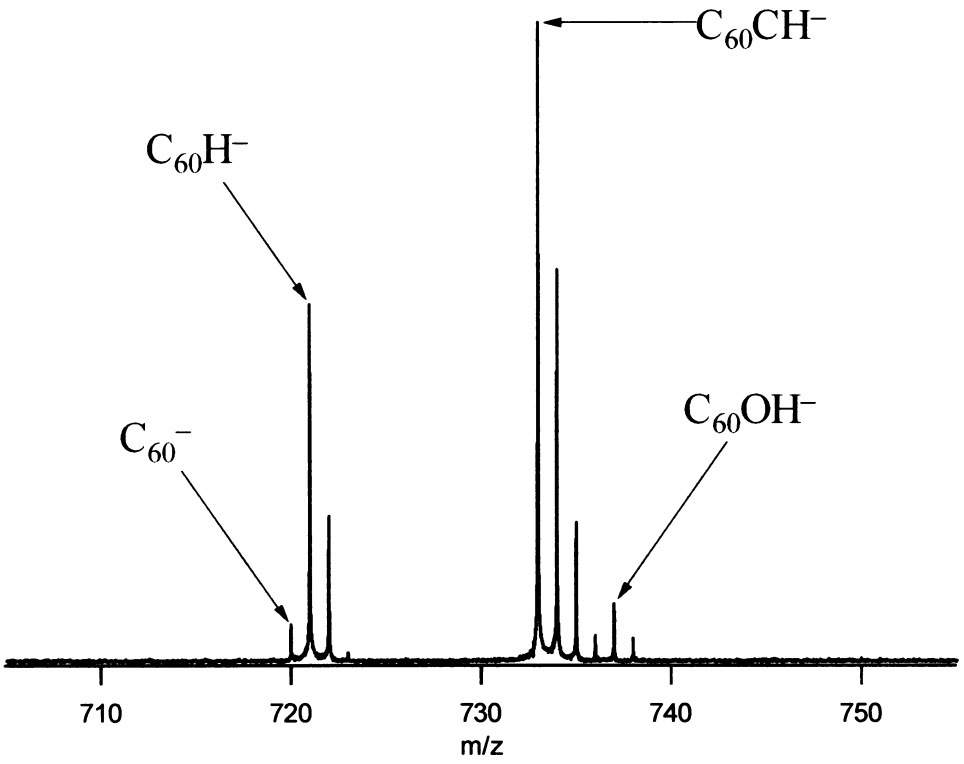

Figure 5-07 SORI-CID-FTICR mass spectrum of $C_{60}CH^-$.

5.2.1.3 Semi-Empirical Calculations on Fullerene Derivative I and its Related Species

Semi-empirical calculations using the AM1 approximation with the MOPAC program[40] were carried out on a few neutral and ionic species that are related to the fullerene derivative ***I***, including both monomeric and dimeric examples. With increasing molecular size and for radical species MOPAC has difficulties with both SCF and geometric convergence. Consequently some species are not included in the results presented in Table 5-01.

The structures obtained for the energetically preferred monomer anion species are illustrated in Figure 5-08. Among the species considered $C_{60}CH^-$ is found to be of C_{2V} symmetry with the negative charge delocalized on the cyclopropyl moiety rather than being localized on the methano group or on the C_{60}, which would confer C_s symmetry. The $C_{60}CHCOO^-$ anion is of the expected C_s symmetry with equivalent oxygen atoms aligned symmetrically relative to the C_{60} sphere. The dicarboxylic acid $C_{60}C(COOH)_2$ prefers C_2 over C_s symmetry by 3 kJ/mol, but its anion $C_{60}C(COOH)COO^-$ has no symmetry. The energies for deprotonation show the expected trend with the dicarboxylic acid being more reactive than the monocarboxylic acid, with the methanofullerene[60] showing least reactivity.

The unusual fragmentation product in the C/S-CID, $C_{60}CHOOH^-$, is shown to prefer the structure with a complete COOH group and the negative charge delocalized into the C_{60} sphere. The other possible structure, the 1,2– di-adduct with H and COO^- groups is found to be less stable by 47 kJ/mol. Since $C_{60}COOH^-$ has lost its methano carbon, the possible mechanism of its formation remains unknown.

The observed dimeric species $[C_{60}CHCOOH][C_{60}CHCOO]^{x-}$ with x =1 and 2 are likely to comprise a classical –O–H···O hydrogen-bond as their essential structural feature. Their neutral progenitor $[C_{60}CHCOOH]_2$ is expected to show the classical

TABLE 1. MOPAC / AM1 results for selected methanofullerene[60] molecules and anions: calculated ionization energies, IE (in eV) and standard heats of formation, ΔH_f^o, with the derived deprotonation energies, ΔH_{dp}^o (in kJ mol^{-1}).

Molecule	**Symmetry**	**IE**	ΔH_f^o	ΔH_{dp}^o
C_{60}	I_h	9.64	4072	
C_{60}^-	I_h	3.31	3771	
$C_{60}CH_2$	C_{2v}	9.34	4057	–33
$C_{60}CH^-$	C_{2v}	3.84	4024	
$C_{60}CHCOOH$	C_s	9.43	3717	–157
$C_{60}CHCOO^-$	C_s	5.74	3559	
$C_{60}CCOOH^-$	C_s	4.65	3601	
$C_{60}CCOOHCOOH$	C_2	9.51	3407	–188
$C_{60}CCOOHCOOH$	C_s	9.52	3410	–190
$C_{60}CCOOHCOO^-$	C_1	6.20	3219	
$C_{60}HCOOH$	C_s	9.39	3571	–241
$C_{60}COOH^-$	C_s	4.91	3330	
$C_{60}HCOO^-$	C_s	6.04	3377	

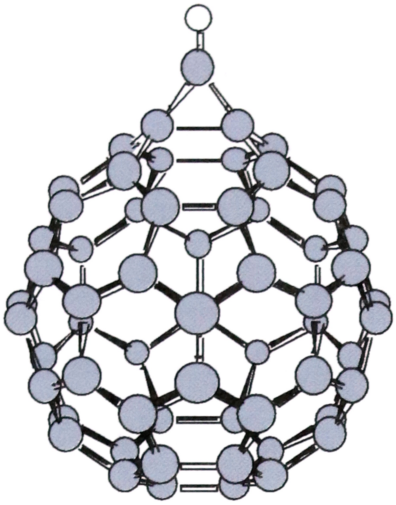

$C_{60}CH^-$

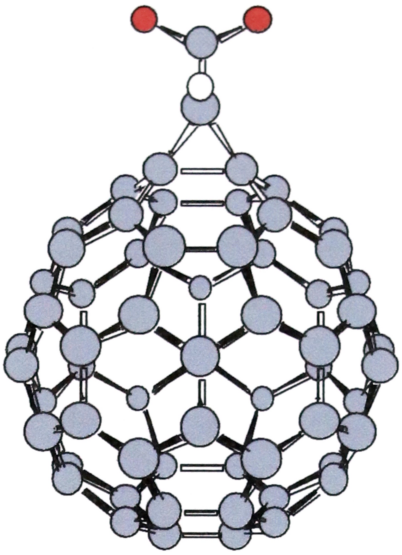

$C_{60}CHCOO^-$

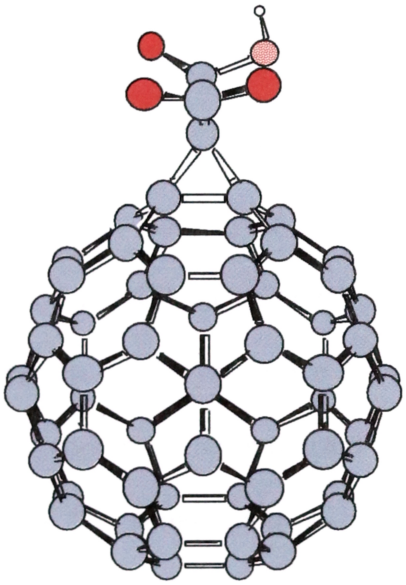

$C_{60}C(COOH)COO^-$

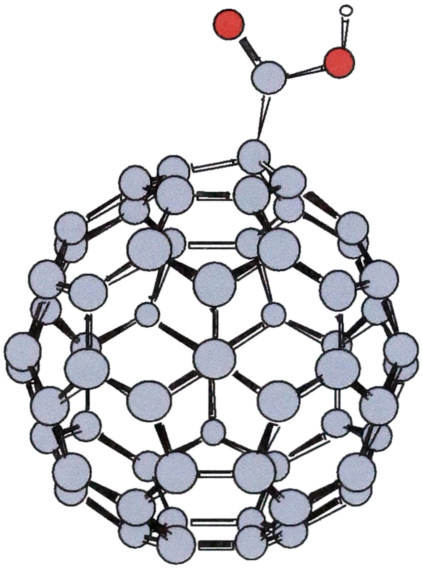

$C_{60}COOH^-$

Figure 5-08 Calculated (MOPAC) structures of fullerene derivatives' anion that are observed by ESI-FTICR mass spectrometry.

double hydrogen bond with a planar $(CHCOOH)_2$ linkage. This is verified by the MOPAC AM_1 calculation as illustrated in Figure 5-09, for which the H···O distances are 2.110 Å and the dimerization energy is –27 kJ mol^{-1} (or 13 kJ mol^{-1} for each hydrogen-bond energy). These relate well to the experimental values for the gas-phase H_2O dimer of 2.019 Å and 15 kJ mol^{-1} respectively.[41]

Deprotonation of the neutral dimer provides the mono-anion $[C_{60}CHCOOH]$ $[C_{60}CHCOO]^-$ bound through a single hydrogen bond. The AM_1 structure shown in Figure 5-09 retains the planar bridging structure. The H···O distances for this structure are 1.905 Å and 2.459 Å respectively, with the shorter distance being smaller than the hydrogen-bond lengths in the neutral dimer. Perhaps not surprisingly the calculated dimerization energy of –53 kJ mol^{-1} is rather higher than that obtained for the neutral species.

Since the C_{60}^- anion is stable in the gas-phase, the addition of one and two further electrons to the mono-anion dimer to give $[C_{60}CHCOOH][C_{60}CHCOO]^{2-}$ and $[C_{60}CHCOOH][C_{60}CHCOO]^{3-}$ should simply involve delocalized electron density appearing on the respective C_{60} moieties, without necessarily greatly weakening the hydrogen-bond. The optimized AM1 geometry for the tri-anion is little different from that of the mono-anion with H···O distances calculated as 2.015 Å and 2.512 Å respectively, and a dimerization energy of –111 kJ mol^{-1} relative to $C_{60}CHCOOH$ and $C_{60}CHCOO^-$ as fragments with two free electrons. The Koopmans' ionization energies calculated for the two dimeric anions are 6.50 and –0.59 eV respectively, the latter suggesting contrary to observation that the tri-anion is not stable towards electron loss in the gas-phase.

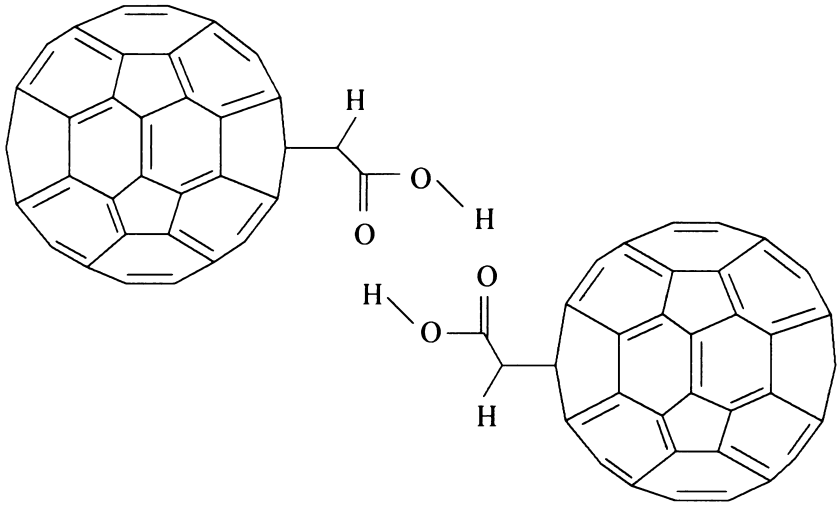

$[C_{60}CHCOOH]_2$ (C_{2h})

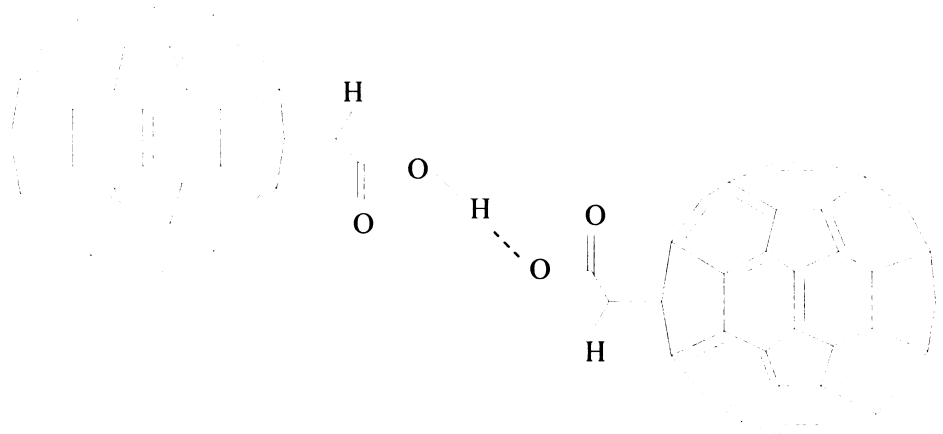

$[C_{60}CHCOOH][C_{60}CHCOO]^-$ (C_s)

Figure 5-09 Calculated (MOPAC) structures for $[C_{60}CHCOOH]_2$ dimer and hydrogen-bond $[C_{60}CHCOOH][C_{60}CHCOO]^-$ anion.

5.2.2 ESI-FTICR Mass Spectrometry Studies of Fullerene Derivative II

The fullerene derivative ***II*** has a molecular mass of 865 Da. The ESI-FTICR mass spectrometry studies of this compound were performed in both positive-ion and negative-ion mode.

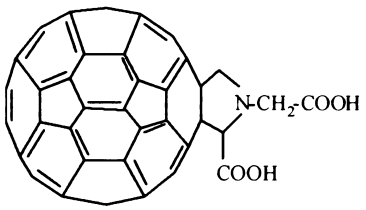

Structure II

The positive-ion ESI-FTICR mass spectrum (Figure 5-10) shows the molecule can add a sodium cation and several hydroxyl groups. The base peak in this mass spectrum is assigned to $(OH)_4M+Na^+$, where M is the neutral fullerene derivative molecule. The addition of hydroxyl groups is also observed for 1,6-methano[60]fullerene-61,61-dicarboxylic acid that has been show above, but in that case, it was observed in the negative-ion mode. A possible explanation for this observation is that these two compounds present different acidity in the electrospray solution, which leads to the addition of hydroxyl groups in different ionization modes.

Figure 5-11 shows the negative-ion ESI-FTICR mass spectrum of fullerene derivative ***II***. A range of oxygen addition products in the form of $[O_nM-H]^-$ (where n = 6 ~ 13; M is the neutral molecule) are observed in this mass spectrum. The major ion in this mass spectrum is assigned to $[O_8M-H]^-$. The number of these oxygen-attached species that can be observed depends on the experimental conditions such as the capillary voltages. It has been observed that the composition of the sample solution undergoes dynamic changes over a period of time. The mass spectrum of the same sample that was stored for more than a week shows many ionic species that are possibly related to the fullerene derivative ***II*** (Figure 5-12). $[O_8M-H]^-$ is still in high abundance, with possible dissociation products such as $C_{60}O^-$ and C_{60}^- that were not observed in the early experiment.

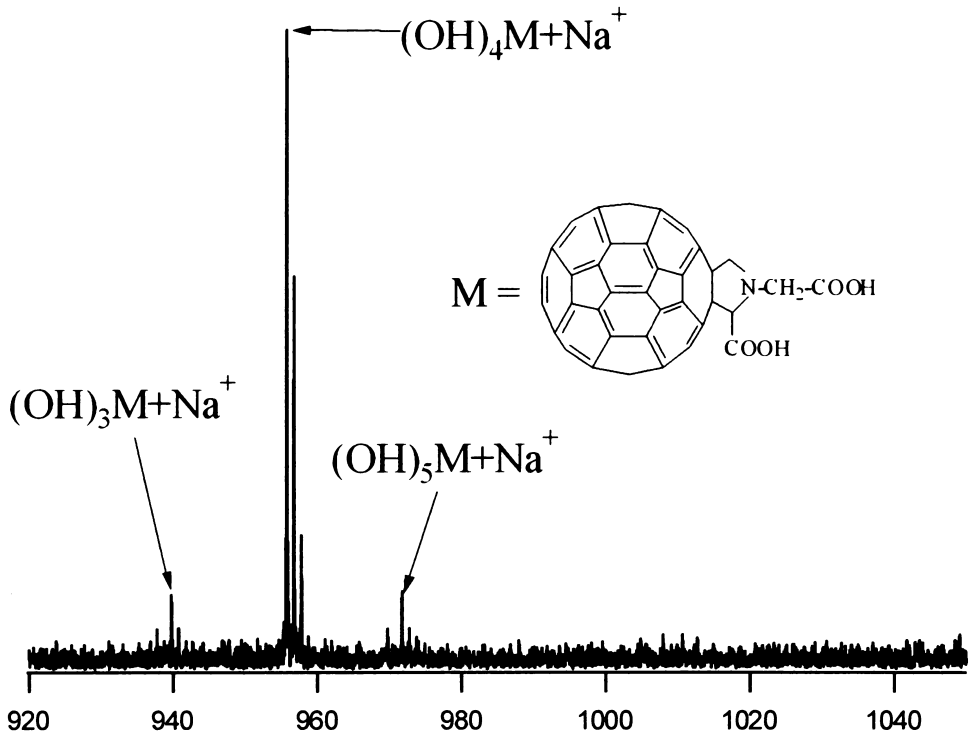

Figure 5-10 Positive-ion ESI-FTICR mass spectrum of fullerene derivative ***II***.

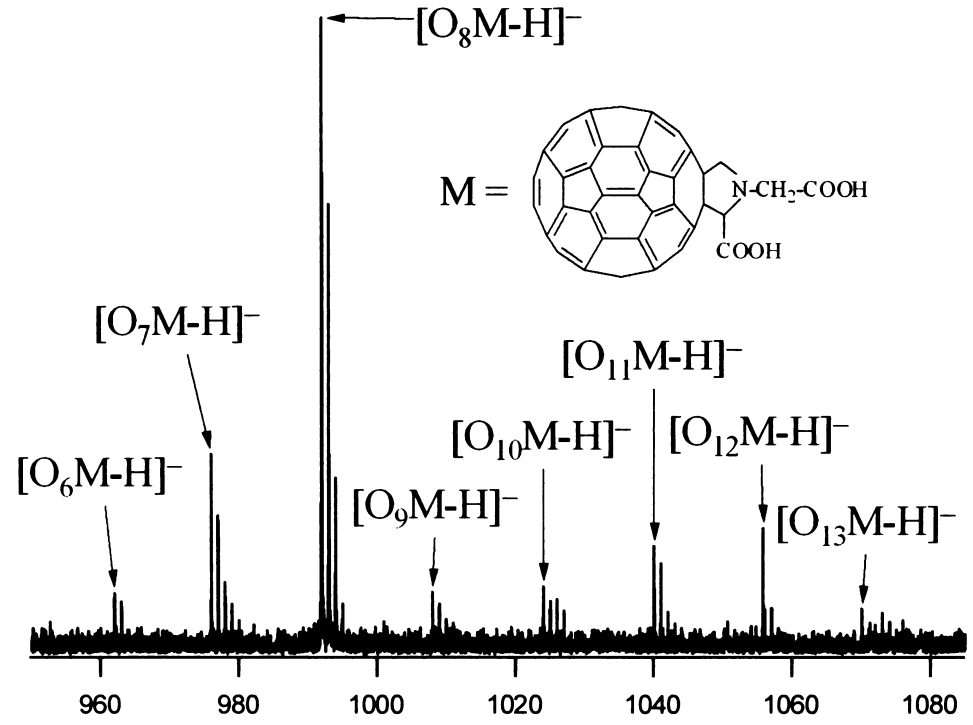

Figure 5-11 Negative-ion ESI-FTICR mass spectrum of fullerene derivative ***II***.

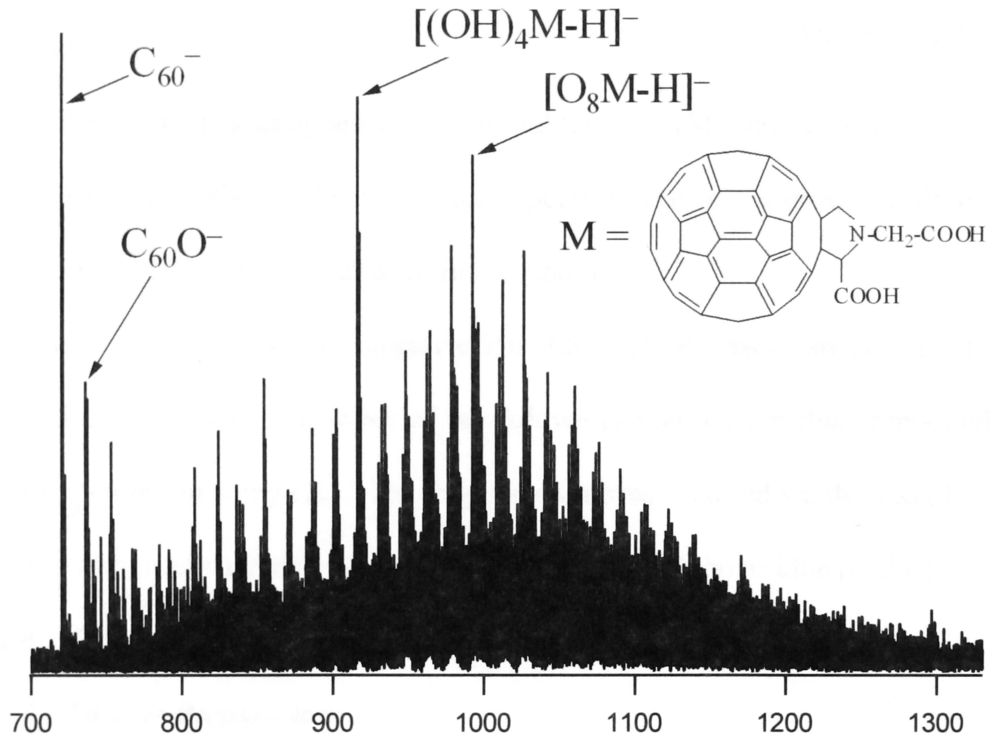

Figure 5-12 Positive-ion ESI-FTICR mass spectrum of fullerene derivative ***II*** after the sample solution stored for a week.

5.2.3 ESI-FTICR Mass Spectrometry Studies of Fullerene Derivative III

Fullerene derivative ***III*** has a molecular mass of 1,010 Da. Figure 5-13 shows the positive-ion ESI-FTICR mass spectrum for this compound. The base peak in this mass spectrum is assigned to $[(CO)M+Na]^+$ where M is the neutral molecule of this compound.

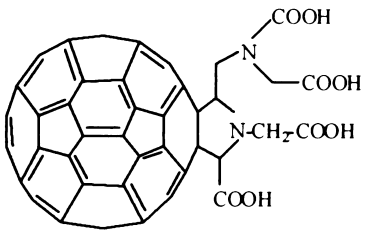

Structure III

A small peak that is assigned to sodium adduct ion $[M+Na]^+$ is also observed in this mass spectrum. Other peaks in this mass spectrum can be assigned to different addition ions or dissociation product ions of this compound.

Figure 5-14 shows the negative-ion ESI-FTICR mass spectrum of fullerene derivative ***III***. There is a series of breakdown products from this compound with the final fragment ion being C_{60}^-. The fragmentation was occurred via the loss of several CO_2 groups, with the formation of carboxylic anion in most of the residue products.

5.2.4 Fullerene Derivative IV ~ VI and Ligand Compounds L_1 and L_2

5.2.4.1 Sample Preparation

Fullerene derivatives ***IV*** ~ ***VI*** were supplied by Dr. Paul Keller of Wollongong University. Compound ***IV*** is a trimethylamine type of fullerene derivative, which was used as a precursor compound for the synthesis of many other fullerene derivatives. Compound ***V*** and ***VI*** contain C_{60} external bridges that are formed by joining two diphenylmethylamide glycine molecules with a benzene molecule on the 'para' and 'meta' position respectively. The respective ligand compounds L_1 and L_2 are also studied by ESI-FTICR mass spectrometry. Reports on the synthesis and characterization of these compounds can be found elsewhere.[42,43]

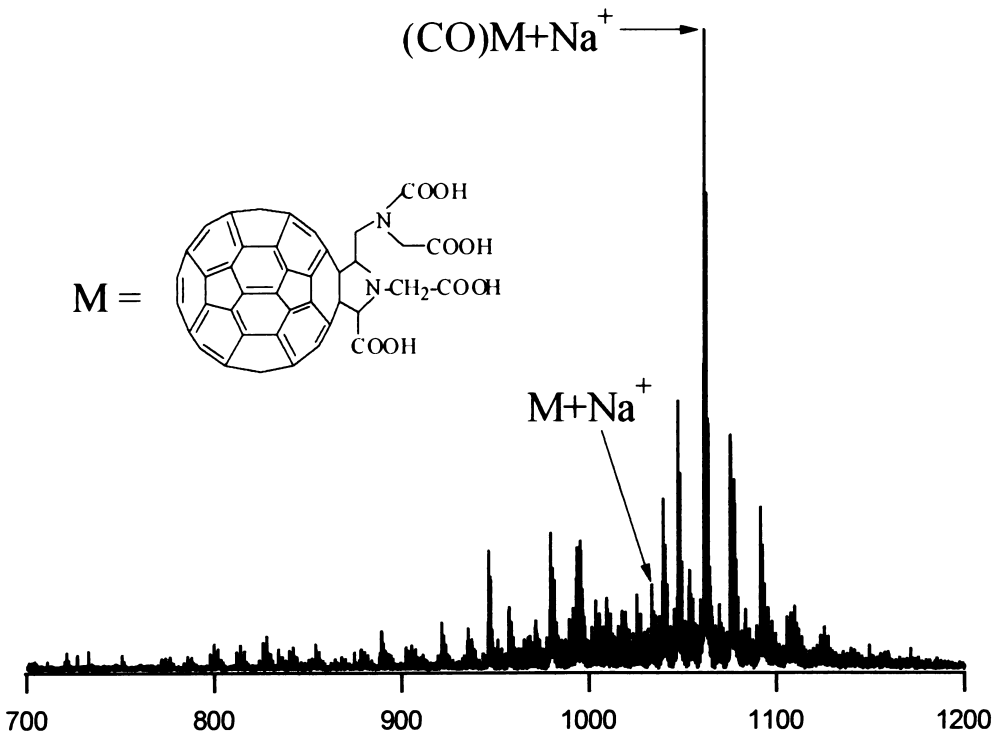

Figure 5-13 Positive-ion ESI-FTICR mass spectrum of fullerene derivative ***III***.

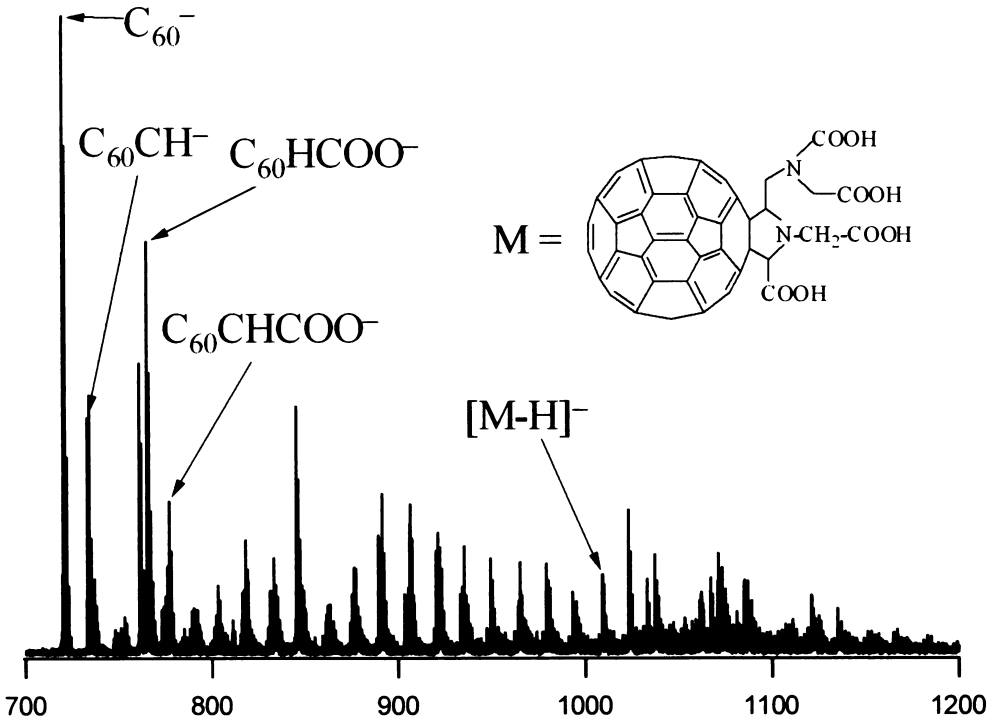

Figure 5-14 Negative-ion ESI-FTICR mass spectrum of fullerene derivative ***III***.

5.2.4.2 ESI-FTICR Mass Spectrometry Studies of Fullerene Derivatives IV ~ VI and Ligand Compounds L_1 and L_2

Unlike the fullerene derivatives ***I*** **-** ***III***, fullerene derivative ***IV*** has no carboxylic acid groups. Figure 5-15 shows a positive-ion ESI-FTICR mass spectrum of this fullerene derivative. The major ion observed in this mass spectrum is $[M+H]^+$. Other minor ions in this spectrum are assigned to impurities.

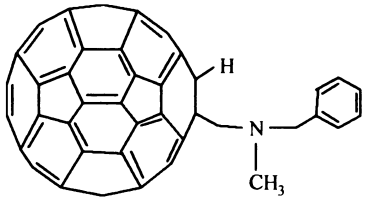

Structure IV

Figure 5-16 shows the negative-ion ESI-FTICR mass spectrum of fullerene derivative ***IV***. The deprotonated anion is shown as the base peak in this mass spectrum. Several smaller ions including $C_{60}(OCH_3)^-$, $C_{60}OH^-$, $C_{60}H^-$ and C_{60}^- can be observed in this mass spectrum.

Figure 5-17 shows the ORI-CID FTICR mass spectrum of the deprotonated anion. It clearly shows that the dissociation process eliminates the whole amine group and the hydrogen atom that was attached to the fullerene frame.

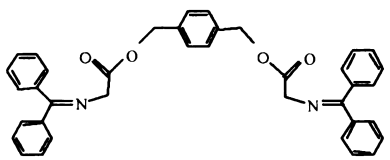

Structure L_1

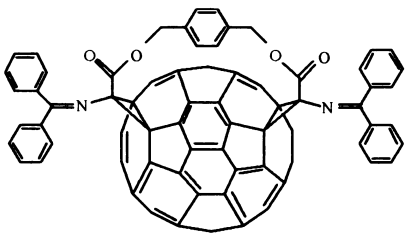

Structure V

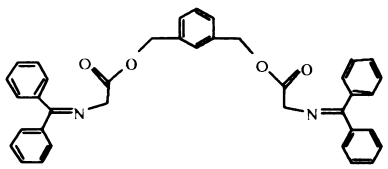

Structure L_2

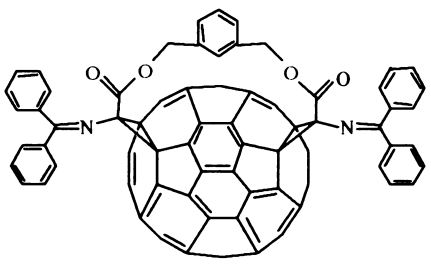

Structure VI

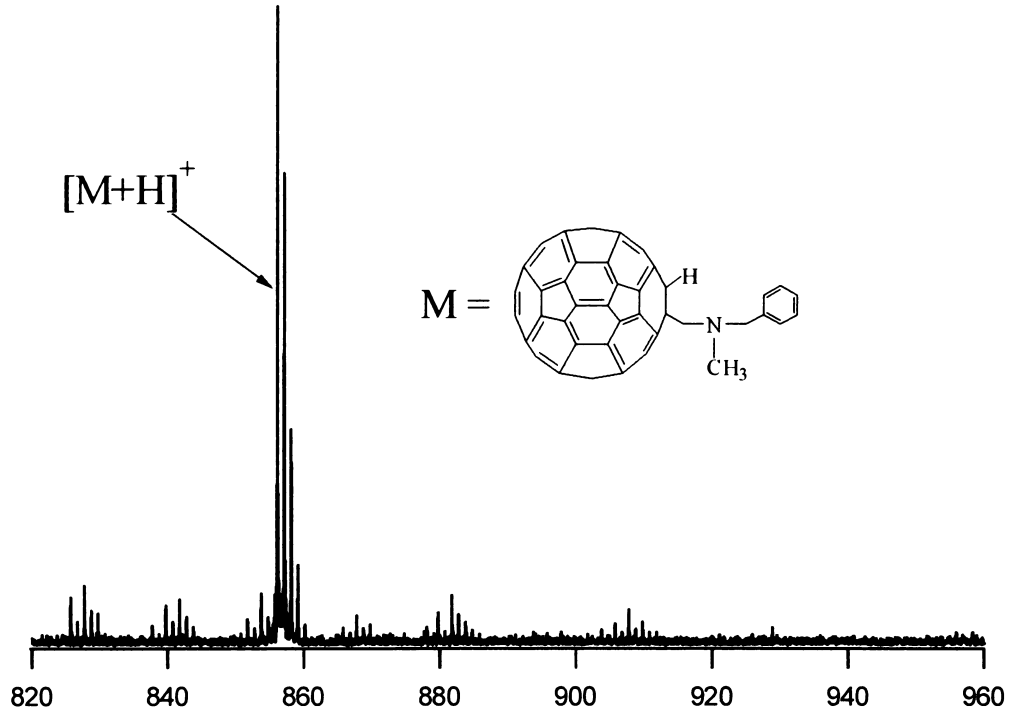

Figure 5-15 Positive-ion ESI-FTICR mass spectrum of fullerene derivative ***IV***.

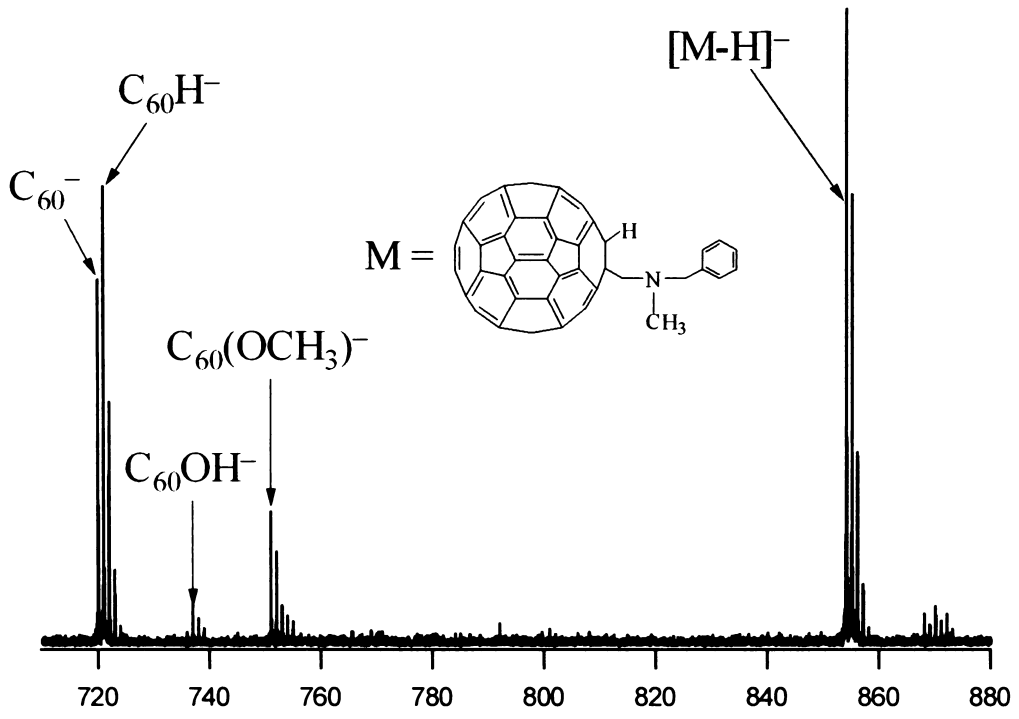

Figure 5-16 Negative-ion ESI-FTICR mass spectrum of fullerene derivative ***IV***.

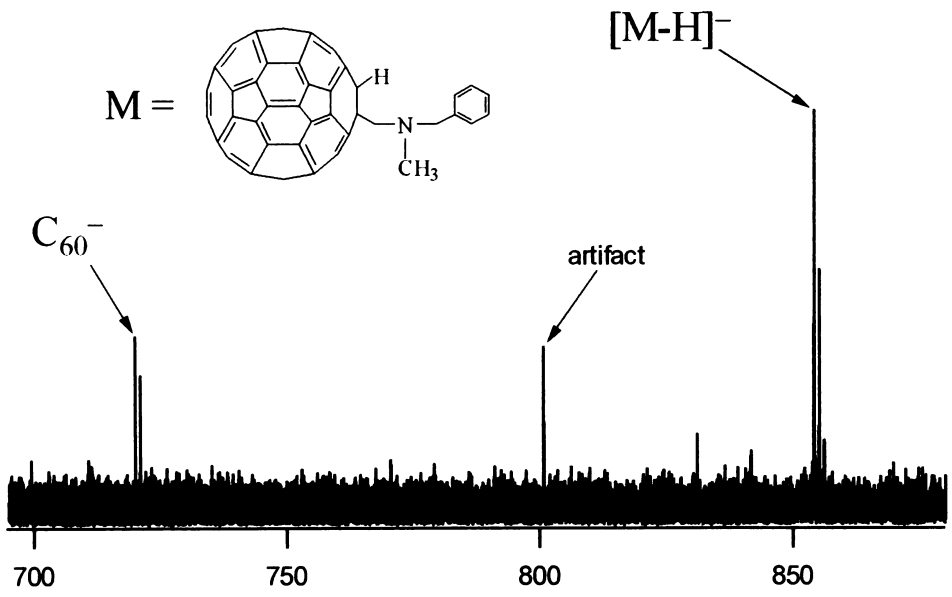

Figure 5-17 ORI-CID FTICR mass spectrum of deprotonated radical anion of fullerene derivative ***IV***.

For fullerene derivatives ***V*** and ***VI***, the ESI-FTICR mass spectrometry studies were first carried out with the ligand compounds L_1 and L_2. Both compounds have a molecular weight of 580 Da. The positive-ion ESI-FTICR mass spectrum for L_1 is shown in Figure 5-18. The sodiated ion $[M+Na]^+$ is the base peak in the mass spectrum. Other addition ions including $[M+H]^+$, $[M+K]^+$ and $[M+Cs]^+$ are also formed. It has been observed that the abundance of $[M+H]^+$ largely depends on the proton affinity of the analyte molecule and the acidity of the solution, whereas the abundance of the alkaline metal adduct ions is proportional to the corresponding metal ions concentration in the solution.

Figure 5-19 is the negative-ion ESI-FTICR mass spectrum of L_1. The major ion in the mass spectrum is the deprotonated anion $[M-H]^-$. The deprotonation is likely to occur on the methyl group in between the carboxylic acid group and the amine group. This is also the binding site for the fullerene derivative ***V***.

Both positive-ion and negative-ion ESI-FTICR mass spectra of L_2 show ionic species that are identical to the compound L_1. ORI-CID experiments are carried out with this compound. Figure 5-20 and 5-21 shows ORI-CID-FTICR mass spectra of the dissociation of sodiated L_2 cation and deprotonated L_2 anion respectively. As indicated in Figure 5-20, the dissociation of sodiated L_2 cation yields a single product ion due to the C-O bond cleavage in one of the carboxylic groups. The CID result for the deprotonated anion $[M-H]^-$ shows two fragmented product ions. The first one is formed by C-O bond cleavage in one of the carboxylic groups and the second one is C-C bond cleavage in the glycine component which yields a radical anion $:C=N=CPh_2^{\cdot -}$.

The positive-ion ESI-FTICR mass spectrum of fullerene derivative ***V*** is shown in Figure 5-22. According to this mass spectrum, $[M+Na]^+$ is the main species observed in

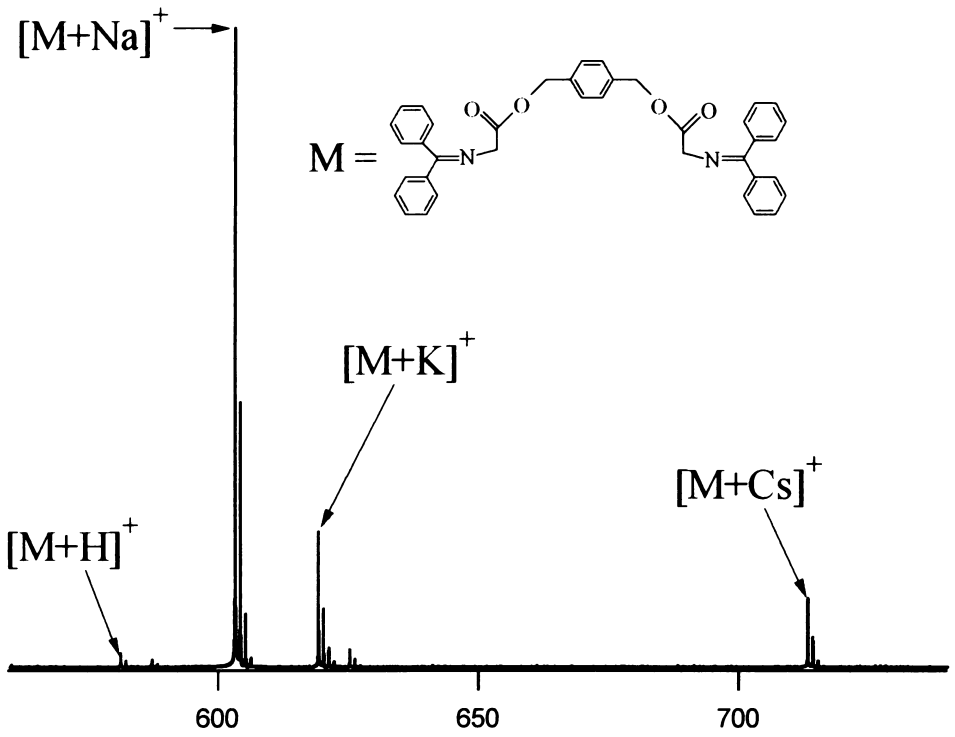

Figure 5-18 Positive-ion ESI-FTICR mass spectrum of ligand compound L_1.

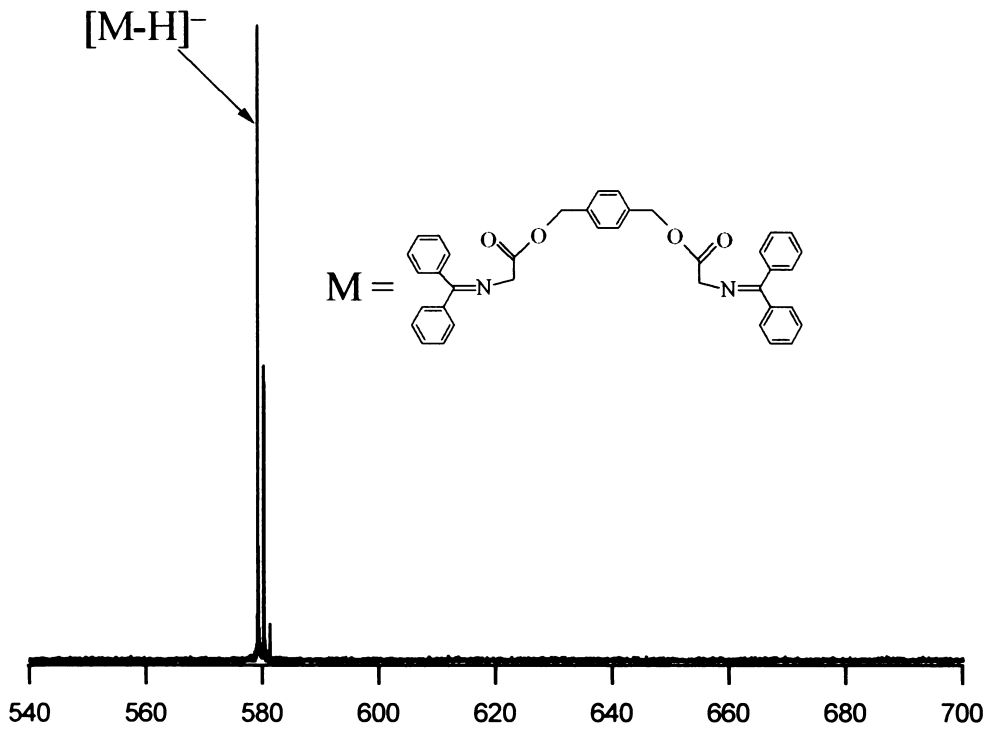

Figure 5-19 Negative-ion ESI-FTICR mass spectrum of ligand compound L_1.

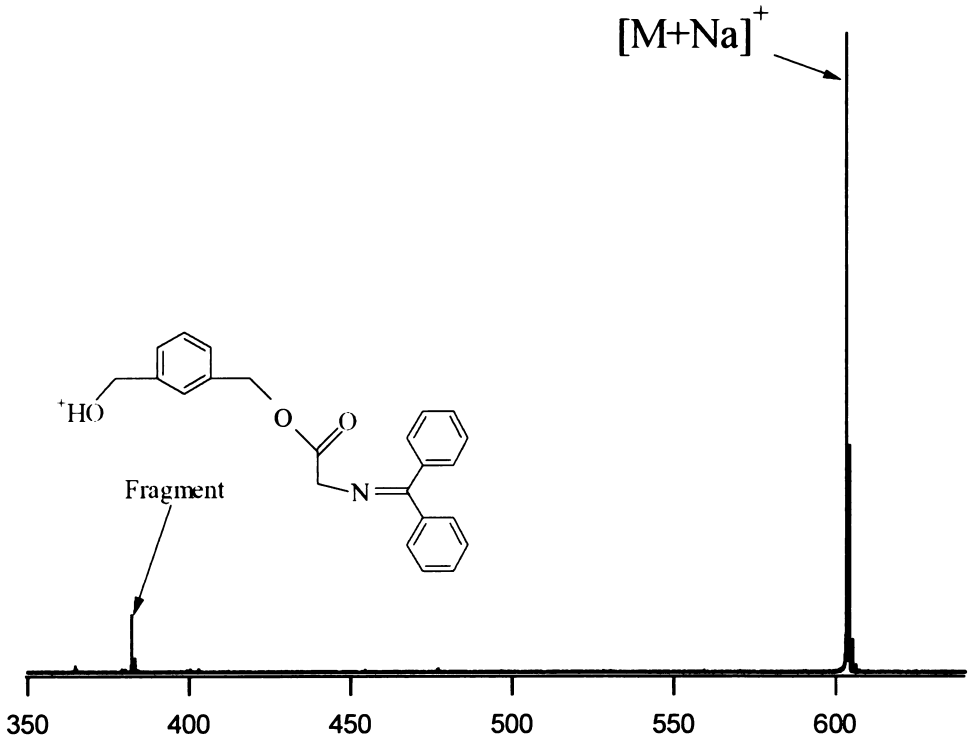

Figure 5-20 ORI-CID-FTICR mass spectrum of sodiated cation of ligand compound L_2.

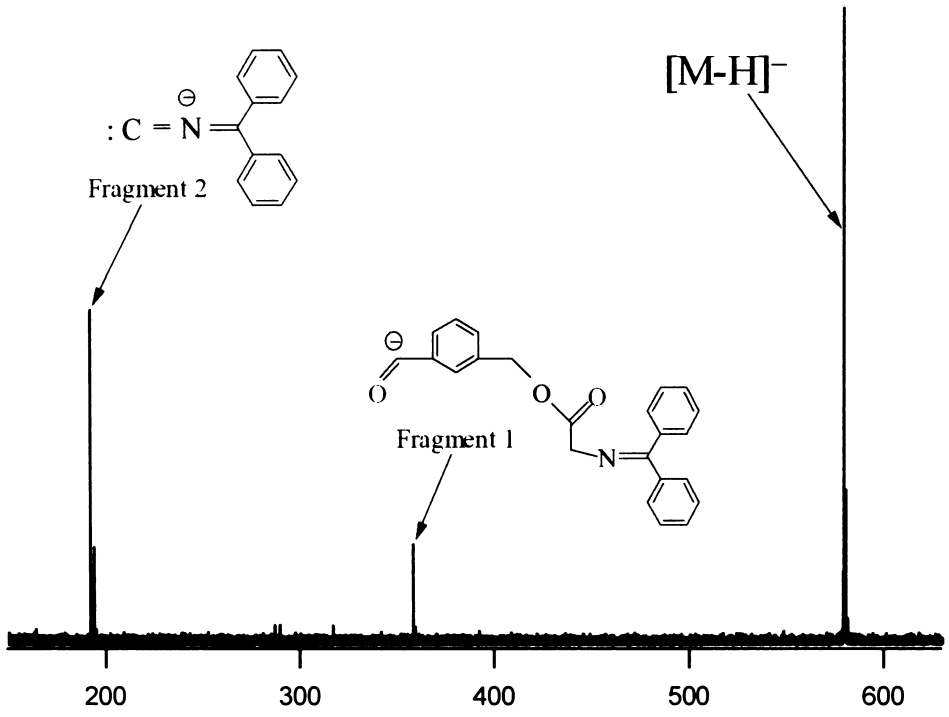

Figure 5-21 ORI-CID-FTICR mass spectrum of deprotonated anion of ligand compound L_2.

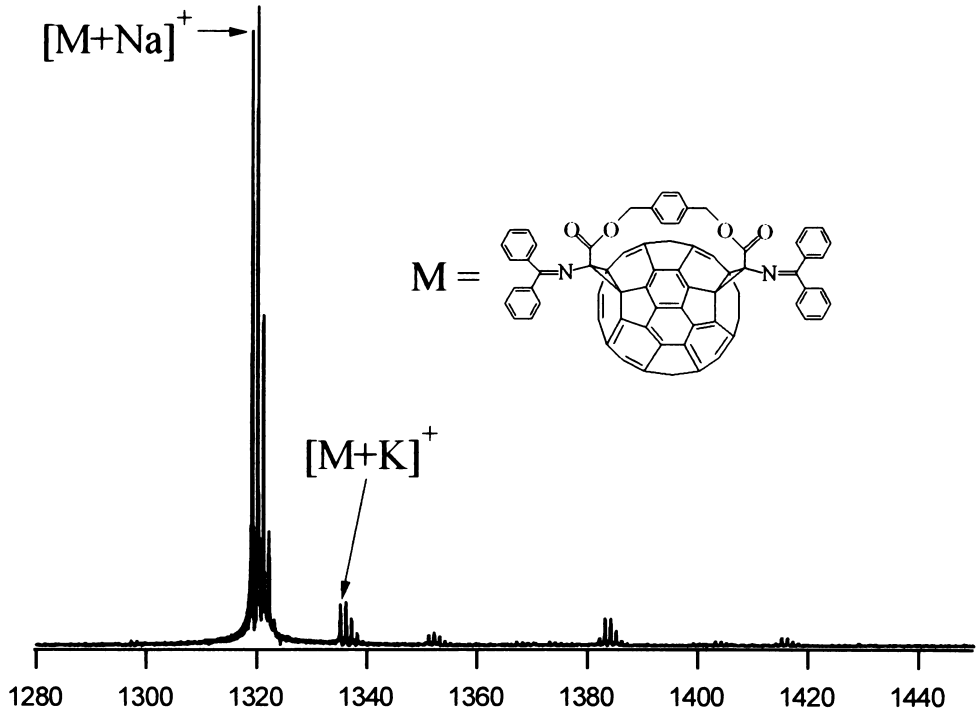

Figure 5-22 Positive-ion ESI-FTICR mass spectrum of fullerene derivative *V*.

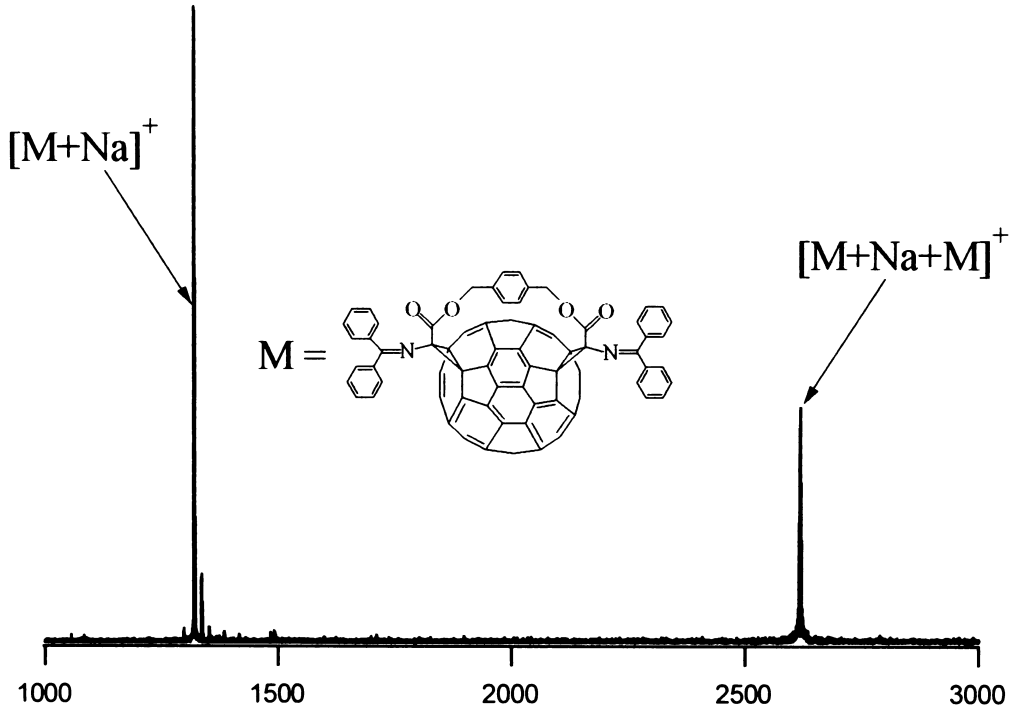

Figure 5-23 Positive-ion ESI-FTICR mass spectrum of fullerene derivative *V*.

this mass spectrum with a small amount of $[M+K]^+$. The sodiated ion can bind with another neutral molecule to form cluster ions of the type of $[M+Na+M]^+$ (Figure 5-23).

The negative-ion ESI-FTICR mass spectrum of fullerene derivative ***V*** is shown in Figure 5-24. In this case, the molecular radical anion $M^{\cdot-}$ is observed together with several addition products including $(CH_3O)M^-$ and $(CH_3O)(CH_3OH)_nM^-$, where n is observed up to four in this mass spectrum. The formation of the molecular radical anion $M^{\cdot-}$ indicates a charge transfer process is involved. The methoxylated anion is possibly formed by the reaction between $M^{\cdot-}$ and solvent methanol molecule or addition of OMe^- to M.

In the study of fullerene derivative ***VI***, a drop of CsI solution was added into the spray solution. Figure 5-25 shows the positive-ion ESI-FTICR mass spectrum of this compound. It shows the caesium ion addition product $[M+Cs]^+$ is the base peak in this mass spectrum with $[M+Na]^+$ being the other major ion in this mass spectrum.

Like the fullerene derivative ***V***, The negative-ion ESI-FTICR mass spectrum of fullerene derivative ***VI*** also shows the molecular radical anion $M^{\cdot-}$ (Figure 5-26). A methoxylated anion and with additional methanol molecules attached anions are also observed in this mass spectrum.

Both the molecular radical anion and the methoxylated anion of ***VI*** were chosen for the CID experiments. Figure 5-27 and Figure 5-28 show the ORI-CID-FTICR mass spectra of these two anions respectively. In Figure 5-27, the dissociation of the molecular radical anion produce two fragment ions. The first fragment has one side of the methano-carbon break away from the fullerene surface with C-O bond cleavage at the end of the carboxylic group that left a dangling radical anion group $-CH_2^{\cdot-}$. This dissociation channel is different from the one that observed for the ligand L_2, where the C-O bond cleavage occurred within the carboxylic group. The other fragment from the

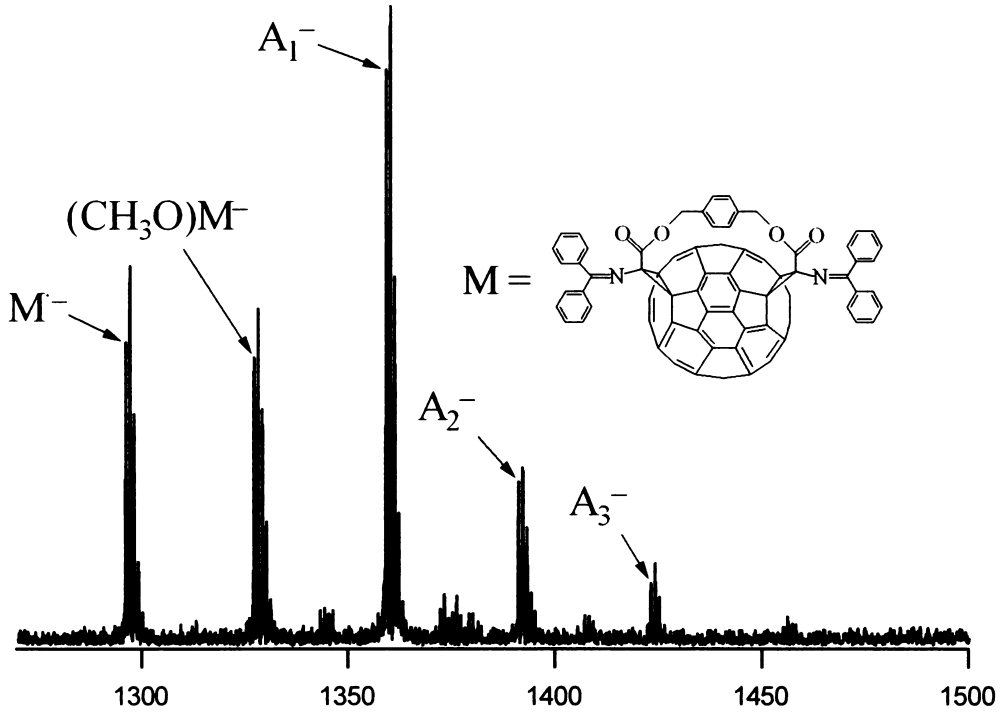

Figure 5-24 Negative-ion ESI-FTICR mass spectrum of fullerene derivative ***V***, where A_1^-, A_2^- and A_3^- represent one, two and three methanol addition to $(CH_3O)M^-$.

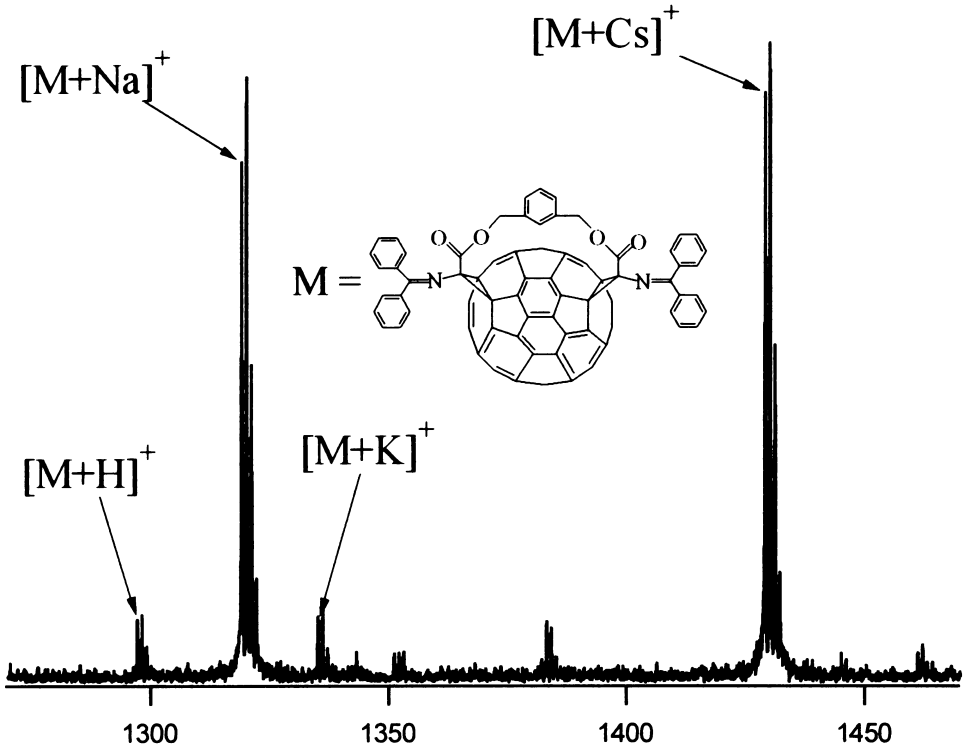

Figure 5-25 Positive-ion ESI-FTICR mass spectrum of fullerene derivative ***VI***.

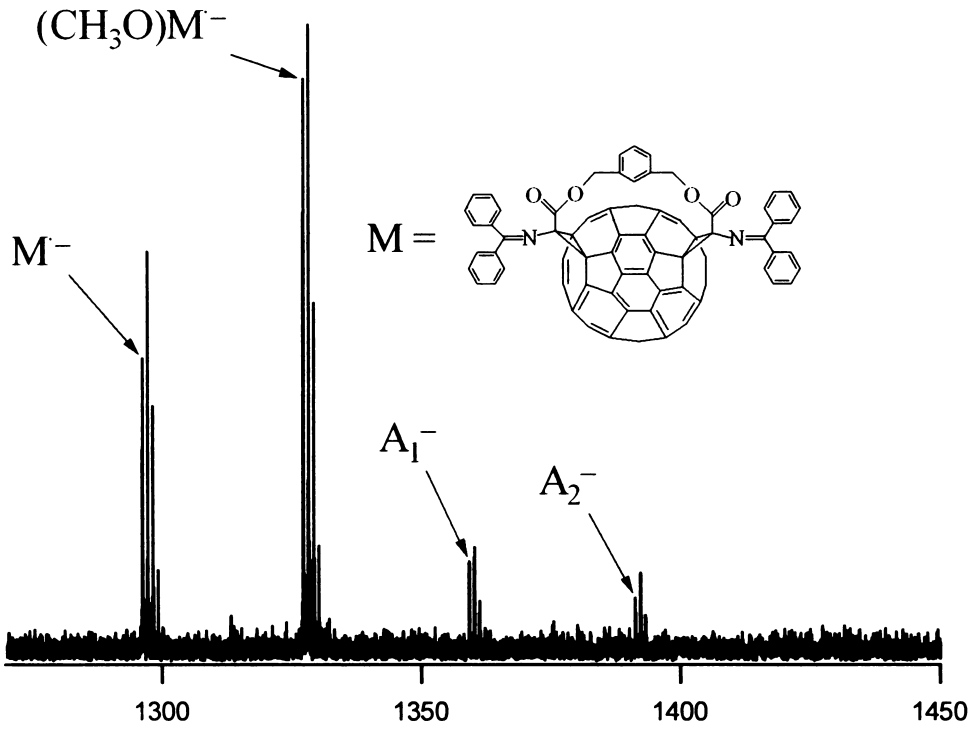

Figure 5-26 Negative-ion ESI-FTICR mass spectrum of fullerene derivative ***VI***, where A_1^- and A_2^- represent single and double methanol addition to $(CH_3O)M^-$.

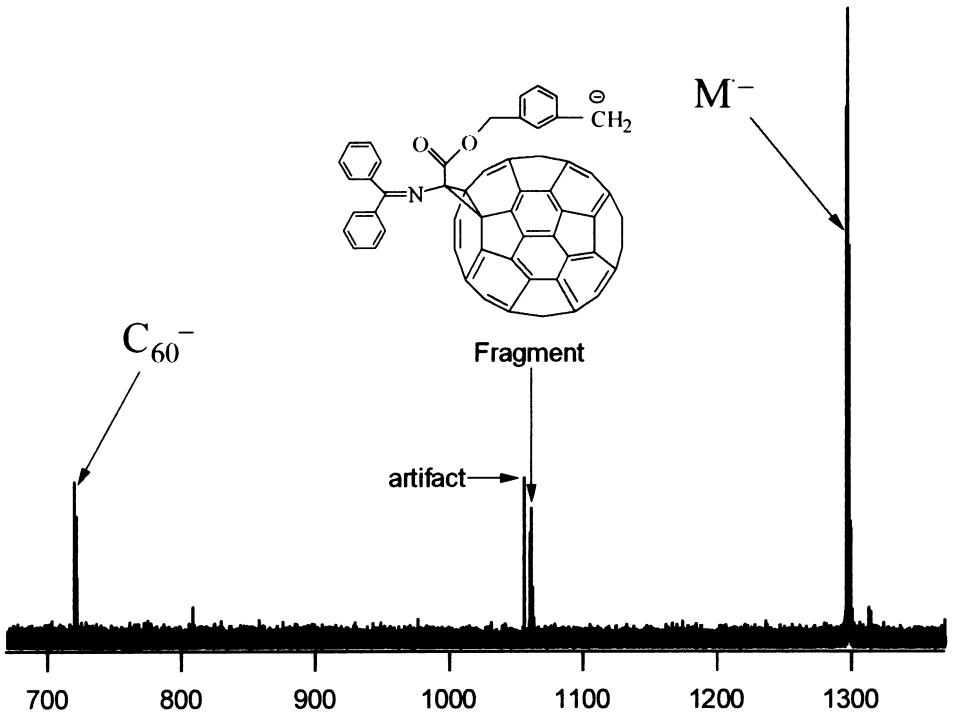

Figure 5-27 ORI-CID-FTICR mass spectrum of molecular radical anion of fullerene derivative *VI*.

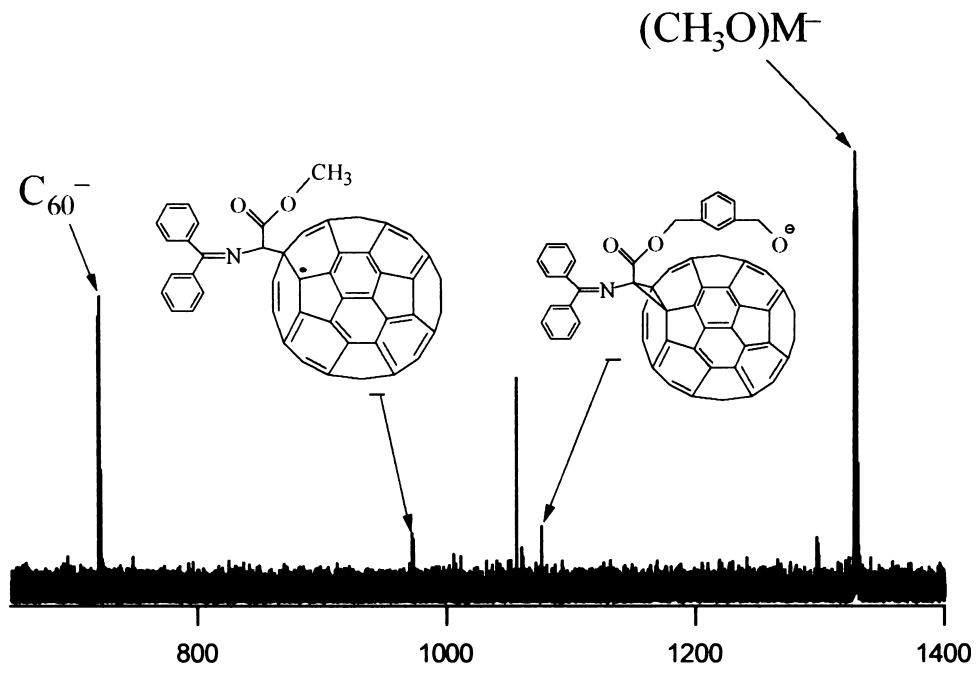

Figure 5-28 ORI-CID-FTICR mass spectrum of methoxylated/deprotonated fullerene derivative *VI* cation.

dissociation of ***VI*** is C_{60}^-. The CID of the methoxylated ion produced three fragment ions as indicated in the mass spectrum in Figure 5-28.

5.2.5 Cyano-Fullerene Derivatives

5.2.5.1 Sample Preparation

The cyano-fullerene derivatives were prepared by reacting fullerene C_{60} with NaCN. 18 mg of pure fullerene C_{60} (99.9%, from MER Co. USA) was dissolved in chlorobenzene which yields a purple colored solution. 180 mg NaCN was then dissolved in dimethylformamide. The two solutions were mixed together and the final solution changes in color to dark red. Storing over-night allowed a crystalline material to precipitate from the solution. The crystals were separated by filtration and it was found that this material was water-soluble. The aqueous solution of this material was diluted in the methanol about a hundred times prior to the ESI-FTICR mass spectrometry analysis.

5.2.5.2 ESI-FTICR Mass Spectrometry Studies of Cyano-Fullerene Derivatives

The study of cyano-fullerenes was carried out mainly in the negative-ion mode, as cationic species are unlikely to be observed for cyano-fullerenes. Figure 5-29 shows a negative-ion ESI-FTICR mass spectrum showing a series of cyano-fullerenes. The main species in this mass spectrum are assigned to $C_{60}(CN)_n^-$, (where n = 0 – 8), with $C_{60}(CN)_3^-$ is assigned to the base peak in this mass spectrum. Many minor species are assigned to $C_{60}O_n^-$ ($n < 5$), or $C_{60}O(CN)_n^-$ type of ions where n is in the same range as $C_{60}(CN)_n^-$. C_{60}^- is observed as the base peak ion in the mass spectrum and since the reaction rate for cyano-addition reaction is unknown, it is possible that certain amount of unreacted fullerene C_{60} remained in the spray solution.

Some reports have shown doubly charged cyano-fullerene anions can be formed by ESI process,[28,29] Tuinman and Compton have also observed the formation of multiply

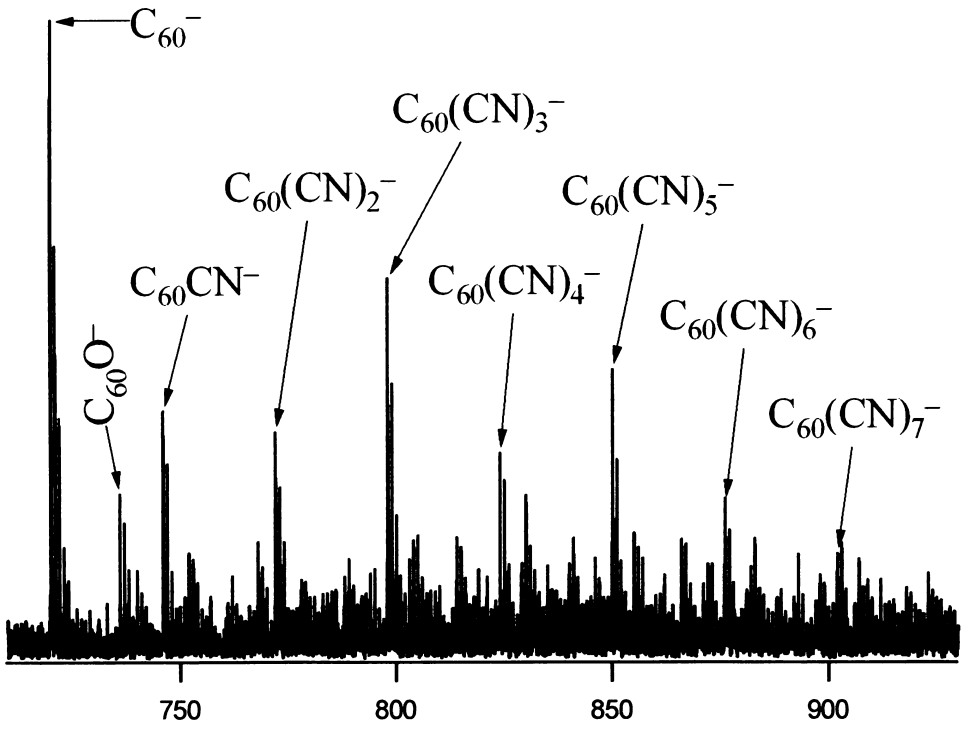

Figure 5-29 Negative-ion ESI-FTICR mass spectrum of cyano-fullerenes.

charged ions from fullerene derivatives involving radical anions of the cyano adduct of C_{60}.[44] They reported that the negative-ion ESI mass spectra of solutions containing C_{60} and a 100-fold molar excess of NaCN display numerous polyanionic species of the general form $(C_{60})_nCN_m^{x-}$ where n = 1-3, m = 1-7, and x = 1-3.

In this present study, however, no doubly charged cyano-fullerenes anions are observed. As in the ESI-FTICR mass spectrometry experiments, the observation of cyano-fullerenes requires some extreme electrospray conditions for which the maximum capillary voltage (400 V, exit end) has to be applied. The multiply charged ions may not survive after many high-energy collisions.

5.2.6 Fluorinated Fullerenes

5.2.6.1 Sample Preparation

The fluorinated fullerenes were supplied by Dr. Gerry Gadd from the Australian Nuclear Science and Technology Organization (ANSTO). The fluorinated fullerenes were synthesized by reacting fullerene C_{60} with SF_6 under high pressure (~ 200 bar). The reaction product was a brownish colored powder, which was extracted in methanol. By rotary evaporation, the methanol-soluble components yielded a yellow colored powder. This sample was then investigated by the ESI-FTICR mass spectrometry.

5.2.6.2 ESI-FTICR Mass Spectrometry Studies of Fluorinated Fullerenes

The ESI-FTICR mass spectrometry study of fluorinated fullerenes results in the observation of a large number of ions. As shown in Figure 5-30, the positive-ion ESI-FTICR mass spectrum shows a broad distribution of cationic species that are centered at m/z ~ 1,400. The attempt to assign the peaks with a general formula of $C_{60}F_x^+$ was unsuccessful. Closer examination of this mass spectrum shows that peaks are generally separated by a unit mass with odd number peaks higher in abundance than the adjacent even number peaks. The first three digits after the decimal point of the ion mass

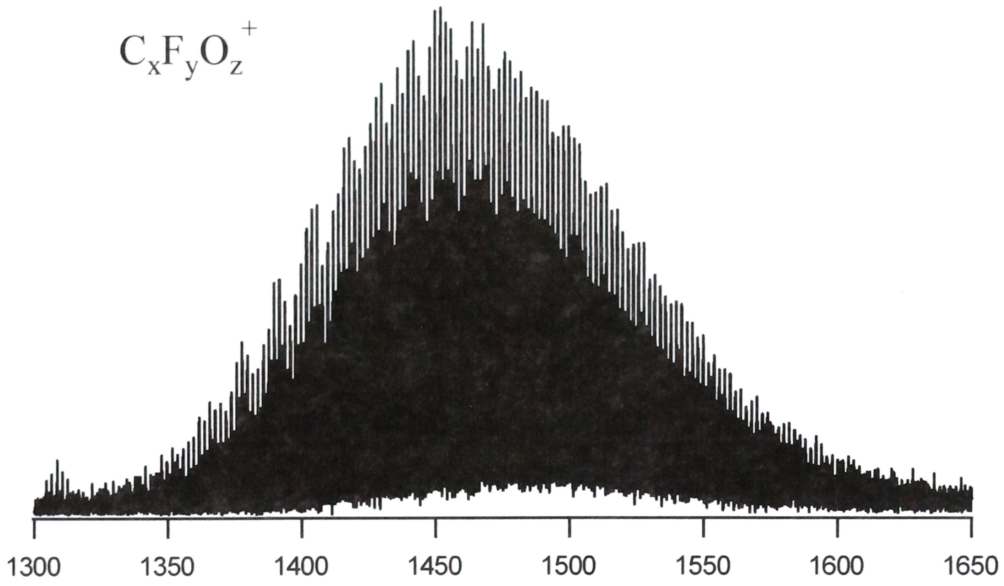

Figure 5-30 Positive-ion ESI-FTICR mass spectrum of fluorinated fullerenes and carbons.

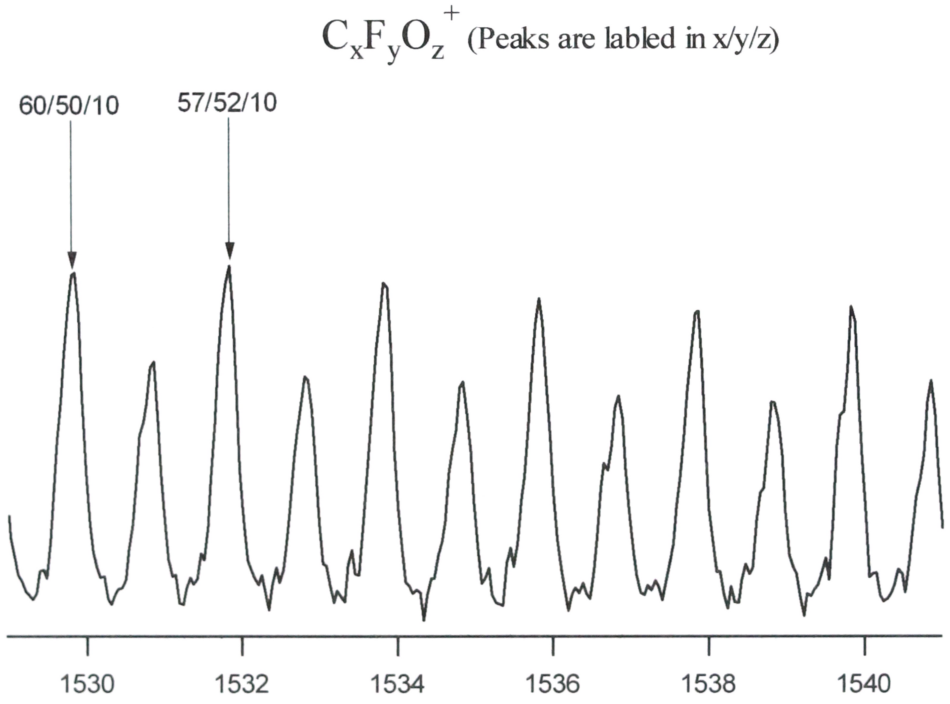

Figure 5-31 The expanded region (m/z 1529 ~ 1541) of the positive-ion ESI-FTICR mass spectrum showing in Figure 5-30.

number ranges between .588 ~ .834 for m/z region of 1,300 ~1,650. Such mass numbers cannot be assigned to pure carbon or carbon-fluorine species. One possible explanation for such mass numbers and the ion distributions is that these species may contain various numbers of oxygen atoms. Also, many of these species may not be fullerene derivative, but large carbon species that are dissociated from C_{60}. The dissociation of fullerene may be caused by the high strain in the fullerene molecule as the result of high degree of fluorination. Using a general formula $C_xO_yH_z^+$, many peaks in this mass spectrum can be assigned to a mass accuracy within a few ppm. For example, a peak that measured m/z value is 1,529.827, has been assigned to $C_{60}O_{50}H_{10}^+$, to within 2 ppm.

The expanded mass region of m/z 1,460 ~ 1,480 of Figure 5-30 is shown in Figure 5-31. It shows that various combinations of the x, y and z values that causes the ion isotope overlapping and ion intensity alternation.

The negative-ion ESI-FTICR mass spectrum (Figure 5-32) has presented very similar ion distributions with more low mass ions (m/z < 1300) observed in this mass spectrum. Closer examination of this mass spectrum shows that peaks are also separated by a unit mass with odd number peaks higher in abundance than the adjacent even number peaks. The first three digits after the decimal point of the ion mass number ranges between 0.217 ~ 0.334 for m/z region 1,300 ~1,650. Possible formulae including $C_{60}F_x^-$, $C_xF_y^-$, $C_xF_yO_z^-$ and $C_xO_yH_z^-$ could not be used to successfully assign the peaks. Using a general formula $C_xF_yH_z^-$, however, most of the peaks in this mass spectrum can be assigned within a few ppm. Figure 5-33 shows an expanded region of m/z 1,400 ~ 1,450 of the mass spectrum show in Figure 5-32. It shows several examples for such mass assignment. The possible combinations of the x, y and z values have indicated a high degree of C_{60} dissociation that may have occurred during the synthesis.

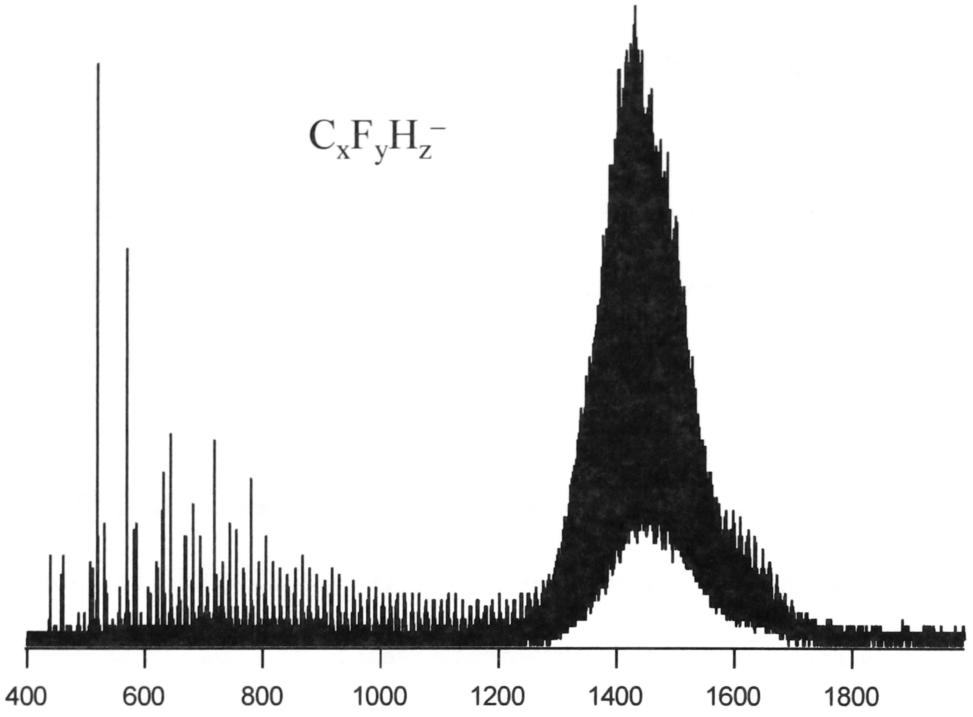

Figure 5-32 Negative-ion ESI-FTICR mass spectrum of fluorinated and hydrolyzed fullerenes.

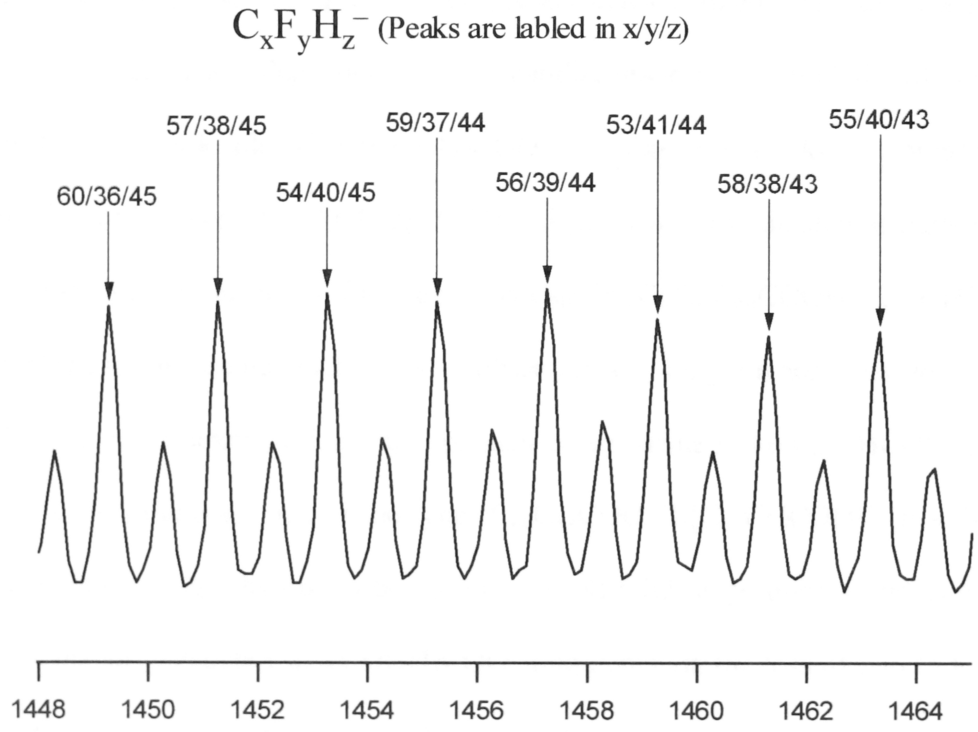

Figure 5-33 The expanded region (m/z 1448 ~ 1465) of the negative-ion ESI-FTICR mass spectrum showing in Figure 5-32.

As discussed in the Chapter one, fullerene hydrogenation and fluorination have been attempted by several research groups,[5,45-50] but full hydrogenation or full fluorination of fullerene C_{60} have not been successful because the high strain that such molecules experienced makes them very unstable. The unstable nature of these molecules may explain why so many dissociation products are observed in this current ESI-FTICR mass spectrometry studies.

5.3 Conclusions

The ESI-FTICR mass spectrometry study of fullerene derivatives ***I*** – ***VI***, cyano-fullerenes and fluorinated fullerenes shows that the combination of electrospray ionization method and FTICR mass spectrometry is a very informative method for the characterization of different types of fullerene derivatives.

The study of 1,6-methano[60]fullerene-61,61-dicarboxylic acid (***I***) in methanol shows that gas phase negative-ions are preferentially formed. The ion distributions in the mass spectra are dependent on the capillary/skimmer potential difference. The deprotonated molecule $C_{60}C(COOH)COO^-$ is observed at low capillary/skimmer potential differences. $C_{60}C(COOH)COO^-$ progressively fragmented at higher potential difference and produced the fragment ions $C_{60}CHCOO^-$, $C_{60}COOH^-$, $C_{60}CH^-$ and C_{60}^-. Gas phase ion-molecule reactions were observed with long ion accumulation delay (d_1 = 2 s) in the rf/dc hexapole ion trap. In such an experiment the $C_{60}CHCOO^-$ anion was found to form cluster ions of the type $[C_{60}CHCOOH]_n[C_{60}CHCOO]^-$ (n = 1-2) which may contain single-hydrogen-bridge(s). SORI-CID experiments indicate that the deprotonated molecule $C_{60}C(COOH)COO^-$ fragments via the loss of two CO_2 groups to form $C_{60}CH^-$ which further dissociates to give $C_{60}^-/C_{60}H^-$.

The semi-empirical molecular orbital calculations using the AM_1 approximation for the neutral and ionic species reveal that most of ionic species have low symmetry.

Exceptions to this result are C_{60}^- and $C_{60}CH^-$ that have I_h and C_{2V} symmetries respectively. A comparison of the calculated energies reveals that the deprotonated dicarboxylic acid derivative is more reactive than the monocarboxylic acid derivative, with the basic methanofullerene[60] showing least reactivity.

The study of fullerene derivative ***II*** and ***III*** revealed that both cationic and anionic species are formed in the electrospray process. In the positive-ion mode, proton addition and alkaline metal ion addition are the main ion formation mechanism. As both compounds contain carboxylic acid groups, the formation of negative-ions was mainly via deprotonation.

Fullerene derivative ***IV*** does not contain any acid groups. ESI-FTICR mass spectra of this compound show that the cationic species is formed by protonation of the neutral molecule, and the anionic species is formed by deprotonation of the neutral molecule.

The study of fullerene derivatives ***V*** and ***VI*** show alkaline metal ion addition for the positive ions. In the negative-ion mode, molecular radical anions are formed. A methoxylated molecular anion is also observed which is possibly the result of the reaction between the molecular radical anion and the solvent molecule methanol. Further addition of neutral solvent molecules is also observed in the spectra.

In the study of cyano-fullerenes, a series of cyano-fullerenes are observed with a general formula $C_{60}(CN)_n^-$ with n up to eight. Minor species in the form of $C_{60}O_n^-$ (n = 1 – 4) and $C_{60}O(CN)_n^-$ (where n = 1 – 8) are also observed.

The ESI-FTICR mass spectrometry study of fluorinated fullerene derivatives shows that these compounds are easy to dissociate and produce ionic species of the form of $C_xO_yH_z^+$ for cations and $C_xF_yH_z^-$ for anions. The observation of such dissociation indicates the high strain in these fluorinated fullerene molecules.

5.4 References

(1) O'Donovan, B. F.; Hitchcock, P. B.; Meidine, M. F.; Kroto, H. W.; Taylor, R.; Walton, D. R. M. *J. Chem. Soc., Chem. Commun.* **1997**, 81.

(2) Shi, Y.; Gan, L.; Wei, X.; Jin, S.; Zhang, S.; Meng, F.; Wang, Z.; Yan, C. *Org. Lett.* **2000**, *2*, 667.

(3) Tumanskii, B. L.; Bashilov, V. V.; Solodovnikov, S. P.; Bubnov, N. N.; Sinyashin, O. G.; Romanova, I. P.; Drozd, V. N.; Knyazev, V. N.; Sokolov, V. I. *Russ. Chem. Bull.* **1999**, *48*, 1786.

(4) Karfunkel, H. R.; Hirsh, A. *Angew. Chem. Int. Ed. Engl.* **1992**, *31*, 1468.

(5) Taylor, R.; Holloway, J. H.; Hope, E. G.; Avent, A. G.; Langley, G. J.; Dennis, T. J.; Hare, J. P.; Kroto, H. W.; Walton, D. R. M. *J. Chem. Soc., Chem. Commun.* **1992**, 665.

(6) Boltalina, O.; Holloway, J. H.; Hope, E. G.; Street, J. M.; Taylor, R. *J. Chem. Soc., Perkin Trans.* **1998**, 1845.

(7) Gan, L.; Zhou, D.; Luo, C.; Tan, H.; Huang, C.; Lue, M.; Pan, J.; Wu, Y. *J. Org. Chem.* **1996**, *61*, 1954.

(8) Tumanskii, B. L.; Kalina, O. G.; Bashilov, V. V.; Usatov, A. V.; Shilova, E. A.; Lyakhovetskii, Y. I.; Solodovnikov, S. P.; Bubnov, N. N.; Novikov, Y. N.; Lobach, A. S.; Sokolov, V. I. *Russ. Chem. Bull.* **1999**, *48*, 1108.

(9) Yoshida, M.; Morinaga, Y.; Iyoda, M.; Kikuchi, K.; Ikemoto, I.; Achiba, Y. *Tetrahedron Letts.* **1993**, *35*, 7629.

(10) Boltalina, O. V.; Avakian, T. V.; Markov, V. Y.; Sorokin, I. D.; Sidorov, L. N.; Taylor, R. *Proc. Electrochem. Soc.* **1998**, *98-8*, 1152.

(11) Grieves, G. A.; Buchanan, J. W.; Reddic, J. E.; Duncan, M. A. *Int. J. Mass Spectrom.* **2001**, *204*, 223.

(12) Birkett, P. R.; Cheetham, A. J.; Eggen, B. R.; Hare, J. P.; Kroto, H. W.; Walton, D. R. M. *Chem. Phys. Lett.* **1997**, *281*, 111.

(13) Bruhwiler, P. A.; Anderson, S.; Dippel, M.; Martensson, N.; Demirev, P. A.; Sundquivist, B. U. R. *Chem. Phys. Lett.* **1993**, *214*, 45.

(14) Hettich, R. L.; Jin, C.; Britt, P. F.; Tuinman, A. A.; Compton, R. N. *Proc. Mater. Res. Soc. Symp.* **1994**, *349*, 133.

(15) Jin, C.; Hettich, R.; Compton, R.; Joyce, D.; Blencoe, J.; Burch, T. *J. Phys. Chem.* **1994**, *98*, 4215.

(16) Birkett, P. R.; Kroto, H. W.; Taylor, R.; Walton, D. R. M. *Mol. Cryst. Liq. Cryst. Sci. Technol., Sect. C* **1996**, *7*, 27.

(17) Adamson, A. J.; Holloway, J. H.; Hope, E. G.; Taylor, R. *Fullerene Sci. Technol.* **1997**, *5*, 629.

(18) Peel, J. B.; Rothwell, R. G. *Aust. J. Chem.* **1994**, *47*, 131.

(19) Diederich, F.; Thilgen, C. *Science* **1996**, *271*, 317.

(20) Hirsch, A. *J. Phys. Chem. Solids* **1997**, *58*, 1729.

(21) Schuster, D. I.; Wilson, S. R.; Schinazi, R. F. *Bioorg. Med. Chem. Lett.* **1996**, *6*, 1253.

(22) Takenaka, S.; Yamashita, K.; Takagi, M.; Hatta, T.; Tsuge, O. *Chem. Lett.* **1999**, *7*, 319.

(23) Takenaka, S.; Yamashita, K.; Takagi, M.; Hatta, T.; Tsuge, O. *Chem. Lett.* **1999**, *7*, 321.

(24) Khan, S. I.; Oliver, A. M.; Paddon-Row, M. N.; Rubin, Y. *J. Am. Chem. Soc.* **1993**, *115*, 4919.

(25) Liu, S.; Lu, Y.; Kappes, M. M.; Ibers, J. A. *Science* **1991**, *254*, 408.

(26) Wilson, S. R.; Wu, Y. H. *J. Am. Chem. Soc.* **1993**, *115*, 10334.

(27) Hiraoka, K.; Kudaka, I.; Fujimaki, S.; Shinohara, H. *Rapid Commun. Mass Spectrom.* **1992**, *6*, 254.

(28) Khairallah, G.; Peel, J. B. *Chem. Commun.* **1997**, 253.

(29) Khairallah, G.; Peel, J. B. *Chem. Phys. Lett.* **1997**, *268*, 218.

(30) Khairallah, G.; Peel, J. B. *J. Phys. Chem. A* **1997**, *101*, 6770.

(31) Dupont, A.; Gisselbrecht, J.; Leize, E.; Wanger, L.; Van Dorsselaer, A. *Tet. Lett.* **1994**, 6083.

(32) Wilson, S. R.; Wu, Y. H. *Org. Mass Spectrom.* **1994**, *29*, 186.

(33) Grayson, M.; Lovett, E.; Dugan, L.; Wang, Y.; Gross, M. *Proc. 47th Am. Soc. Mass Spectrom. Conf. on Mass Spectrom. & Allied Topics* (*American Society for Mass Spectrometry*) **1999**, *Dallas*, 249.

(34) Da Ros, T.; Prato, M. *Chem. Commun.* **1999**, 663.

(35) Sijbesma, R. P.; Srdanov, G.; Wudl, F.; Castora, J. A.; Wilkins, C.; Friedman, S. H.; DeCamp, D. L.; Kenyon, G. L. *J. Am. Chem. Soc.* **1993**, *115*, 6510.

(36) Friedman, S. H.; DeCamp, D. L.; Sijbesma, R. P.; Srdanov, G.; Wudl, F.; Kenyon, G. L. *J. Am. Chem. Soc.* **1993**, *115*, 6506.

(37) Lamparth, I.; Hirsch, A. *J. Chem. Soc., Chem. Commun.* **1994**, *14*, 1727.

(38) Zhao, Y.; Gan, L.; Zhou, D.; Luo, C.; Huang, C.; Jia, G.; Wu, T. *Chin. Sci. Bull.* **1997**, *42*, 1360.

(39) Shi, Y.; Jiang, J.; Gan, L.; Jin, S.; Zhang, W.; Huang, C.; Wu, Y. *Proc. Electrochem. Soc.* **1998**, *98-8*, 1088.

(40) Coolidge, M. B.; Stewart, J. J. P. *MOPAC 7.0 prog.* **1990**.

(41) Hobza, P.; Bludsky, O.; Suhai, S. *Chem. Phys.* **1999**, *1*, 3073.

(42) Burley, G. A.; Keller, P. A.; Pyne, S. G.; Ball, G. E. *J. Chem. Soc., Chem. Commun.* **1998**, 2539.

(43) Burley, G. A.; Keller, P. A.; Pyne, S. G. *Fullerene Sci. Technol.* **1999**, *7*, 973.

(44) Tuinman, A. A.; Compton, R. N. *J. Phys. Chem.* **1998**, *102*, 9791.

(45) Tuiman, A. A.; Mukherjee, P.; Adcock, J. L.; Hettich, R. L.; Compton, R. N. *J. Phys. Chem.* **1992**, *96*, 7584.

(46) Kniaz, K.; Fischer, J. E.; Selig, H.; Vaughan, G. B. M.; Romano, W. J.; Cox, D. M.; Chowdhury, S. K.; McCauley, J. P.; Strongin, R. M.; III, A. B. S. *J. Am. Chem. Soc.* **1993**, *115*, 6060.

(47) Taylor, R.; Langley, G. J.; Brisdon, A. K.; Holloway, J. H.; Hope, E. G.; Kroto, H. W.; Walton, D. R. M. *J. Chem. Soc., Chem. Commun.* **1993**, 875.

(48) Compton, R. N.; Lahamer, A. S.; Tuinman, A. A.; Zhou, L. *Proc. Electrochem. Soc.* **1998**; *98-8*, 1022.

(49) Mitsumoto, R.; Seki, K.; Araki, T.; Ito, E.; Ouchi, Y.; Achiba, Y.; Kikuchi, K.; Yajima, S.; Kawasaki, S. *J. Electron Spectrosc. Relat. Phenom.* **1996**, *78*, 453.

(50) Mitsumoto, R.; Araki, T.; Ito, E.; Ouchi, Y.; Seki, K.; Kikuchi, K.; Achiba, Y.; Kurosaki, H.; Sonoda, T.; Kobayashi, H.; Boltalina, O. V.; Pavlovich, V. K.; Sidorov, L. N.; Hattori, Y.; Liu, N.; Yajima, S.; Kawasaki, S.; Okino, F.; Touhara, H. *J. Phys. Chem. A* **1998**, *102*, 552.

Chapter Six

Brief Summary and Future Work

The research work described in this thesis involves several developing areas in chemistry including fullerenes, fullerene derivatives, endohedral metallofullerenes, gas-phase ion chemistry and DFT quantum chemical calculation of gas-phase clusters. It is clear that this current study has barely scratched the surface of these fields and further investigations are necessary for better understanding of these subjects. Several points are summarized here in order to provide a brief guide for future work.

6.1 Macroscopic Production of Endohedral Metallofullerenes

As shown in Chapter Three, the laser ablation experiment indicates a promising method for macroscopic production of endohedral metallofullerenes. By using polycyclic aromatic hydrocarbon precursors, such as those collected from the pyrolysed KCT-pitch, fullerenes and endohedral metallofullerenes can be produced at room temperature by laser ablation. Further experimental studies are needed if the production conditions are to be optimized. Variables including the laser power density; carrier gas pressure and metal/carbon ratio are of major concerns for the optimization. Purification method for endohedral metallofullerenes also need to improve in order to obtain chemically pure material for macroscopic studies. Characterization of endohedral metallofullerenes by various analytical techniques including FTICR mass spectrometry is a worth for further study, because the chemical and physical properties of these molecules are still not fully understood.

Larger scale production of endohedral metallofullerenes may be achieved by redesigning the laser ablation fullerene and endohedral metallofullerenes generator with the possibility of using larger size of target and higher energy lasers. Using multiple

lasers/multiple targets is another alternative in this aspect. In regard with the carbon precursors, it may be possible to use a single PAH with well-defined structure instead of a range of PAHs such as the pyrolysed KCT-pitch residue. The advantage of such choice is that the laser ablation conditions may be more precisely determined and the yield of endohedral metallofullerenes may be improved. A PAH such as $C_{60}H_{28}$, which is present in the laser desorption FTICR mass spectrum shown in Figure 3-02, would be a suitable candidate for such experiment.

6.2 Further Studies of Gas-Phase Ion Chemistry of Metal-Carbon Clusters

In pursuing the study of gas-phase ion chemistry of metal-carbon clusters that is described in the Chapter Four, metals from different groups in the periodic table need to be investigated by the means of ion-molecule reactions. The gas-phase reactions of yttrium- and lanthanum-carbon clusters demonstrate characteristic reaction pathways in various reactions. As gas-phase reactivity of metal-carbon clusters can reflect their electronic structure, the study of the reaction products by the means of collision-induced-dissociation will provide crucial information on their structures and bonding orders. For example, the CID experiment performed with the endohedral metallofullerene ion $La@C_{60}^+$ shows the emission of carbon atoms from the fullerene cage but not the metal ion. Endohedral metallofullerene ions are also known to be non-reactive towards to many common gas-phase organic reagents such as methanol or benzene while the related small metal-carbon clusters such as yttrium- and lanthanum-carbon clusters have shown high reactivity towards these reagent molecules.

6.3 Further Studies of Metal-Carbon Clusters by DFT Calculations

In pursuing the theoretical studies on the metal-carbon clusters described in the Chapter Four, investigation on metal-carbon clusters with larger carbon ligands or with other metals needs to be carried out and the outcome of these investigations may

provide crucial knowledge on the formation of metal-carbon clusters including endohedral metallofullerenes and Metcars. It also provides a better understanding of the formation of these clusters which may shine light on how to improve their macroscopic production.

Also, as demonstrated in Chapter Four, the studies of weak covalent-bond structures such as $La(C_6H_4)(C_6H_6)_3^+$ is challenging for theoretical chemical calculations. Improved methodology should be adopted in order to achieve a better description of such system. The understanding of this type of structures can have major implications in biological science since the formation of many biomolecules largely involves non-covalent interactions such as hydrogen bonding.

6.4 ESI-FTICR Mass Spectrometry Studies of Fullerene Derivatives

The ESI-FTICR mass spectrometry studies of fullerene derivatives described in the Chapter Five show characteristic behavior of these molecules in the electrospray process. The high resolution of FTICR instruments provides unparallel resolving power for correct ion mass assignment, which enables precise elemental composition analysis. It is still not clear though how the ions, especially fullerene molecules are formed in the electrospray process. Understanding the formation of proton or alkaline metal ion adducts and molecular ions are very important for many large compounds such as biopolymers. The formation of multiply charged species is also of major concern in understanding the ESI process.

On the other hand, the current study has shown that ESI-FTICR mass spectrometry is a very informative method in the characterization of fullerene derivatives. The soft ionization nature of ESI often enables the observation of the molecular species of these chemically labile fullerene derivatives. ESI-FTICR mass spectrometry has also made it possible to study fullerene derivatives in both solution phase and gas-phase.

List of Publications

1. **Carbon Black: A Precursor for Fullerene and Metallofullerene Production**

   Femia G. Hopwood, Keith J. Fisher, Paul Greenhill, Gary Willett and **Rui Zhang**

   The Journal of Physical Chemistry B **1997**,*101*,10704-10708

2. **Laser Ablation Mass Spectrometry of Pyrolyzed Koppers Coal-Tar Pitch: A Precursor for Fullerenes and Metallofullerenes**

   Rui Zhang, Yohji Achiba, Keith J. Fisher, Gerry E. Gadd, Femia G. Hopwood, Toshinobu Ishigaki, Derek R. Smith, Shinzo Suzuki and Gary D. Willett

   The Journal of Physical Chemistry B **1999**,*103*, 9450-9458

3. **Electrospray Studies of a Water Soluble Platinum (II) Phosphine Complex, Chlorotris(1, 3, 5-triaza-7-phosphaadamantane)platinum (II) Chloride $(TPA)_3PtCL_2$**

   Keith J. Fisher, Ian G. Dance, Gary Willett and **Rui Zhang**

   European Journal of Mass Spectrometry **2000**, *6*, (1) 23-30

4. **An Electrospray Ionization Fourier Transform Ion Cyclotron Resonance Mass Spectrometry Study of 1,6-methano[60]fullerene-61,61-dicarboxylic Acid**

   Rui Zhang, Keith J. Fisher, Liangbing Gan, Zhen Gao, J. Barrie Peel, Yaru Shi, Derek R. Smith and Gary Willett

   European Journal of Mass Spectrometry **2000**, *6*, (2) 161-168

5. **Sub-ppt Detection Limits for Copper Ions with Gly-Gly-His Modified Electrodes**

   Wenrong Yang, David Jaramillo, J. Justin Gooding, D. Brynn Hibbert, **Rui Zhang**, Gary D. Willett, Keith J. Fisher

   Chemical Communications **2001**, *19*, 1982-1983